HELSINKI INSTITUTE OF PHYSICS INTERNAL REPORT SERIES

HIP-2005-03

The Nature of Primordial Perturbations in the Light of CMB Observations

Jussi Väliviita

Helsinki Institute of Physics
P.O. Box 64, FI-00014 University of Helsinki, Finland

ACADEMIC DISSERTATION
To be presented for public criticism, with the permission of the Faculty of Science of the University of Helsinki, in Auditorium E204 at Physicum, Gustaf Hällströmin katu 2, on June 22, 2005, at 12 a.m.

Helsinki 2005

ISBN 952-10-1691-4 (printed version)
ISSN 1455-0563
Helsinki 2005
Yliopistopaino

ISBN 952-10-1692-2 (pdf version)
http://ethesis.helsinki.fi
Helsinki 2005
Helsingin yliopiston verkkojulkaisut

I dedicate this thesis to my beloved grandmother
who passed away on the 8^{th} of March 2005
at the age of 91 years.

Acknowledgments

This thesis is based on the research carried out at the Theoretical Physics Division of the Department of Physical Sciences at the University of Helsinki and at Helsinki Institute of Physics during the years 2000–2004. I thank the personnel of the both institutes for a pleasant working atmosphere. I acknowledge the Academy of Finland, Magnus Ehrnrooth Foundation, and Science Foundation of the University of Helsinki for financial support, and CSC – Scientific Computing Ltd. for computational resources.

I acknowledge my supervisors Prof. Kari Enqvist and Dr. Hannu Kurki-Suonio for collaboration. In particular, I want to mention Kari's physical intuition. He arranged most of the funding and encouraged me to attend various conferences. He pushed me on to continue the research when I had got stuck with some problem and even when I felt that the results of my work would not be of any interest to other cosmologists. Perhaps most importantly, Kari has built up a high quality cosmology research group in Helsinki. I admire Hannu's carefulness and ability to find solutions to cosmological problems within a moment whenever I bothered him. Hannu also gave three excellent courses on cosmology. He is the best teacher I know on physics.

I thank the referees of this thesis, Dr. Iiro Vilja and Dr. Arttu Rajantie, for the careful reading of the manuscript.

I would like to thank my former officemates Dr. Martin Snoager Sloth, Dr. Asko Jokinen, Antti Väihkönen, Vesa Muhonen, Dr. Syksy Räsänen, and Janne Högdahl for many enjoyable and enlightening discussions. I have also a pleasure to know an enthusiastic cosmologist and Planck scientist, Dr. Elina Keihänen. I am thankful for her clarifying comments on many questions and, in particular, for numerous Matlab tips.

I thank Vesa for collaboration with papers III and V. I am grateful to Syksy and Dr. Francesc Ferrer, who I have actually never met, for inspiring collaboration with paper IV.

I am eternally thankful to my mother for continuous support and encouragement. I want to mention my friends and (former) fellow students Ossi, Pekko, Vuokko, Tommi, Joonas, Juha, Petja, and Tiina who have had the greatest impact on my life. In particular, I thank Tiina. During the years of struggling with papers of this thesis skiing trips in Finnish Lapland with Martin, Asko, Elina, Tiina, Mika, and Ossi have kept me alive and in adequate physical and mental health.

Helsinki, spring 2005

Väliviita, Jussi: The Nature of Primordial Perturbations in the Light of CMB Observations, University of Helsinki, 2005, 143 p., Helsinki Institute of Physics Internal Report Series, HIP-2005-03, ISSN 1455-0563, ISBN 952-10-1691-4 (printed version), ISBN 952-10-1692-2 (pdf version).

Classification (INSPEC): A9870V, A9880B, A9880D
Keywords: cosmology, cosmic microwave background radiation, early universe

Abstract

The universe is filled with nearly isotropic cosmic microwave background (CMB) radiation, which has a blackbody spectrum of temperature $T \approx 2.73\,\mathrm{K}$. In addition, there are tiny direction dependent deviations δT from the mean temperature, $\delta T/T \lesssim 10^{-4}$. These CMB anisotropies result from small primordial perturbations. The initial conditions, deep in the radiation-dominated universe, can be a mixture of two different modes: adiabatic and isocurvature perturbations. The former means a primordial perturbation in the spatial curvature of the universe, whereas the latter means a spatial perturbation in the relative number densities of different particle species. Adiabatic and isocurvature primordial perturbations lead to a distinct imprint on the observed angular power — the CMB temperature variance $\langle(\delta T)^2\rangle$ as a function of angular scale in the sky. Often, in the literature, a pure adiabatic primordial perturbation mode has been assumed.

We review the linear cosmological perturbation theory in the Newtonian gauge, and show how the primordial perturbations evolve into the observed anisotropies. According to the recent precision CMB data, the primordial perturbations are predominantly adiabatic. We constrain the amplitude of a primordial cold dark matter (CDM) isocurvature perturbation in phenomenological models where the adiabatic and isocurvature perturbations can be correlated or uncorrelated, and have a power-law spectrum with an independent spectral index for each component. Perturbations of this type arise naturally in multi-field inflationary models, in inflaton-curvaton models, and in the pre-Big Bang model with axion and dilaton. Cosmic strings, quintessence, or brane collision could also give rise to isocurvature perturbations.

We find at the 95% confidence level that at most only 18% of the total primordial perturbation power can be in the form of the CDM isocurvature perturbation. In the observed temperature variance, an upper limit to the non-adiabatic contribution is 7.5%.

The determination of the conventional cosmological parameters can be affected by the possible presence of an isocurvature mode. We scan the likelihood function in an 11-dimensional parameter space by a sophisticated Markov Chain Monte Carlo method, and conclude that, of the standard parameters, the determination of the physical CDM density ω_c and the sound horizon angle θ (or the expansion rate of the universe, the Hubble parameter H_0) are affected the most. The physical baryon density ω_b retains nearly the same value as in the standard adiabatic ΛCDM model. These results suggest that the CDM isocurvature can play an important role in inferring the dark matter and dark energy contents of the universe.

List of accompanying papers

This Ph.D. thesis consists of an introduction to the cosmic microwave background physics and the following five research articles:

I K. Enqvist, H. Kurki-Suonio and J. Valiviita,
"Limits on isocurvature fluctuations from Boomerang and Maxima",
Phys. Rev. D **62**, 103003 (2000) [arXiv:astro-ph/0006429].

II K. Enqvist, H. Kurki-Suonio and J. Valiviita,
"Open and closed CDM isocurvature models contrasted with the CMB data",
Phys. Rev. D **65**, 043002 (2002) [arXiv:astro-ph/0108422].

III J. Valiviita and V. Muhonen,
"Correlated adiabatic and isocurvature CMB fluctuations in the wake of WMAP",
Phys. Rev. Lett. **91**, 131302 (2003) [arXiv:astro-ph/0304175].

IV F. Ferrer, S. Rasanen and J. Valiviita,
"Correlated isocurvature perturbations from mixed inflaton-curvaton decay",
JCAP **0410**, 010 (2004) [arXiv:astro-ph/0407300].

V H. Kurki-Suonio, V. Muhonen and J. Valiviita,
"Correlated primordial perturbations in light of CMB and LSS data",
Phys. Rev. D **71**, 063005 (2005) [arXiv:astro-ph/0412439].

Author's contribution

Paper I: On the day when the first Boomerang results came out in May 2000 Prof. Kari Enqvist and Dr. Hannu Kurki-Suonio suggested me to study mixed adiabatic and isocurvature perturbations by using the CMBfast code and the new data. I performed the Fortran programming for calculating grids of mixed models. I analyzed the results with Matlab programs written by me and made all the data analysis as well as produced the published results. I also worked out the figures needed to visualize the results. Hannu Kurki-Suonio and Kari Enqvist supervised and helped me by suggesting what kind of 2d figures could be of the greatest interest to the cosmology community. The introduction was written by Kari Enqvist and the other text mainly by Hannu Kurki-Suonio based on my results and our discussions.

Paper II: After paper **I** it still seemed possible to fit pure isocurvature models to the data by relaxing the flatness requirement as suggested us by Dr. Alessandro Melchiorri. In **I** we had restricted the analysis to the flat models partially because of the computing resources problems of calculating larger grids and partially because of some theoretical problems in non-flat models. When we had finished paper **I**, I engaged myself for solving these problems. Kari Enqvist wrote the beginning of Introduction. I did all the other work including the programming, data analysis, theoretical considerations, and the actual writing of the publication. Hannu Kurki-Suonio supervised me and we discussed the reasonable regions of the parameter space to scan through. He also helped with the conclusions section. When finalizing the paper, improved Boomerang and Maxima results were published, and I decided to reanalyze the models with these new data, which cost me an additional four months.

Paper III: Shortly after the release of the first results of the Wilkinson Microwave Anisotropy Probe (WMAP) I found a questionable simplification from the WMAP group analysis of correlated adiabatic and isocurvature initial conditions. I immediately began to plan a better way to study general correlated models. I studied the theory, programmed the routines to calculate correlated angular powers by CAMB and did the actual writing of the publication. A new Ph.D. student M.Sc. Vesa Muhonen helped me with a parallelized driver program to scan large grids of models by a supercomputer. Together we optimized the algorithms to throw away uninteresting models and to store the results from our huge grid.

Paper IV: The idea to study the decay of the curvaton field in the general case, in which the curvaton cannot be treated as dust, came from Dr. Syksy Räsänen. He asked me whether curvaton model could lead to lower CMB quadrupole than the ordinary pure

adiabatic ΛCDM model. I pointed out that the negative correlation with inflaton decay products could suppress the angular power in the Sachs-Wolfe region, and suggested that in the paper, in addition to the curvaton decay calculation, one should compare the predictions to the measured angular power. Finally, the responsibility was divided as follows: Syksy Räsänen was the combining force and writer. He did most of the theoretical considerations of the curvaton decay. Dr. Francesc Ferrer wrote and parallelized C programs to perform the decay calculation numerically, and checked Syksy's formulas. I used my expertise to fit the resulting spectrum to the CMB data. This included a month of editing the CAMB code to allow for the type of correlation we were studying, then about 4 months of studying the Monte Carlo method (and editing the CosmoMC program), since the grid method which I was familiar with appeared to be far too slow for scanning our 11-dimensional parameter space. Finally I controlled the CosmoMC runs, analyzed the results and wrote a draft of the 15 pages' "data fit" part of the paper in some 10 weeks.

Paper V: I did the work to fit our model to the data by implementing the Markov Chain Monte Carlo method to our problem. I wrote and debugged the Fortran code, suggested the ways to proceed, and solved a dozen of technical problems. Vesa Muhonen controlled the creation of the Markov Chains by the CosmoMC program, and we had many enlightening discussions with Hannu Kurki-Suonio. We all investigated jointly the problems (related, for example, to the marginalization integration measure) that we found when analyzing the preliminary Markov Chains. As, in the end, I was busy with finalizing my Ph.D. thesis, the actual writing work of the first draft was due to Hannu Kurki-Suonio, and the figures due to Vesa Muhonen. I wrote about one third of the final text.

In papers **I**, **II**, **IV**, and **V** authors are listed in alphabetical order according to the particle physics convention. I am the "first author" of papers **I**, **II**, **III** and **V**. The work and results in paper **IV** are equally due to all three authors.

Contents

Chapter 1

Introduction

The universe is filled with nearly isotropic cosmic microwave background (CMB) radiation, which has a blackbody spectrum of temperature $T \approx 2.7$ K [1]. In addition, there are tiny direction dependent deviations δT from the mean temperature T called CMB perturbations, $\delta T/T \lesssim 10^{-4}$. The existence of a few Kelvin thermal [2] radiation as a remnant of the Big Bang was predicted in 1948 [3–7] and first observed in 1965 [8, 9]. The thermal spectrum and near isotropy were confirmed in the following years [10–12].

The theory of cosmological perturbations began to develop rapidly [13–16]. However, it was not until 1992 that the Cosmic Microwave Background Explorer (COBE) measured the perturbations at large angular scales ($\theta \sim 7^\circ$) [17, 18], which launched the golden age of observational CMB cosmology. The ultimate goal is to measure the temperature perturbation as a function of the angular scale in the sky, *the angular power spectrum*, with a high accuracy down to angular scales $\theta \sim 5$ arcmin. On smaller scales, the angular power falls off by the Silk (diffusion) damping [19].

On scales probed by the COBE satellite the angular power spectrum is described by the Sachs-Wolfe (SW) plateau [13, 20] and the integrated Sachs-Wolfe effect (ISW). The power starts to rise towards the first acoustic peak on the scale $\theta \sim 1^\circ$. After that there is a series of acoustic peaks. The precise shape of the angular power spectrum depends on the whole history of the universe: The SW plateau contains information mostly about the gravitational and expansion effects. The positions and spacings of the acoustic peaks yield information about the geometry of the universe and about the initial conditions of the primordial perturbations. The relative heights of the successive peaks encode the baryon content of the universe as well as the cold dark matter, which generates the required gravitational potential wells. This comes about because the acoustic peak structure arises as a result of a competition between gravitational collapse and photon pressure in the photon-baryon fluid.

Detailed comparison of theoretical predictions and the measured angular power spectrum became possible in the year 2000 when the first acoustic peak was definitely observed by the Boomerang [21, 22] and Maxima [23, 24] balloon borne experiments. These measurements gave rise to an exponential interest in the CMB cosmology. At present, the most accurate temperature perturbation data is provided by the Wilkinson Microwave

Anisotropy Probe (WMAP) satellite experiment [25, 26]. The WMAP and improved Boomerang [27, 28] and Maxima [29, 30] data are supplemented by ground based interferometers like DASI [31–33], CBI [34–37], VSA [38–42], and by a bolometer experiment ACBAR [43–45] as well as by balloon borne test flights of the Planck satellite's high frequency instrument, Archeops [46–48].

Polarization properties of the CMB perturbations include valuable information in particular about the ionization history of the universe. Polarization measurements are important for breaking certain degeneracies, too [49]. (Many theoretical models produce a similar temperature angular power but a distinct polarization power.) The polarization signal has been observed by ground based interferometer experiments like DASI [50–52] and CBI [53], and by the WMAP [54] satellite. In the near future (launch 2007), the Planck satellite [55] will provide the most accurate measurements on both the temperature and polarization of CMB.

As the CMB perturbations provide a snapshot of the universe as it was at the time of last scattering, the angular power is an ideal tool for studying the very early universe. (For nice reviews see e.g. [56, 57].) The CMB perturbations and perturbations in the matter content (galaxies etc) evolve from small primordial perturbations which are amplified by gravitation. For example, quantum fluctuations that freeze in and turn into classical at horizon exit during inflation can produce the required primordial perturbation power.

The evolution of the primordial perturbations into the observed angular power (and matter power) is described by a group of second order differential equations. From a mathematical point of view there are two types of equally possible independent solutions. The primordial perturbations (i.e. the initial conditions) can be of adiabatic or isocurvature type, see Fig. 1 in [58] for a simplified explanation. The former means that the seed for the observed perturbations is a small perturbation of the comoving curvature $\mathcal{R}$ (or the Newtonian gravitational potential Ψ) in the very early, radiation-dominated universe. The latter means that there is no perturbation in the curvature initially, but instead the seed for perturbations is provided by a perturbation of the specific entropy $\mathcal{S}$. In this case the relative particle number densities of different particle species are not spatially constant. In inflationary models, this is the generic situation if more fields than just one are excited, like in the double inflation [59–61] or in the minimally supersymmetric standard model (MSSM) with flat directions [62].

For the purpose of CMB analysis, it is enough to consider four particle species. They are photons (γ), neutrinos (ν), baryons (b), and cold dark matter (CDM, c). As a result there can be several entropy perturbation modes: $\mathcal{S}_{\nu\gamma}$, $\mathcal{S}_{b\gamma}$, $\mathcal{S}_{c\gamma}$ for densities, and in addition to these, the so called neutrino velocity mode. It can be shown that the most general initial conditions for growing mode perturbations include the adiabatic mode, the listed four isocurvature modes, and correlations between those. So the initial conditions can be described by a 5×5 matrix [63, 64]. However, the baryon isocurvature $\mathcal{S}_{b\gamma}$ and CDM isocurvature $\mathcal{S}_{c\gamma}$ leave a similar imprint on the CMB [63, 65]. Thus, in the general case, it is enough to study the initial conditions specified by a 4×4 matrix.

Even within standard cosmology the determination of cosmological parameters from

the measured angular and matter power depends crucially on the chosen initial conditions. Usually, the adiabatic initial condition is adopted in the CMB analysis. The motivation for this is simplicity in two respects. Since the fit of the pure adiabatic models to the data is very good, the other initial perturbation modes only yield unnecessary complications. The second argument is that inflation (which is, in most studies, assumed to be responsible for the primordial perturbations) with one scalar field cannot give rise to isocurvature perturbations [66].

To summarize, from a pragmatic point of view the pure adiabatic model is appealing, since the theory becomes very simple. In papers **I**–**V** the opposite attitude is taken. Since the two types of the initial modes are mathematically equally acceptable and theoretically motivated, they should be treated on an equal basis in the CMB analysis, and the isocurvature mode should not be neglected. Furthermore, if there is one scalar field responsible for inflation, it would be natural to expect that there exists a whole bunch of scalar fields leading to a mixture of isocurvature and adiabatic perturbations. The mixture of perturbations arises naturally also in alternative theories to the inflation, such as the pre-Big Bang [67–71], the pre-Big Bang curvaton model [72, 73], or the inflaton-curvaton model [65, 74–82].

The objective of papers **I**–**V** is to study how much CDM isocurvature is allowed by the CMB data (together with some astrophysical observations, which are necessary for breaking the degeneracies), and how allowing for the CDM isocurvature mode affects the values of cosmological parameters extracted from the measured angular power. The two neutrino isocurvature modes are neglected since, in the type of models studied in papers **I**–**V**, they would yield a too high dimensional parameter space — hard to scan within accessible supercomputer resources. Other motivation for dropping the neutrino modes is that neutrinos and photons are tightly coupled in the very early universe. Thus, at time of neutrino decoupling, their velocities are equal. To get any neutrino velocity isocurvature perturbations, there should exist some generating mechanism after neutrino decoupling. In addition, assuming that there is no net lepton number, the neutrinos and photons end up having identical density perturbations by virtue of being locally in thermal equilibrium [63, 76, 83]. So, in this case, there are no neutrino density isocurvature perturbations either.

We contrast the data with a more general form of the initial power spectrum than done so far in the literature.[1] Thus it would not be motivated to include too many less studied additions at the same time. By adding only the CDM (and effectively the baryon) isocurvature mode we can discuss more quantitatively its role in the data fit. Studying the neutrino modes at same time would blur the analysis also because the acoustic peak structure of the neutrino modes is close to that of the adiabatic mode [63, 64]. There are other studies [85–89] where the whole 4×4 (or 5×5) matrix of the initial conditions is investigated but the shape of the initial power spectra is more restricted than in our

[1] However, when writing this introduction, one paper with a power spectrum nearly similar to ours appeared [84].

analysis. In [85–89] an identical shape of the primordial power spectrum for all modes is assumed whereas we study models where adiabatic and isocurvature modes can have a different spectral shape, more precisely different spectral indices.

In papers **I–V** the underlying theory is regarded to be standard cosmology with inflation (including several scalar fields) responsible for the primordial perturbations. Nevertheless, the results can be applied to many other cosmological scenarios too, since the treatment and the shape of the primordial power spectra have been kept as general as possible.

We start this chapter by introducing some concepts of standard cosmology and the notation used later in this thesis. Then we comment on perturbation generation from quantum fluctuations during inflation and also mention some other mechanisms leading to (correlated) adiabatic and isocurvature primordial perturbations. Finally, we introduce the metric for our universe with small perturbations, and discuss the ambiguity in the division to unperturbed background and perturbations, called gauge freedom.

As the study of CMB perturbations and evolution of the universe demands a deep understanding of a wide range of different fields of physics, such as special and general relativity, particle physics, quantum mechanics, statistical physics, and standard cosmology itself, it is out of scope of this thesis to give a self-contained review. Many formulas appearing in this thesis are derived step by step in my Master's thesis [90]. It is a "complete" review of the relevant theory scattered into about 50 publications between the years 1960 and 2000. There the theoretical angular power is derived from the first principles following mostly the Ph.D. thesis by Hu [91]. Nowadays, good textbooks are also available [92–94]. The most recent of these [94] deals with CMB in the greatest detail. Although less focused on CMB, the classic Kolb and Turner [95] is a valuable source of information.

1.1 Standard cosmology and some notation

The standard model of cosmology is based on two fundamental observations. Firstly, the universe is very homogeneous and isotropic on large scales. This allows us to use the *Friedmann-Robertson-Walker* (FRW) metric. Secondly, the farther away the observed object (galaxy, supernova) is, the faster it seems to recede from us.

From the theory of general relativity (from the Einstein equation) with FRW metric one can derive the *Friedmann equation*, which describes the dynamics of the universe. With the help of it, the second observation is interpreted as an expansion of space, first observed by Hubble in 1929 [96]. The size of the universe is described by a *scale factor* $a(t)$, which is a growing function of time at present.

Solving the "history of the universe" from the Friedmann equation we find that the scale factor has been smaller and the universe has been much denser and hotter at earlier times. Going far enough backward in time we eventually reach the conditions where the energy density was extremely high, the scale factor was small, and the expansion was

very fast. It is believed that for a proper description in these conditions (also) the gravity should be quantized. The leading framework for quantizing gravity together with all the other interactions of Nature is string theory. As the understanding of physics at near-Planckian conditions is still incomplete, we just call the extremely hot and dense, rapidly expanding, initial phase of the universe, the *Big Bang*.

The evolution of the universe after the Big Bang can be summarized as follows. The universe cools due to the adiabatic expansion. The energies of particles decrease, and all kinds of phase transitions may happen (e.g. GUT, electroweak, QCD transition). In the beginning, all particle species are relativistic (i.e. they behave like radiation). The massive particle species become non-relativistic, when the temperature gets smaller than their mass. In addition, the rate of pair production of particles and antiparticles of a particular species decreases and therefore the number density drops steeply as the temperature falls below the rest mass of that species. For example, nucleons and antinucleons annihilate shortly after the QCD transition ($T \sim 150\,\mathrm{MeV}$) leaving a small excess of nucleons in the universe. Below the temperature $T \sim 100\,\mathrm{MeV}$ pions and muons annihilate. Later, at the temperature $T < 500\,\mathrm{keV}$, the electron-positron annihilation leaves a small excess of electrons. The nucleons, the only baryons left, are strictly non-relativistic. The only relativistic species are the photons and massless (or low mass) neutrinos.

The energy density of the relativistic species (radiation) is proportional to a^{-4} while the energy density of the non-relativistic particles (matter) behaves as a^{-3}. Therefore the relativistic species dominate the energy density of the universe at the early times when the scale factor a is very small. As a grows with time, the relative contribution of the matter to the total energy density increases. Hence the universe is first radiation dominated but becomes matter dominated. The instant when the radiation and matter energy densities are equal is called the time of matter to radiation equality or briefly the *time of equality*. We will denote the scale factor at that time by a_{eq}. The present value of the scale factor is denoted by a_0. For the scale factor at an arbitrary instant of time we often write just a dropping the argument t.

Thermal ionization prevents the nucleons and electrons from forming atoms until the temperature falls well below the binding energy of the hydrogen atom. At this stage ($T \sim 0.3\,\mathrm{eV}$) the photons have so small energy that they cannot ionize the hydrogen any more. The neutral atoms can finally form. This process is called *recombination*.

Before recombination, the Compton scattering of the photons from free electrons made the universe opaque. When recombination proceeds, the number density of free electrons (or ionization fraction x_e) gets smaller and the mean free path of the photons increase. Finally, the photons *decouple* from the matter; they do not scatter any more. This means that since the time of *last scattering* the photons have streamed freely in the universe, i.e., the universe has been transparent. Only a small fraction of photons have scattered on their way to us because of *reionization* (ionization of the intergalactic gas). (As Dodelson points out in [94] the few free electrons are still tightly coupled to photons after the decoupling, since the photon number density is many orders of magnitude larger than the electron number density.)

Due to the finite speed of light, when observing distant objects we see backward in time. In particular, when observing the microwave radiation coming from different directions in the sky, we "see" a spherical shell called the *last scattering surface*, which is practically an image of the universe as it was about 379 000 years [25] after the Big Bang.

Since the last scattering the scale factor has grown by a factor of about 1100 (1089 according to WMAP [25]). The temperature is proportional to the inverse of the scale factor, and thus the universe has been 10^3 times hotter at the time of the last scattering than today. The observed cosmic microwave background (CMB) radiation is nearly isotropic and obeys the blackbody distribution with the characteristic temperature of 2.725 K [1].

Although we will mainly explain the notations where they first appear, let us introduce some of them here. The speed of light is throughout this thesis $c = 1$. In addition, we set the Boltzmann constant $k_B = 1$, and the reduced Planck constant $h/(2\pi) = 1$. We use the Einstein summation convention: summation over repeated indices is assumed and the indices are raised or lowered by the metric tensor, e.g. $x_\mu = g_{\mu\nu}x^\nu$. Greek indices take values $0, 1, 2, 3$ and Latin indices run usually over spatial dimensions only, $1, 2, 3$.

The relative speed of expansion, the *Hubble parameter*, is defined as

$$H \stackrel{\text{def}}{=} \frac{\frac{da}{dt}}{a(t)} = \frac{\frac{da}{d\eta}\frac{d\eta}{dt}}{a} = \frac{a_0}{a}\frac{\dot{a}}{a} \stackrel{\text{def}}{=} \frac{a_0}{a}\mathcal{H}, \tag{1.1}$$

where an over-dot refers to the derivative with respect to the conformal time η,

$$\dot{} \stackrel{\text{def}}{=} \frac{\partial}{\partial\eta}, \tag{1.2}$$

and we defined the conformal Hubble parameter $\mathcal{H} = \dot{a}/a$. Throughout this thesis we will employ mostly the conformal time defined by the equation

$$\frac{d\eta}{dt} = \frac{a_0}{a}. \tag{1.3}$$

The present value of the Hubble parameter is $H_0 = h\,100\,\frac{\text{km/s}}{\text{Mpc}}$, where $h \approx 0.4 \ldots 1.0$ according to a conservative estimate. Assuming adiabatic primordial perturbations the WMAP team derived a value $h = 0.71^{+0.04}_{-0.03}$ [25]. The Hubble Space Telescope Key Project gives $h = 0.72 \pm 0.08$ [97].

The dynamics and geometry of the universe depend on its energy contents. The critical density of the universe is $\rho_{\text{crit}}(t) = \frac{3H^2}{8\pi G}$, where G is Newton's gravitational constant. It is common to define the *reduced Planck mass* by $M_{\text{Pl}} = 1/\sqrt{8\pi G}$ (and Planck mass by $m_{\text{Pl}} = 1/\sqrt{G} = \sqrt{8\pi}M_{\text{Pl}}$). Now the critical density can be written as $\rho_{\text{crit}} = 3M_{\text{Pl}}^2H^2$. The ratio of the total energy density ρ to the critical density is called the (total energy) density parameter $\Omega_{\text{tot}}(t) = \rho(t)/\rho_{\text{crit}}(t)$. As indicated, this is a function of time unless $\rho(t) = \rho_{\text{crit}}(t)$, i.e., $\Omega_{\text{tot}}(t) = 1$. For brevity, we will write just Ω_{tot} when referring to the present value, and explicitly $\Omega_{\text{tot}}(t)$ when referring to the value at any other time t. Similarly we define other density parameters such as $\Omega_m(t) = \rho_m(t)/\rho_{\text{crit}}(t)$ for matter energy density, $\Omega_r(t) = \rho_r(t)/\rho_{\text{crit}}(t)$ for radiation en-

ergy density, and $\Omega_\Lambda(t) = \rho_v/\rho_{\rm crit}(t)$ for vacuum energy density. Now the total energy density parameter is given by $\Omega_{\rm tot}(t) = \Omega_m(t)+\Omega_r(t)+\Omega_\Lambda(t)$. The matter energy density consists of baryons and dark matter, $\Omega_m(t) = \Omega_b(t) + \Omega_{dm}(t)$. Furthermore, in addition to CDM, part of the dark matter can be in form of massive neutrinos sometimes called hot dark matter (HDM): $\Omega_{dm}(t) = \Omega_c(t) + \Omega_{\nu m}(t)$. Here $\Omega_{\nu m} = f_{\nu m}\Omega_{dm}$ is the contribution of the massive neutrino species. The massive neutrino fraction[2] $f_{\nu m}$ defines how much of the dark matter (dm) actually is in the form of massive neutrinos. The radiation part consist of photons and massless neutrinos. Hence $\Omega_r(t) = \Omega_\gamma(t)+\Omega_\nu(t)$, where $\Omega_\nu = X_\nu\Omega_r$ and $\Omega_\gamma = (1-X_\nu)\Omega_r$. (Massless neutrino fraction X_ν tells how much of the radiation is in the form of neutrinos.) From here on also all these density parameters refer to the present values unless we write explicitly the argument t. Occasionally, we also use *physical density parameters* defined by $\omega_i \stackrel{\rm def}{=} h^2\Omega_i$.

Let λ_p describe a physical length scale of some phenomenon. It could be, for example, the wave length of electromagnetic radiation. The expansion of space stretches this physical length so that $\lambda_p \propto a$. Often, it is convenient to define a constant *comoving* quantity $\lambda_c = (a_0/a)\lambda_p$. This is just the physical length scaled to today's value: as can be seen $\lambda_{p0} = \lambda_c$. The cosmological perturbation theory is usually done in the Fourier space. There the physical wave number corresponding to λ_p is $k_p \propto a^{-1}$. Thus we define the comoving wave number by $k_c = (a/a_0)k_p$. We will mainly work with comoving quantities. From here on we drop the subscript c. The quantities should be regarded as the comoving ones unless explicitly stated by a subscript or superscript p that they are the physical ones.

1.1.1 FRW metric and Friedmann equation

Since the vacuum energy density ρ_v is constant and $\rho_r \propto a^{-4}$ and $\rho_m \propto a^{-3}$, we can write

$$\Omega_{\rm tot}(t) = \left[\Omega_r\left(\frac{a_0}{a}\right)^4 + \Omega_m\left(\frac{a_0}{a}\right)^3 + \Omega_\Lambda\right]\left(\frac{H_0}{H}\right)^2 . \tag{1.4}$$

If the energy density of the universe is exactly the critical one, then $\Omega_{\rm tot}(t) = 1$. From the Friedmann equation it can be shown that, if this is the case once, it will be preserved unchanged forever. Similarly the condition $\Omega_{\rm tot}(t) < 1$ cannot change to $\Omega_{\rm tot}(t') > 1$. Because of these three distinct possibilities, the present value of the energy density parameter $\Omega_{\rm tot}$ can be used to characterize the cosmological models:

$$\rho(t) > \rho_{\rm crit}(t) \Leftrightarrow \Omega_{\rm tot} > 1 \quad \text{(closed model, elliptic spatial geometry)}$$
$$\rho(t) = \rho_{\rm crit}(t) \Leftrightarrow \Omega_{\rm tot} = 1 \quad \text{(flat model, euclidean spatial geometry)}$$
$$\rho(t) < \rho_{\rm crit}(t) \Leftrightarrow \Omega_{\rm tot} < 1 \quad \text{(open model, hyperbolic spatial geometry).}$$

So, the geometry of a homogeneous and isotropic 3-space with a constant curvature

[2] In paper **IV** we use a symbol f_ν without specifying that we mean massive neutrino fraction, since there we assume all three species to be massive. So we do not have massless neutrinos today.

K can be elliptic or spherical (a 3-sphere), flat (euclidean), or hyperbolic (a pseudo sphere):

- In spherical coordinates the metric of a unit 3-sphere is
  $ds_3^2 = d\tilde{\chi}^2 + \sin^2\tilde{\chi}(d\theta^2 + \sin^2\theta d\varphi^2), \quad \tilde{\chi} \in [0,\pi],\ \theta \in [0,\pi],\ \varphi \in [0,2\pi[\,,$
- In spherical coordinates the metric of a 3-dimensional flat space is
  $ds_3^2 = d\tilde{\chi}^2 + \tilde{\chi}^2(d\theta^2 + \sin^2\theta d\varphi^2), \quad \tilde{\chi} \in [0,\infty[\,,$
- In hyperbolic coordinates the metric of a unit 3-hyperboloid is
  $ds_3^2 = d\tilde{\chi}^2 + \sinh^2\tilde{\chi}(d\theta^2 + \sin^2\theta d\varphi^2), \quad \tilde{\chi} \in [0,\infty[\,,$

where $\tilde{\chi}$ is a dimensionless radial coordinate. From these one can derive the metric of space-time, whose surfaces of constant time are homogeneous and isotropic [98, 99]. It is of the form $ds^2 = -dt^2 + (a/a_0)^2|K|^{-1}ds_3^2$, where, as explained, the scale factor a describes the stretching of the space part of the metric, i.e., the expansion of the universe. As a shorthand notation we will write this FRW metric as

$$ds^2 = g_{\mu\nu}dx^\mu dx^\nu = (a/a_0)^2[-d\eta^2 + \gamma_{ij}dx^i dx^j]\,, \tag{1.5}$$

where the three-metric reads

$$\gamma_{ij}\,dx^i\,dx^j = |K|^{-1}\Big[|K|\,d\chi^2 + \sin_K^2(|K|^{1/2}\chi)\,(\,d\theta^2 + \sin^2\theta\;d\varphi^2)\Big], \tag{1.6}$$

with $\sin_K(|K|^{1/2}\chi)$ defined as

$$\sin_K(|K|^{1/2}\chi) = \begin{cases} \sin(|K|^{1/2}\chi), & \text{if } K > 0 \text{ (closed universe)} \\ \sinh(|K|^{1/2}\chi), & \text{if } K < 0 \text{ (open universe)} \end{cases}. \tag{1.7}$$

With this notation the radial coordinate χ has a dimension of length. It is related to the dimensionless radial coordinate by $\tilde{\chi} = |K|^{1/2}\chi$. Letting $K \to 0$ from above or below in (1.6) the flat space metric follows;

$$\gamma_{ij}\,dx^i\,dx^j = \,d\chi^2 + \chi^2(\,d\theta^2 + \sin^2\theta\;d\varphi^2). \tag{1.8}$$

The Friedmann equation connects the relative expansion rate H to the geometry and energy contents of the universe as follows

$$H^2 \equiv \left(\frac{a_0}{a}\frac{\dot{a}}{a}\right)^2 = -\left(\frac{a_0}{a}\right)^2 K + \frac{8\pi G}{3}\rho\,, \tag{1.9}$$

where we consider the vacuum energy density ρ_v as a part of the total energy density. Nowadays the non-vanishing vacuum energy density seems so obvious (see e.g. [25, 100]) that it is natural to include it in the total energy density. Historically, the vacuum energy density has been written as a separate term in the Friedmann equation, and ρ has been reserved for an ordinary energy density only. Then there would have been two energy density terms on the right hand side: $8\pi G\rho/3 + 8\pi G\rho_v/3 = 8\pi G\rho/3 + \Lambda/3$, where $\Lambda = 8\pi G\rho_v$ is Einstein's famous cosmological constant.

The Friedmann equation in its perhaps most compact form can now be written as

$$\Omega_{\rm tot}(t) = 1 + \frac{1}{H^2}\left(\frac{a_0}{a}\right)^2 K\,. \tag{1.10}$$

Solving the constant K from this equation we get $K = -H_0^2(1 - \Omega_{\rm tot})$. (Since K is a constant we can evaluate the right hand side at present as well as at any other time.) We define the "curvature density parameter" $\Omega_k \stackrel{\rm def}{=} 1 - \Omega_{\rm tot} = 1 - \Omega_m - \Omega_\Lambda$, so that we have $\Omega_k < 0$ in the closed model and $\Omega_k > 0$ in the open model [94]. Substituting $K = -H_0^2\Omega_k$ and $\Omega_{\rm tot}(t)$ from equation (1.4) into (1.10) we get

$$H^2 = H_0^2 \left[\Omega_r \left(\frac{a_0}{a}\right)^4 + \Omega_m \left(\frac{a_0}{a}\right)^3 + \Omega_k \left(\frac{a_0}{a}\right)^2 + \Omega_\Lambda \right] . \tag{1.11}$$

Given the present values Ω_r, Ω_m, and Ω_Λ, the time evolution of the scale factor is determined by this differential equation[3]. When $a \gg a_{\rm eq}$ the radiation term can be neglected, since $\Omega_r = (1 - X_\nu)^{-1}\Omega_\gamma \sim \Omega_\gamma = 2.47 \times 10^{-5} h^{-2}$ [93], while $\Omega_m \simeq \Omega_\Lambda \simeq 1$. Here we employed the radiation law $\rho_\gamma = g\pi^2 T^4/30$, where the number of degrees of freedom is $g = 2$ for photons. In addition, we used the fact $0 \le X_\nu \le 0.405$ [94] which ensures that $(1 - X_\nu)^{-1} \sim 1$.

1.1.2 Dynamics of the universe, supernovae observations

According to equation (1.11), the future of the universe depends on the total energy density and on how that is divided between matter and vacuum energy. The behaviour of the scale factor can be studied by the method of effective potential [99]. A flat universe with matter only expands forever with decreasing speed ($d^2a/dt^2 < 0$). If some of the total energy density is in the form of positive vacuum energy, then the expansion is first decelerating as in the pure matter case but when the vacuum energy (negative pressure, $p_v = -\rho_v$) starts to contribute significantly, the expansion speed begins to increase. On the contrary, negative vacuum energy causes positive pressure. Hence the expansion ends and turns into accelerating contraction in the flat models with $\Omega_\Lambda < 0$. Actually, this is also true for the closed and open models with $\Omega_\Lambda < 0$. So there are models where the history of the universe ends by a Big Crunch. Also the closed model with matter only leads to decelerating expansion that eventually turns into accelerating contraction. A small positive vacuum energy contribution does not change this behaviour, but if the vacuum energy contribution exceeds a certain matter density dependent critical value $\Omega_{\Lambda_c} = 4\Omega_m \left[\cos\left(\frac{1}{3}\cos^{-1}(\Omega_m^{-1} - 1) + \frac{4\pi}{3}\right)\right]^3$ [93, 105], then the negative pressure wins

[3]Note that for a fluid x whose equation of state is $p_x(t) = w_x\rho_x(t)$ the continuity equation (2.6) leads to $\rho_x \propto a^{-3(1+w_x)}$. Putting $w_r = 1/3$ for radiation, $w_m = 0$ for matter, and $w_v = -1$ for vacuum energy we regain the results used to write equation (1.4). Recently, models with modified equation of state for the "vacuum" have become popular. The common term for all mysterious energy that is not in the form of the radiation or matter (and has negative w) is *dark energy* (*de*). Assuming $w_{de} \neq -1$ we would need to replace Ω_Λ in (1.4) and (1.11) by $\Omega_{de}(a_0/a)^{3(1+w_{de})}$. A refinement to this generalization would, in turn, be time varying equation of state $w_{de}(t)$ for the dark energy. See [100, 101] for attempts to directly constrain w_{de} as a function of redshift from supernovae data. Complementary constraints derived from the metallicities of the stellar populations in cluster galaxies are in good agreement with supernovae results [102]. Actually, the current data allows even $w_{de} < -1$ [103, 104]. Whatever the dark energy is, according to combined CMB and supernovae observations its contribution to the present total energy density can be as large as about 70%.

	$\Omega_\Lambda = 0$	$\Omega_\Lambda > 0$		$\Omega_\Lambda < 0$
Flat $\Omega_{\rm tot} = 1$ $\Omega_k = 0$ $K = 0$	Decelerating expansion forever	Expansion forever; first decelerating, then accelerating		First decelerating expansion, then accelerating contraction
Closed $\Omega_{\rm tot} > 1$ $\Omega_k < 0$ $K > 0$	First decelerating expansion, then accelerating contraction	$\Omega_\Lambda < \Omega_{\Lambda_c}(\Omega_m)$ First decelerating expansion, then accelerating contraction	$\Omega_\Lambda > \Omega_{\Lambda_c}(\Omega_m)$ Expansion forever; first decelerating, then accelerating	First decelerating expansion, then accelerating contraction
Open $\Omega_{\rm tot} < 1$ $\Omega_k > 0$ $K < 0$	Decelerating expansion forever	Expansion forever; first decelerating, then accelerating		First decelerating expansion, then accelerating contraction

Table 1.1: Dynamics of the universe. The decelerating expansion means that $da/dt > 0$ and $d^2a/dt^2 < 0$. In the phase of accelerating expansion $d^2a/dt^2 > 0$. Note that even then $dH/dt < 0$, unless $(d^2a/dt^2)/a > H^2$.

and the decelerating expansion turns eventually into accelerating expansion instead of contraction. (If Ω_Λ is large enough a can never have evolved to a_0, so there has not been the Big Bang. This critical value of Ω_Λ is obtained from the above relation by dropping $\frac{4\pi}{3}$ and replacing cos with cosh for $\Omega_m < 0.5$.) Finally, in the open case, the universe expands forever unless $\Omega_\Lambda < 0$.

The behaviour of the scale factor is summarized in table 1.1. In the first column we also summarize our notation. See also Fig. 3.2 on page 62, where we, among others, indicate whether we are now in an accelerating or in a decelerating period. Most easily this is determined by defining the deceleration parameter $q \stackrel{\rm def}{=} -\frac{d^2a}{dt^2}\frac{a}{(da/dt)^2} = -(d^2a/dt^2)/(aH^2)$ [93]. Now, derivating the Friedmann equation (1.9) and using (1.11) along with the continuity equation (2.6) we find that $q(t) = \Omega_m(t)/2 + \Omega_r(t) - \Omega_\Lambda(t)$. The expansion is accelerating whenever $q < 0$, i.e., $\Omega_\Lambda(t) > \Omega_m(t)/2 + \Omega_r(t)$. The present favourite parameter values ($\Omega_m \simeq 0.3, \Omega_\Lambda \simeq 0.7$) tell that we live in the universe which should be expanding forever. Moreover, we should be already on the period of accelerating expansion, $q_0 \simeq -0.55$.

The supernovae observations [100, 106–111] confirm that the universe is undergoing a phase of accelerating expansion.[4] The radio galaxy data [119–121] give further support to this crucial observation that in the time of first publication [106] in 1998 came as a surprise to the majority of the cosmology community. (Cosmologists had for a while believed that no cosmological constant was needed. The acceleration together with $\Omega_m < 0.5$ meant that a significant dark energy contribution was indeed needed.) From table 1.1 (see column $\Omega_\Lambda > 0$) we find that, in the past, the expansion should have been

[4]High-redshift supernovae appear to be fainter than expected in the decelerating case. A good fit to the magnitude-redshift data is achieved in models where dark energy accelerates the expansion. Note however, that the dimming of supernovae could be explained by more unconventional way, too. For example, some of the photons could oscillate into light axions, and then a good fit would result even without acceleration [112–116]. There are also other models where the acceleration is not needed [117, 118].

decelerating. Actually, very recently also this has been observed from the supernovae data [100].

Moreover, when the accuracy (and number of data points) of the supernovae and radio galaxy measurements increase, it becomes possible to measure the deceleration parameter directly by studying objects at different coordinate distances. In principle, the data determines the coordinate distance of supernovae, χ in our terminology, as a function of the redshift z. However, there are many possible error sources in the data, among others the identification of standard candles. Fortunately, calculating q from $\chi(z)$ with help of the Friedmann equation includes only differentials of the coordinate distance: $q(z) = -1 - (1+z)(d\chi/dz)^{-1}(d^2\chi/dz^2)$ in the flat case [121]. This dramatically reduces the error sources and allows one to use the data from various experiments at the same time without introducing systematics [101, 122]. The approach is model independent – "everything" that is needed is the relation between the scale factor and redshift, $a_0/a = 1+z$, and the choice of the geometry. In particular, the above formula for determining $q(z)$ from the data does not depend on the form of the dark energy. In the flat case, a preliminary analysis yields $q_0 = -0.35 \pm 0.10$ [101] to be compared to the "theoretical" value (-0.55) given above. Note that the theoretical value is very sensitive to the form of dark energy. For $p_{de} = w_{de}\rho_{de}$ one would get $q(t) = \Omega_m(t)/2 + \Omega_r(t) + [1+3w_{de}(t)]\Omega_{de}(t)/2$ [105, 122]. For example, in [123] where a time varying equation of state is considered the best-fit model has $q_0 = -0.9$. Hence, an accurate direct measurement of $q(z)$ will provide an essential test for different theories of dark energy.

Like for q also the equation of state for the dark energy w_{de} can, in principle, be measured directly: $w_{de}(z) = -[1+(2/3)(1+z)(d\chi/dz)^{-1}(d^2\chi/dz^2)]/[1-(d^2\chi/dz^2)\Omega_m(1+z)^3]$. However, here an independent knowledge of Ω_m is necessary. Assuming $\Omega_m = 0.3$ Daly and Djorgovski [122] find $w_{de}(0) = -0.9 \pm 0.1$, which is consistent with $w_v = -1$. However, at present, it is premature to draw any strong conclusions from the values of q and w obtained directly from supernovae and radio galaxy searches. From now on, we assume that dark energy can be described by the cosmological constant ($w_{de} = w_v = -1$).

Let us finally emphasize that the accelerating expansion does not mean $dH/dt > 0$. From the identity $dH/dt = (d^2a/dt^2)/a - H^2$ we see that the expansion rate H increases with time only when $(d^2a/dt^2)/a > H^2$. This is not the case today, since $(d^2a/dt^2)/a|_0 = -H_0^2 q_0 \simeq 0.55 H_0^2 < H_0^2$.

1.1.3 Horizons

In all three possibilities for the spatial geometry there can exist a *particle horizon* because of the finite speed of light. The horizon length is a distance to the Big Bang along the geodesic of light. It is the maximum distance one can "see". Since the speed of light is the maximum velocity of propagation of any information, the regions farther from each other than the size of the particle horizon can never have been in causal connection.

The exact size of the particle horizon is the comoving distance to the Big Bang, $s_{\rm PH} = \int_{\chi_i}^{\chi_0} d\chi$, where $\chi_i = 0$ is the "radial coordinate of the Big Bang" and χ_0 our

position. Hence we have $s_{\rm PH} = (\chi_0 - \chi_i)$. To find χ_0 we consider photons moving radially along the line of sight. For them we have $ds^2 = 0$ leading to $d\chi = d\eta$. So we have $s_{\rm PH} = \int_{\eta_i}^{\eta_0} d\eta$. The integration over η can be converted to the integration over the scale factor a with help of the Friedmann equation (1.11). Moreover, the scale factor can be written in terms of the redshift: $a/a_0 = 1/(1+z)$ and $da/a_0 = -dz/(1+z)^2$. Finally, substituting $1/(1+z) = x$ we arrive at

$$\chi_0 - \chi_i = \chi(z_0) - \chi(z_i) = H_0^{-1}\mathcal{I}(z_i, z_0)\,, \tag{1.12}$$

where

$$\mathcal{I}(z_i, z_0) = \int_{1/(1+z_i)}^{1/(1+z_0)} \frac{dx}{\sqrt{\Omega_\Lambda x^4 + \Omega_k x^2 + \Omega_m x + \Omega_r}}\,. \tag{1.13}$$

The horizon distance is now $s_{\rm PH_0} = \lim_{z_i\to\infty} H_0^{-1}\mathcal{I}(z_i, 0)$. In the general case in which $\Omega_{\rm tot}$ differs from unity or Ω_m is far from unity the integral $\mathcal{I}$ in (1.13) has to be calculated numerically (see also [124] for a semi-analytical approach). For $(\Omega_m \simeq 0.3, \Omega_\Lambda \simeq 0.7)$ we get $s_{\rm PH_0} \simeq 3.3H_0^{-1} = h^{-1}9900\,{\rm Mpc}$. In the simple pure matter case the integral gives just $\mathcal{I} = 2\Omega_m^{-1/2}[1/\sqrt{1+z_0} - 1/\sqrt{1+z_i}]$. Then the horizon distance would be $2\Omega_m^{-1/2}H_0^{-1} = 2\Omega_m^{-1/2}h^{-1}3000\,{\rm Mpc}$. In the pure radiation era we get $s_{\rm PH} = H^{-1}$.

The *event horizon*, $s_{\rm EH} = \lim_{t\to\infty}\int_{\eta_0}^{\eta(t)} d\eta'$, determines the size of the region that will be in causal contact with us in the future. It is the distance a light ray emitted today will be able to travel. If the event horizon is infinite, then points in a sphere of arbitrarily large fixed radius r will eventually be in causal contact with each other.

The most important concept when studying cosmological perturbations is the Hubble radius $cH^{-1}(t)$ (also called the Hubble length). In our units this is the same as the Hubble time $H^{-1}(t)$, which gives the time scale of the expansion. Within one Hubble time light can travel one Hubble radius. Hence, the Hubble radius determines whether two points can be in "temporal" causal contact at time t. (With "temporal" we mean "within one Hubble time".) From here on, we call the Hubble radius just the *horizon* or horizon length. This is the commonly used terminology in the CMB and inflation literature. We divide the treatment of the perturbations into subhorizon and superhorizon modes. Consequently, no causal microphysics can affect the superhorizon modes $[\lambda_p(t) \gg H^{-1}(t),\ k_p(t) \ll H(t)$ or in terms of the comoving quantities $\lambda \gg (a_0/a)H^{-1}(t) = \mathcal{H}^{-1}(t),\ k \ll (a/a_0)H(t) = \mathcal{H}(t)]$.

Although the conceptual difference between the particle horizon and the horizon (the Hubble radius) is clear, they have the same value in a radiation-dominated universe $s_{\rm PH} = H^{-1}$. We saw above that in the matter-dominated (or partially matter-dominated) case $s_{\rm PH} \sim \mathcal{O}(1...10)H^{-1}$. Sometimes the coincidence $s_{\rm PH} \sim H^{-1}$ causes confusion, since it does not matter which one is called the horizon. However, during inflation (and pure Λ case) the situation is different. Then $s_{\rm PH} = \infty$, but H^{-1} is practically a finite constant of time.

The importance of the horizon length comes about because in the evolution equations for cosmological perturbations (in Fourier space) one can very often identify the combination $k(aH/a_0)^{-1} = k(\dot{a}/a)^{-1} = k\mathcal{H}^{-1}$. This is negligible on superhorizon scales,

but affects the evolution on subhorizon scales.

We will also meet the term *sound horizon*, which is the distance that the sound has had time to travel during the age of the universe. Denoting the sound speed by c_s the sound horizon is $r_s(\eta) = \int_{\eta_i}^{\eta} c_s(\eta')d\eta'$.

We end this section by giving some important relations. Denoting the "initial" values of η and a by η_i and a_i, respectively, and assuming that the universe has been all the time from η_i to η purely radiation dominated (RD), matter dominated (MD), curvature dominated (CD), or vacuum energy dominated (ΛD) the Friedmann equation (1.11) leads to

$$\eta - \eta_i \propto \begin{cases} a - a_i & \text{pure RD} \\ \sqrt{a} - \sqrt{a_i} & \text{pure MD} \\ \ln(a/a_i) & \text{pure CD} \\ 1/a - 1/a_i & \text{pure } \Lambda\text{D} \end{cases} . \tag{1.14}$$

In the radiation- and matter-dominated cases we can set $\eta_i = a_i = 0$. Hence we find

$$\mathcal{H} = \frac{\dot{a}}{a} = \begin{cases} 1/\eta & \text{RD} \\ 2/\eta & \text{MD} \end{cases} . \tag{1.15}$$

The superhorizon condition can now be expressed as $k\eta \ll 1$ for RD/MD.

Finally, we need some results in terms of the scale factor. The ratio $a/a_{\rm eq}$ appears so frequently that we define a shorthand notation

$$y(t) \stackrel{\rm def}{=} \frac{a(t)}{a_{\rm eq}} = \frac{\rho_m(t)}{\rho_r(t)} , \tag{1.16}$$

in particular, $y_0 = a_0/a_{\rm eq}$. The last equality follows from the definition of the time of equality. In terms of density parameters it is $\Omega_r y_0^4 = \Omega_m y_0^3$, which gives $\Omega_r = y_0^{-1}\Omega_m$. Substituting this into the Friedman equation (1.11) yields

$$H^2 = H_0^2 \left[\Omega_m \frac{a_{\rm eq} + a}{a_0} y_0^4 y^{-4} + \Omega_k y_0^2 y^{-2} + \Omega_\Lambda \right] . \tag{1.17}$$

At matter to radiation equality the curvature and vacuum energy terms are negligible. Thus we arrive at

$$H_{\rm eq} = H_0 \left[\Omega_m \frac{2a_{\rm eq}}{a_0} y_0^4 \right]^{1/2} = y_0 \left(2\Omega_m H_0^2 y_0 \right)^{1/2} \stackrel{\rm def}{=} y_0 k_{\rm eq} = k_{\rm eq}^p . \tag{1.18}$$

Here we defined (by $k_{\rm eq}^p H_{\rm eq}^{-1} = 1$) the wavenumber $k_{\rm eq}$ that corresponds to the horizon length at the time of equality. Now the Friedmann equation (1.17) takes a very compact form $H^2 = \frac{1}{2}(1+y)y^{-4}(k_{\rm eq}^p)^2$, RD/MD. This yields the relations

$$\frac{\dot{a}}{a} = \frac{\sqrt{1+y}}{y\sqrt{2}} k_{\rm eq} , \qquad \eta = \frac{2\sqrt{2}}{k_{\rm eq}} (\sqrt{1+y} - 1) , \qquad \text{RD/MD} \tag{1.19}$$

which we later use extensively.

Let us derive some numbers: From the definition (1.16) we have $y_{\rm eq} = 1$, $y_0 = \Omega_m/\Omega_r = \Omega_m/(4.183 \times 10^{-5} h^{-2}) = \omega_m/(4.183 \times 10^{-5})$, and

$$y_* = y_0/z_* = \omega_m/(4.183 \times 10^{-5})/z_* = \omega_m \times (10^3/z_*) \times 23.9 . \tag{1.20}$$

For $\omega_m = 0.147$ and $z_* = 1100$ these read $y_0 = 3514$ and $y_* = 3.2$, which tells that the

last scattering surface is very near to the equality. From the definition (1.18) we find now

$$k_{\rm eq} = \left[2\omega_m \frac{\omega_m}{4.183\times10^{-5}}\right]^{1/2} \frac{1}{3000\ {\rm Mpc}} = \omega_m \times 0.0729\ {\rm Mpc}^{-1}. \qquad (1.21)$$

1.2 Inflation

The theory described so far has at least two obvious problems (see e.g. [95, 125]).

- At the end of Sec. 3.3 we will find that the horizon length at the last scattering surface is so small that it covers only an angle $\theta < 5^\circ$ in the observed sky. However, the CMB temperature is very precisely isotropic on all scales ($\delta T/T \lesssim 10^{-4}$). This large-scale isotropy needs an explanation, since the observed CMB radiation seems to originate from several hundred or thousand causally disconnected areas at the last scattering surface.
- According to observations the universe is nearly flat today. In adiabatic models $\Omega_{\rm tot}$ can differ from 1 to a few per cent level only [25, 126, 127]. The Friedmann equation (1.10) with $H^2 \propto a^{-3}$ (MD) and $H^2 \propto a^{-4}$ (RD) from (1.11) gives an estimate $|\Omega_{\rm tot}(t) - 1|/|\Omega_{\rm tot} - 1| \approx (a/a_{\rm eq})^2(a_{\rm eq}/a_0) = [T_{\rm eq}/T(t)]^2(T_0/T_{\rm eq})$ for the deviation from flatness at times before the matter to radiation equality. At the last step we used for temperature $T \propto a^{-1}$. Substituting $T_0 = 2.348\times10^{-4}\,{\rm eV}$, $T_{\rm eq} \simeq 1\,{\rm eV}$, and $T(t_{\rm Nucl}) \simeq 1\,{\rm MeV}$, we find that, at the time of nucleosynthesis $\Omega_{\rm tot}(t)$ has been about 10^{16} times closer to 1 than today, and at the Planck time, $T(t_{Pl}) \simeq 10^{19}\,{\rm GeV}$, by a factor 10^{60} closer to 1 than today. Hence, in the Big Bang cosmology, there arises a (philosophical) question why the universe has been so close to the flat one, i.e., why the initial conditions have been extremely flat.

A phase of accelerating expansion (inflation), driven by vacuum energy of a scalar field (inflaton, φ) in the very early universe, was originally introduced in order to solve these horizon (non-causality) and flatness problems [128–130]. In 25 years, inflation has been cemented in the main stream of cosmological model building. There is an overwhelming number of publications where different types of scalar field potentials are studied and all kinds of problems and solutions to them have been discussed. We do not review the basic inflationary scenarios here, but just refer to the standard textbooks [92, 93, 95] and the original articles and reviews such as [131–146] and [147–149].

In most inflationary models the resulting primordial perturbations have a Gaussian scale-invariant (Harrison–Zel'dovich [150, 151]) spectrum or a nearly scale-invariant power-law spectrum. Nowadays, this is the most powerful argument for inflation, since a power-law spectrum fits the CMB (and matter clustering) data extremely well and is hard to produce by any other means. Thus we introduce and discuss some concepts related to a perturbation spectrum generated by inflation.

1.2.1 Generating primordial perturbations

During inflation the quantum fluctuations initially of subhorizon physical scale are stretched to superhorizon ones because of the rapid expansion. Then they are frozen in, since causal microphysics ceases acting. On the superhorizon scales the quantum fluctuations turn into classical perturbations [92, 147].

Consider a scalar perturbation described by a field ξ and its canonical conjugate Π. To quantize the theory we promote these fields to operators $\hat{\xi}$ and $\hat{\Pi}$, respectively. Using the Heisenberg picture in which the states are time-independent but the operators evolve, we impose the canonical equal-time commutation relations

$$\left[\hat{\xi}(\eta,\vec{x}),\hat{\xi}(\eta,\vec{x}')\right] = \left[\hat{\Pi}(\eta,\vec{x}),\hat{\Pi}(\eta,\vec{x}')\right] = 0\,, \quad \left[\hat{\xi}(\eta,\vec{x}),\hat{\Pi}(\eta,\vec{x}')\right] = i\delta^{(3)}\left(\vec{x}-\vec{x}'\right). \quad (1.22)$$

The field operator can be written as a Fourier transformation

$$\hat{\xi}(\eta,\vec{x}) = \frac{1}{(2\pi)^3}\int d^3\vec{k}\hat{\xi}(\eta,\vec{k})e^{i\vec{k}\cdot\vec{x}} \quad \text{with} \quad \hat{\xi}(\eta,\vec{k}) = \hat{a}_{\vec{k}}(\eta_i)f_k(\eta) + \hat{a}^\dagger_{-\vec{k}}(\eta_i)f_k^*(\eta)\,, \quad (1.23)$$

where $\hat{a}_{\vec{k}}(\eta_i)$ is the annihilation operator of the initial vacuum state

$$\hat{a}_{\vec{k}}(\eta_i)\left|0\right\rangle_{\eta_i} = 0\,. \quad (1.24)$$

The time evolution of the vacuum state is taken into account by functions $f_k(\eta)$ and $f_k^*(\eta)$. The commutation relations (1.22) are inherited by $\hat{a}_{\vec{k}}$ as

$$\left[\hat{a}_{\vec{k}}(\eta),\hat{a}^\dagger_{\vec{k}'}(\eta)\right] = (2\pi)^3\delta^{(3)}(\vec{k}-\vec{k}')\,, \quad (1.25)$$

which implies that ${}_{\eta_i}\!\left\langle 0\right|\hat{\xi}^\dagger(\eta,\vec{k})\hat{\xi}(\eta,\vec{k}')\left|0\right\rangle_{\eta_i} \propto (2\pi)^3\delta^{(3)}(\vec{k}-\vec{k}')$. This observable is commonly written in the form

$${}_{\eta_i}\!\left\langle 0\right|\hat{\xi}^\dagger(\eta,\vec{k})\hat{\xi}(\eta,\vec{k}')\left|0\right\rangle_{\eta_i} \overset{\text{def}}{=} (2\pi)^3\delta^{(3)}(\vec{k}-\vec{k}')\frac{2\pi^2}{k^3}\mathcal{P}_\xi(\eta,k)\,, \quad (1.26)$$

where $\mathcal{P}_\xi$ is called the *power spectrum* of ξ. According to equation (1.23) it is $\mathcal{P}_\xi(\eta,k) = \frac{k^3}{2\pi^2}|f_k(\eta)|^2$. Often, another convention (P) for power spectrum is used, $P(k) \overset{\text{def}}{=} \frac{2\pi^2}{k^3}\mathcal{P}(k)$.

In the Heisenberg picture the operator $\hat{\xi}$ satisfies the same equation of motion as the classical field ξ. Hence, we can solve the classical equation of motion on the subhorizon scales and on the superhorizon scales. The above quantum mechanical considerations are then used to properly normalize the subhorizon solution. Finally, the superhorizon solution should be smoothly matched to the subhorizon solution. In the simplest one-field case of slow roll inflation the equation for the scalar field ξ, describing the physical degrees of freedom of the perturbations, becomes so simple that it can be solved analytically for all scales. Then the matching of subhorizon and superhorizon scales is guaranteed immediately, and we just need to normalize in the subhorizon limit.

The equation of motion gives us $f_k(\eta)$. On the subhorizon scales we demand that the initial state corresponds to the usual Minkowski space vacuum with no particles. When we go backward in time during inflation $\eta \to -\infty$. Hence we perform the normalization

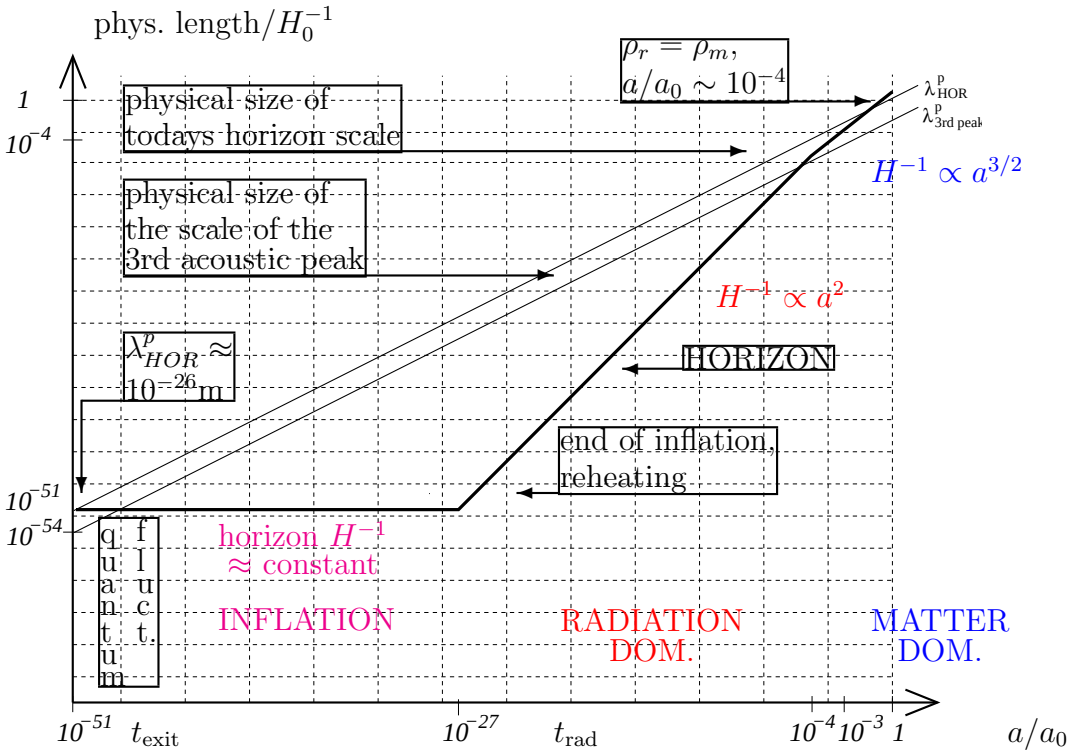

Figure 1.1: **The evolution of horizon and perturbations in standard cosmology with inflationary beginning.** On the vertical axis we represent physical length scales in units of today's horizon H_0^{-1}. In the end of inflation and at the time of reheating the evolution can take a more complicated form than indicated in this simplified presentation.

in the "infinite" past. To put this precisely, we demand that

$$\hat{\xi}(\eta, \vec{k}) \to \hat{\xi}_{\rm Minkowski} = \frac{1}{\sqrt{2k}} \left[e^{-ik\eta} \hat{a}_{\vec{k}}(\eta_i) + e^{ik\eta} \hat{a}^\dagger_{-\vec{k}}(\eta_i) \right] , \tag{1.27}$$

when $\eta, \eta_i \to -\infty$. This implies that $f_k(\eta) \to (1/\sqrt{2k}) e^{-ik\eta}$.

Writing φ for the mean of the inflation field and $\delta\varphi$ for the perturbations, the power spectrum turns out to be $\mathcal{P}_{\delta\varphi}(k) = (\frac{H}{2\pi})^2\big|_{\rm exit}$ in the slow roll limit [92, 93]. The possible scale dependence comes from the slight time dependence of H, since the right hand side is evaluated at the time of horizon exit of the scale in question, i.e., at $k = aH$.

The comoving curvature perturbation $\mathcal{R}$ is the most convenient perturbation variable for characterizing seeds for adiabatic perturbations. This is because (in the pure adiabatic case) it remains constant on superhorizon scales [143, 152]. In terms of the inflaton field it can be written as $\mathcal{R} = -\frac{\mathcal{H}}{\dot{\varphi}}\delta\varphi + \Phi$ [153], where Φ is a perturbation to the unit spatial length in the space part of the metric in the Newtonian gauge, to be defined in Sec. 1.3.4. In the slow roll case the first term dominates, since $\mathcal{H}/\dot{\varphi} \gg 1$. Now the power spectrum takes a simple form

$$\mathcal{P}_{\mathcal{R}}(k) = \left(\frac{\mathcal{H}}{\dot{\varphi}}\right)^2 \mathcal{P}_{\delta\varphi}(k) = \left(\frac{\mathcal{H}}{\dot{\varphi}}\right)^2 \left(\frac{H}{2\pi}\right)^2\Big|_{\rm exit} . \tag{1.28}$$

The ratio of the largest to the smallest cosmologically interesting (observable) scale

is about 10^4. This means that the largest observable scale (corresponding to today's horizon) crosses the horizon $\ln(10^4) = 9$ e-folds before the smallest one. In other words, the classical cosmological perturbations "are created" within 9 Hubble times. During that time the changes in H and $\dot{\varphi}$ are so small that to a good approximation we can write $\mathcal{P}_\mathcal{R}(k) = A(k/k_0)^{n-1}$, where A is the expression (1.28) evaluated at the horizon exit of the mode k_0, i.e. with $aH = k_0$ in (1.28). The constant n is called the *spectral index*. In the extreme slow roll limit the k dependence disappears ($n = 1$). Then the spectrum is *scale invariant*.

A general definition of the (adiabatic) spectral index is

$$n(k) - 1 = \frac{d \ln \mathcal{P}_\mathcal{R}(k)}{d \ln k} \,. \tag{1.29}$$

The k dependence of n will be very weak: $dn/d\ln k$ is of second order in the slow roll parameters [92]. The more the actual situation at the time of the horizon exit of cosmologically interesting scales differs from the slow roll, the more scale variant the resulting curvature perturbation power spectrum is. When $n < 1$ the spectrum is called *negatively tilted* or *red* since large scales (small wavenumbers) have more power. When $n > 1$ the spectrum is *positively tilted* or *blue*. If the spectral index is (weakly) scale dependent, then the spectral index is said to be *running*. For this type of inflationary models see e.g. [154, 155].

1.2.2 Horizon exit and re-entry

In Fig. 1.1 we summarize the behaviour of perturbations and horizon length in the standard Big Bang cosmology with an inflationary early phase (see also, for example, [92] or [95]). During inflation the physical horizon H^{-1} remains nearly constant. In the beginning, all the perturbations are of subhorizon physical size. As the space expands exponentially the wavelengths of quantum fluctuations are stretched, the fluctuations exit the horizon and turn into classical perturbations of $\mathcal{R}$ (or $\mathcal{S}$) — first large scales, later smaller scales. We denote the time of horizon exit by $t_{\rm exit}$.

When inflation ends, all the energy density of the universe is in the scalar field(s) and the universe is very cold, but in the process called *reheating* the particle species of standard model emerge and the energy of the scalar field(s) is converted into radiation. We denote the time of the early radiation-dominated era by $t_{\rm rad}$. This is the "initial" time for the CMB perturbation calculations, since, from this on, the evolution is determined by the standard radiation-dominated picture. The horizon length evolves according to (1.11) as $H^{-1} \propto a^2$. Finally, around $a/a_0 \sim 10^{-4}$, the matter energy density exceeds the radiation energy density, and we have $H^{-1} \propto a^{3/2}$. The perturbations of small scales re-enter the horizon, i.e., turn into subhorizon ones, first, and large scales later. This forms the rule mentioned in many textbooks: "first out, last in — last out, first in". The reason for re-entering the horizon is that the space always stretches as a, but during radiation and matter domination the horizon expands faster. In Fig. 1.1 we indicate perturbations of two different length scales. The scale corresponding to today's horizon is just entering

the horizon while the smaller scale (that actually corresponds to the scale of the third acoustic peak in CMB) has already entered during radiation domination.

Let us comment on the perturbation spectrum arising from (1.28). Actually, instead of being exactly constant, in most slow roll models, H slightly decreases with time during inflation. Since large scales exit first, their amplitude will be larger than the amplitude of smaller scales. Hence the expected spectrum is not entirely scale invariant, but instead slightly red. For typical slow roll predictions ($n \simeq 0.9 - 1.0$) see [156].

1.2.3 More than one scalar field — entropy perturbation

Consider now two scalar fields excited during inflation. In the basic scenario the inflaton field would, at reheating, decay into ordinary particles and the other field would form the CDM. The mean values of these fields, $\varphi(t)$ and $\chi(t)$ form the background trajectory in the field space. Instead of studying the "original" field perturbations $\delta\varphi(t,\vec{x})$ and $\delta\chi(t,\vec{x})$ one can perform a rotation in the field space, and study a perturbation in the direction of the background trajectory (say $\delta\sigma$) and a perturbation perpendicular to that one (say δs). This makes the analysis much simpler as illustrated by Gordon et al. [153, 157].

The perturbation along the trajectory is the "adiabatic perturbation" while δs is the entropy perturbation. In terms of these new fields the curvature perturbation will be $\mathcal{R}|_{\rm exit} = \left(-\frac{\mathcal{H}}{\dot\sigma}\delta\sigma + \Phi\right)|_{\rm exit}$, and the entropy (isocurvature) perturbation $\mathcal{S} \stackrel{\rm def}{=} \mathcal{H}\left(\frac{\delta p}{\dot p} - \frac{\delta\rho}{\dot\rho}\right)$, which we discuss in detail in Sec. 2.1.2, will be $\mathcal{S}|_{\rm exit} \propto \delta s|_{\rm exit}$. At the horizon exit, the values of $\mathcal{R}$ and $\mathcal{S}$ are generically independent random variables.[5] If the background trajectory is a straight line during and after the horizon exit, then the curvature perturbation remains constant as long as it is superhorizon[6] (just as in the pure adiabatic case), but if the background trajectory is curved, the entropy perturbation seeds the curvature perturbation [143, 152]. In the treatment by Gordon et al. [153, 157] this becomes particularly transparent. An earlier, worked-out realization, is for example a double inflation study by Langlois [59, 60].

So, the generic prediction for inflation generated perturbations is [159]

$$\begin{bmatrix} \hat{\mathcal{R}}(t_{\rm rad},\vec{k}) \\ \hat{\mathcal{S}}(t_{\rm rad},\vec{k}) \end{bmatrix} = \begin{bmatrix} 1 & T_{\mathcal{RS}}(k) \\ 0 & T_{\mathcal{SS}}(k) \end{bmatrix} \begin{bmatrix} \hat{\mathcal{R}}(t_{\rm exit},\vec{k}) \\ \hat{\mathcal{S}}(t_{\rm exit},\vec{k}) \end{bmatrix}, \tag{1.30}$$

The transfer functions $T_{xy}(k)$ describe how the perturbations evolve from the time of in-

[5] Being independent degrees of freedom $\delta\varphi$ and $\delta\chi$ acquire independent random values due to quantum fluctuations. In Fourier space we get then $\langle\delta\varphi^*(t,\vec{k})\chi(t,\vec{k})\rangle = 0$. The new perturbations are linear combinations of the original perturbations, $\delta\sigma = \cos\theta\delta\varphi + \sin\theta\delta\chi$ and $\delta s = -\sin\theta\delta\varphi + \cos\theta\delta\chi$, where θ is an angle between φ and the trajectory (or σ). Now it follows that $\langle\delta\sigma^*(t,\vec{k})\delta s(t,\vec{k})\rangle = 0$, and $\langle\delta\sigma^*(t,\vec{k})\delta\sigma(t,\vec{k}')\rangle = \frac{2\pi^2}{k^3}\left(\cos^2\theta\,\mathcal{P}_{\delta\varphi} + \sin^2\theta\,\mathcal{P}_{\delta\chi}\right)(2\pi)^3\delta(\vec{k}-\vec{k}')$. For $\langle|\delta s|^2\rangle$ just change $\cos \leftrightarrow \sin$.

[6] This holds to first order in perturbations. In the second order perturbation theory the entropy perturbation sources the curvature perturbation on long wavelengths even for straight trajectories, but if the trajectory is a geodesic in the field space the evolution of entropy and curvature perturbations decouple [158].

flation to the beginning of the radiation-dominated era. The exact form of these functions is model dependent. By the hat we remind that the quantities generated by quantum fluctuations are random variables, so only their statistical properties (e.g. variance or power spectrum) can be predicted by theory.

From (1.30) we find the general initial condition for any CMB (or matter power) calculation

$$\mathcal{P}_{\mathcal{R}}(t_{\rm rad},k) = \mathcal{P}_{\mathcal{R}}(t_{\rm exit},k) + T^2_{\mathcal{RS}}(k)\mathcal{P}_{\mathcal{S}}(t_{\rm exit},k), \tag{1.31}$$

$$\mathcal{P}_{\mathcal{S}}(t_{\rm rad},k) = T^2_{\mathcal{SS}}(k)\mathcal{P}_{\mathcal{S}}(t_{\rm exit},k), \tag{1.32}$$

$$\mathcal{C}_{\mathcal{RS}}(t_{\rm rad},k) \stackrel{\rm def}{=} \frac{k^3}{2\pi^2}\langle\mathcal{R}^*(t_{\rm rad},\vec{k})\mathcal{S}(t_{\rm rad},\vec{k})\rangle \tag{1.33}$$

$$= T_{\mathcal{RS}}(k)T_{\mathcal{SS}}\mathcal{P}_{\mathcal{S}}(t_{\rm exit},k) = \mathcal{C}_{\mathcal{SR}}(t_{\rm rad},k), \tag{1.34}$$

where the last equality follows from the reality of $\mathcal{R}(t,\vec{x})$ and $\mathcal{S}(t,\vec{x})$ which imply $\mathcal{R}^*(t,\vec{k}) = \mathcal{R}(t,-\vec{k})$ and $\mathcal{S}^*(t,\vec{k}) = \mathcal{S}(t,-\vec{k})$. At least in the slow roll case, the scale dependence of the power spectra and transfer functions becomes weak. Then the power laws $\mathcal{P}_{\mathcal{R}}(t_{\rm exit},k) \propto (k/k_0)^{n_1}$, $\mathcal{P}_{\mathcal{S}}(t_{\rm exit},k) \propto (k/k_0)^{n_2}$, $T_{\mathcal{RS}}(k) \propto (k/k_0)^{n_3}$, and $T_{\mathcal{SS}}(k) \propto (k/k_0)^{n_4}$ are good approximations, and we end up with

$$\mathcal{P}_{\mathcal{R}}(t_{\rm rad},k) = A_r^2\Big(\frac{k}{k_0}\Big)^{n_{\rm ad1}-1} + A_s^2\Big(\frac{k}{k_0}\Big)^{n_{\rm ad2}-1}, \tag{1.35}$$

$$\mathcal{P}_{\mathcal{S}}(t_{\rm rad},k) = B^2\Big(\frac{k}{k_0}\Big)^{n_{\rm iso}-1}, \tag{1.36}$$

where $n_{\rm ad1} = n_1 + 1$, $n_{\rm ad2} = n_2 + 2n_3 + 1$, and $n_{\rm iso} = n_2 + 2n_4 + 1$. The three components are the usual adiabatic mode, a second adiabatic mode generated by the entropy perturbation, and the usual isocurvature mode, with constant amplitudes A_r, A_s and B at the pivot scale $k = k_0$, respectively. (Analytical formulas and consistency relations for the spectral indices can be found in [160].) The initial cross-correlation between the adiabatic and the isocurvature component is now

$$\mathcal{C}_{\mathcal{RS}}(t_{\rm rad},k) = \mathcal{C}_{\mathcal{SR}}(t_{\rm rad},k) = A_s B\Big(\frac{k}{k_0}\Big)^{n_{\rm cor}-1}, \tag{1.37}$$

where $n_{\rm cor} = n_2 + n_3 + n_4 + 1 = (n_{\rm iso} + n_{\rm ad2})/2$. The correlation is between the second adiabatic and the isocurvature component as is natural since these components have the same source, namely entropy perturbation. Although, for simplicity, we considered only two scalar fields, the formalism is straightforward to generalize to the case of several scalar fields.

In papers **III** & **V** we study constraints the CMB data set to the primordial spectra of shape (1.35) – (1.37). Specific examples of double inflation can be found from [59, 137, 139, 161–163]. Similar type of spectra could arise also, for example, in the curvaton scenario. However, as shown in **IV**, in the curvaton model it is motivated to include also the "second isocurvature mode" with spectral index $n_{\rm iso2}$ in addition to the second adiabatic mode, and one would have a constraint $n_{\rm iso2} = n_{\rm ad2}$ (and $n_{\rm iso} = n_{\rm ad1}$) [80, 164, 165]. In paper **I** the adiabatic and isocurvature modes are assumed to be uncor-

related, i.e., $A_s = 0$, which is motivated (as we have seen) if the scalar field potential is such that the trajectory in the field space is a straight line during inflation. Moreover, in realistic supersymmetric GUT theories, cosmic strings are typically produced after inflation, leading to isocurvature perturbations [166], which are usually considered to be uncorrelated with the pre-existing adiabatic perturbations from the inflationary era. In paper **II** we rule out pure CDM isocurvature perturbations, $A_s = A_r = 0$.

Here we have left unmentioned many important concepts of the standard cosmology, which we will need in the following chapters. Let us just refer to the standard textbooks [92–95, 105, 167, 168]. We have now discussed some possible mechanisms that produce (correlated) adiabatic and isocurvature primordial perturbations. From here on, we assume for the initial state of our analysis the radiation-dominated standard FRW universe with small perturbations. From Fig. 1.1 we understand that perturbations of any cosmologically interesting scale are initially superhorizon, if we choose the "initial time", $t_{\rm rad}$, deep enough in the radiation-dominated era.

1.3 Perturbed FRW universe

In the linear regime the perturbations can be treated in the Fourier space. For example, a scalar perturbation quantity A is written as in the previous section

$$A(\eta, \vec{x}) = \frac{1}{(2\pi)^3} \int d^3\vec{k} A(\eta, \vec{k}) Q(\vec{x}, \vec{k}) \,. \tag{1.38}$$

In the flat space $Q(\vec{x}, \vec{k}) = e^{i\vec{k}\cdot\vec{x}}$. (See Appendix A.1 for a generalization of the Fourier transformation to open and closed cases.) Vector and tensor perturbation quantities A_i and A_{ij}, respectively, are given by

$$A_i(\eta, \vec{x}) = \frac{1}{(2\pi)^3} \int d^3\vec{k} A(\eta, \vec{k}) Q_i(\vec{x}, \vec{k}) \,, \quad A_{ij}(\eta, \vec{x}) = \frac{1}{(2\pi)^3} \int d^3\vec{k} A(\eta, \vec{k}) Q_{ij}(\vec{x}, \vec{k}) \cdot$$

In the flat space $Q_j = -i(k_j/|\vec{k}|)Q$ and $Q_{ij} = [(k_i k_j/k^2) + (1/3)\gamma_{ij}]Q$. (See again Appendix A.1 for the general case.) The evolution equations of various quantities are usually written up to first or second order in perturbations.

The perturbations in the energy density, curvature, temperature etc. induce perturbations to the FRW metric. Generally, the FRW-type metric perturbed by *scalar perturbations* can be written in terms of four independent functions of time and wave vector (A^G, B^G, H_L^G and H_T^G) in the form [15]

$$\begin{aligned} g_{00}(\eta, \vec{x}) &= -\textstyle\int \frac{d^3\vec{k}}{(2\pi)^3} \, (a/a_0)^2 [1 + 2A^G(\eta, \vec{k}) Q(\vec{x}, \vec{k})] \,, \\ g_{0j}(\eta, \vec{x}) &= -\textstyle\int \frac{d^3\vec{k}}{(2\pi)^3} \, (a/a_0)^2 B^G(\eta, \vec{k}) Q_j(\vec{x}, \vec{k}) \,, \\ g_{ij}(\eta, \vec{x}) &= \textstyle\int \frac{d^3\vec{k}}{(2\pi)^3} \, (a/a_0)^2 [\gamma_{ij} + 2H_L^G(\eta, \vec{k}) Q(\vec{x}, \vec{k}) \gamma_{ij} + 2H_T^G(\eta, \vec{k}) Q_{ij}(\vec{x}, \vec{k})] \,, \end{aligned} \tag{1.39}$$

where G is a reminder that the actual values depend on the gauge choice as will be explained in Sec. 1.3.3. A^G is the amplitude of the perturbation in the ratio of the proper time distance to the coordinate time distance between two nearby hypersurfaces of

constant time. B^G represents the perturbation in the rate of deviation of a constant space coordinate line from a line normal to a constant time hypersurface. H_L is the perturbation in the unit spatial length and H_T is an anisotropic distortion of each constant time hypersurface. For brevity, we occasionally drop the k integrations.

1.3.1 Energy-momentum tensor

Within the scope of this thesis, it is sufficient to consider the universe consisting of five components x with $x \in \{\gamma, \nu, b, c, v\}$, where v stands for the vacuum (or, more generally, for any dark energy) component. The total energy-momentum tensor is then

$$T_{(T)}{}^{\mu}{}_{\nu} = \sum_x T_{(x)}{}^{\mu}{}_{\nu}\,, \tag{1.40}$$

where the energy-momentum tensor for individual components x is given by [15] (see also [99] and [98] for general discussion of the energy-momentum tensor)

$$\begin{aligned}
T_{(x)}{}^{0}{}_{0} &= -(1+\delta_x Q)\rho_x,\\
T_{(x)}{}^{0}{}_{i} &= (\rho_x + p_x)V_x Q_i,\\
T_{(x)}{}^{j}{}_{0} &= -(\rho_x + p_x)V_x Q^j,\\
T_{(x)}{}^{i}{}_{j} &= p_x(\delta^i{}_j + \frac{\delta p_x}{p_x}\delta^i{}_j Q + \tilde{\Pi}_x Q^i{}_j)\,.
\end{aligned} \tag{1.41}$$

Here ρ_x is the homogeneous background energy density of the component x, p_x is the pressure, $\delta_x = \delta\rho_x/\rho_x \ll 1$ is the energy density perturbation, V_x is the velocity potential (the Fourier components of the fluid velocity are $-i(k^i/|\vec{k}|)V_x$ in the flat case), and we use a shorthand notation $\tilde{\Pi}_x = \frac{3}{2}(1-3K/k^2)^{-1/2}\Pi_x$, where Π_x is the anisotropic stress of the component x.

From the form of the total energy-momentum tensor (1.40) we see that the total matter variables have to be defined in terms of the individual components of the fluid in the following way:

$$\begin{aligned}
\rho_T &= \sum_x \rho_x\,, & p_T &= \sum_x p_x\,,\\
\delta_T\rho_T &= \sum_x \delta_x\rho_x\,, & \delta p_T &= \sum_x \delta p_x\,,\\
(\rho_T + p_T)V_T &= \sum_x (\rho_x + p_x)V_x\,, & p_T\tilde{\Pi}_T &= \sum_x p_x\tilde{\Pi}_x.
\end{aligned} \tag{1.42}$$

With (1.42) in mind, we can use (1.41) also for the whole fluid; just replace x by T.

1.3.2 The temperature perturbation Θ

Perturbations in the energy-momentum tensor introduce the temperature perturbation

$$\Theta \stackrel{\text{def}}{=} \frac{\delta T}{T}\,. \tag{1.43}$$

The plain Fourier expansion (1.38) is not alone a convenient way to describe the temperature perturbation on different scales because, in addition to the time and position, it depends on direction. This comes about because the energy of photons coming from different directions may differ. If we observe photons at a fixed position $\vec{x}$ we relate a larger temperature to more energetic photons. Defining $\vec{\gamma}$ to be a unit vector in the direction of propagation of photons [for details, see (2.42) and discussion thereon] we conclude that $\Theta = \Theta(\eta, \vec{x}, \vec{\gamma})$. In Appendices A.2 and A.3 we present a multipole expansion of this type of a function with direction dependence in curved space. The end result is (A.47) with the basis functions G_ℓ defined in (A.35).

In the flat space the expressions of Appendices A.2 and A.3 reduce to $G_\ell(\vec{x}, \vec{\gamma}, \vec{k}) = (-i)^\ell P_\ell(\mu) e^{i\vec{k}\cdot\vec{x}}$, where $\mu = k^{-1}\vec{\gamma}\cdot\vec{k}$ defines the direction of the wave vector with respect to the direction of propagation of photons. Then $\Theta(\eta, \vec{x}, \vec{\gamma}) = \frac{1}{(2\pi)^3}\int d^3\vec{k} e^{i\vec{k}\cdot\vec{x}}\Theta(\eta, \vec{k})$ with

$$\Theta(\eta, \vec{k}) = \Theta(\eta, k, \mu) = \sum_{\ell=0}^{\infty}(-i)^\ell P_\ell(\mu)\Theta_\ell(\eta, k)\,. \tag{1.44}$$

Multiplying this by $(2\ell'+1)P_{\ell'}(\mu)/[2(-i)^{\ell'}]$, integrating over μ, and using the orthogonality of the Legendre polynomials $\int_{-1}^{1} d\mu P_\ell(\mu)P_{\ell'}(\mu) = 2\delta_{\ell\ell'}/(2\ell+1)$ we obtain

$$\Theta_\ell(\eta, k) = \int_{-1}^{1}\frac{d\mu}{2(-i)^\ell}(2\ell+1)P_\ell(\mu)\Theta(\eta, k, \mu)\,. \tag{1.45}$$

The function Θ_ℓ depends on time and $k = |\vec{k}|$ only. The direction dependence is tracked by the multipole number ℓ. Note that factors of $(2\ell+1)$ can be absorbed in the definition of Θ_ℓ if in (1.44) we use $(2\ell+1)(-i)^\ell P_\ell(\mu)$ as a basis function instead of $(-i)^\ell P_\ell(\mu)$. This is similar to the ambiguity of 2π factors in the usual Fourier transformation and its inverse transformation. E.g. Dodelson [94] defines $\Theta_\ell(\eta, k) = \int_{-1}^{1}\frac{d\mu}{2(-i)^\ell}P_\ell(\mu)\Theta(\eta, k, \mu)$, which implies $\Theta_\ell^{\rm Dodelson} = \Theta_\ell^{\rm Our}/(2\ell+1)$. This difference is, of course, reflected to any equation that contains ℓ factors; for example to one of our main goals in the next chapter, the Boltzmann hierarchy (2.52). Hence, great care is needed when taking formulas from different sources in the literature.

The definition of the last scattering surface (in a perturbed universe) needs a refinement. First of all, even in the homogeneous background universe the last scattering surface has a finite thickness, because of the finite photon mean free path. We can define a reference value η_* corresponding to the conformal time in the background universe where the ionization fraction has dropped to a level where the photon mean free path exceeds the Hubble length. For a more precise definition in terms of the optical depth see the discussion beginning just above the equation (2.123). Secondly, the (mean) last scattering of photons (over a small region) in a perturbed universe does not happen at the same coordinate time η_* everywhere. For individual photons the last scattering can take place before or after that time. In the homogeneous background universe the temperature and optical depth are constant on the last scattering surface defined by $\eta = \eta_* = \text{const}$. In the perturbed universe the temperature or ionization fraction are not any more constants on this $\eta = \eta_* = \text{const.}$ surface, but we still keep referring to this

surface as the last scattering surface, since these perturbations are anyway smaller than the thickness of the last scattering surface.

1.3.3 Gauge freedom

According to the principles of general relativity preferred coordinates do not exist. Thus we can choose the coordinate system arbitrarily. For example, even an unperturbed homogeneous and isotropic FRW metric can be recast into an inhomogeneous form by wrapping the time slicing with a suitable coordinate transformation. This means that the actual value and the physical interpretation of the perturbations depend on the choice of a coordinate system. Put another way: the coordinate transformation can change the correspondence between the perturbed world and the unperturbed background. This kind of coordinate transformation is called a gauge transformation. The resulting ambiguity in the definition of perturbations, i.e., in the choice of gauge, is called *gauge freedom*.

In the linear perturbation theory it is enough to consider infinitesimal gauge transformations, $x^\xi \mapsto \tilde{x}^\xi$, which can be expressed as

$$\tilde{x}^\xi = x^\xi + \delta x^\xi \,, \tag{1.46}$$

with $x^0 = \eta$ and

$$\begin{aligned} \delta x^0 &= TQ \,, \\ \delta x^i &= LQ^i \,, \end{aligned} \tag{1.47}$$

where T and L are arbitrary functions of time corresponding to the choice of the time slicing and spatial coordinate grid, respectively.

Let us find how the metric (1.39) transforms in (1.46). The comparison between the transformed metric $\tilde{g}_{\mu\nu}$ and the ordinary metric $g_{\mu\nu}$ should be made at the same physical point. $P = (x^\xi)$ in the new coordinates, corresponds $(x^\xi - \delta x^\xi)$ in the old coordinates. Hence we have

$$\tilde{g}_{\mu\nu}[(x^\xi)] = \frac{\partial x^\alpha}{\partial \tilde{x}^\mu} \frac{\partial x^\beta}{\partial \tilde{x}^\nu} g_{\alpha\beta}[(x^\xi - \delta x^\xi)] \,, \tag{1.48}$$

where $\partial x^\alpha / \partial \tilde{x}^\mu \approx \delta^\alpha_\mu - (\delta x^\alpha)_{,\mu}$ from (1.46), and $g_{\alpha\beta}[(x^\xi - \delta x^\xi)] \approx g_{\alpha\beta}[(x^\xi)] - \delta x^\lambda g_{\alpha\beta,\lambda}[(x^\xi)]$ from the Taylor expansion. Thus we get to first order

$$\tilde{g}_{\mu\nu}[(x^\xi)] = g_{\mu\nu}[(x^\xi)] - (\delta x^\alpha)_{,\mu}\, g_{\alpha\nu}[(x^\xi)] - (\delta x^\beta)_{,\nu}\, g_{\beta\mu}[(x^\xi)] - \delta x^\lambda\, g_{\mu\nu,\lambda}[(x^\xi)] \,, \tag{1.49}$$

which leads to

$$\begin{aligned} \tilde{g}_{00} &= -(a/a_0)^2 \left[1 + 2\left(A^G - \dot{T} - (\dot{a}/a)T\right) Q\right] , \\ \tilde{g}_{0j} &= -(a/a_0)^2 \left(B^G + \dot{L} + kT\right) Q_j , \\ \tilde{g}_{ij} &= (a/a_0)^2 \left[\gamma_{ij} + 2\left(H_L^G - (k/3)L - (\dot{a}/a)T\right) Q\gamma_{ij} + 2\left(H_T^G + kL\right) Q_{ij}\right] . \end{aligned}$$

Comparing this with (1.39), the gauge transformation properties of the metric perturbations read as

$$A^{\tilde{G}} = A^G - \dot{T} - (\dot{a}/a)T \,,$$

$$
\begin{aligned}
B^{\tilde{G}} &= B^G + \dot{L} + kT\,, \\
H_L^{\tilde{G}} &= H_L^G - (k/3)L - (\dot{a}/a)T\,, \\
H_T^{\tilde{G}} &= H_T^G + kL\,. \qquad (1.50)
\end{aligned}
$$

Hence none of A, B, H_L or H_T is gauge invariant. Nevertheless, we can find gauge invariant combinations of these. For example

$$
\begin{aligned}
\mathcal{A} &= A^G - a^{-1}\frac{d}{d\eta}\left[\frac{a^2}{\dot{a}}\left(H_L^G + \frac{1}{3}H_T^G\right)\right] \qquad \text{and} \\
\mathcal{B} &= B^G + (\dot{a}/a)^{-1}k[H_L^G + (1/3)H_T^G] - k^{-1}\dot{H}_T^G \qquad (1.51)
\end{aligned}
$$

are two independent gauge invariants as can easily be checked by employing (1.50).

To first order the energy-momentum tensor in the new coordinate system stands as

$$
\begin{aligned}
\tilde{T}^\mu_\nu[(x^\xi)] &= \frac{\partial\tilde{x}^\mu}{\partial x^\alpha}\frac{\partial x^\beta}{\partial\tilde{x}^\nu}T^\alpha_\beta[(x^\xi - \delta x^\xi)] \\
&= [\delta^\mu_\alpha + (\delta x^\mu)_{,\alpha}][\delta^\beta_\nu - (\delta x^\beta)_{,\nu}]T^\alpha_\beta[(x^\xi)] - \delta x^\lambda\delta^\mu_\alpha\delta^\beta_\nu T^\alpha_{\beta,\lambda}[(x^\xi)] \\
&= T^\mu_\nu[(x^\xi)] + (\delta x^\mu)_{,\alpha}\,T^\alpha_\nu[(x^\xi)] - (\delta x^\beta)_{,\nu}\,T^\mu_\beta[(x^\xi)] - \delta x^\lambda\,T^\mu_{\nu,\lambda}[(x^\xi)]\,.
\end{aligned}
$$

Putting here the explicit form of T^μ_ν from (1.41) and following the same lines as in the case of the metric, we get

$$
\begin{aligned}
V_x^{\tilde{G}} &= V_x^G + \dot{L}\,, \\
\delta_x^{\tilde{G}} &= \delta_x^G + 3(1+w_x)\frac{\dot{a}}{a}T\,, \\
\delta p_x^{\tilde{G}} &= \delta p_x^G + 3c_x^2\rho_x(1+w_x)\frac{\dot{a}}{a}T\,, \\
\Pi_x^{\tilde{G}} &= \Pi_x^G\,. \qquad (1.52)
\end{aligned}
$$

From these we see that the only gauge invariant building block of our energy-momentum tensor is the anisotropic stress Π_x. In fact, in our case of scalar perturbations, any quadrupole or higher order quantity (e.g. Θ_ℓ with $\ell \geq 2$, see Sec. 1.3.2) is evidently gauge invariant, since the gauge transformation is defined by a scalar function (TQ) describing the wrapping of the time slicing and a vector in space (LQ^i) to boost the system. Clearly these leave the tensor quantities unchanged. This observation is of crucial importance. When we later derive the angular power C_ℓ that describes the observed anisotropy, we can rely on the fact that its numerical value for $\ell > 1$ does not depend on the gauge where the calculations are performed. However, for the monopole and dipole the division into background and perturbed parts is not unique: The monopole C_0 and dipole C_1 receive different numerical values in different gauges. Thus the comparison of their theoretical and possibly measured values is meaningless. (See also footnote 3 on page 64). Finally, we note that the velocity difference between two particle species x and y, $V_x - V_y$, is gauge invariant according to (1.52).

We assumed the FRW metric to be given and added there small perturbations. However, it would be better justified to start from the metric of our real, perturbed, universe.

Then one should construct a homogeneous and isotropic background by some averaging process. As one could guess, since the spatial averaging process depends on the hypersurfaces of constant time, there is not an obvious way to do this [169]. In the case of very small perturbations the problem becomes less severe, since the difference in the metric resulting from two different averaging processes is at most of the order of perturbations. Hence, this difference can be regarded as a small perturbation and included in the perturbed part of the metric.

Finding genuine gauge invariant perturbation quantities and using only them as building blocks of the theory would also be possible [169, 170] and, in some sense, more justified. However, we choose here the simplicity and intuitivity of the Newtonian gauge.

1.3.4 Newtonian gauge

Newtonian gauge (conformal Newtonian gauge, longitudinal gauge) is a time slicing, in which the expansion is isotropic, i.e. $B^N = H_T^N = 0$, see (1.39). Putting $\tilde{G} = N$ in (1.50) we get

$$\begin{aligned} 0 &= B^N = B^G + \dot{L} + kT \qquad \text{and} \\ 0 &= H_T^N = H_T^G + kL\,. \end{aligned} \tag{1.53}$$

The second of these gives $L = -H_T^G/k$, and the first one $T = -B^G/k - \dot{L}/k = -B^G/k + \dot{H}_T^G/k^2$. This shows that the Newtonian gauge is reached from an arbitrary gauge G by performing the gauge transformation (1.46) with

$$T = -B^G/k + \dot{H}_T^G/k^2, \qquad \text{and} \qquad L = -H_T^G/k. \tag{1.54}$$

Let us define the *"Newtonian potentials"* by $\Psi \stackrel{\text{def}}{=} A^N$ and $\Phi \stackrel{\text{def}}{=} H_L^N$. Substitution of T and L from (1.54) into equations (1.50) and (1.52) gives the Newtonian perturbations in terms of perturbations in an arbitrary gauge:

$$\begin{aligned} \Psi &= A^G + \frac{1}{a}\frac{d}{d\eta}[aB^G/k - a\dot{H}_T^G/k^2]\,, \\ \Phi &= H_L^G + \frac{1}{3}H_T^G + \frac{\dot{a}}{a}(B^G/k - \dot{H}_T^G/k^2)\,, \\ \delta_x^N &= \delta_x^G + 3(1+w_x)\frac{\dot{a}}{a}(-B^G/k + \dot{H}_T^G/k^2)\,, \\ \delta p_x^N &= \delta p_x^G + 3c_x^2\rho_x(1+w_x)\frac{\dot{a}}{a}(-B^G/k + \dot{H}_T^G/k^2)\,, \\ V_x^N &= V_x^G - \dot{H}_T^G/k\,, \end{aligned} \tag{1.55}$$

where $c_x \stackrel{\text{def}}{=} \sqrt{\dot{p}_x/\dot{\rho}_x}$ is the sound speed in fluid x.

In this thesis we will work in the Newtonian gauge. Any equation or quantity can be recast from an arbitrary gauge to the Newtonian gauge (and vice versa) by the transformations (1.55). In this sense the treatment can be regarded as general. Note however, that e.g. the neutrino velocity isocurvature perturbation becomes singular at very early times in the Newtonian gauge [63]. This has to be a coordinate singularity,

because there are gauges where the singularity disappears. We can use the Newtonian gauge, since we do not consider the neutrino velocity isocurvature mode. Hence, our metric reads

$$\begin{aligned} g_{00} &= -(a/a_0)^2(1+2\Psi Q), \\ g_{0i} &= 0, \\ g_{ij} &= (a/a_0)^2(1+2\Phi Q)\gamma_{ij}\,. \end{aligned} \tag{1.56}$$

Note that some authors (e.g. [93, 153, 167]) change the role of Ψ and Φ. In the literature, the sign conventions may also differ from ours [92]. Our convention is used e.g. in [90, 91, 94, 171–174]. Later, from equation (2.27), we find that in the absence of anisotropic stress ($\Pi_T = 0$) we have simply one independent variable, since then $\Phi = -\Psi$.

In papers **III**–**V** we characterize the primordial adiabatic perturbation by the comoving curvature perturbation (see e.g. [135, 153, 175]) $\mathcal{R}$ instead of the Newtonian potential Ψ (and Φ). These are related by [147]

$$\mathcal{R} = \Phi + \frac{H}{\dot{H}}\left(-\dot{\Phi} + H\Psi\right)\,. \tag{1.57}$$

On superhorizon scales, in the early radiation-dominated era, the relation becomes very simple. The primordial perturbations of $\mathcal{R}$ in terms of Ψ and Φ are [92]

$$\begin{aligned} \mathcal{R}(t_{\rm rad},\vec{k}) &= -\frac{3}{2}\left(1+\tfrac{4}{15}X_\nu\right)\Psi(t_{\rm rad},\vec{k}) \\ &= \frac{3}{2}\left(1+\tfrac{4}{15}X_\nu\right)\left(1+\tfrac{2}{5}X_\nu\right)^{-1}\Phi(t_{\rm rad},\vec{k})\,. \end{aligned} \tag{1.58}$$

Actually, in paper **IV** we use an opposite sign convention for $\mathcal{R}$.

Let us finally define a shorthand notation for the initial values: $\mathcal{R}_i \stackrel{\rm def}{=} \mathcal{R}(t_{\rm rad},\vec{k})$, $\Psi_i \stackrel{\rm def}{=} \Psi(t_{\rm rad},\vec{k})$, etc. From here on, in most equations, we put $X_\nu = 0$, i.e., we neglect the 10% contribution ($X_\nu = 0.405$) from the anisotropic stress caused by neutrinos.

In the following chapters we make also other approximations, which are valid only roughly. The actual calculations of the angular power are performed accurately numerically, the main approximation being the treatment to first order in perturbations, i.e., the use of linear perturbation theory. The approximative analytical formulas that we review in this thesis are intended for gaining insight into the behaviour of the anisotropies and their origin instead of merely relying on the "black-box" numerical results. The validity of the approximations can be confirmed numerically case by case. Hence, we do not always devote much space to proving the validity of approximations in detail. In principle, the approximations can be divided into four categories: (1) We neglect all the second or higher order terms in perturbations. (2) We neglect the anisotropic stress. (3) On subhorizon scales we neglect terms containing $\mathcal{H}/k$ and on superhorizon scales $k/\mathcal{H}$. (4) On subhorizon scales, before recombination we make an expansion in the Compton scattering time $\dot{\tau}^{-1}$, which is small compared to the time scale of expansion of the universe.

Chapter 2

Evolution of background, perturbations, and anisotropies

In this chapter we review the equations governing the evolution of the background and perturbations. We also provide approximative analytic solutions. We explain the meaning of the entropy perturbation and show (also by intuitive arguments) how it arises in the multi-component fluid. We derive a basic tool of all CMB analyse, the brightness equation and the Boltzmann hierarchy of the temperature perturbation multipoles. Finally, we show how this leads to acoustic oscillations, and demonstrate the line of sight integration method by which the perturbations at the last scattering surface can conveniently be converted into the anisotropy multipoles observed today.

Throughout, for shortness, we neglect the anisotropic stress Π, since including it in the analysis is not necessary for understanding the basic properties of the angular power spectrum to be discussed in the next chapter. We neither consider the equations for polarization multipoles. However, polarization feeds back into the temperature quadrupole equation resulting in a larger diffusion damping scale than in the case of unpolarized radiation. We comment on this at the end of Sec. 2.7.3. The full treatment including the anisotropic stress and polarization can be found e.g. in [172]. The anisotropic stress would just lead to correction factors $1 + \frac{4}{15}X_\nu$ and $1 + \frac{2}{5}X_\nu$ along the lines of (1.58).

2.1 Conservation equations

The total energy-momentum of a fluid is conserved: ${T_{(T)}}^{\mu\nu}{}_{;\mu} = 0$ where $_{;\mu}$ means a covariant derivative with respect to x^μ. However, the energy-momentum of the individual components is not necessarily conserved, since interactions can transport the energy and momentum between different particle species. Thus we write

$${T_{(x)}}^{\mu\nu}{}_{;\mu} = {F_{(x)}}^{\nu}, \tag{2.1}$$

where the source term ${F_{(x)}}^{\nu}$ is to be determined later. Conservation of the total energy-momentum now implies that

$$\sum_x {F_{(x)}}^{\nu} = 0. \tag{2.2}$$

By defining ${F_{(T)}}^{\nu} = 0$ we can use equation (2.1) also for the total matter. Note that the source term is also zero for a particle species x, which does not interact with other species. In our model ${F_{(c)}}^{\nu} = {F_{(\nu)}}^{\nu} = 0$ and then, according to the constraint (2.2),

$$ {F_{(\gamma)}}^{\nu} = -{F_{(b)}}^{\nu}. \tag{2.3} $$

The interchange of energy-momentum between photons and baryons arises before last scattering (and after reionization) because of Compton interaction.

Assuming that the fractional energy shift in the Compton scattering is small, at most of first order, the energy transfer rate ${F_{(\gamma)}}^{\nu}$ is also at most of first order, i.e., to zeroth order we put ${F_{(x)}}^{\nu} = 0$ for all species $x = T,\ b,\ c,\ \gamma,\ \nu,\ v$. Note that we include the possible vacuum energy here. Now we may write F explicitly in k-space as

$$ \begin{aligned} {F_{(x)}}^{0} &= (a_0/a)^2 \zeta_x Q, \\ {F_{(x)}}^{i} &= (a_0/a)^2 \xi_x Q^i, \end{aligned} \tag{2.4} $$

where we include the scale factor $(a_0/a)^2$ just for later convenience. Now, $\zeta_x = \xi_x = 0$ for $x = T,\ c,\ \nu$, while for photons and baryons we have

$$ \zeta_b = -\zeta_\gamma \qquad \text{and} \qquad \xi_b = -\xi_\gamma. \tag{2.5} $$

These possibly nonzero source terms will be specified in Sec. 2.6. Actually, it turns out that also $\zeta_b = \zeta_\gamma = 0$, so the only non-zero source terms are ξ_b and ξ_γ.

2.1.1 Continuity equations

The $\nu = 0$ equation in (2.1) gives the continuity equation while the $\nu = i$ equations are related to momentum conservation and give the Euler equation. Here we just present the end results (for derivation see e.g. [90]).

To zeroth order the $\nu = 0$ equation, the *continuity equation* of the homogeneous background, reads as

$$ \dot{\rho}_x = -3(1 + w_x)\frac{\dot{a}}{a}\rho_x, \tag{2.6} $$

where $w_x \stackrel{\text{def}}{=} \frac{p_x}{\rho_x}$ defines the equation of state for the fluid-component x. If w_x is constant, we get $\rho_x \propto a^{-3(1+w_x)}$. This leads to the already mentioned relations for radiation ($w_r = 1/3$) and for non-relativistic matter ($w_m = 0$): $\rho_r \propto a^{-4}$ and $\rho_m = a^{-3}$.

The first order equation in perturbations with $\nu = 0$ in (2.1) is the *continuity equation for perturbations*

$$ \dot{\delta}_x = -(1 + w_x)(kV_x + 3\dot{\Phi}) - 3\frac{\dot{a}}{a}\left(\frac{\delta p_x}{\delta \rho_x} - w_x\right)\delta_x + \zeta_x/\rho_x\,, \tag{2.7} $$

where $\delta_x = \delta\rho_x/\rho_x$ as in Sec. 1.3.1.

2.1.2 Entropy perturbation

In this subsection we give a formal definition of the entropy perturbation and motivate the terminology. To this end we notice that the middle source term in the perturbation

continuity equation (2.7) is due to the spatial perturbation of the equation of state. Indeed, keeping the perturbations up to first order only, we get

$$\delta w_x = \frac{p_x + \delta p_x}{\rho_x + \delta\rho_x} - w_x = \frac{1}{\rho_x}\left(p_x + \delta p_x\right)\left(1 - \frac{\delta\rho_x}{\rho_x}\right) = \left(\frac{\delta p_x}{\delta\rho_x} - w_x\right)\delta_x. \tag{2.8}$$

On the other hand, if the pressure is a function of energy density only, $p_x = p_x(\rho_x) = w_x\rho_x$, then $\delta p_x = (\partial p_x/\partial\rho_x)\delta\rho_x = (\dot{p}_x/\dot{\rho}_x)\delta\rho_x = c_x^2\delta\rho_x$, where the sound speed is $c_x \stackrel{\text{def}}{=} \sqrt{\dot{p}_x/\dot{\rho}_x}$. This is the adiabatic pressure perturbation.

Employing equation (2.7) we get

$$\frac{d}{d\eta}\left(\frac{\delta_x}{1+w_x}\right) = -(kV_x + 3\dot{\Phi}) - \frac{1}{1+w_x}3\mathcal{H}\left(\frac{\delta p_x}{\delta\rho_x} - w_x\right)\delta_x - \frac{\delta_x}{(1+w_x)^2}\dot{w}_x + \frac{\zeta_x/\rho_x}{1+w_x}\,. \tag{2.9}$$

Using the continuity equation (2.6) $\dot{w}_x$ in the second last term can be expressed as

$$\dot{w}_x = \frac{\dot{p}_x}{\rho_x} - \frac{p_x}{\rho_x^2}\dot{\rho}_x = \frac{\dot{\rho}_x}{\rho_x}\left(\frac{\dot{p}_x}{\dot{\rho}_x} - w_x\right) = -3(1+w_x)\mathcal{H}(c_x^2 - w_x)\,. \tag{2.10}$$

Now defining the entropy perturbation

$$\mathcal{S}_x \stackrel{\text{def}}{=} \mathcal{H}\left(\frac{\delta p_x}{\dot{p}_x} - \frac{\delta\rho_x}{\dot{\rho}_x}\right) \tag{2.11}$$

we end up with

$$\frac{d}{d\eta}\left(\frac{\delta_x}{1+w_x}\right) = -(kV_x + 3\dot{\Phi}) + 9\mathcal{H}c_x^2\mathcal{S}_x + \frac{\zeta_x/\rho_x}{1+w_x}. \tag{2.12}$$

Note that in terms of $\mathcal{S}_x$ the pressure perturbation in (2.8) and (2.7) reads $\delta p_x = c_x^2\left[\delta_x - 3(1+w_x)\mathcal{S}_x\right]\rho_x$. The last term $-3(1+w_x)\rho_x c_x^2\mathcal{S}_x$ is the non-adiabatic pressure perturbation. Many authors like to use this as a basic quantity instead of $\mathcal{S}_x$. For example, in [90, 91, 144, 171], $p_x\Gamma_x \stackrel{\text{def}}{=} \delta p_x - c_x^2\delta\rho_x = -3(1+w_x)\rho_x c_x^2\mathcal{S}_x$ is used.

The entropy perturbation vanishes for individual matter and radiation fluids, since $\delta p_x = w_x\delta\rho_x$ and $c_x^2 = w_x$ for them. However, in the two-component fluid consisting of both matter and radiation $\mathcal{S}_T$ is not necessarily zero. This is due to different equations of state of the individual components. Actually, as can be seen from (2.8), the entropy perturbation would be nonzero even for single particle fluid, if for example its equation of state parameter was not spatially constant. That could happen in the case of not strictly non-relativistic matter, if its temperature varied spatially due to some astrophysical process, which locally injects energy into the fluid [91].

Now we proceed to find $\mathcal{S}_T$ of (2.11) in radiation-matter fluid, and show that it is proportional to the perturbation of the relative number densities of matter and radiation particles. Finally, we motivate the term entropy perturbation. For radiation-matter fluid we have $\delta p_T = \frac{1}{3}\delta\rho_r$, $\delta\rho_T = \delta\rho_r + \delta\rho_m$, $\dot{p}_T = \dot{p}_r = \frac{1}{3}\dot{\rho}_r = -\frac{4}{3}\mathcal{H}\rho_r$, and $\dot{\rho}_T = \dot{\rho}_r + \dot{\rho}_m = -4\mathcal{H}\rho_r - 3\mathcal{H}\rho_m$, where in the last two equalities we employed the continuity equation (2.6) for radiation and matter separately. Substituting these results into the definition (2.11) we find

$$\mathcal{S}_T = -\frac{1}{4}\delta_r + \frac{\delta\rho_r + \delta\rho_m}{4\rho_r + 3\rho_m} = -\frac{1}{4}\delta_r + \frac{\rho_r\delta_r + y\rho_r\delta_m}{4\rho_r + 3y\rho_r} = \frac{y}{4+3y}\left(\delta_m - \frac{3}{4}\delta_r\right)\,. \tag{2.13}$$

From this we identify an entropy perturbation between matter and radiation

$$\mathcal{S}_{mr} \stackrel{\rm def}{=} \delta_m - \frac{3}{4}\delta_r = \frac{\delta_m}{1+w_m} - \frac{\delta_r}{1+w_r} = \frac{\delta n_m}{n_m} - \frac{\delta n_r}{n_r} = \frac{\delta(n_m/n_r)}{n_m/n_r}\,, \tag{2.14}$$

where n_m and n_r are the number densities of matter and radiation particles, respectively.[1] Here we have $\rho_m = \rho_c + \rho_b$, $\delta\rho_m = \delta\rho_c + \delta\rho_b$, $\rho_r = \rho_\gamma + \rho_\nu$, and $\delta\rho_r = \delta\rho_\gamma + \delta\rho_\nu$. Hence $\delta_m = X_c\delta_c + X_b\delta_b$ and $\delta_r = X_\gamma\delta_\gamma + X_\nu\delta_\nu$, where $X_c = \rho_c/(\rho_c+\rho_b) = \Omega_c/\Omega_m = 1 - X_b$ and $X_\gamma = \rho_\gamma/(\rho_\gamma+\rho_\nu) = 1 - X_\nu$.

Defining the general entropy perturbation between two particle species x and y by

$$\mathcal{S}_{xy} \stackrel{\rm def}{=} -3\mathcal{H}\left(\frac{\delta\rho_x}{\dot\rho_x} - \frac{\delta\rho_y}{\dot\rho_y}\right) = \frac{\delta_x}{1+w_x} - \frac{\delta_y}{1+w_y}\,, \tag{2.15}$$

we realize that, in the photon-neutrino-CDM-baryon fluid, there can be several entropy perturbation modes. However, not all of them are independent. Taking photons as a reference we can have $\mathcal{S}_{c\gamma}$, $\mathcal{S}_{b\gamma}$, and $\mathcal{S}_{\nu\gamma}$. As we do not consider the neutrino isocurvature mode $\mathcal{S}_{\nu\gamma} = (3/4)(\delta_\nu - \delta_\gamma) = 0$ initially, i.e., $\delta_{r_i} = \delta_{\nu_i} = \delta_{\gamma_i}$. Thus our final formula for the matter-radiation entropy perturbation will be

$$\mathcal{S}_{mr} = X_c\delta_c + X_b\delta_b - \frac{3}{4}\delta_\gamma = X_c\mathcal{S}_{c\gamma} + X_b\mathcal{S}_{b\gamma}. \tag{2.16}$$

As pointed out in Introduction, we do not actually study the baryon isocurvature either. So, in papers **I**–**V**, we have $\mathcal{S}_{mr} = X_c\mathcal{S}_{c\gamma} = X_c\frac{\delta(n_c/n_\gamma)}{n_c/n_\gamma}$, and $\mathcal{S}_T = [y/(4+3y)]\mathcal{S}_{mr}$. Employing the gauge transformations (1.52) we see that $\mathcal{S}_{xy}$ defined in (2.15) and $\mathcal{S}_x$ are automatically gauge invariant.

Instead of using the total entropy of the universe, $S_{\rm tot}$, it is more common to consider entropy per particle, the specific entropy $s_x = S_{\rm tot}/N_x$, where N_x is the number of x particles. Now $s_x = (S_{\rm tot}/V)/(N_x/V) = s/n_x$, where the entropy density s is dominated by the contribution of relativistic particles [95]. Thus we can use the relation $s \propto T^3 \propto a^{-3}$. On the other hand $n_\gamma \propto T^3$, which leads to $s \propto n_\gamma$, and $s_x \propto n_\gamma/n_x$. We can call the perturbation in s_x as entropy perturbation. But according to (2.14) and (2.15) it coincides (up to a sign) to our earlier definition of entropy perturbation, namely we get $\delta(s_x)/s_x = \delta(n_\gamma/n_x)/(n_\gamma/n_x) = -\mathcal{S}_{x\gamma}$, and we have $\mathcal{S}_{c\gamma} = -\delta(s_c)/s_c$. The sign we chose in (2.15) is the most common in the literature, since with this convention a positive initial value of $\mathcal{S}_{c\gamma}$ corresponds to an initial CDM overdensity.

Let us finally derive some intuitive understanding of the perturbation continuity equation (2.12). Consider first a single particle fluid x. In the footnote 1 on page 30 we saw that $\delta_x/(1+w_x) = \delta n_x/n_x$ for $x = r, m$. Thus the left hand side of (2.12) is just the rate of change in the number density perturbation $\frac{d}{d\eta}(\delta n_x/n_x)$. Apart from the factor $-3\dot\Phi$, equation (2.12) is the normal continuity equation for the number density of particles: $\frac{\partial}{\partial\eta}(\delta n_x/n_x)(\eta,\vec{x}) = -\nabla\cdot v_x(\eta,\vec{x})$, i.e., in k-space $\frac{d}{d\eta}(\delta n_x/n_x) = -kV_x$. The

[1] In the case of non-relativistic particles $\rho_x = m_x n_x$, where m_x is the mass of the particle and n_x is the number density. Thus $\delta_m/(1+w_m) = \delta\rho_m/\rho_m = \delta n_m/n_m$. For radiation $\rho_r \propto T^4$ and $n_r \propto T^3$, where T is the temperature. This implies $\rho_r \propto n_r^{4/3}$ and $\delta_r/(1+w_r) = (3/4)\delta\rho_r/\rho_r = \delta n_r/n_r$.

term $-3\dot{\Phi}$ can be identified as space stretching. In the metric (1.56) the equal time proper length is $ds \propto (a/a_0)\sqrt{1+2\Phi} \approx (a/a_0)(1+\Phi)$. Thus for a non-flowing fluid, whose particles are at "equally" spaced coordinate points, the number density is $n_x \propto [(a/a_0)(1+\Phi)]^{-3} \approx (a/a_0)^{-3}(1-3\Phi)$, and we arrive at $\delta n_x/n_x \approx -3\delta a/a - 3\Phi$, i.e. $\frac{d}{d\eta}(\delta n_x/n_x) = -3\dot{a}/a - 3\dot{\Phi}$. The term $-3\dot{a}/a$ yields just the zeroth order continuity equation (2.6), and $-3\dot{\Phi}$ gives the first order equation (2.12) without the flow term V_x, which we already explained. Thus we could have found equation (2.12) by Newtonian arguments, but we missed $\mathcal{S}_x$. However, for individual particle species this is not an error, since in most cases $\mathcal{S}_x$ $(x \neq T)$ vanishes.

The simple equation, which we above derived by intuitive means,

$$\frac{d}{d\eta}\left(\frac{\delta_x}{1+w_x}\right) = -kV_x - 3\dot{\Phi} \tag{2.17}$$

can, actually, be used to derive the perturbation continuity equation (2.12) for the total radiation-matter fluid. First, we note that

$$\begin{aligned}\frac{d}{d\eta}\left(\frac{\delta_T}{1+w_T}\right) = \frac{\rho_m+p_m}{\rho_T+p_T}\frac{d}{d\eta}\left(\frac{\delta_m}{1+w_m}\right) + \frac{\rho_r+p_r}{\rho_T+p_T}\frac{d}{d\eta}\left(\frac{\delta_r}{1+w_r}\right) \\ + \frac{\delta_m}{1+w_m}\frac{d}{d\eta}\left(\frac{\rho_m+p_m}{\rho_T+p_T}\right) + \frac{\delta_r}{1+w_r}\frac{d}{d\eta}\left(\frac{\rho_r+p_r}{\rho_T+p_T}\right),\end{aligned} \tag{2.18}$$

where $p_m = 0$. The time derivatives in the first two terms can be picked from (2.17). Using the definitions (1.42) and $w_T = p_T/\rho_T = p_r/(\rho_r+\rho_m)$ we then realize that those first two terms form just the right hand side of (2.17) with x replaced by T. Employing $\rho_m/\rho_r = y$ from (1.16) and $\dot{y} = \dot{a}/a_{\rm eq} = (\dot{a}/a)y$, the last two time derivatives in (2.18) get a form

$$\frac{d}{d\eta}\left(\frac{\rho_r+p_r}{\rho_T+p_T}\right) = \frac{d}{d\eta}\left(\frac{4}{4+3y}\right) = -\frac{\dot{a}}{a}\frac{12y}{(4+3y)^2} = -\frac{d}{d\eta}\left(\frac{\rho_m+p_m}{\rho_T+p_T}\right). \tag{2.19}$$

Hence, we have got the total matter perturbation continuity equation

$$\frac{d}{d\eta}\left(\frac{\delta_T}{1+w_T}\right) = -(kV_T + 3\dot{\Phi}) + \mathcal{H}\frac{12y}{(4+3y)^2}\mathcal{S}_{mr}\,, \tag{2.20}$$

where $\mathcal{S}_{mr}$ can be written as $\mathcal{S}_{mr} = [(4+3y)/y]\mathcal{S}_T$, see (2.13). Hence the last term simplifies to $12\mathcal{H}\mathcal{S}_T/(4+3y)$. The sound speed in the total fluid is

$$c_T^2 = \frac{\dot{p}_T}{\dot{\rho}_T} = \frac{\dot{p}_r}{\dot{\rho}_m+\dot{\rho}_r} = \frac{4}{3}\frac{\rho_r}{3\rho_m+4\rho_r} = \frac{4}{3}\frac{1}{4+3y}\,, \tag{2.21}$$

so the last term in (2.20) reduces to $9\mathcal{H}c_T^2\mathcal{S}_T$, and we have re-invented the full perturbation continuity equation (2.12). Here we did not consider the energy transfer term ζ, since for the total fluid it is automatically zero, see (2.2) – (2.5).

In what follows we encounter often c_T^2 and the equation of state parameter w_T. Thus is is worth pointing out that these are not equal. For radiation-matter fluid we have

$$w_T = \frac{p_T}{\rho_T} = \frac{1}{3}\frac{1}{1+y}. \tag{2.22}$$

2.1.3 Euler equation

To zeroth order the $\nu = i$ equations in (2.1) are identically zero. The first order result is the *Euler equation*

$$\dot{V}_x + \frac{\dot{a}}{a}(1-3c_x^2)V_x \\ = k\Psi + \frac{1}{1+w_x}\left[kc_x^2\delta_x - k3(1+w_x)c_x^2\mathcal{S}_x - k(1-3K/k^2)\tfrac{2}{3}w_x\tilde{\Pi}_x - \tfrac{\xi_x}{\rho_x}\right]. \quad (2.23)$$

In the absence of the right hand side terms, this equation gives just the effect of the expansion to the particle velocity. Consider again a single-particle fluid with constant c_x (for matter $c_m^2 \approx 0$ and for radiation $c_r^2 = 1/3$). From (2.23) it then follows that $dV_x = -(1/a)da(1-3c_x^2)V_x$. We observe that V_r is a constant while $V_m \propto a^{-1}$. Thus the expansion has a different effect on radiation than on matter. This happens because the expansion redshifts momenta of massive particles as a^{-1} and consequently the particle velocity decays as a^{-1} whereas, in the case of radiation, it is the energy (temperature), which redshifts as $T \propto a^{-1}$. Another argument for $V_r =$ constant is that $V_r \propto \Theta_1$, which has a dipole signature, so isotropic expansion cannot affect it.

On the right hand side of (2.23) there is (as one could guess) the gradient of the gravitational potential (in k-space), $k\Psi$. The other three terms are stress terms, which try to prevent a gravitational infall. There is an anisotropic component $\tilde{\Pi}_x$ as well as a pressure component, which is separated into the two parts: acoustic (adiabatic) $\propto c_x^2\delta_x$ and entropy (non-adiabatic) $\propto -3(1+w_x)c_x^2\mathcal{S}_x = w_x\Gamma_x$, which again can contribute if the fluid consists of more than one particle species.

2.2 Einstein equations

The conservation equations (2.6), (2.12) and (2.23) do not yet form a closed set of dynamical equations, since they do not specify the evolution of potentials Ψ and Φ. The feedback between these metric perturbations [see (1.56)] and the perturbations in the energy-momentum [see (1.41)] is established through the Einstein equations

$$G_{\mu\nu} = 8\pi G T_{\mu\nu}, \quad (2.24)$$

where $G_{\mu\nu}$ is the Einstein tensor, and the possible vacuum energy contribution is included in the energy-momentum tensor.

To zeroth order (i.e. for the background), the space-space Einstein equations give just the conservation equations of the previous section. The time-space components vanish identically and the time-time component gives the Friedmann equation (1.9) that connects the geometry of the universe and the evolution of the scale factor to the energy contents.

The first order Einstein equations give three different equations for Ψ and Φ. The

time-time part becomes

$$3\left(\frac{\dot{a}}{a}\right)^2\Psi - 3\frac{\dot{a}}{a}\dot{\Phi} - (k^2-3K)\Phi = -4\pi G\left(\frac{a}{a_0}\right)^2\rho_T\delta_T. \tag{2.25}$$

Recall that $\dot{a}/a = \mathcal{H}$ and the Friedmann equation gives $4\pi G(a/a_0)^2\rho_T = (3/2)\mathcal{H}^2$. Substituting these into the above and following equations they would take a more compact form. The time-space equation is

$$\frac{\dot{a}}{a}\Psi - \dot{\Phi} = 4\pi G\left(\frac{a}{a_0}\right)^2(1+w_T)\rho_T V_T/k, \tag{2.26}$$

and the space-space $i \neq j$ equation says

$$k^2(\Psi+\Phi) = -8\pi G\left(\frac{a}{a_0}\right)^2 p_T\tilde{\Pi}_T. \tag{2.27}$$

When we multiply equation (2.26) with $3(\dot{a}/a)$ and subtract (2.25) from the resulting equation, we obtain the *generalized Poisson equation*

$$(k^2-3K)\Phi = 4\pi G\left(\frac{a}{a_0}\right)^2\rho_T[\delta_T + 3\frac{\dot{a}}{a}(1+w_T)V_T/k]. \tag{2.28}$$

This reduces to the normal Poisson equation familiar from (non-relativistic) Newtonian theory, if $K = 0$ and the last term in square brackets is negligible. Rewriting (2.28) as

$$(k^2-3K)\Phi = \tfrac{3}{2}\mathcal{H}^2[\delta_T + 3\mathcal{H}(1+w_T)V_T/k] \tag{2.29}$$

we see immediately that the last term is negligible, if $\mathcal{H}/k \ll 1$. Thus we regain the Newtonian theory on subhorizon scales, $k \gg \mathcal{H}$.

2.3 Large-scale solution

By defining a new density perturbation quantity $\Delta_T = \delta_T + 3(\dot{a}/a)(1+w_T)V_T/k$ the Poisson equation takes a simple form

$$(k^2-3K)\Phi = 4\pi G(a/a_0)^2\rho_T\Delta_T\,. \tag{2.30}$$

After some algebra, the Friedmann equation, the perturbation continuity equation, and the Euler equation lead to

$$\begin{aligned}\ddot{\Delta}_T \;-\; &\left[3(2w_T - c_T^2) - 1\right](\dot{a}/a)\dot{\Delta}_T + \left[(\tfrac{9}{2}w_T^2 - 12w_T - \tfrac{3}{2} + 9c_T^2)(\dot{a}/a)^2 + (\tfrac{9}{2}w_T^2 - \tfrac{3}{2})K\right.\\ &+\; \left.(1-3K/k^2)k^2c_T^2 + (3/2)(a/a_0)^2\Omega_\Lambda H_0^2(1+w_T)(1-3w_T)\right]\Delta_T = \mathcal{F},\end{aligned} \tag{2.31}$$

where the source term is

$$\begin{aligned}\mathcal{F} = \;& -3(1+w_T)c_T^2(1-\tfrac{3K}{k^2})k^2\mathcal{S}_T - 2w_T\tfrac{\dot{a}}{a}(1-\tfrac{3K}{k^2})\dot{\tilde{\Pi}}_T + 2\Big[(3w_T^2 - 2w_T + 3c_T^2)(\tfrac{\dot{a}}{a})^2 +\\ &(3w_T^2 + 2w_T)K + \tfrac{1}{3}w_T(1-\tfrac{3K}{k^2})k^2 - \tfrac{3}{2}(\tfrac{a}{a_0})^2\Omega_\Lambda H_0^2 w_T(1+w_T)\Big](1-\tfrac{3K}{k^2})\tilde{\Pi}_T.\end{aligned}$$

We conclude that the entropy perturbation and the anisotropic stress act as sources for the density perturbation Δ_T. However, the anisotropic stress is very small so that in

what follows we neglect it.

On superhorizon scales ($k\eta \ll 1$) the only growing solution to equation (2.31) is [171, 174]

$$\Delta_T = \Phi_i U_A(\tilde{a}) + \mathcal{S}_i U_I(\tilde{a}), \tag{2.32}$$

where Φ_i is primordial (initial) value of the potential, $\mathcal{S}_i$ is primordial entropy perturbation between matter and radiation, $\mathcal{S}_i \stackrel{\text{def}}{=} \mathcal{S}_{mr}(t_{\rm rad}, \vec{k})$, and

$$U_A(\tilde{a}) = \frac{6}{5}\left(\frac{k}{k_{eq}}\right)^2 \left(1 - \frac{3K}{k^2}\right) \left[\tilde{a}^3 + \frac{2}{9}\tilde{a}^2 - \frac{8}{9}\tilde{a} - \frac{16}{9} + \frac{16}{9}\sqrt{\tilde{a}+1}\right] \frac{1}{\tilde{a}(\tilde{a}+1)}\,,$$

$$U_I(\tilde{a}) = \frac{4}{15}\left(\frac{k}{k_{eq}}\right)^2 \left(1 - \frac{3K}{k^2}\right) \frac{3\tilde{a}^2 + 22\tilde{a} + 24 + 4(4+3\tilde{a})(1+\tilde{a})^{1/2}}{(1+\tilde{a})(4+3\tilde{a})[1+(1+\tilde{a})^{1/2}]^4} \tilde{a}^3\,.$$

Here $\tilde{a}$ is given by

$$\tilde{a} = \tfrac{1}{a_{\rm eq}} \times \tfrac{5}{2} a_0^3 \Omega_m\, g(a) \int_{a_i}^{a} \tfrac{1}{a'^3 g^3(a')} da'\,, \tag{2.33}$$

with

$$g^2(a) = \left(\tfrac{a_0}{a}\right)^3 \Omega_m + \left(\tfrac{a_0}{a}\right)^2 \Omega_k + \Omega_\Lambda\,. \tag{2.34}$$

At the radiation-dominated epoch and early matter-dominated epoch $\tilde{a} = a/a_{\rm eq} = y$, but later, at curvature- or vacuum energy-dominated epochs $\tilde{a}$ starts slowly differ from y.

Now we can give the asymptotic solutions at each epoch of the evolution of the universe. Deep at the radiation-dominated epoch $\tilde{a} \ll 1$ while well after the time of matter to radiation equality $\tilde{a} \gg 1$. Keeping the leading terms of y we arrive at

$$\Delta_T = \frac{1}{30}\left(\frac{k}{k_{\rm eq}}\right)^2 \left(1 - \frac{3K}{k^2}\right) \times \begin{cases} 40y^2\Phi_i + 5y^3\mathcal{S}_i & \text{RD} \\ 36y\,\Phi_i + 8y\,\mathcal{S}_i & \text{MD} \\ 36\tilde{a}\,\Phi_i + 8\tilde{a}\,\mathcal{S}_i\,. & \text{CD/}\Lambda\text{D} \end{cases} \tag{2.35}$$

The Poisson equation gives immediately the potential

$$\Phi = \begin{cases} \Phi_i + \frac{1}{8} y \mathcal{S}_i & \text{RD} \\ \frac{9}{10}\Phi_i \quad + \frac{1}{5}\mathcal{S}_i & \text{MD} \\ \frac{9}{10}\frac{\tilde{a}}{y}\Phi_i + \frac{1}{5}\frac{\tilde{a}}{y}\mathcal{S}_i\,. & \text{CD/}\Lambda\text{D} \end{cases} \tag{2.36}$$

As we are neglecting the anisotropic stress, $\tilde{\Pi}_T = 0$, equation (2.27) relates the potentials by $\Psi = -\Phi$. Hence we have a solution for Ψ also. The velocity from equation (2.26) becomes

$$\begin{aligned} V_T &= \frac{k}{k_{\rm eq}} \times \begin{cases} \frac{\sqrt{2}}{2} y \Psi \; - \frac{1}{k_{\rm eq}} y^2 \dot{\Phi} & \text{RD} \\ \frac{2\sqrt{2}}{3} y^{1/2} \Psi - \frac{1}{k_{\rm eq}} \frac{4}{3} y \dot{\Phi} & \text{MD/CD/}\Lambda\text{D} \end{cases} \\ &= -\frac{k}{k_{\rm eq}} \times \begin{cases} \frac{\sqrt{2}}{2} y \Phi_i \quad + \frac{\sqrt{2}}{8} y^2 \mathcal{S}_i & \text{RD} \\ \frac{3\sqrt{2}}{5} y^{1/2} \Phi_i + \frac{2\sqrt{2}}{15} y^{1/2} \mathcal{S}_i & \text{MD} \\ \frac{6}{5}\frac{1}{k_{\rm eq}} \dot{\tilde{a}} \Phi_i \; + \frac{4}{15}\frac{1}{k_{\rm eq}} \dot{\tilde{a}} \mathcal{S}_i\,. & \text{CD/}\Lambda\text{D} \end{cases} \end{aligned} \tag{2.37}$$

Our final goal is to determine the temperature perturbation. Hence we need δ_r^N, which is related to the total density perturbation by

$$\delta_T^N = \frac{\rho_m \delta_m^N + \rho_r \delta_r^N}{\rho_m + \rho_r} = \frac{y}{1+y}\delta_m^N + \frac{1}{1+y}\delta_r^N\,. \tag{2.38}$$

On superhorizon scales we have $\dot{\mathcal{S}}_{mr} = 0$, since there is no causal microphysics that could change the relative particle number densities. Hence, we can write $\delta_m^N = \mathcal{S}_i + \frac{3}{4}\delta_r^N$. Substituting this into the above equation leads to

$$\delta_r^N = \frac{1+y}{1+\frac{3}{4}y}\left(\delta_T^N - \frac{y}{1+y}\mathcal{S}_i\right) \tag{2.39}$$

Knowing Δ_T and V_T the Newtonian total density perturbation δ_T^N can be solved from the definition of Δ_T at the beginning of this section. Then the above equation gives the radiation density perturbation. Neglecting the possible neutrino isocurvature modes we have $\delta_\gamma^N = \delta_\nu^N = \delta_r^N$. After these considerations we end up with the monopole temperature perturbation [91]

$$\Theta_0 = \frac{\delta_\gamma^N}{4} = \begin{cases} \frac{1}{2}\Phi_i - \frac{1}{8}y\mathcal{S}_i & \text{RD} \\ \frac{3}{5}\Phi_i \;\; - \frac{1}{5}\mathcal{S}_i & \text{MD} \\ \left(\frac{3}{2} - \frac{9}{10}\frac{\tilde{a}}{y}\right)\Phi_i - \frac{1}{5}\frac{\tilde{a}}{y}\mathcal{S}_i\,. & \text{CD/}\Lambda\text{D} \end{cases} \tag{2.40}$$

2.4 Brightness equation

At temperatures of our interest the baryons and CDM can be treated as non-relativistic pressureless dust characterized by density and velocity. The relativistic species (photons and massless neutrinos) cannot be described by a simple velocity field, but by a distribution function $f(t, \vec{x}, p^0, \vec{p})$, where p^μ is the four-momentum of photons. Furthermore, before decoupling the evolution of photons and baryons is connected due to the Compton scattering.

As will be explained, the tight coupling between photons and baryons ensures that the dominant perturbations at the last scattering surface are monopole and dipole perturbations Θ_0 and Θ_1, respectively. When photons start to stream freely these monopole and dipole perturbations are mapped onto all multipoles Θ_ℓ. Hence, for an approximate result, it is enough to know $\Theta_0(\eta_*)$ and $\Theta_1(\eta_*)$. Note however that the small quadrupole perturbation $\Theta_2(\eta_*)$ can be seen in the polarization measurements.

To find the temperature perturbation Θ we need a Boltzmann equation to describe the evolution of the (photon) distribution function f

$$\frac{df}{d\eta} \equiv \frac{\partial f}{\partial \eta} + \frac{\partial f}{\partial x^i}\frac{dx^i}{d\eta} + \frac{\partial f}{\partial p^\mu}\frac{dp^\mu}{d\eta} = \frac{a}{a_0}C[f]\,. \tag{2.41}$$

Here $C[f]$ is a (physical) collision term which takes into account the Compton scattering. The left hand side contains the (general relativistic) gravitational effects. As is obvious from the above notation we will work in x space in this section.

Calculating Θ requires knowing the energy of photons. It is the zeroth component of the four momentum in the locally orthonormal frame $\epsilon = \hat{p}^0 = (a/a_0)\sqrt{1+2\Psi}\,p^0$. Instead of p^i we will characterize the direction of propagation of the photons by

$$\gamma_p^i = \frac{\hat{p}^i}{\hat{p}^0} = \frac{\sqrt{1+2\Phi}}{\sqrt{1+2\Psi}}\frac{p^i}{p^0} = \frac{\sqrt{1+2\Phi}}{\sqrt{1+2\Psi}}\frac{dx^i}{d\eta}\,. \tag{2.42}$$

This has a nice property that the comoving vector $\gamma^i = (a_0/a)\gamma_p^i$ is a unit vector with respect to the unperturbed three metric, $(a/a_0)^2\gamma_{ij}\gamma^i\gamma^j = 1$.

With help of the geodesic equation of photons (see e.g. [90, 91, 94, 176]) the fractional rate of change in the energy of photons reads

$$\frac{1}{\epsilon}\frac{d\epsilon}{d\eta} = -\left(\mathcal{H} + \frac{\partial\Phi}{\partial\eta} + \gamma_p^i\frac{\partial\Psi}{\partial x^i}\right). \tag{2.43}$$

The physical interpretation is easy. The first term accounts for the redshift due to the expansion of the universe. The second term describes the stretching of space by perturbations. The third term counts the energy gain/loss of photons falling to/climbing out of the gravitational potential wells.

Equation (2.43) is crucial for the theory of CMB perturbations, since it states that if the spectrum in a given instant is of the blackbody type, it will remain such forever. This comes because the fractional energy shift is independent of the frequency of the photons. To show this let us study a small perturbation $\delta\epsilon$ to the energy. The perturbed energy of photons is then $\epsilon' = \epsilon + \delta\epsilon = \epsilon[1 + (\delta\epsilon/\epsilon)]$. Now we have

$$f(\epsilon, T) = [\mathrm{e}^{\frac{\epsilon}{T}} - 1]^{-1} = [\mathrm{e}^{\frac{\epsilon'}{T(1+\frac{\delta\epsilon}{\epsilon})}} - 1]^{-1} = [\mathrm{e}^{\frac{\epsilon'}{T'}} - 1]^{-1} = f'(\epsilon', T'), \tag{2.44}$$

where $T' \stackrel{\mathrm{def}}{=} T(1 + \frac{\delta\epsilon}{\epsilon})$. So we notice that the functional form of f and f' is same, and $\delta T/T = \delta\epsilon/\epsilon$.

The temperature perturbation at point $(\eta, \vec{x})$ seen in the direction $\vec{n} = -\vec{\gamma}$ is

$$\Theta(\eta, \vec{x}, \vec{\gamma}) = \frac{\delta T}{\overline{T}} = \frac{T(\eta, \vec{x}, \vec{\gamma}) - \overline{T}(\eta)}{\overline{T}(\eta)}, \tag{2.45}$$

where $\overline{T}(\eta) = (1/V)\int d^3\vec{x}\int\frac{d\Omega}{4\pi}T(\eta, \vec{x}, \vec{\gamma})$ is the space and direction averaged value of the temperature at time η.

Because the energy density of the photons, ρ_γ, is proportional to T^4, we get $4\Theta = \delta\rho_\gamma/\overline{\rho}_\gamma = \frac{\rho(\eta,\vec{x},\vec{\gamma})}{\overline{\rho}_\gamma(\eta)} - 1$, where $\overline{\rho}_\gamma(\eta) = (1/V)\int d^3\vec{x}\rho_\gamma(\eta, \vec{x})$. The density of states in the phase space is $g/(2\pi)^3$, where $g = 2$ for photons. Thus we have

$$\rho_\gamma(\eta, \vec{x}) = \frac{2}{(2\pi)^3}\int d^3\vec{p}\,\epsilon\, f[\epsilon, T(\eta, \vec{x}, \vec{\gamma})] = \frac{1}{\pi^2}\int_0^\infty d\epsilon\,\epsilon^3\int\frac{d\Omega}{4\pi}f[\epsilon, T(\eta, \vec{x}, \vec{\gamma})], \tag{2.46}$$

The direction dependent energy density can be defined by dropping the integral over directions, $\rho(\eta, \vec{x}, \vec{\gamma}) = \frac{1}{\pi^2}\int_0^\infty d\epsilon\,\epsilon^3\, f[\epsilon, T(\eta, \vec{x}, \vec{\gamma})]$. This leads to

$$4\Theta = \frac{1}{\pi^2\overline{\rho}_\gamma}\int_0^\infty \epsilon^3\, f\, d\epsilon - 1. \tag{2.47}$$

From now on we will omit the overline on the averaged energy density.

As we have derived the temperature perturbation Θ in terms of the photon distribution function we can now find a differential equation for Θ using the Boltzmann equation (2.41). Changing from p^μ to our new variables $(\epsilon, \vec{\gamma}_p)$, multiplying by ϵ^3 and integrating over energy it becomes

$$\frac{\partial}{\partial\eta}\int\epsilon^3 f\, d\epsilon + \frac{dx^i}{d\eta}\frac{\partial}{\partial x^i}\int\epsilon^3 f\, d\epsilon + \frac{d\gamma_p^i}{d\eta}\frac{\partial}{\partial\gamma_p^i}\int\epsilon^3 f\, d\epsilon + \int\frac{1}{\epsilon}\frac{d\epsilon}{d\eta}\epsilon^4\frac{\partial f}{\partial\epsilon}\, d\epsilon = \frac{a}{a_0}\int\epsilon^3 C[f]\, d\epsilon\,.$$

The fractional energy shift $\frac{1}{\epsilon}\frac{d\epsilon}{dt}$ is independent of the energy and can be taken out from the integrand in the last term on the left hand side. So we get an integral $\int_0^\infty \epsilon^4 \frac{\partial f}{\partial \epsilon}\, d\epsilon$, which can be simplified by integration by parts to give $-4\int_0^\infty \epsilon^3 f\, d\epsilon$. When we use these results and equation (2.47), we obtain

$$\pi^2 \left\{ \frac{\partial}{\partial \eta} + \frac{dx^i}{d\eta}\frac{\partial}{\partial x^i} + \frac{d\gamma_p^i}{d\eta}\frac{\partial}{\partial \gamma_p^i} + 4\left(\frac{1}{a}\frac{da}{d\eta} + \frac{\partial \Phi}{\partial \eta} + \gamma_p^i \frac{\partial \Psi}{\partial x^i}\right)\right\} [\rho_\gamma(4\Theta+1)] = \frac{a}{a_0}\int_0^\infty \epsilon^3 C[f]\, d\epsilon\,.$$

Recall that the average energy density of photons is proportional the a^{-4}. Thus $\frac{\partial \rho_\gamma}{\partial \eta} = -4\rho_\gamma \frac{1}{a}\frac{da}{d\eta}$. With this and definition (2.42) the above equation reads to the first order

$$\frac{\partial \Theta}{\partial \eta} + \gamma_p^i \frac{\partial}{\partial x^i}(\Theta + \Psi) + \frac{d\gamma_p^i}{d\eta}\frac{\partial \Theta}{\partial \gamma_p^i} + \frac{\partial \Phi}{\partial \eta} = \frac{a}{a_0}\frac{1}{4\pi^2 \rho_\gamma}\int_0^\infty \epsilon^3 C[f]\, d\epsilon\,. \tag{2.48}$$

Here Ψ is not a function of $\vec{\gamma}$ and $\gamma_p^i = \frac{dx^i}{d\eta}$ to the zeroth order. So we arrive at the very compact form

$$\frac{d}{d\eta}(\Theta + \Psi) + \frac{\partial}{\partial \eta}(\Phi - \Psi) = \frac{a}{a_0}\frac{1}{4\pi^2 \rho_\gamma}\int_0^\infty \epsilon^3 C[f]\, d\epsilon\,, \tag{2.49}$$

which is called the *brightness equation*.

The collision term appearing in (2.49) is tedious to derive. The familiar formulas for Compton scattering from particle physics cannot be used, since we need a low energy (Thomson scattering) limit whereas in particle physics the high energy limit is the interesting one. In particle physics the electron mass can be neglected (or more precisely the results can be written as a Taylor series of mass). In our case, the temperature (energy) is less than the electron mass. Thus we need an expansion in terms of $1/m_e$. After about 20 pages of calculations one gets up to the second order [90, 91]

$$C[f] = C_0 + C_{v_b} + C_{v_b^2} + C_{T_e/m_e} + C_{p/m_e} + C_{v_b p/m_e} + C_{(p/m_e)^2}\,.$$

Upon integration on the right hand side of (2.49) only terms C_0 and C_{v_b} lead to the zeroth and first order contributions. C_0 accounts for the direction dependence of the photon distribution function. C_{v_b} describes the Doppler effect of photons scattering from baryons that have velocity v_b. The end result is

$$\frac{d}{d\eta}(\Theta + \Psi) + \frac{\partial}{\partial \eta}(\Phi - \Psi) = \frac{d\tau}{d\eta}[(\Theta_0 - \Theta) + \frac{1}{16}\gamma_i\gamma_j \Pi_\gamma^{ij} + \gamma_i v_b^i]\,, \tag{2.50}$$

where the anisotropic stress Π^{ij} comes from the quadrupole moment of the photon distribution function. It is given by

$$\Pi_\gamma^{ij} = \int \frac{d\Omega}{4\pi}\left[3\gamma^i\gamma^j - \left(\frac{a}{a_0}\right)^2 \gamma^{ij}\right] 4\Theta\,. \tag{2.51}$$

The optical depth τ due to Thomson scattering is defined through the scattering rate $d\tau/dt = n_{\text{free}}(t)\sigma_T$, where $n_{\text{free}} = x_e n_e$ is the number density of free electrons, $\sigma_T = 8\pi\alpha^2/3m_e^2$ is the Thomson cross section, and $\alpha = 1/137.03599976$ is the fine structure constant. Returning to SI units $\sigma_T = 8\pi\alpha^2(h/2\pi)^2/(3m_e^2c^2) = 6.65246 \times 10^{-29}\text{m}^2$. (Actually, α could be time varying, but the CMB data indeed implies that the difference to

today's value is at most of a few per cent [177–180].)

The brightness equation (2.50) is our basic tool in calculating the evolution of temperature perturbations. The evolution equations of previous sections for other perturbations are needed to complete our set of equations to solve $\vec{v}_b$, Ψ, Φ and Π^{ij} appearing in the brightness equation.

2.5 Decomposed brightness equation, the Boltzmann hierarchy

In Appendix A.2 we present a multipole expansion for a function with a position and direction dependence. [In the flat space it simplifies to (1.44).] As the temperature perturbation function Θ in the brightness equation (2.50) is of this type we plug in there the multipole expansion and read the resulting equation for each individual multipole (see Appendix A.3). The result is a Boltzmann hierarchy for the temperature perturbation, see e.g. [91, 172, 174, 181],

$$\begin{aligned}
\dot{\Theta}_0 &= -\frac{k}{3}\Theta_1 - \dot{\Phi},\\
\dot{\Theta}_1 &= k\left[\Theta_0 + \Psi - \frac{2}{5}K_2^{1/2}\Theta_2\right] - \dot{\tau}(\Theta_1 - V_b),\\
\dot{\Theta}_2 &= k\left[\frac{2}{3}K_2^{1/2}\Theta_1 - \frac{3}{7}K_3^{1/2}\Theta_3\right] - \dot{\tau}\frac{9}{10}\Theta_2,\\
\dot{\Theta}_\ell &= k\left[\frac{\ell}{2\ell-1}K_\ell^{1/2}\Theta_{\ell-1} - \frac{\ell+1}{2\ell+3}K_{\ell+1}^{1/2}\Theta_{\ell+1}\right] - \dot{\tau}\Theta_\ell \quad (\ell > 2)\,,
\end{aligned} \tag{2.52}$$

where

$$K_\ell = 1 - (\ell^2 - 1)K/k^2, \quad \ell \geq 1. \tag{2.53}$$

Now we have achieved from the Boltzmann equation (2.41) a set of coupled differential equations for Θ_ℓ, which could be solved numerically. In a typical calculation of the angular power spectrum the whole hierarchy (2.52) must be solved up to $\ell_{\max} \sim 2 \times 10^3$. This takes enormous computer time. Thus, in practice, instead of solving the full Boltzmann hierarchy, the line of sight integration method is used. (See Sec. 2.8 for an implementation of this method.)

We will return to the Boltzmann hierarchy in Secs. 2.6 and 2.7. However, let us say something already at this stage. The relative velocity of the photon fluid and the background frame causes the temperature shift through the Doppler effect: $\frac{\delta T}{T} = \vec{v_\gamma}\cdot\vec{\gamma}$. So it produces a dipole perturbation. Writing this in k-space, we get $\Theta_1 = V_\gamma$, where V_γ is defined similar to V_b in (A.48). Before recombination the multiple scattering tends to make the photon distribution isotropic in the electron (baryon) rest frame. Hence, before the time of recombination, it is a good approximation to take $V_\gamma \approx V_b$ and $\Theta_\ell \approx 0$ for $\ell > 1$. This means that basically we have only monopole (Θ_0) and dipole (Θ_1) perturbations at the last scattering surface. Then the perturbations start to spread towards higher and higher multipoles as the photons freely stream to us. Actually, this is easy to see from (2.52). First the time derivative of Θ_2 is positive (if $\Theta_1(\eta_*)$ is positive)

while the time derivatives of Θ_3 etc. are zero. Thus Θ_2 begins to grow. As it becomes positive the time derivative of Θ_3 turn from zero to positive and Θ_3 starts to grow and so on. (Note that after the last scattering $\dot{\tau}$ is zero, if there is no reionization.) This mapping of spatial perturbations of the last scattering surface into the anisotropies seen today is just what one would have expected.

We can use the same equation (2.52) for (massless, non-interacting) neutrinos, too. If we denote neutrino temperature perturbations by $N(\eta, \vec{x}, \vec{\gamma})$, we just have to replace Θ_ℓ with N_ℓ. Since neutrinos decouple at very early times, we can set $\dot{\tau} = 0$ in any practical neutrino calculation.

2.6 Identifying the source terms

Now it is time to identify the source terms ζ_x and ξ_x appearing in (2.12) and (2.23), respectively. As already mentioned these are zero for the total matter as well as for noninteracting species such as CDM and neutrinos.

Substituting $\Theta_0 = \delta_\gamma/4$ and $\Theta_1 = V_\gamma$ into the first equation of the Boltzmann hierarchy (2.52) gives

$$\dot{\delta}_\gamma = -(4/3)kV_\gamma - 4\dot{\Phi} = -(1 + w_\gamma)(kV_\gamma + 3\dot{\Phi})\,, \tag{2.54}$$

where $w_\gamma = 1/3$. Comparison of this equation with (2.12) leads to $\zeta_\gamma = 0$. From (2.5) we get $\zeta_b = 0$. Hence we can immediately write equation (2.12) for baryons ($w_b = 0$)

$$\dot{\delta}_b = -kV_b - 3\dot{\Phi}. \tag{2.55}$$

Together equations (2.54) and (2.55) lead to a very useful relation

$$\dot{\delta}_b - \frac{3}{4}\dot{\delta}_\gamma = k(V_\gamma - V_b), \tag{2.56}$$

which gives the evolution of the perturbation in the photon entropy per baryon, see definition (2.15),

$$\dot{\mathcal{S}}_{b\gamma} = k(V_\gamma - V_b)\,. \tag{2.57}$$

This result should be easy to believe on intuitive grounds, too. If the photon and baryon velocities are equal, then their relative number density at a fixed point remains constant and thus also the entropy perturbation is constant in time. On the other hand, if the velocities differ, then for example more baryons than photons flow from one area to another, and the relative number density changes. The rate of this change is just $k(V_\gamma - V_b)$ when expressed in k-space.

Similarly, because $\zeta_x = 0$ for $x \in \{b, c, \gamma, \nu\}$, we find that

$$\mathcal{H}^{-1}\dot{\mathcal{S}}_{x\gamma} = -\mathcal{H}^{-1}\, k\, (V_x - V_\gamma) \tag{2.58}$$

holds for all of our particle species. Hence, the relative entropy perturbation $\mathcal{S}_{x\gamma}$ remains constant on superhorizon scales $\mathcal{H}^{-1}k \ll 1$.

To derive the other source term, ξ_γ, we substitute into the second equation in (2.52)

again $\Theta_0 = \delta_\gamma/4$ and $\Theta_1 = V_\gamma$, which leads to

$$\dot{V}_\gamma = \frac{1}{4}k\delta_\gamma - \frac{2}{5}(1-3K/k^2)^{1/2}k\Theta_2 + k\Psi - \dot{\tau}(V_\gamma - V_b). \tag{2.59}$$

On the other hand, remembering that $c_\gamma^2 = 1/3 = w_\gamma$ and $\mathcal{S}_\gamma = 0$, we have from the Euler equation (2.23)

$$\dot{V}_\gamma = \frac{1}{4}k\delta_\gamma - \frac{2}{3}\frac{1}{4}(1-3K/k^2)k\tilde{\Pi}_\gamma + k\Psi - \frac{3}{4}\frac{\xi_\gamma}{\rho_\gamma}. \tag{2.60}$$

Equations (2.59) and (2.60) are valid after recombination as well as before it. After recombination there is no Compton scattering i.e. the photons do not interact with baryons. Hence the Compton scattering term $\dot{\tau}$ in (2.59) and source term ξ_γ in (2.60) both vanish after the last scattering. Now, comparison of these two equations allows us to make an identification

$$\frac{2}{5}(1-3K/k^2)^{1/2}k\Theta_2 = \frac{2}{3}\frac{1}{4}(1-3K/k^2)k\tilde{\Pi}_\gamma.$$

Recalling that $\tilde{\Pi}_\gamma = \frac{3}{2}(1-3K/k^2)^{-1/2}\Pi_\gamma$ (see comment after equation (1.41)), this relation gives the anisotropic stress in terms of the quadrupole temperature perturbation,

$$\Pi_\gamma = \tfrac{8}{5}\Theta_2. \tag{2.61}$$

Before recombination $\dot{\tau}$ and ξ_γ are nonzero due to the Compton scattering. In this case, again the comparison of equations (2.59) and (2.60) gives

$$\xi_\gamma = \frac{4}{3}\rho_\gamma\dot{\tau}(V_\gamma - V_b). \tag{2.62}$$

Actually, this is not an interesting result, since we already knew this from the previous section. However, using (2.5) we get something new, i.e., we find that

$$\xi_b = -\frac{4}{3}\rho_\gamma\dot{\tau}(V_\gamma - V_b). \tag{2.63}$$

Hence the Euler equation (2.23) for baryons ($w_b = c_b = \mathcal{S}_b = 0$) reads as

$$\dot{V}_b = -\frac{\dot{a}}{a}V_b + k\Psi + \frac{4}{3}\frac{\rho_\gamma}{\rho_b}\dot{\tau}(V_\gamma - V_b). \tag{2.64}$$

2.7 Small-scale solution

2.7.1 Tight coupling approximation

As a particular k-mode enters the horizon, the velocities of different particle species start to evolve differently. Before recombination, photons and baryons still have equal velocities above the photon diffusion scale because of the tight coupling caused by Compton scattering. On the other hand, decoupled components, such as neutrinos, stream freely leading to a change in the entropy perturbation, e.g., change in $\mathcal{S}_{\nu\gamma}$.

In this section we investigate the photon-baryon fluid. We start with the tight coupling approximation, i.e., we assume that the Compton scattering time $\dot{\tau}^{-1}$ is very small, which yields the equation for (driven) acoustic oscillations, where the photon pressure resists the gravitational compression. In Sec. 2.7.3 we repeat the calculations up to second order

in $\dot\tau^{-1}$ and find that the oscillations are damped by photon diffusion. We emphasize that even before recombination the tight coupling approximation fails on superhorizon scales, since for them $\dot\tau = 0$. For this reason we have treated also the temperature perturbation Θ separately for superhorizon case at the end of Sec. 2.3.

Before recombination, on subhorizon scales the decomposed Boltzmann equation (2.52) can be solved iteratively with help of the baryon perturbation continuity equation (2.55) and the baryon Euler equation (2.64). So we are looking for a solution to the following coupled equations:

$$\dot\Theta_0 = -\frac{k}{3}\Theta_1 - \dot\Phi, \tag{2.65}$$

$$\Theta_1 - V_b = \dot\tau^{-1}[-\dot\Theta_1 + k(\Theta_0 + \Psi)], \tag{2.66}$$

$$\dot\delta_b = -kV_b - 3\dot\Phi, \tag{2.67}$$

$$\dot V_b = -\frac{\dot a}{a}V_b + k\Psi + \dot\tau(V_\gamma - V_b)/R, \tag{2.68}$$

where we put

$$R \stackrel{\text{def}}{=} \frac{3\rho_b}{4\rho_\gamma} = \frac{3\rho_b(\eta_{\rm eq})\, y^{-3}}{4\rho_\gamma(\eta_{\rm eq})\, y^{-4}} = y\,\frac{3\rho_b(\eta_{\rm eq})}{4\rho_\gamma(\eta_{\rm eq})} = yR_{\rm eq}, \tag{2.69}$$

and recall $\Theta_1 = V_\gamma$. Note that at the time of equality $\rho_r = \rho_m$ but ρ_b and ρ_γ are not necessarily equal. Thus, in general, $R_{\rm eq} \neq 3/4$ and R differs from $(3/4)y$. In fact, using the conventions of Sec. 2.1.2 we may write

$$R_{\rm eq} = \frac{3}{4}\frac{(\Omega_b/\Omega_m)\rho_m(\eta_{\rm eq})}{(1-X_\nu)\rho_r(\eta_{\rm eq})} = \frac{3}{4}X_b(1-X_\nu)^{-1}. \tag{2.70}$$

Equation (2.68) can be rewritten as

$$V_b = \Theta_1 - \dot\tau^{-1}R\left(\dot V_b + \tfrac{\dot a}{a}V_b - k\Psi\right). \tag{2.71}$$

Actually it is this equation, which we will iterate to find V_b. Then V_b is put into (2.66) in order to find an equation for the dipole temperature perturbation Θ_1.

To zeroth order in $\dot\tau^{-1}$ (that is when $\dot\tau^{-1} = 0$) equation (2.71) gives $V_b^{(0)} = \Theta_1$, i.e., $V_b^{(0)} = V_\gamma$. The higher multipole equations in (2.52) lead to $\Theta_\ell = 0$ for $\ell \geq 2$. Now substituting $\dot\Phi$ from (2.65) into (2.67) we obtain $\dot\Theta_0 = \dot\delta_b/3$. In addition, from (2.57) we find that $\dot{\mathcal{S}}_{b\gamma} = 0$, which leads to $\dot\delta_b - 3\dot\delta_\gamma/4 = 0$.

Putting the zeroth order result $V_b^{(0)} = \Theta_1$ back into the right hand side of (2.71) we find the iterative first order result

$$V_b^{(1)} = \Theta_1 - \dot\tau^{-1}R\left(\dot\Theta_1 + \tfrac{\dot a}{a}\Theta_1 - k\Psi\right). \tag{2.72}$$

Substituting this into (2.66) gives the differential equation for Θ_1, see (2.74) below. Note that equation (2.65) remains unchanged and $R\dot a/a$ can be written with help of the continuity equation (2.6) as $\dot R$. Hence the first order result for the temperature perturbations is

$$\dot\Theta_0 = -\frac{k}{3}\Theta_1 - \dot\Phi, \tag{2.73}$$

$$\dot\Theta_1 = -\frac{\dot R}{1+R}\Theta_1 + \frac{1}{1+R}k\Theta_0 + k\Psi. \tag{2.74}$$

These are usually combined into a single second order differential equation for Θ_0. This is done by differentiating the upper equation, and then substituting into the resulting equation the terms $\dot{\Theta}_1$ from the lower and Θ_1 from the upper equation. By this way we arrive at the *basic equation for acoustic oscillations* [91, 94, 172–174]

$$\ddot{\Theta}_0(\eta) + \frac{\dot{R}(\eta)}{1+R(\eta)}\dot{\Theta}_0(\eta) + k^2\tilde{c}_s^2(\eta)\Theta_0(\eta) = G(\eta), \tag{2.75}$$

where

$$G = -\ddot{\Phi} - \frac{\dot{R}}{1+R}\dot{\Phi} - \frac{k^2}{3}\Psi \tag{2.76}$$

is the "gravitational" forcing function and

$$\tilde{c}_s^2 = \frac{1}{3}\frac{1}{1+R} \tag{2.77}$$

is the square of the sound speed in the photon-baryon fluid.[2]

Adding on and subtracting a term $k^2\tilde{c}_s^2\Phi$ we see that (2.75) takes a form [94]

$$\left\{\frac{d^2}{d\eta^2} + \frac{\dot{R}}{1+R}\frac{d}{d\eta} + k^2\tilde{c}_s^2\right\}[\Theta_0 + \Phi] = F\,, \tag{2.78}$$

with $F \stackrel{\text{def}}{=} \frac{k^2}{3}\left(3\tilde{c}_s^2\Phi - \Psi\right)$. Note that if the sound speed $\tilde{c}_s$ (and R) was a constant and the forcing function F was zero (or constant), we would get a (forced) harmonic oscillator with an angular frequency $\omega = k\tilde{c}_s$. As a shorthand notation we start to write $A(\eta) \stackrel{\text{def}}{=} \Theta_0(\eta) + \Phi(\eta)$, since this quantity will undergo acoustic oscillations.

2.7.2 The WKB approximation

Now we derive an approximative general solution to equation (2.78). Our first task is to solve the homogeneous ($F = 0$) equation. This is done by the WKB approximation (see e.g. [182]). Since equation (2.78) is very similar to the harmonic oscillator, we try an oscillating solution of the form [183]

$$A = \exp[iu(\eta)], \tag{2.79}$$

where $u(\eta)$ is an arbitrary continuous function. Actually, in the absence of the "friction term" $\dot{R}/(1+R)$ in (2.78) u would be just $k\tilde{c}_s$. The friction is expected to cause only a little difference in a form of damping: $u = k\tilde{c}_s + iB$, where B is a function of R.

To proceed we need to assume

$$k^2\tilde{c}_s^2 \gg \frac{\dot{R}^2}{(1+R)^2} \quad \text{(approximation 1)}. \tag{2.80}$$

[2]The photon-baryon sound speed squared is

$$\tilde{c}_s^2 \stackrel{\text{def}}{=} \frac{\dot{p}_\gamma}{\dot{\rho}_\gamma + \dot{\rho}_b} = \frac{1}{3}\frac{1}{1+\dot{\rho}_b/\dot{\rho}_\gamma} = \frac{1}{3}\frac{1}{1+R},$$

where the last step follows from the continuity equation (2.6) and we put tilde in order to make a difference with the sound speed in the whole fluid.

This is clearly valid if we consider small enough scale (large enough k). Indeed, from $\dot{R} = R(\dot{a}/a) = R\mathcal{H}$ it follows that

$$\frac{\dot{R}^2}{(1+R)^2} = \frac{R^2}{(1+R)^2}\mathcal{H}^2. \tag{2.81}$$

Thus, the assumption (2.80) can be rewritten as

$$k^2 \gg \frac{3R^2}{1+R}\mathcal{H}^2 \stackrel{\text{def}}{=} f_1(R)\mathcal{H}^2. \tag{2.82}$$

The R factor $f_1(R)$ is a growing function of time. So we have $f_1(R) \leq f_1(R_*)$, since we consider the time before recombination. With $X_\nu = 0.405$ we find from (2.69) with help of (2.70) and (1.20)

$$R_* = y_* \frac{3}{4}\frac{\omega_b}{\omega_m} \times 1.68 \simeq 30\omega_b(10^3/z_*)\,, \tag{2.83}$$

where z_* depends only weakly on ω_m and ω_b, see [184]. For $\omega_b = 0.02$ we obtain $R_* = 0.55$ and even for $\omega_b = 0.04$ we have $R_* = 1.09$. Thus for realistic models $R_* \lesssim 1$, which yields $\sqrt{f_1(R)} < \sqrt{3/2} \approx 1.2$. Therefore the assumption (2.80) is valid for small enough subhorizon scales that obey $k/\mathcal{H} \gg 1.2$. Note that we obtained the number 1.2 by demanding that (2.80) is valid before the last scattering. However, the numerical factor would be less than 0.2 (for $\omega_b = 0.02$ and $\omega_m = 0.147$), if we wanted the validity only until equality. Hence, (2.80) is clearly true for all subhorizon modes before equality.

In parallel with (2.80) we need to assume that $\ddot{R}/(1+R)$ is small compared to $(k\tilde{c}_s)^2$ and $(k\tilde{c}_s)\dot{R}/(1+R)$. But $\ddot{R} = \frac{d}{d\eta}(R\mathcal{H}) = R(\mathcal{H}^2 + \dot{\mathcal{H}})$, and differentiating the Friedmann equation (1.11)

$$\mathcal{H}^2 = H_0^2\left[\Omega_r\left(\frac{a_0}{a}\right)^2 + \Omega_m\left(\frac{a_0}{a}\right) + \Omega_k + \Omega_\Lambda\left(\frac{a}{a_0}\right)^2\right] \tag{2.84}$$

we find a formula for $2\mathcal{H}\dot{\mathcal{H}}$, which finally leads to

$$\mathcal{H}^2 + \dot{\mathcal{H}} = H_0^2\left[\frac{1}{2}\Omega_m\left(\frac{a_0}{a}\right) + \Omega_k + 2\Omega_\Lambda\left(\frac{a}{a_0}\right)^2\right]. \tag{2.85}$$

In the pure RD era this is zero, in the MD era $\frac{1}{2}\mathcal{H}^2$, in the CD era $\mathcal{H}^2$, and in the ΛD era $2\mathcal{H}^2$. As we consider here the RD era and the beginning of the MD era, we conclude that $\mathcal{H}^2 + \dot{\mathcal{H}} < \mathcal{H}^2$. Now $\ddot{R}/(1+R) < [R/(1+R)]\mathcal{H}^2$, and we arrive at

$$\frac{\ddot{R}}{1+R}\Big/\tilde{c}_s^2 < 3R\mathcal{H}^2 \stackrel{\text{def}}{=} f_2(R)\mathcal{H}^2. \tag{2.86}$$

Therefore we have

$$\frac{\ddot{R}}{1+R} \ll k^2\tilde{c}_s^2, \quad \text{(approximation 2)} \tag{2.87}$$

if $k/\mathcal{H} \gg \sqrt{f_2(R)}$, where $f_2(R) = 3R < 3R_* \lesssim 3$ (for $\omega_b < 0.04$). So we need $k/\mathcal{H} \gg 1.7$ in order that (2.87) is surely valid. Finally,

$$\frac{\ddot{R}}{1+R}\Big/\frac{\tilde{c}_s\dot{R}}{1+R} = \frac{R(\mathcal{H}^2+\dot{\mathcal{H}})}{R\mathcal{H}}\sqrt{3(1+R)} < \frac{\mathcal{H}^2}{\mathcal{H}}\sqrt{3(1+R)} = \mathcal{H}f_3(R) \tag{2.88}$$

where $f_3(R) = \sqrt{3(1+R)}$. Thus

$$\frac{\ddot{R}}{1+R} \ll k\tilde{c}_s \frac{\dot{R}}{1+R}\,, \quad \text{(approximation 3)} \tag{2.89}$$

if $k/\mathcal{H} \gg f_3(R)$, i.e., $k/\mathcal{H} \gg 2.4$ for $\omega_b < 0.04$.

As we now know that assumptions (2.80), (2.87), and (2.89) are valid when the perturbation is well inside the horizon, we can continue to find u of (2.79). Substituting (2.79) into (2.78) gives

$$\dot{u}^2 = i\ddot{u} + \tfrac{\dot{R}}{1+R} i\dot{u} + k^2\tilde{c}_s^2. \tag{2.90}$$

To first approximation we assume that $\ddot{u}$ is negligible, which can be shown to hold on subhorizon scales along the similar lines as the previous approximations. Thus from (2.90) we obtain a second degree equation for $\dot{u}$ with the solution

$$\dot{u}_0 = \tfrac{i}{2}\tfrac{\dot{R}}{1+R} \pm k\tilde{c}_s, \tag{2.91}$$

where we used the assumption (2.80) and put the subscript zero to remind that this is only a zeroth order approximation. Integrating this we get

$$u_0 = \tfrac{i}{2}\ln|1+R| \pm k\textstyle\int^\eta \tilde{c}_s(\eta')d\eta'. \tag{2.92}$$

We continue to find an iterative first order solution u_1 by substituting u_0 into the right hand side of (2.90)

$$\begin{aligned}\dot{u}_1^2 &= i\ddot{u}_0 + \frac{\dot{R}}{1+R} i\dot{u}_0 + k^2\tilde{c}_s^2 \\ &= -\tfrac{1}{2}\tfrac{\ddot{R}}{1+R} \pm \tfrac{i}{2}\tfrac{\dot{R}}{1+R} k\tilde{c}_s + k^2\tilde{c}_s^2\,.\end{aligned} \tag{2.93}$$

Applying the approximations (2.87) and (2.89) we can drop the $\ddot{R}/(1+R)$ term and write

$$\begin{aligned}\dot{u}_1 &\approx \pm k\tilde{c}_s\left[1 \pm \tfrac{i}{2}\tfrac{\dot{R}}{1+R}/(k\tilde{c}_s)\right]^{1/2} \\ &\approx \pm k\tilde{c}_s + \tfrac{i}{4}\tfrac{\dot{R}}{1+R}\,,\end{aligned} \tag{2.94}$$

where, in the second step, we took two first terms of the Taylor expansion. Finally we get

$$A = e^{iu} \approx e^{iu_1} = e^{-\frac{1}{4}\int^\eta \frac{\dot{R}}{1+R}d\eta' \pm ik\int^\eta \tilde{c}_s d\eta'}. \tag{2.95}$$

Performing the integrals, we find two independent solutions to the homogeneous equation (2.78). They are

$$\begin{aligned}A_a(\eta) &= [1+R(\eta)]^{-1/4} e^{-ikr_s(\eta)} \\ A_b(\eta) &= [1+R(\eta)]^{-1/4} e^{ikr_s(\eta)},\end{aligned} \tag{2.96}$$

where the sound horizon is

$$\begin{aligned}r_s(\eta) &= \int_{\eta_i}^{\eta} \tilde{c}_s d\eta' = \frac{1}{\sqrt{3}}\int_0^R \frac{1}{\sqrt{1+R'}}\frac{d\eta'}{dy'}\frac{dy'}{dR'}dR' \\ &= \frac{1}{\sqrt{3}}\int_0^R \frac{1}{\sqrt{1+R'}}\frac{1}{\dot{y}'}\frac{1}{R_{\rm eq}}dR'\end{aligned}$$

$$
\begin{aligned}
&= \frac{\sqrt{2}}{\sqrt{3}}\frac{1}{k_{\rm eq}}\frac{1}{\sqrt{R_{\rm eq}}}\int_0^R \frac{1}{\sqrt{R_{\rm eq}y'R + (R_{\rm eq}y' + R_{\rm eq}R') + R_{\rm eq}}}dR' \\
&= \frac{\sqrt{2}}{\sqrt{3}}\frac{1}{k_{\rm eq}}\frac{1}{\sqrt{R_{\rm eq}}}\int_0^R \frac{1}{\sqrt{R'^2 + (1+R_{\rm eq})R' + R_{\rm eq}}}dR' \\
&= \frac{\sqrt{2}}{\sqrt{3}}\frac{1}{k_{\rm eq}}\frac{1}{\sqrt{R_{\rm eq}}}\ln\frac{2\sqrt{R^2 + (1+R_{\rm eq})R + R_{\rm eq}} + 2R + R_{\rm eq} + 1}{2\sqrt{R_{\rm eq}} + R_{\rm eq} + 1} \\
&= \frac{\sqrt{2}}{\sqrt{3}}\frac{1}{k_{\rm eq}}\frac{1}{\sqrt{R_{\rm eq}}}\ln\left(\frac{\sqrt{1+R} + \sqrt{R+R_{\rm eq}}}{1+\sqrt{R_{\rm eq}}}\right)^2 \\
&= \frac{2}{3}\frac{1}{k_{\rm eq}}\sqrt{\frac{6}{R_{\rm eq}}}\ln\frac{\sqrt{1+R} + \sqrt{R+R_{\rm eq}}}{1+\sqrt{R_{\rm eq}}}. \qquad (2.97)
\end{aligned}
$$

In the first line we used equation (2.69) to get $\frac{dy}{dR} = 1/R_{\rm eq}$, then we wrote $\dot{y} = \frac{\sqrt{1+y}}{\sqrt{2}}k_{\rm eq}$, and used again (2.69) to write $R_{\rm eq}y = R$. Finally, the integral was taken from tables.[3]

Using an elementary method called *variation of constants*[4] we construct a particular solution A_p to the full equation (2.78)

$$
\begin{aligned}
A_p(\eta) &= \int_{\eta_i}^{\eta} \frac{A_a(\eta')A_b(\eta) - A_a(\eta)A_b(\eta')}{A_a(\eta')\dot{A}_b(\eta') - \dot{A}_a(\eta')A_b(\eta')}F(\eta')d\eta' \\
&= \frac{\sqrt{3}}{k}[1+R(\eta)]^{-1/4}\int_{\eta_i}^{\eta}[1+R(\eta')]^{3/4}\sin[kr_s(\eta) - kr_s(\eta')]F(\eta')d\eta'. \qquad (2.98)
\end{aligned}
$$

Now the full solution is

$$
\hat{A} = \tilde{C}_1 A_a + \tilde{C}_2 A_b + A_p = C_1[1+R]^{-1/4}\cos kr_s + C_2[1+R]^{-1/4}\sin kr_s + A_p, \qquad (2.99)
$$

where $C_1 = \tilde{C}_1 + \tilde{C}_2$, $C_2 = i(\tilde{C}_2 - \tilde{C}_1)$ and the hat reminds us of the fact that this is the undamped, i.e., the first order solution in the Compton scattering time $\dot{\tau}^{-1}$.

The initial conditions are

$$
\hat{A}(\eta_i) = A(\eta_i) \qquad \text{and} \qquad \dot{\hat{A}}(\eta_i) = \dot{A}(\eta_i), \qquad (2.100)
$$

since the diffusion damping has not had time to alter the amplitude of the perturbation yet. Realizing that $R(\eta_i) = r_s(\eta_i) = 0$ and $\dot{r}_s = \tilde{c}_s$, we find the constants C_1 and C_2. (Note that we set the initial condition in very early radiation-dominated era when $y \ll 1$.) The final solution is

$$
[1+R(\eta)]^{1/4}\hat{A}(\eta) = A(\eta_i)\cos kr_s(\eta) + \frac{\sqrt{3}}{k}[\dot{A}(\eta_i) + \frac{1}{4}\dot{R}(\eta_i)A(\eta_i)]\sin kr_s(\eta)
$$

---

[3] Mathematical handbook [185] gives

$$
\int \frac{dx}{\sqrt{ax^2+bx+c}} = \frac{1}{\sqrt{a}}\ln\left(2\sqrt{a}\sqrt{ax^2+bx+c} + 2ax + b\right).
$$

Since the logarithm obeys $\ln(a^b) = b\ln a$, it is possible to write the answer in tens of forms. We wrote the final expression for r_s in three different forms in order to make it easier to compare with the literature.

[4] Terms "variation of parameters" and "Lagrange's method" are also commonly used , see [186, 187].

$$+ \frac{\sqrt{3}}{k}\int_{\eta_i}^{\eta} d\eta'[1+R(\eta')]^{3/4}\sin[kr_s(\eta)-kr_s(\eta')]F(\eta'). \qquad (2.101)$$

Using (2.73) this gives immediately also the dipole perturbation, $\hat{\Theta}_1 = -\frac{3}{k}\dot{\hat{A}}$.

2.7.3 Diffusion damping

From physical intuition we know that diffusion damping affects very small scales (see Fig. 2.1), i.e., well below the sound horizon r_s, which is always smaller than the horizon $\sim \eta$. Let us show that on these scales the potentials can be neglected in the first approximation at the late radiation-dominated epoch.

From the Poisson equation (2.30) with (1.15) we have $\Phi \sim (k\eta)^{-2}\Delta_T$, where $\Delta_T \sim \Delta_\gamma = 4(\Theta_0 + \frac{\dot{a}}{a}V_T/k) = 4(\Theta_0 + \frac{1}{k\eta}V_T)$. But Θ_0 is oscillating and $\frac{1}{k\eta}V_T$ is small on subhorizon scales $k\eta \gg 1$. Thus the potentials Φ and Ψ are damped as $(k\eta)^{-2}$. The same kind of analysis shows that also the derivatives of the potentials decay away. So we set $F = 0$ in (2.78) and use the solution of the homogeneous equation

$$\hat{\Theta}_0 = C_A[1+R]^{-1/4}\cos kr_s + C_I[1+R]^{-1/4}\sin kr_s \qquad (2.102)$$

on small scales in the late radiation-dominated epoch. To get a diffusion damped solution we introduce a damping factor such that

$$\Theta_0 = \mathcal{D}(\eta,k)\hat{\Theta}_0, \qquad (2.103)$$

where

$$\mathcal{D}(\eta,k) = e^{-(k/k_D)^2}. \qquad (2.104)$$

Here k_D^{-1} is the damping scale. The magnitude of this is easy to guess. The mean free path of the photons is the Compton scattering time $\lambda_C = \dot{\tau}^{-1}$. The photon scatters $N = \eta/\lambda_C$ times in time η. On the other hand, the theory of random walk processes gives the diffusion scale $\lambda_D \sim \sqrt{N}\lambda_C = \sqrt{\lambda_C\eta} = \sqrt{\eta/\dot{\tau}}$, and we get $k_D^{-2} \sim \int \dot{\tau}^{-1}d\eta$.

To find an accurate diffusion scale we iterate (2.65) – (2.68) up to second order in $\dot{\tau}^{-1}$. The second order iterative solution for V_b is found by substituting the first order result $V_b^{(1)}$ from (2.72) into the right hand side of equation (2.71)

$$\begin{aligned}
V_b^{(2)} &= \Theta_1 - \dot{\tau}^{-1}R\left\{\dot{V}_b^{(1)} + \tfrac{\dot{a}}{a}V_b^{(1)} - k\Psi\right\} \\
&= \Theta_1 - \dot{\tau}^{-1}R\left\{\frac{d}{d\eta}\left[\Theta_1 - \dot{\tau}^{-1}R\left(\dot{\Theta}_1 + \tfrac{\dot{a}}{a}\Theta_1 - k\Psi\right)\right]\right. \\
&\qquad \left. + \frac{\dot{a}}{a}\left[\Theta_1 - \dot{\tau}^{-1}R\left(\dot{\Theta}_1 + \tfrac{\dot{a}}{a}\Theta_1 - k\Psi\right)\right] - k\Psi\right\} \\
&= \Theta_1 - \dot{\tau}^{-1}R(\dot{\Theta}_1 + \tfrac{\dot{a}}{a}\Theta_1 - k\Psi) \\
&\qquad + \dot{\tau}^{-2}R^2\Big[\ddot{\Theta}_1 + 3\frac{\dot{R}}{R}\dot{\Theta}_1 + \Big(\frac{\ddot{R}}{R} + \frac{\dot{R}^2}{R^2}\Big)\Theta_1 - k\Big(2\frac{\dot{R}}{R}\Psi + \dot{\Psi}\Big)\Big] \\
&\qquad + \dot{\tau}^{-1}\frac{d}{d\eta}\Big(\dot{\tau}^{-1}\Big)R^2\left(\dot{\Theta}_1 + \tfrac{\dot{a}}{a}\Theta_1 - k\Psi\right). \qquad (2.105)
\end{aligned}$$

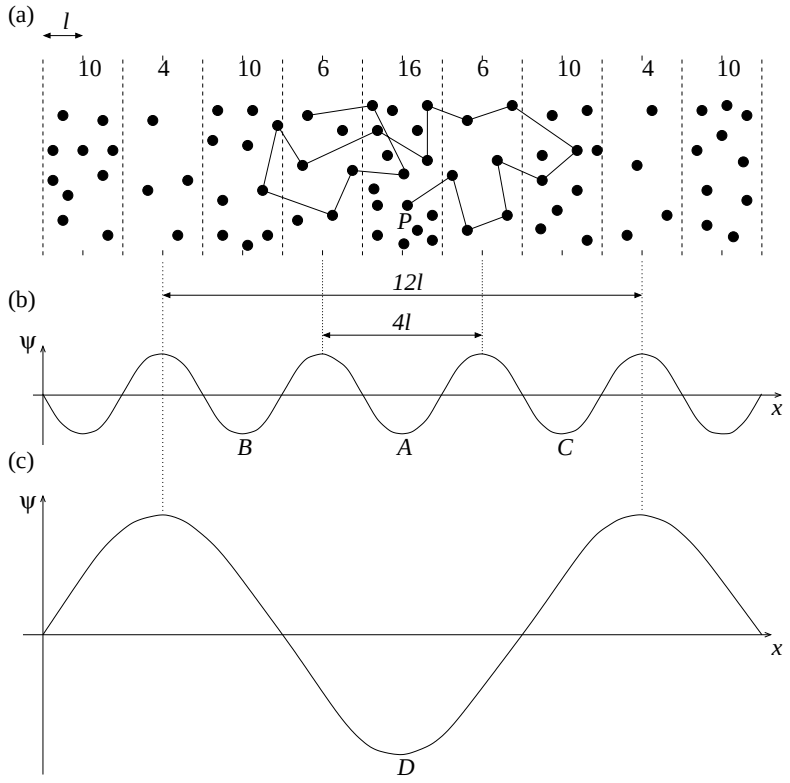

Figure 2.1: **The diffusion damping. (a)** Each point represents an electron, and l is a unit length. The number above each block of length $2l$ tells how many baryons there are in that block. The baryons are distributed spatially in a periodic way. At least two different periods can be found, $4l$ and $12l$. The average potentials on these scales are plotted in **(b)** and **(c)**, respectively. Here we show a situation where the tight coupling approximation is still valid on the larger scale ($\lambda = 12l$) but fails on the smaller scale ($\lambda = 4l$). We have plotted a path of one photon starting from point P as it random walks between the baryons. The mean free path is approximately $1.4l$. When observed on larger scale the photon stays in the potential well D where it started from. Instead, when looking on smaller scale, it starts from the potential well A but is able to climb up to the neighbouring hills or even to random walk to the nearest wells B or C. Thus, on this smaller scale, the photon distribution cannot retain the information about the potential wells and the spatial temperature differences are smoothed out.

On the last line, we have well before recombination $\frac{d}{d\eta}(\dot{\tau}^{-1}) = -\dot{\tau}^{-2}\ddot{\tau} \simeq 2\dot{\tau}^{-1}\frac{\dot{a}}{a}$, since the ionization fraction is practically a constant ($x_e = 1$) so that $(a_0/a)\dot{\tau} \propto n_{\rm free} \propto a^{-3}$.

As we know that the first order (i.e. undamped) result $\Theta_1^{(1)} \equiv \hat{\Theta}_1$ is oscillating (see the line after (2.101) with $F = 0 = \dot{\Phi}$), it is reasonable to assume that also to second order Θ_1 takes an oscillating form

$$\Theta_1^{(2)}(\eta) \propto e^{i\int^\eta \omega(\eta')d\eta'}, \tag{2.106}$$

where the angular frequency ω (possibly) depends on time. Again we expect that ω does not differ much from our previous first order (in $\dot{\tau}^{-1}$) solution $k\tilde{c}_s$.

Recall that $R = yR_{\rm eq}$ from (2.69) and $\dot{a}/a = \mathcal{H}$ from (1.15). Substituting these with (2.106) into (2.105), approximating $\omega \simeq k\tilde{c}_s$ when necessary, and performing similar

considerations that led to (2.80), (2.87), and (2.89) we find that all the terms containing $\dot{a}/a$, $\dot{R}$, or $\ddot{R}$ are small compared to the other terms if $k/\mathcal{H} \gg f(R)$, where $f(R)$ is some function of R for each term. The maximum value of $f(R)$ is for every term at most of the order of 1. So, again our approximation is valid for modes well inside the horizon before recombination. Assuming, in addition, that $\dot{\Psi}$ is negligible the second order result from (2.105) reads

$$V_b^{(2)} = \Theta_1 - \dot{\tau}^{-1}R(i\omega\Theta_1 - k\Psi) - \dot{\tau}^{-2}R^2\omega^2\Theta_1. \tag{2.107}$$

With this V_b, equation (2.66) gives

$$i\omega(1+R)\Theta_1 = k[\Theta_0 + (1+R)\Psi] - \dot{\tau}^{-1}R^2\omega^2\Theta_1. \tag{2.108}$$

Now we differentiate this. Assuming again that the potentials Ψ and Φ and the baryon to photon energy ratio R are very slowly varying when compared to ω, i.e., regarding terms containing $\dot{\omega}$, $\dot{R}$, $\dot{\Psi}$, or $\dot{\Phi}$ as higher order corrections [which is true for $k/\mathcal{H} \gg \mathcal{O}(1)$], the result is

$$-\omega^2(1+R)\Theta_1 = k\dot{\Theta}_0 - \dot{\tau}^{-1}R^2 i\omega^3\Theta_1. \tag{2.109}$$

Substituting $\dot{\Theta}_0 = -k\Theta_1/3$ from (2.65) we arrive at

$$(1+R)\omega^2 = k^2/3 + i\dot{\tau}^{-1}R^2\omega^3 \tag{2.110}$$

Of course, it would be possible to solve this third degree equation for ω exactly. However, in the spirit of iterative solution, we put the first order solution into the right hand side, $\omega^3 = \omega\omega^2 \approx \omega(k\tilde{c}_s)^2 = \omega\frac{k^2}{3}\frac{1}{1+R}$. Thus we get

$$(1+R)\omega^2 = \tfrac{k^2}{3} + i\dot{\tau}^{-1}\tfrac{k^2}{3}\tfrac{R^2}{1+R}\omega, \tag{2.111}$$

which has solutions

$$\begin{aligned}\omega &= \pm\frac{k}{\sqrt{3(1+R)}} + \frac{i}{6}k^2\dot{\tau}^{-1}\frac{R^2}{(1+R)^2} \\ &= \pm k\tilde{c}_s + \tfrac{i}{6}k^2\dot{\tau}^{-1}\tfrac{R^2}{(1+R)^2},\end{aligned} \tag{2.112}$$

where we dropped $\dot{\tau}^{-2}$ terms. Recall that we started from $\Theta_1 \propto e^{i\int^\eta \omega(\eta')d\eta'}$, which now gives

$$\Theta_1(\eta) \propto \exp\{\pm ikr_s(\eta)\}\exp\left\{-\frac{1}{6}k^2\int_{\eta_i}^{\eta}\dot{\tau}^{-1}(\eta')\frac{R^2(\eta')}{[1+R(\eta')]^2}d\eta'\right\}. \tag{2.113}$$

From here we read the damping factor to be $\mathcal{D} = e^{-(k/k_D)^2}$, with

$$k_D^{-2} = \frac{1}{6}\int_{\eta_i}^{\eta}\frac{1}{\dot{\tau}}\frac{R^2}{(1+R)^2}d\eta'. \tag{2.114}$$

Note that we ignored the quadrupole temperature perturbation Θ_2, which is also of second order. Fortunately, the effect of this is easy to take into account. Think of the third equation in the decomposed Boltzmann equation (2.52). With $\Theta_3 \approx 0 \approx \dot{\Theta}_2$, it gives

$$\Theta_2 = \frac{10}{9}\frac{2}{3}K_2^{1/2}\dot{\tau}^{-1}k\Theta_1. \tag{2.115}$$

This leads to the additional term $-\frac{2}{5}K_2\frac{10}{9}\frac{2}{3}\dot{\tau}^{-2}k^2\Theta_1 \approx -\frac{8}{27}\dot{\tau}^{-2}k^2\Theta_1$ to the right hand side of the second decomposed Boltzmann equation in (2.66), which in turn gives the contribution $-\frac{8}{27}\dot{\tau}^{-1}k^2\Theta_1$ to the right hand side of (2.108). Here we wrote $K_2 = 1 - 3K/k^2 \approx 1$, which is clearly valid on small scales. Now solving the resulting equation

$$(1+R)\omega^2 = \tfrac{k^2}{3} + i\dot{\tau}^{-1}k^2(\tfrac{1}{3}\tfrac{R^2}{1+R} + \tfrac{8}{27})\omega \tag{2.116}$$

instead of (2.111), leads finally to the accurate damping scale

$$k_D^{-2} = \frac{1}{6}\int_{\eta_i}^{\eta}\frac{1}{\dot{\tau}}\left[\frac{1}{1+R}\left(\frac{R^2}{1+R}+\frac{8}{9}\right)\right]d\eta'. \tag{2.117}$$

The R factor in the square brackets has the value $8/9$ when $R = 0$, the minimum value 0.69 is reached when $R = 8/10$, and after that it approaches 1 when $R \to \infty$. Thus it is all the time close to one, and we get $k_D^{-2} \approx \frac{1}{6}\int\frac{1}{\dot{\tau}}d\eta'$, which is in accordance with our earlier order of magnitude consideration.

One could derive a Boltzmann hierarchy very similar to (2.52) for CMB polarization multipoles Θ_ℓ^P (see e.g. equation A-4 in [172]). Actually, the polarization changes also (2.52) a little. The last term in the third line should read $-\dot{\tau}\left(\frac{9}{10}\Theta_2 - \frac{1}{10}\Theta_2^P - \frac{1}{2}\Theta_0^P\right)$ instead of $-\dot{\tau}\frac{9}{10}\Theta_2$, which we derived. To first order in $\dot{\tau}^{-1}$ one has $\Theta_2^P = \Theta_0^P = \frac{1}{4}\Theta_2$. Thus, instead of $\frac{10}{9}$ in (2.115) we should have $\left(\frac{9}{10} - \frac{1}{10}\frac{1}{4} - \frac{1}{2}\frac{1}{4}\right)^{-1} = \frac{4}{3}$. This is reflected in (2.117) by changing $\frac{8}{9}$ to $\frac{16}{15}$. So, polarization causes the diffusion damping to start on larger scales than in the case of unpolarized radiation.

2.7.4 Matching to the large-scale solution

In the beginning, perturbation of any scale has been a superhorizon one, if we go far enough backward in time. Thus the initial conditions for subhorizon perturbations, i.e., the constants in front of the cosine and sine in (2.101) or C_A and C_I in (2.102), should actually be determined at the time of horizon crossing $\eta_k^{\rm hor}$ to match the superhorizon solution. The exact numerical values of C_A and C_I depend on the total effect of the gravitational forcing function F in (2.98).

In the adiabatic case, finding C_A (or $\Theta_0(\eta_k^{\rm hor}) + \Phi(\eta_k^{\rm hor})$) is particularly easy, since Θ_0 and Φ remain constant in the radiation-dominated era. The results (2.36) and (2.40) lead to

$$C_A = \frac{3}{2}\Phi_i\,. \tag{2.118}$$

In the isocurvature case, the superhorizon solution (2.40) is $|\Theta_0| = \frac{1}{8}y|\mathcal{S}_i|$, which is a growing function of time. Thus the initial amplitude for the subhorizon solution is the larger the longer time the perturbation has stayed superhorizon: larger scales will acquire larger "initial amplitude". Employing (1.19) we find that $\dot{\Theta}_0 = -\frac{1}{8}\dot{y}\mathcal{S}_i = -\frac{1}{8}\frac{\dot{a}}{a}y\mathcal{S}_i = -\frac{1}{8}\frac{\sqrt{1+y}}{y\sqrt{2}}k_{\rm eq}y\mathcal{S}_i \approx -\frac{\sqrt{2}}{16}k_{\rm eq}\mathcal{S}_i = -\dot{\Phi}$, as $y \ll 1$. Comparing to (2.101) and (2.102) we deduce $C_I \propto \frac{k_{\rm eq}}{k}\mathcal{S}_i$. Kodama and Sasaki [171] find the matching condition (see also [172])

$$C_I = -\frac{\sqrt{6}}{4}\frac{k_{\rm eq}}{k}\mathcal{S}_i\,. \tag{2.119}$$

This k dependence of the isocurvature amplitude will be essential for understanding the different behaviour of adiabatic and isocurvature angular power on small scales. In Sec. 3.4.2 we note that if the k dependence of $\mathcal{R}_i$ (Φ_i) and $\mathcal{S}_i$ is identical, the ratio of the isocurvature to adiabatic power will decrease as $(k_{\rm eq}/k)^2$ when $k > k_{\rm eq}$.

2.8 Line of sight integration method

In Sec. 2.3 we gave a solution for the temperature perturbation on superhorizon scales, and in Sec. 2.7 we derived a solution valid before recombination on subhorizon scales. Given the primordial perturbations (i.e. the initial conditions) deep at the radiation-dominated epoch (just after inflation and reheating) the monopole, dipole, and quadrupole temperature perturbations at the last scattering surface are now known.

We employed analytical approximations, but in practical calculations the differential equations [continuity (2.6), perturbation continuity (2.12), Euler (2.23), time-space Einstein (2.26), space-space Einstein (2.27), generalized Poisson (2.28)] are solved numerically together with the Boltzmann hierarchy (2.52). Until recombination $\ell \gtrsim 4$ equations of the Boltzmann hierarchy are not needed, since Θ_ℓ with $\ell > 2$ are negligible. This is because of the tight coupling as we have already mentioned. However, after the last scattering surface the perturbations start to spread to larger multipoles as briefly described at the end of Sec. 2.5. Then it would be an enormous computational task the solve today's temperature perturbation multipoles $\Theta_\ell(\eta_0)$ directly from the Boltzmann hierarchy.

In this section we review a method where it is enough to calculate first the monopole, dipole, (and quadrupole) perturbations at the last scattering surface as described above. Then today's observed multipoles $\Theta_\ell(\eta_0)$ are obtained by integrating along the path of the photons coming from the last scattering surface. This method is called the line of sight integration method [188].

We demonstrate the method in the flat space generalizing only the final result to open and closed cases. To simplify the treatment we again drop the small anisotropic stress term from the brightness equation (2.50). Then it reads

$$\frac{d}{d\eta}(\Theta + \Psi) = \dot{\Psi} - \dot{\Phi} + \dot{\tau}[(\Theta_0 - \Theta) + \gamma_i v_b^i]. \tag{2.120}$$

Substituting the Fourier expansions the left hand side of (2.120) becomes

$$\frac{d}{d\eta}[\Theta + \Psi](\eta, \vec{x}, \vec{\gamma}) = \frac{1}{(2\pi)^3}\int d^3\vec{k}\left\{[\dot{\Theta} + \dot{\Psi}](\eta, k, \mu)e^{i\vec{k}\cdot\vec{x}} + [\Theta + \Psi](\eta, k, \mu)\frac{d}{d\eta}e^{i\vec{k}\cdot\vec{x}}\right\}.$$

For definition of the functions of (η, k, μ) see equation (1.44). Although $e^{i\vec{k}\cdot\vec{x}}$ is not an explicit function of time, the last term does not vanish since it contains the total differential. From Fig. 2.2 we find that for the photons moving radially along the line of sight we have $\vec{x}(\eta) = (\eta - \eta_0)\vec{\gamma}$. This leads to

$$\frac{d}{d\eta}e^{i\vec{k}\cdot\vec{x}} = e^{-i\eta_0\vec{k}\cdot\vec{\gamma}}\frac{d}{d\eta}e^{i\eta\vec{k}\cdot\vec{\gamma}} = i(\vec{k}\cdot\vec{\gamma})e^{-i\eta_0\vec{k}\cdot\vec{\gamma}}e^{i\eta\vec{k}\cdot\vec{\gamma}} = i(\vec{k}\cdot\vec{\gamma})e^{i\vec{k}\cdot\vec{x}} = ik\mu e^{i\vec{k}\cdot\vec{x}}. \tag{2.121}$$

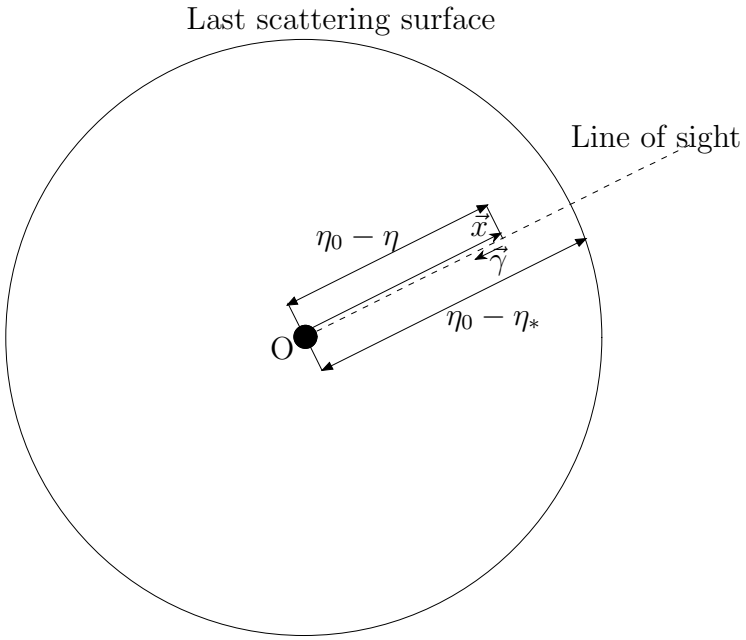

Figure 2.2: **Line of sight integration in the flat space.** Choose the origin (O) of the coordinate system to be at the location of our detector. The distance to the last scattering surface is $\chi_* = \eta_0 - \eta_*$. The photons travel radially towards the origin. At time η they are at the position $\chi = \eta_0 - \eta$. For radially moving photons the direction of propagation $\vec{\gamma}$ is parallel to the line of sight. Recalling that $|\vec{\gamma}| = 1$, we may write the position of the photons at time η as $\vec{x}(\eta) = (\eta - \eta_0)\vec{\gamma}$. Note that with these notations we have $d\eta = -d\chi$ unlike in the other sections where we chose $d\eta = d\chi$.

Altogether, equation (2.120) gives for each k-mode

$$[\dot{\Theta}+\dot{\Psi}](\eta,k,\mu)+ik\mu[\Theta+\Psi](\eta,k,\mu) = [\dot{\Psi}-\dot{\Phi}](\eta,k)+\dot{\tau}\left\{[\Theta_0-\Theta](\eta,k,\mu) - i\mu V_b(\eta,k,\mu)\right\}.$$

Rearranging the terms, we arrive at

$$(\dot{\Theta}+\dot{\Psi}) + (ik\mu+\dot{\tau})(\Theta+\Psi) = \dot{\Psi} - \dot{\Phi} + \dot{\tau}(\Theta_0 + \Psi - i\mu V_b). \tag{2.122}$$

This is a first order differential equation for $(\Theta + \Psi)$. All quantities on the right hand side are known, and thus it is a known function. Also the multiplier of $(\Theta + \Psi)$ in the second term is a known function of time. The integrating factor[5] of this equation is

$$u(\eta) = \exp\left\{\int_{\eta_0}^{\eta} [ik\mu + \dot{\tau}(\eta')]\, d\eta'\right\} = e^{ik\mu(\eta-\eta_0)}e^{-\tau(\eta,\eta_0)},$$

[5]Recall from the theory of ordinary differential equations that an equation

$$y' + p(x)y = q(x)$$

has the solution

$$y(x) = \frac{1}{u(x)}\int_{x_0}^{x} u(\tilde{x})q(\tilde{x})d\tilde{x},$$

where $u(x) = \exp\left[\int^x p(\tilde{x})d\tilde{x}\right]$ is the integrating factor.

where $\tau(\eta,\eta_0)=\int_\eta^{\eta_0}\dot\tau(\eta')d\eta'$ is the optical depth measured from η to the present.

Now we get the solution

$$[\Theta+\Psi](\eta_0,k,\mu)=\int_{\eta_i}^{\eta_0}\left\{\dot\Psi-\dot\Phi+\dot\tau[\Theta_0+\Psi-i\mu V_b]\right\}e^{-\tau(\eta,\eta_0)}e^{ik\mu(\eta-\eta_0)}d\eta, \qquad (2.123)$$

where the integration is performed along the line of sight.

From the integrand in (2.123) we find the combination $\dot\tau e^{-\tau(\eta,\eta_0)}$, which is called the visibility function. From the theory of random walk processes we know that it is the probability density that a photon last scattered at time η. Thus $\dot\tau(\eta)e^{-\tau(\eta,\eta_0)}d\eta$ gives the probability that a photon last scattered within η and $\eta+d\eta$. Of course, the visibility function is nearly zero elsewhere and has a sharp peak at the time of last scattering epoch. In the limit of instantaneous decoupling of photons we get

$$e^{-\tau(\eta,\eta_0)}\to\theta(\eta-\eta_*) \quad \text{and} \quad \dot\tau(\eta)e^{-\tau(\eta,\eta_0)}\to\delta(\eta-\eta_*), \qquad (2.124)$$

where θ is a step function and δ is the Dirac delta function. The argument for this goes as: Before decoupling the tight coupling approximation is valid, i.e., $\dot\tau^{-1}=0$. Thus we have $\dot\tau=\infty$ and $\dot\tau e^{-\tau}=\lim_{x\to\infty}xe^{-x}=0$. After decoupling the Compton cross section becomes zero and thus $\dot\tau=0$. This gives again $\dot\tau e^{-\tau}=0$. So far we have got $\dot\tau e^{-\tau}=0$ for all $\eta\neq\eta_*$. However, we find that $\int_0^{\eta_0}\dot\tau(\eta)e^{-\tau(\eta,\eta_0)}d\eta=\int_0^{\eta_0}\frac{d}{d\eta}e^{-\tau(\eta,\eta_0)}d\eta=\not{}_0^{\eta_0}e^{-\tau(\eta,\eta_0)}=\not{}_\infty^0e^{-x}=1$. Hence, in the case of an instantaneous decoupling, the visibility function obeys all the properties of the Dirac delta function. Another way to see this is to realize that $\tau(\eta,\eta_0)\to\infty$ when $\eta<\eta_*$, and $\tau(\eta,\eta_0)=0$ when $\eta>\eta_*$. Thus $e^{-\tau}$ is a step function with the value 0 before and the value 1 after the decoupling. The visibility function is a derivative of this step function. But the derivative of a step function is just a Dirac delta function.

Now we are finally able to derive an equation for the observed multipoles $\Theta_\ell(\eta_0,k)$. The last exponent function in (2.123) can be rewritten as $e^{i\vec k\cdot\vec x(\eta)}$. Employing the result (2.121) from the right to the left, we write equation (2.123) in the form

$$[\Theta+\Psi](\eta_0,k,\mu)=\int_{\eta_i}^{\eta_0}\left\{\left[\dot\Psi-\dot\Phi+\dot\tau(\Theta_0+\Psi)\right]e^{i\vec k\cdot\vec x(\eta)}-\frac{1}{k}V_b\dot\tau\frac{d}{d\eta}\left[e^{i\vec k\cdot\vec x(\eta)}\right]\right\}e^{-\tau(\eta,\eta_0)}d\eta. \qquad (2.125)$$

The exponent function can be expanded as

$$\begin{aligned}
e^{i\vec k\cdot\vec x} &= 4\pi\sum_\ell\sum_m i^\ell j_\ell(k\chi)Y_{\ell m}(\theta,\varphi)Y^*_{\ell m}(\theta_k,\varphi_k)\\
&= 4\pi\sum_\ell i^\ell j_\ell(k\chi)\frac{2\ell+1}{4\pi}P_\ell(\hat k\cdot\hat x)\\
&= \sum_\ell i^\ell(2\ell+1)j_\ell(k\chi)P_\ell(-\hat k\cdot\vec\gamma)\\
&= \sum_\ell(-i)^\ell(2\ell+1)j_\ell(k\chi)P_\ell(\mu), \qquad (2.126)
\end{aligned}$$

where the last step follows from the fact that $P_\ell(-\mu)=(-1)^\ell P_\ell(\mu)$. We also wrote $\hat k=\vec k/|\vec k|$ and $\hat x=\vec x/|\vec x|=-\vec\gamma$, see Fig. 2.2.

Writing the left hand side of equation (2.125) in terms of the expansion (1.44) and substituting (2.126) to the right hand side, we arrive at

$$\sum_\ell (-i)^\ell P_\ell(\mu)[\Theta+\Psi]_\ell(\eta_0,k) = \sum_\ell (-i)^\ell P_\ell(\mu)(2\ell+1)$$
$$\times \int_{\eta_i}^{\eta_0} \left\{ \left[\dot\Psi - \dot\Phi + \dot\tau(\Theta_0+\Psi)\right] j_\ell(k\chi) - \frac{1}{k} V_b \dot\tau \frac{d}{d\eta}\Big[j_\ell(k\chi)\Big] \right\} e^{-\tau(\eta,\eta_0)} d\eta.$$

Because Ψ is a scalar perturbation and a function of position only (not function of direction) we have $\Psi_\ell = 0$ for $\ell > 0$. Reading the equation for each $\ell > 0$ we get

$$\frac{\Theta_\ell(\eta_0,k)}{2\ell+1} = \int_{\eta_i}^{\eta_0} \left\{ \left[\dot\Psi - \dot\Phi + \dot\tau(\Theta_0+\Psi)\right] j_\ell(k\chi') - \frac{1}{k} V_b \dot\tau \frac{d}{d\eta'}\Big[j_\ell(k\chi')\Big] \right\} e^{-\tau(\eta',\eta_0)} d\eta' \,.$$

Here we have $\chi' = \eta_0 - \eta'$ or $\frac{d}{d\eta'} = -\frac{d}{d\chi'}$, see Fig. 2.2. However, in the previous sections and in Appendix we have used $d\eta = d\chi$. To maintain this notation, we must replace in the above equation χ' with $\chi_0 - \chi'$. Substituting the tight coupling value $V_b = V_\gamma = \Theta_1$, we arrive at

$$\frac{\Theta_\ell(\eta,k)}{2\ell+1} = \int_{\eta_i}^{\eta} \left\{ \left[\dot\Psi - \dot\Phi + \dot\tau(\Theta_0+\Psi)\right] j_\ell\Big(k(\eta-\eta')\Big) \right.$$
$$\left. - \frac{1}{k}\Theta_1 \dot\tau \frac{d}{d\eta'}\Big[j_\ell\Big(k(\eta-\eta')\Big)\Big] \right\} e^{-\tau(\eta',\eta)} d\eta'. \qquad (2.127)$$

Of course, this result should be used in precise calculations, but let us proceed toward a little bit simpler formula.

As already indicated in (2.124), in the limit of an instantaneous decoupling the combination $\dot\tau e^{-\tau(\eta',\eta)}$ is the Dirac delta function and $e^{-\tau(\eta',\eta)}$ reduces to the step function. Thus we can easily perform the integration in (2.127) with the result

$$\frac{\Theta_\ell(\eta,k)}{2\ell+1} = [\Theta_0+\Psi](\eta_*,k)\, j_\ell[k(\eta-\eta_*)] - \frac{1}{k}\Theta_1(\eta_*,k)\frac{d}{d\eta'} j_\ell[k(\eta-\eta')]\Big|_{\eta'=\eta_*}$$
$$+ \int_{\eta_*}^{\eta} [\dot\Psi - \dot\Phi](\eta',k) j_\ell[k(\eta-\eta')] d\eta'. \qquad (2.128)$$

We come back to the three terms of this result in detail in the next chapter. The first term includes the intrinsic spatial temperature perturbation at the last scattering surface and a gravitational effect Ψ. Photons coming from gravitational potential wells $\Psi < 0$ loose energy when climbing up from the well. The combination $\Theta_* + \Psi_*$ determines the ordinary SW effect [13]. The third term is purely gravitational and takes into account the energy loss and gain (and space stretching) of photons coming through time varying potentials. It is called the integrated SW effect. The second term proportional to $\Theta_1(\eta_*) = V_\gamma(\eta_*)$ describes the Doppler effect. Regions with photons moving toward us seem warmer.

Had we left $\frac{d}{kd\eta} e^{i\vec k\cdot\vec x}$ in (2.125) in the form $ik^{-1}\vec k\cdot d\vec x/d\eta e^{i\vec k\cdot\vec x} = i\mu e^{i\vec k\cdot\vec x}$, we would have got for the Doppler term $i\mu\Theta_1 j_\ell[k(\eta-\eta_*)]$. In the next chapter we use this form for the Doppler term. However, the form of (2.128) gives a hint of how to obtain the open and closed space generalizations.

The analogy of formula (2.128) in curved space follows simply by replacing the spher-

ical Bessel function $j_\ell[k(\eta-\eta_*)]$ by its generalization $X_\nu^\ell(\tilde\chi-\tilde\chi_*)$, see (A.13) and (A.20). Let us prove this. From (2.52) we can derive a recursion relation for $\frac{\Theta_\ell(\eta)}{2\ell+1}$. We find that it is the same recursion relation which X_ν^ℓ obeys, see equation (A.20). Hence, one solution is $\frac{\Theta_\ell(\eta)}{2\ell+1} \propto X_\nu^\ell(\tilde\chi-\tilde\chi_*)$. Evaluating this at $\eta=\eta_*$ the constant of proportionality comes $[\Theta_0+\Psi](\eta_*,k)$. But looking at the recursion relation (A.20) of X_ν^ℓ, we notice that $\frac{dX_\nu^\ell(\tilde\chi)}{d\eta}$ satisfies it, too. Thus in addition to $X_\nu^\ell(\tilde\chi)$ also $\frac{\Theta_\ell(\eta)}{2\ell+1} = C\frac{d}{d\eta'}X_\nu^\ell\left[|K|^{1/2}(\chi-\chi')\right]|_{\eta'=\eta_*}$, is (another independent) solution. The constant of proportionality C is fixed by the initial conditions at the last scattering surface. For $\ell=0$ the right hand side vanishes, but for $\ell=1$ we get $\frac{\Theta_1(\eta_*)}{3} = -C\frac{1}{3}kX_\nu^0(0) = -C\frac{1}{3}k$ leading to $C=-\Theta_1(\eta_*)\frac{1}{k}$.

We have proved that in the instantaneous decoupling approximation the dipole $\Theta_1(\eta_*)$ at the last scattering surface is mapped onto anisotropies seen today as

$$\frac{\Theta_\ell(\eta_0,k)}{2\ell+1} = -\frac{1}{k}\Theta_1(\eta_*,k)\left.\frac{dX_\nu^\ell\left[|K|^{1/2}(\chi_0-\chi')\right]}{d\eta'}\right|_{\eta'=\eta_*} \tag{2.129}$$

while the monopole perturbations at the last scattering surface are mapped by

$$\frac{\Theta_\ell(\eta_0,k)}{2\ell+1} = [\Theta_0+\Psi](\eta_*,k)\,X_\nu^\ell\left[|K|^{1/2}(\chi_0-\chi_*)\right]\ . \tag{2.130}$$

One refinement of our analytic approximation is worth doing. In Sec. 2.7.3 we found that we should not use the undamped solutions $\hat\Theta_0$ and $\hat\Theta_1$ from equations such as (2.101) and (2.102). Instead we should substitute into (2.128) the diffusion damped versions from (2.103). However, multiplying the undamped solutions just by $\mathcal{D}(\eta_*,k) = e^{-[k/k_D(\eta_*)]^2}$ would underestimate the effect of damping, since the damping starts before the last scattering. Although we already integrated over η when deriving the instantaneous decoupling approximation (2.128), it is useful to "restore" this integration to the definition of the damping factor. Thus we redefine the damping factor as weighted by the visibility function

$$\mathcal{D}(\eta_*,k) = \int_0^{\eta_*}\dot\tau e^{-\tau(\eta,\eta_0)}e^{-[k/k_D(\eta)]^2}d\eta. \tag{2.131}$$

Note that this same damping factor should be used for the potentials on small scales. In the limit of the instantaneous decoupling this definition coincides with our earlier definition (2.104).

The ionization history of the universe appears both in the visibility function $\dot\tau e^{-\tau}$ and in the damping term $e^{-[k/k_D(\eta)]^2}$ via the damping length k_D^{-1} defined in (2.117). To first approximation, we could use the Saha equation [91, 95] to find the evolution of the ionization fraction x_e and thus $\dot\tau$. (Recall that $\dot\tau = \frac{a}{a_0}x_e n_e\sigma_T$, where σ_T is the Thomson cross section and n_e the total number density of electrons.)

Chapter 3

Angular power

In papers **I**–**V**, for a given primordial power spectrum, the resulting theoretical temperature (and polarization) angular power spectra are calculated numerically by modified versions of publicly available Fortran programs CMBfast [189] described in detail in [188, 190–192] and CAMB [193] described in [194, 195]. However, in **I**–**V** there is a lot of discussion about the qualitative features of the end results. These considerations rely on a deep understanding of the effects of various physical phenomena on the angular power. In this chapter, we list some anisotropy sources and comment on their role at a more qualitative level than in the previous rather technical chapter.

We start by explaining how the spatial temperature perturbations at the last scattering surface are mapped onto the anisotropy seen today. We discuss the Sachs-Wolfe effect and, in particular, the series of acoustic peaks in the angular power. Not all the observed anisotropy reflects the properties of the primordial perturbations or even the properties of the perturbations at the last scattering surface. This is due to many *foreground sources* like emission from the intergalactic gas and dust, our own Milky way, and the point sources. In principle, these can be distinguished from the CMB anisotropies by their different spectral shape. In papers **I**–**V** we assume that the experimental teams have properly removed the foreground effects from the angular power they provide. However, for completeness, we comment on some foreground sources. As important as it is, removing all the foreground is an extremely difficult task and can be done only partially. There is always some contamination in the angular power, and actually, for example in the case of the WMAP first year data, there are implications of severe foreground contamination on the largest scales [196–200].

3.1 Angular power and measurements

The last scattering surface is like a sphere surrounding us. Since the temperature at its surface varies from point to point, we will associate a different temperature to the radiation coming from different directions: the spatial temperature perturbations at the last scattering surface are seen as anisotropies in CMB today. Because of the spherical

geometry it is convenient to expand the observed anisotropy in spherical harmonics

$$\frac{\delta T}{T}(\vec{n}) = \sum_{\ell=0}^{\infty} \sum_{m=-\ell}^{\ell} a_{\ell m} Y_{\ell m}(\vec{n}), \tag{3.1}$$

where $\vec{n}$ is a unit vector in the direction of the line of sight. [Occasionally we will write the pair (θ, φ) instead of $\vec{n}$.] T is the direction averaged temperature $T = \int d\Omega T(\theta, \varphi)$, and $\delta T(\vec{n}) \equiv \delta T(\theta, \varphi) = T(\theta, \varphi) - T$ is the deviation in the direction $\vec{n}$. The coefficients $a_{\ell m}$ obey the relation

$$\langle a_{lm} a^*_{l'm'} \rangle = \delta_{ll'} \delta_{mm'} C_\ell \,, \tag{3.2}$$

since the mean square temperature perturbation cannot depend on the direction. Here the angle brackets denote an (*ensemble*) average to be explained later.

Equation (3.2) defines the angular power C_ℓ. To get more insight into this definition, consider the expectation value of the two-point correlation function of temperature perturbation between directions $\vec{n}$ and $\vec{n}'$ separated from each other by an angle θ, $\vec{n} \cdot \vec{n}' = \cos\theta$,

$$\begin{aligned} \left\langle \tfrac{\delta T}{T}(\vec{n}) \, \tfrac{\delta T^*}{T}(\vec{n}') \right\rangle &= \sum_{\ell\ell' mm'} \langle a_{\ell m} a^*_{\ell' m'} \rangle \, Y_{\ell m}(\vec{n}) Y^*_{\ell' m'}(\vec{n}') = \sum_{\ell=0}^{\infty} C_\ell \sum_{m=-\ell}^{\ell} Y_{\ell m}(\vec{n}) Y^*_{\ell m}(\vec{n}') \\ &= \sum_{\ell} \frac{2\ell+1}{4\pi} C_\ell P_\ell(\vec{n} \cdot \vec{n}') \,. \end{aligned} \tag{3.3}$$

Hence $(2\ell+1) C_\ell P_\ell(\cos\theta)$ is the contribution of the ℓth multipole to the temperature perturbation correlation function of angular scale θ. Taking the limit $\theta \to 0$ we have $P_\ell(1) = 1$ and consequently

$$\left\langle \left| \tfrac{\delta T}{T}(\vec{n}) \right|^2 \right\rangle = \frac{1}{4\pi} \sum_{\ell=0}^{\infty} (2\ell+1) C_\ell \,. \tag{3.4}$$

So, $(2\ell+1)C_\ell$ represents the contribution of the ℓth multipole to the mean square temperature perturbation in the sky.

Coefficients $a_{\ell m}$ in the expansion (3.1) describe the temperature perturbation, which is proportional to the primordial perturbation in the curvature, $\mathcal{R}_i$ (Φ_i), in the pure adiabatic case, and entropy perturbation, $\mathcal{S}_i$, in the isocurvature case. In general, $a_{\ell m} = g^{\rm ad}_{\ell m} \mathcal{R}_i + g^{\rm iso}_{\ell m} \mathcal{S}_i$, where g is a constant of proportionality. But theory (such as inflation) does not predict the actual values of $\mathcal{R}_i$ and $\mathcal{S}_i$; instead their probability distribution (variance) is known[1]: $\langle \hat{a}^*_{\ell m} \hat{a}_{\ell m} \rangle = (g^{\rm ad}_{\ell m})^2 \langle |\hat{\mathcal{R}}_i|^2 \rangle + (g^{\rm iso}_{\ell m})^2 \langle |\hat{\mathcal{S}}_i|^2 \rangle + 2 g^{\rm ad}_{\ell m} g^{\rm iso}_{\ell m} \langle \hat{\mathcal{R}}^*_i \hat{\mathcal{S}}_i \rangle$, where, as

[1] In the simplest inflationary scenarios, each Fourier component of quantum fluctuations of an effectively massless [$m^2 \ll (\frac{3}{2})^2 H^2$] scalar field has a Gaussian probability distribution with zero mean. Even if the individual Fourier components are not Gaussian, their sum (Fourier integral) will have a Gaussian probability distribution function according to the central limit theorem [92]. Thus, rather generally, $\hat{\mathcal{R}}_i(\vec{x})$ and $\hat{\mathcal{S}}_i(\vec{x})$ are Gaussian random variables. However, in some inflationary models, the "entropy field" s acquires a large effective mass due to interactions between scalar fields, or its background value s vanish so that the mean energy density attached to the field s results from its perturbations: $\rho_s \propto \langle |\delta s|^2 \rangle$. Then one must consider second order perturbations, and obtains $\mathcal{P}_{\mathcal{S}} \propto \mathcal{P}_{(\delta s)^2}$ which obeys

in Sec. 1.2.3, hat reminds us that the actual value is picked from a random distribution.

Now it is evident that $C_\ell = \langle|\hat{a}_{\ell m}|^2\rangle$ is a purely theoretical quantity that cannot be measured. This comes about because C_ℓ is an expectation value of a random variable, but there is only one realization of the universe. So we can only measure the actual value of $|\hat{a}_{\ell m}|^2$ in our universe, not its expectation value. However, we can proceed to find an as good as possible estimator $\tilde{C}_\ell$ for C_ℓ.

First, consider an ideal experiment. From (3.1) we obtain

$$\hat{a}_{\ell m} = \int \tfrac{\hat{\delta T}}{T}(\vec{n}) Y^*_{\ell m}(\vec{n}) d\Omega \,. \tag{3.5}$$

If we were able to perform a noise-free measurement of $\hat{\delta T}/T$ at many pixels that cover the entire sky, we could evaluate this integral very accurately by

$$\hat{a}_{\ell m} = \frac{4\pi}{N_{\rm pix}} \sum_{p=1}^{N_{\rm pix}} \frac{\hat{\delta T}}{T}(\vec{n}_p) Y^*_{\ell m}(\vec{n}_p) \,, \tag{3.6}$$

where $N_{\rm pix}$ is the total number of pixels and $\vec{n}_p$ is the unit vector in the direction of the pixel p. So, for each fixed ℓ, we can measure $2\ell+1$ quantities $\hat{a}_{\ell m}$. However, as explained above, this set of $2\ell+1$ quantities is only one sample from the distribution for $\hat{a}_{\ell m}$. The best we can do is, for instance, to calculate the average of the measured quantities

$$\tilde{C}_\ell = \frac{1}{2\ell+1} \sum_{m=-\ell}^{\ell} |\hat{a}_{\ell m}|^2 \,. \tag{3.7}$$

The mean square error made when approximating C_ℓ by $\tilde{C}_\ell$ is

$$\begin{aligned}
\left\langle (\tilde{C}_\ell - C_\ell)^2 \right\rangle &= \left\langle \tilde{C}_\ell^2 \right\rangle - 2C_\ell \left\langle \tilde{C}_\ell \right\rangle + C_\ell^2 \\
&= \frac{1}{(2\ell+1)^2} \left[\sum_m \left(\left\langle |\hat{a}_{\ell m}|^4 \right\rangle + \sum_{m' \neq m} \left\langle |\hat{a}_{\ell m}|^2 |\hat{a}_{\ell m'}|^2 \right\rangle \right) \right] \\
&\quad - 2C_\ell \frac{1}{2\ell+1} \sum_m \left\langle |\hat{a}_{\ell m}|^2 \right\rangle + C_\ell^2 \\
&= \frac{2}{2\ell+1} C_\ell^2 \,.
\end{aligned} \tag{3.8}$$

The last step follows from assuming a Gaussian distribution for $\hat{a}_{\ell m}$, since in addition to relation (3.2), we then have $\langle \hat{a}_{\ell m} \rangle = 0$ and $\langle |\hat{a}_{\ell m}|^4 \rangle = 3C_\ell^2$. The quantity (3.8) is *cosmic variance*. Due to it the fractional uncertainty of the measured angular power $\tilde{C}_\ell$ compared to the theoretically predicted power, C_ℓ, is

$$\frac{\sqrt{\langle (\tilde{C}_\ell - C_\ell)^2 \rangle}}{C_\ell} = \sqrt{\frac{2}{2\ell+1}} \tag{3.9}$$

χ^2 statistics as δs is Gaussian (see e.g. [141, 201] for a simple realization). Possible non-Gaussianities of the CMB temperature maps [202] and the theoretical (e.g. inflationary) predictions for the amount of non-Gaussianity form a field of active research. However, we just refer to an excellent review by Bartolo et al. [203].

even in the perfect experiment. As one could have guessed, the possibility of a large error is largest at low multipoles, since there we have the smallest sample.[2] The uncertainty for C_2 is 63%, for C_5 43%, for C_{10} 31%, and even for C_{100} we have an uncertainty of 10%. And all this in the case of an otherwise idealized experiment. Interestingly, WMAP has so good performance that the estimates for the measurement error (experimental error bars) are dominated by cosmic variance up to the multipole $\ell \simeq 350$ [204].

In real experiments there is always some noise in the data. This is due to all kind of contamination (see Sec. 3.6) and due to electronic receiver noise of the actual apparatus used in measurements. Thus the pth data point consists of a signal and noise,

$$d_p = \frac{\hat{\delta T}}{T}(\vec{n}_p) + c_p, \tag{3.10}$$

where c_p is the noise in the point p. Now we do not find the exact values for $\hat{a}_{\ell m}$ as in (3.6), but some slightly different quantities

$$\hat{a}^c_{\ell m} = \frac{4\pi}{N_{\rm pix}} \sum_{p=1}^{N_{\rm pix}} d_p Y^*_{\ell m}(\vec{n}_p)\,, \tag{3.11}$$

where c refers to the "contamination" by noise. Assuming that the noise in each pixel is independent and has a Gaussian distribution with variance σ, we obtain

$$\langle |\hat{a}^c_{\ell m}|^2 \rangle = C_\ell + \frac{4\pi}{N_{\rm pix}}\sigma^2\,. \tag{3.12}$$

Thus we have $C_\ell = \langle |\hat{a}^c_{\ell m}|^2 \rangle - \frac{4\pi}{N_{\rm pix}}\sigma^2$. Following the same principles as in the case of the idealized experiment, we approximate this theoretical C_ℓ by a measurable quantity [205]

$$\tilde{C}_\ell = \frac{1}{2\ell+1} \sum_{m=-\ell}^{\ell} |\hat{a}_{\ell m}|^2 - \frac{4\pi}{N_{\rm pix}}\sigma^2\,. \tag{3.13}$$

[2]The difference between the measured average and the ensemble average is easy to understand by the following way. Consider n dice, each with the spots 1, 2, 3, 4, 5, and 6. Throw them on the table. The ensemble average of the spots is $(1+2+3+4+5+6)/6 = 3.5$. If we could repeat the experiment hundreds of times, the average of the measured spots would approach the number 3.5. So, if we were able to perform many measurements, we would get a very accurate approximation for the ensemble average. However, if we can perform only one experiment, i.e., throw the dice only once on the table, then the best we can do is to calculate the mean of the spots of those n dice. If n was very large, we would still find the measured mean to be very close to the ensemble average 3.5. (More precisely, the probability that the measured average was close to 3.5 would be high.) But if n was small, then the measured average could differ significantly from 3.5. For example, with three dice we could get the spots 4, 5, and 6. So our estimate for the ensemble average would be as worse as 5. But how is this example related to the concept of cosmic variance? For fixed ℓ one can think that we allot the values of $\hat{a}_{\ell m}$ by dropping $n = 2\ell+1$ dice on the table. If we could repeat the allotting infinite times, we could "measure" the ensemble average accurately. However, there is only one universe (that is, one realization or sample of the set of random variables) to be observed. So the allotting is made only once and we can only measure those $2\ell+1$ values. As already explained, especially for small $n = 2\ell+1$ the average of these quantities may differ significantly from the ensemble average.

Now the mean square error is larger than in the idealized case. In fact, we find

$$\sqrt{\left\langle (\tilde{C}_\ell - C_\ell)^2 \right\rangle} = \sqrt{\frac{2}{2\ell+1}} \left(C_\ell + \frac{4\pi}{N_{\rm pix}} \sigma^2 \right) . \tag{3.14}$$

Moreover, there are several other complications in the real measurements. Let us just mention the incomplete sky coverage. So far, the best coverage has been achieved by the WMAP satellite experiment, but as the Galactic plane of the Milky Way is too contaminated, only about 80% of the sky is usable. In the absence of the data points from some directions, it is impossible to calculate each individual quantity $a_{\ell m}$ from the formula (3.6). So an estimator $\tilde{C}_\ell$ for C_ℓ will depend on the other C_ℓs.

Let us finally comment on the common practice in the literature. When discussing temperature anisotropies the quantity $\ell(\ell+1)C_\ell/(2\pi)$ is often plotted instead of the plain C_ℓ or $(2\ell+1)C_\ell/(4\pi)$ that appeared in expansion (3.4). The first reason is historical: in the simplest (scale invariant, flat, $\Omega_m = 1$) model $\ell(\ell+1)C_\ell$ is constant as a function of ℓ in the Sachs-Wolfe part of the spectrum ($\ell \lesssim 20$, see Sec. 3.4.1.) However, if $\Omega_{\rm tot} \neq 1$ or $\Omega_\Lambda \neq 0$, the integrated Sachs-Wolfe effect (see e.g. Sec. 3.5.1) adds power on the largest angular scales, i.e., at the lowest values of ℓ. This effect erases the "plateau" of the simplest model. As the effect becomes less pronounced on smaller scales, there may occur a valley between the smallest ℓ-values and the first acoustic peak. The second motivation to plot $\ell(\ell+1)C_\ell/2\pi$ is that, to see better the SW part, logarithmic ℓ axis is often used. Then the area below the plotted curve between ℓ_1 and ℓ_2 is just the contribution of the multipole interval $[\ell_1, \ell_2]$ to the total CMB temperature anisotropy. This can be seen by replacing the summation in (3.4) by integration as follows:

$$\left\langle \left| \tfrac{\delta T}{T}(\vec{n}) \right|^2 \right\rangle \approx \int \tfrac{2\ell+1}{4\pi} C_\ell \, d\ell = \int \tfrac{\ell(2\ell+1)}{4\pi} C_\ell \, d(\log \ell) \approx \int \tfrac{\ell(\ell+1)}{2\pi} C_\ell \, d(\log \ell) \, , \tag{3.15}$$

The last approximation holds the better the larger ℓ is.

3.2 Projection

In this section we find how a given scale $\lambda = 2\pi/k$ is projected onto the observed multipoles, or vice versa, what scales of temperature perturbations at the last scattering surface contribute to the angular power at a given multipole ℓ.

Substituting into (1.44) $P_\ell(\mu) = \frac{4\pi}{2\ell+1} \sum_m Y^*_{\ell m}(\hat{k}) Y_{\ell m}(\vec{\gamma})$ we arrive at

$$\frac{\hat{\delta T}}{T}(\vec{n}) = \Theta(\eta_0, \vec{x}_0, \vec{\gamma}) = \sum_{\ell=0}^{\infty} \sum_{m=-\ell}^{\ell} \left[\frac{1}{(2\pi)^3} \int d^3\vec{k} e^{i\vec{k}\cdot\vec{x}_0} \frac{\Theta_\ell(\eta_0, k)}{2\ell+1} 4\pi (-i)^\ell Y^*_{\ell m}(\hat{k}) \right] Y_{\ell m}(\vec{\gamma}) \, .$$

Here $\vec{\gamma} = -\vec{n}$, and the spherical harmonics obey $Y_{\ell m}(-\vec{x}) = (-1)^\ell Y_{\ell m}(\vec{x})$ [206]. Thus comparing to expansion (3.1) we identify the term in square brackets to be $(-1)^\ell a_{\ell m}$. Now we plug $a_{\ell m}$ into the definition of the angular power (3.2), and find

$$C_\ell = \left\langle |a_{\ell m}|^2 \right\rangle = \frac{1}{(2\pi)^3} \int k^2 dk \left\langle \left| \frac{\Theta_\ell(\eta_0, k)}{2\ell+1} \right|^2 \right\rangle (4\pi)^2 d\Omega_{\hat{k}} Y^*_{\ell m}(\hat{k}) Y_{\ell m}(\hat{k})$$

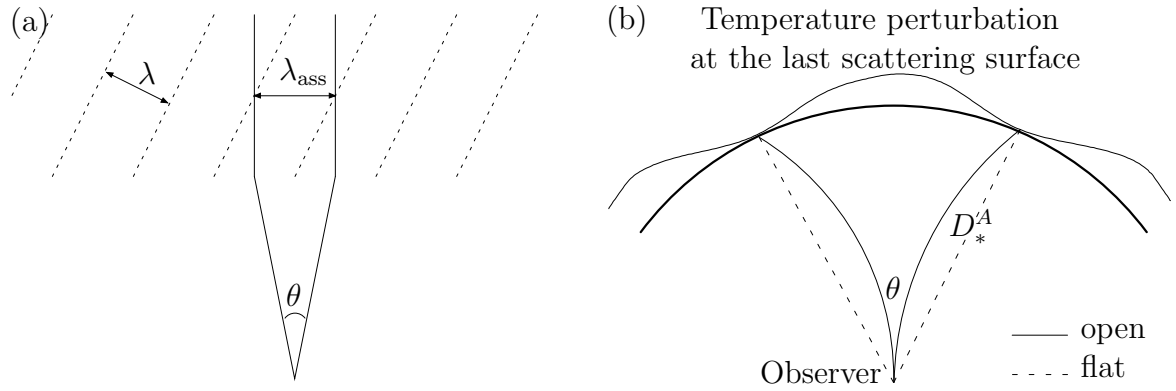

Figure 3.1: **The projection effects. (a)** A plane wave with wavelength $\lambda = 2\pi k^{-1}$ at the last scattering surface. Since the wave vector $\vec{k}$ is not perpendicular to the line of sight, we will associate to the wave the wavelength $\lambda_{\rm ass} > \lambda$. **(b)** A perturbation of a fixed physical length at the last scattering surface is mapped onto smaller angular scale θ (larger ℓ) in an open universe than in the flat case, since the angular diameter distance D_*^A becomes larger. In closed universe the same λ would be mapped onto larger θ (smaller ℓ).

$$= 4\pi \int_0^\infty \frac{dk}{k} \frac{k^3}{2\pi^2} \left\langle \left| \frac{\Theta_\ell(\eta_0, k)}{2\ell + 1} \right|^2 \right\rangle . \tag{3.16}$$

Here we relied on the fact that $\Theta(\eta_0, \vec{k})$ is proportional to the primordial perturbations, and hence according to (1.26) we have $\langle \Theta^*(\eta_0, \vec{k}')\Theta(\eta_0, \vec{k})\rangle \propto (2\pi)^3 \delta^{(3)}(\vec{k}' - \vec{k})$, which kills one of the k integrals that would otherwise appear in (3.16). Had we considered curved space (see Appendix A), we should have replaced k e.g. by $\tilde{k} = \sqrt{|K|}\nu = \sqrt{k^2 + K}$ in (3.16).

In the instantaneous decoupling approximation the monopole (i.e. spatial) perturbation at the last scattering surface is projected onto multipoles according to the result (2.130) as $\Theta_\ell(\eta_0, k)/(2\ell + 1) = [\Theta_0 + \Psi](\eta_*, k) X_\nu^\ell \left[|K|^{1/2}(\chi_0 - \chi_*) \right]$. Let us discuss this relation in detail in flat space case, where $X_\nu^\ell(\tilde{\chi}_0 - \tilde{\chi}_*) = j_\ell[k(\eta_0 - \eta_*)]$. The argument is practically $k\eta_0$, since $\eta_0 \gg \eta_*$. The spherical Bessel function $j_\ell^2(k\eta_0)$ produces a decreasing series of peaks starting from $k\eta_0 \sim \ell$. Being the highest, the first peak at $k\eta_0 \sim \ell$ is the most significant upon integration. We conclude that the main contribution of a given k-mode appears at $\ell_k \sim k\eta_0$. The other peaks of $j_\ell^2(k\eta_0)$ cause some power to bleed to smaller values of ℓ. Think, for instance, that $k\eta_0 = 90$. Now, $j_{90}^2(k\eta_0)$ is the largest and quantities $j_\ell^2(k\eta_0)$ with $\ell > 90$ are approximately zero. But any $j_\ell^2(k\eta_0)$ with $\ell < 90$ can differ from zero. However, $j_{90}^2(k\eta_0) \gg j_{60}^2(k\eta_0) > j_{30}^2(k\eta_0) > 0$. Thus the main angular power of the mode $k = 90/\eta_0$ occurs at $\ell \sim 90$, but this k mode produces also some power at the lower values of ℓ.

This aliasing of a plane wave with a given wavelength $\lambda = 2\pi/k$ to $\ell \leq 2\pi\eta_0/\lambda$ is easy to understand, when we realize that the wave vector $\vec{k}$ is not necessarily perpendicular to the line of sight. To $\vec{k} \perp \vec{n}$ we will associate the right wavelength $\lambda = 2\pi/k$ and get $\ell \sim k\eta_0$. To the wave vectors with same length but other direction we will associate a larger wavelength ($\lambda_{\rm ass} > 2\pi/k$) and thus a smaller ℓ, see Fig. 3.1a. In the limit of the

wave vector parallel to the line of sight we would actually get $\lambda_{\rm ass} \to \infty$.

There appears also another projection effect because of the possible curvature of the universe, which causes the geodesic deviation of the path of the photons coming from the last scattering surface. In an open universe a given physical scale will be projected onto smaller angular scale than in the flat universe, see Fig. 3.1b. Thus all the features of the angular power spectrum are shifted toward higher values of ℓ. In a closed universe the opposite happens. This geometric projection effect comes from the properties of the radial function $[X_\nu^\ell(\tilde\chi_0 - \tilde\chi_*)]^2$. As we have seen, it peaks at wave numbers satisfying $k(\chi_0 - \chi_*) \sim \ell$ in the flat case. However, the peak in the curved case appears when the wave number satisfies $k|K|^{-1/2} \sin_K \left[|K|^{1/2}(\chi_0 - \chi_*)\right] \sim \ell$. This property can be derived from the recursion relation (A.20) as well as all other properties of X_ν^ℓ.

Define $D_*^A = |K|^{-1/2} \sin_K \left[|K|^{1/2}(\chi_0 - \chi_*)\right]$ in the curved case, which reduces to $D_*^A = \chi_0 - \chi_*$ in the flat case. Now, we have derived the correspondence between the observed anisotropies and the spatial perturbations of scale $\lambda = 2\pi/k$ at the last scattering surface. It is

$$\ell_k = kD_*^A, \;\; \ell_\lambda = 2\pi D_*^A/\lambda, \;\; \theta_k = 2\pi/\ell_k = 2\pi/(kD_*^A), \text{ and } \theta_\lambda = 2\pi/\ell_\lambda = \lambda/D_*^A, \quad (3.17)$$

with

$$D_*^A = H_0^{-1} \times \begin{cases} |\Omega_k|^{-1/2} \sin_K \left[|\Omega_k|^{1/2} \mathcal{I}(z_*, 0)\right], & \text{open/closed} \\ \mathcal{I}(z_*, 0)\,, & \text{flat} \end{cases} \quad (3.18)$$

where we used $|K|^{1/2} = H_0|\Omega_k|^{1/2}$, read $\chi_0 - \chi_*$ from (1.12) and $\mathcal{I}$ from (1.13). The last equality in (3.17) motivates a commonly used term *angular diameter distance* for D^A. In many textbooks the angular diameter distance is just given without any motivation. Here we presented a short derivation of it. In the flat case, D_*^A coincides with the comoving distance to the last scattering. Since $\sin x < x < \sinh x$, we see that in closed universe D_*^A is smaller and in open universe larger than the comoving distance.

Note that we used the comoving wave number k and the comoving scale λ. Hence, the projection of a given physical scale $\lambda_p = (a/a_0)\lambda$ appears to be $\ell = k_p(1+z_*)^{-1}D_*^A = 2\pi(1+z_*)^{-1}D_*^A/\lambda_p$.

In Fig. 3.2 we show the values of D_*^A in $(\Omega_m, \Omega_\Lambda)$ plane. Using relations (3.17) we see, for example, that a perturbation with wave number $k = 0.05\,\mathrm{Mpc}^{-1}$ gives rise to angular power around $\ell \sim 0.05\,\mathrm{Mpc}^{-1} \times 14\,000\,\mathrm{Mpc} = 700$, when $\Omega_m = 0.3$, $\Omega_\Lambda = 0.7$, and $h = 0.7$ (marked with an asterisk in Fig. 3.2). This correspondence is used in papers **III**–**V** when discussing the role of a pivot scale $k_0 = 0.05\,\mathrm{Mpc}^{-1}$.

3.3 Superhorizon and subhorizon perturbations

The evolution of temperature perturbations is described by the brightness equation (2.50) where the Compton scattering term (i.e. the right hand side) is zero after the last scattering for all scales. But for large enough scales, $k \ll \mathcal{H}_*$, which become subhorizon only after decoupling, it is zero at all times. Then the temperature anisotropy will be affected by purely gravitational effects only. Let us find a typical wave number

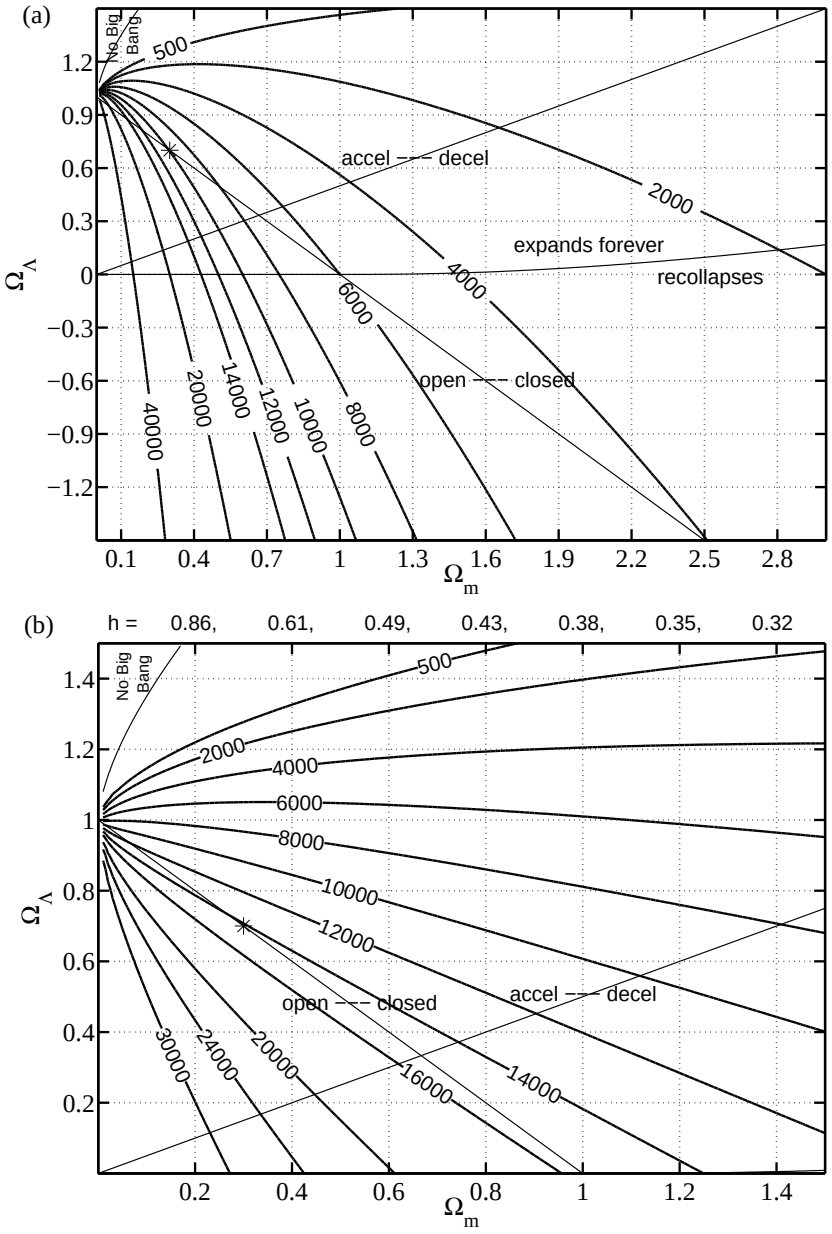

Figure 3.2: **The angular diameter distance to the last scattering surface D_*^A. (a)** The contours with quoted values represent D_*^A in units of h^{-1} Mpc, i.e., to obtain D_*^A in Mpc the quoted values should be divided by h. **(b)** Same as (a) but zoomed and changed parametrization so that the physical matter density is fixed to $\omega_m = 0.147$. Now $h = \sqrt{\omega_m/\Omega_m}$ has become a derived parameter, which is included in the quoted values of D_*^A.

$k_*^{\rm hor} = \mathcal{H}_* = (a_*/a_0)H_*$ that cross the horizon at decoupling. According to (1.11) the result is

$$k_*^{\rm hor} = (1+z_*)^{-1} H_0 \left[\Omega_r (1+z_*)^4 + \Omega_m (1+z_*)^3 + \Omega_k (1+z_*)^2 + \Omega_\Lambda\right]^{1/2}. \qquad (3.19)$$

With $h = 0.7$, $\Omega_r = 4.183 \times 10^{-5} h^{-2}$, $\Omega_m = 0.3$, $\Omega_\Lambda = 0.7$, and $z_* = 1089$ this gives $k_*^{\rm hor} = 0.00483{\rm Mpc}^{-1}$ corresponding to $\ell_* = k_*^{\rm hor} D_*^A \approx 0.00483{\rm Mpc}^{-1} \times 14000{\rm Mpc} \approx 70$. Note that ℓ_* depends only weakly on h, since H_0 in $k_*^{\rm hor}$ and H_0^{-1} in D_*^A cancel each other. The h dependence comes then practically from Ω_r only. Generally, in the flat case,

it is safe to assume that the Compton scattering term does not affect multipoles $\ell \lesssim 50$. See however Sec. 3.5.3 where we discuss reionization.

From the above calculation we realize that the horizon length at the last scattering surface spans only an angle $\theta = 2\pi/70 = 5^\circ$ in the observed sky. Hence, without inflation it is hard to explain the large-scale isotropy.

3.4 Primary anisotropy sources

After the decoupling there are few free electrons (neglecting the possible reionization). Hence, in an idealized situation the photons would stream freely to our detector. The observed CMB anisotropies would, in addition to the projection, depend only on the phenomena before and at the last scattering surface called the *primary anisotropy sources*. (We follow closely the classification of [207] when discussing the primary, secondary, and other, i.e., tertiary anisotropies.)

The photons coming from the last scattering surface carry three different imprints of the region where they last scattered [208]:

- If they last scattered in a potential well ($\Psi < 0$), they will experience a gravitational redshift when climbing out of the well. Note that this semi-Newtonian interpretation is a little dangerous, since it is the full general relativistic treatment that one should apply all the time [209].
- The energy of the photons at a particular point at the last scattering surface depends on the density perturbation at that point. For example, adiabatic perturbations obey the relation $\Theta_0(\eta_*) = \frac{1}{3}\delta_b(\eta_*)$.
- The photons last scattered by the matter, which was moving away from us, will suffer a Doppler redshift.

Taking these effects together we can write schematically today's temperature anisotropy in the form

$$\frac{\delta T}{T}(\vec{n}) = \left[\Psi + \Theta_0 - \vec{n}\cdot\vec{v}\right]_{\eta=\eta_*}, \tag{3.20}$$

where $\vec{n}$ is a unit vector in the direction of observation as before and $\vec{v}$ is the peculiar velocity of the baryon-photon fluid ($\vec{v} = \vec{v}_b = \vec{v}_\gamma$) at the observed point at the last scattering surface.

Here we gave an intuitive explanation for the terms appearing in the observed temperature in the direction $\vec{n}$. We have already presented a full mathematical derivation of this result: The first two terms of equation (2.128) represent the equation (3.20) in Fourier space in terms of the multipole moments.

3.4.1 Large scales, Sachs-Wolfe effect

Assume that, on large scales, there is no explicit time evolution in the potentials Ψ and Φ after the last scattering. Then the brightness equation (2.50) is trivial to integrate

over η to obtain the observed temperature perturbation in the direction $\vec{n}$,

$$\frac{\delta T}{T}(\vec{n}) = \Theta(\eta_*, \vec{x}_*) + \Psi(\eta_*, \vec{x}_*) - \Psi(\eta_0, \vec{x}_0)\,. \tag{3.21}$$

By the first term on the right hand side we actually mean the spatial (i.e. monopole) temperature perturbation Θ_0, since we separated the Doppler (Θ_1) term in (3.20). In addition, we can set the last term to zero[3], so that we end up with

$$\frac{\delta T}{T}(\vec{n}) = \left[\Theta_0 + \Psi\right](\eta_*, \vec{x}_*)\,. \tag{3.22}$$

This combination of the intrinsic temperature perturbation at the last scattering surface and the gravitational redshift is called the *ordinary Sachs-Wolfe effect* [13]. Comparing the MD values of equations (2.36) and (2.40) we find that $\Theta_0(\eta_*) = -\frac{2}{3}\Psi(\eta_*)$ in the adiabatic case. This gives $\frac{\delta T}{T}(\vec{n}) = \frac{1}{3}\Psi(\eta_*)$. On the other hand, the isocurvature initial conditions lead to $\Theta_0(\eta_*) = \Psi(\eta_*)$, and we get $\frac{\delta T}{T}(\vec{n}) = 2\Psi(\eta_*)$. Hence, in the isocurvature case, the same perturbation in the Newtonian potential Ψ at the last scattering surface leads to a SW effect that is 6 times larger than in the adiabatic case. Because $C_\ell \propto [(\Theta_0 + \Psi)_*]^2$, the SW effect on C_ℓ becomes 36 times larger in the isocurvature case.

The SW effect alone dominates the multipoles $\ell \lesssim 20$. Any time evolution of potentials would give an additional contribution called integrated SW effect, see Sec. 3.5.1. Assuming that recombination occurs well after the equality, the result (2.36) tells us that the potentials are constant, $\Psi = -\Phi = \frac{9}{10}\Psi_i - \frac{1}{5}\mathcal{S}_i$. However, if the last scattering surface is close to time of equality, then in the adiabatic case Ψ is decaying from the RD value Ψ_i to the MD value $\frac{9}{10}\Psi_i$. In the isocurvature case, the opposite is happening: Ψ is growing from the initial value zero to the constant value $-\frac{1}{5}\mathcal{S}_i$, which it has in the matter-dominated era. At late times Λ domination causes decay of the potentials.

Above, we gave the SW effect in terms of the temperature and potential perturbations at the last scattering surface. The focus in this thesis is in the role of initial conditions (nature of the primordial perturbations). If recombination happens in the matter-dominated era the MD values from (2.36) and (2.40) lead to

$$\frac{\delta T^{SW}}{T}(\vec{n}) = (\Theta_0 + \Psi)_* = \frac{3}{10}\Psi_i - \frac{2}{5}\mathcal{S}_i = -\frac{1}{5}\mathcal{R}_i - \frac{2}{5}\mathcal{S}_i\,, \tag{3.23}$$

[3] In practice, we cannot measure the spatial temperature perturbation today, since our detectors are at fixed positions in the universe (near to the earth). Therefore the monopole Θ_0 today is unmeasurable and the only meaningful quantities are the higher multipoles Θ_ℓ, which are measured by comparing the temperature of the radiation coming from different directions $\vec{n}$ in the sky. Since the potential at our location, $\Psi(\eta_0, \vec{x}_0)$, affects identically the radiation coming from all directions, it does not alter the absolute differences in the temperature associated with different directions. This means that our own potential affects only the monopole perturbation $\Theta_0(\eta_0)$ and leaves $\Theta_\ell(\eta_0)$ unchanged whenever $\ell > 0$. So, when calculating the multipoles Θ_ℓ and the angular power C_ℓ, we can set $\Psi(\eta_0, \vec{x}_0) = 0$. Note that also $\Theta_1(\eta_0)$ is usually thrown away as a contaminated quantity, because it is somewhat problematic to measure because of the dipole caused by our own velocity with respect to the background radiation. In other words, the meaning of "background" and "perturbation" is not unique in the case of velocity (dipole), since it is not a gauge invariant. Our observation in Sec. 1.3.3 that the higher multipole perturbations are gauge invariants guarantees that Θ_ℓ with $\ell > 1$ has a unique meaning.

where the last step follows from (1.58). Primordial isocurvature perturbation of amplitude $\mathcal{S}_i = A$ on the large scales leads to C_ℓ that are four times as large as would result from the adiabatic $\mathcal{R}_i = A$.

The line of sight integration result (2.128) gives now

$$\left\langle \left| \frac{\Theta_\ell^{SW}(\eta_0,k)}{2\ell+1} \right|^2 \right\rangle = \left\langle \left| -\tfrac{1}{5}\hat{\mathcal{R}}_i(\vec{k}) - \tfrac{2}{5}\hat{\mathcal{S}}_i(\vec{k}) \right|^2 \right\rangle j_\ell^2[k(\eta_0-\eta_*)]$$
$$= \tfrac{2\pi^2}{k^3}\left[\tfrac{1}{25}\mathcal{P}_{\mathcal{R}_i}(k) + \tfrac{4}{25}\mathcal{P}_{\mathcal{S}_i}(k) + \tfrac{4}{25}\mathcal{C}_{\mathcal{R}_i\mathcal{S}_i}(k)\right] j_\ell^2(kD_*^A) \qquad (3.24)$$

Assuming the power law primordial power spectra $\mathcal{P}_{\mathcal{R}_i}(k) = A^2(k/k_0)^{n_{\rm ad}-1}$, $\mathcal{P}_{\mathcal{S}_i}(k) = B^2(k/k_0)^{n_{\rm iso}-1}$, and $\mathcal{C}_{\mathcal{R}_i\mathcal{S}_i}(k) = C(k/k_0)^{n_{\rm cor}-1}$ the angular power from (3.16) reads[4]

$$C_\ell^{SW} = 4\pi\left[\tfrac{1}{25}A^2 I(n_{\rm ad}) + \tfrac{4}{25}B^2 I(n_{\rm iso}) + \tfrac{4}{25}C I(n_{\rm cor})\right] , \qquad (3.25)$$

with

$$I(n) \stackrel{\rm def}{=} \int_0^\infty \left(\frac{k}{k_0}\right)^{n-1} j_\ell^2(kD_*^A)\frac{dk}{k} = \pi 2^{n-4}(k_0 D_*^A)^{1-n}\frac{\Gamma(3-n)\Gamma(\ell+\frac{n-1}{2})}{\Gamma^2(\frac{4-n}{2})\Gamma(\ell+\frac{5-n}{2})}. \qquad (3.26)$$

For $n = 1$ the result is particularly simple: $I(1) = \frac{\pi}{8}\frac{4}{\pi}\frac{1}{\ell(\ell+1)} = \frac{1}{2}\frac{1}{\ell(\ell+1)}$.

If all the spectra are scale invariant, $n_{\rm ad} = n_{\rm iso} = n_{\rm cor} = 1$, we end up with

$$\frac{\ell(\ell+1)}{2\pi}C_\ell^{SW} = \frac{1}{25}A^2 + \frac{4}{25}B^2 + \frac{4}{25}C = \text{constant}. \qquad (3.27)$$

As already explained in Sec. 3.1, it is a common practice to plot this quantity against ℓ (or $\log\ell$) when discussing the power spectra. The Sachs-Wolfe contribution is now flat, so that it is easy to find the differences between some more complicated model and this simplest (scale invariant, flat) model.

Note that, if the primordial perturbations in $\mathcal{R}$ and $\mathcal{S}$ were 100% (anti)correlated with each other on all scales, we would have $C = AB$ and $n_{\rm cor} = (n_{\rm ad} + n_{\rm iso})/2$. The sign of correlation, sign(C), depends on the relative signs of A and B. With $C = AB$ the result (3.27) can be written as $\frac{1}{25}(A+2B)^2$. Thus the SW contribution can be set to zero by a negative correlation component by adjusting the amplitudes to $A = -2B$. In the CMB data there is less power at lowest multipoles ($\ell = 2, 3$) than predicted by typical adiabatic ΛCDM models. One of motivations of paper **IV** was to find out how much the cancellation by negative correlation could improve the fit to the data. Actually, we allowed for both positive and negative correlation, and a scale dependence.

---

[4]From tables [210] we find the formulas

$$j_\ell(x) = \sqrt{\tfrac{\pi}{2x}}J_{\ell+1/2}(x)\,,$$
$$\int_0^\infty t^{-\lambda}J_{\ell+1/2}^2(at)dt = \frac{1}{2^\lambda a^{-\lambda+1}}\frac{\Gamma(\frac{2\ell+2-\lambda}{2})}{\Gamma(\frac{2\ell+3}{2})\Gamma(\frac{\lambda+1}{2})}F(\frac{2\ell+2-\lambda}{2},\frac{-\lambda+1}{2};\frac{2\ell+3}{2};1)\,,$$
$$F(a,b;c;1) = \frac{\Gamma(c)\Gamma(c-a-b)}{\Gamma(c-a)\Gamma(c-b)}.$$

3.4.2 Small scales, acoustic oscillations

Consider for simplicity the case where the baryon to photon ratio R is constant. Now, the solution (2.101) for the adiabatic mode reads

$$\Theta_0(\eta) + \Phi(\eta) = \frac{3}{2}\Phi_i \cos(kr_s) + \int_{\eta_i}^{\eta} k\tilde{c}_s \left[\Phi(\eta') - (1+R)\Psi(\eta')\right] \sin\left[kr_s(\eta) - kr_s(\eta')\right] d\eta', \quad (3.28)$$

see also (2.78), (2.102), and (2.118). Note that the only thing we miss by assuming $\dot{R} = 0$, is the $(1+R)^{-1/4}$ damping from (2.95). With $\dot{r}_s = \tilde{c}_s = \frac{1}{\sqrt{3(1+R)}}$ and $\Psi \approx -\Phi$ integration by parts gives for the integral

$$\int_{\eta_i}^{\eta} (2+R)\Phi(\eta') \cos\left[kr_s(\eta) - kr_s(\eta')\right] - \int_{\eta_i}^{\eta} (2+R)\dot{\Phi}(\eta') \cos\left[kr_s(\eta) - kr_s(\eta')\right] d\eta'. \quad (3.29)$$

Since $r_s(\eta_i) = 0$, the substitution gives just $(2+R)\Phi(\eta) - (2+R)\Phi_i \cos[kr_s(\eta)]$. Due to the SW effect we observe the combination $\Theta_0 + \Psi$ at the last scattering surface. It will be

$$\Theta_0(\eta_*) + \Psi(\eta_*) = [\Theta_0(\eta_*) + \Phi(\eta_*)] - 2\Phi(\eta_*) = R\Phi(\eta_*) - \frac{1}{2}(1+2R)\Phi_i \cos[kr_s(\eta_*)] - \int_{\eta_i}^{\eta_*} (2+R)\dot{\Phi}(\eta) \cos\left[kr_s(\eta_*) - kr_s(\eta)\right] d\eta. \quad (3.30)$$

In the large-scale limit ($k \to 0$) the integral gives $-(2+R)\Delta\Phi = -(2+R)[\Phi(\eta_*) - \Phi_i]$. If the last scattering surface was deep in the radiation-dominated era, this contribution would be zero. On the other hand, in the matter-dominated era $\Phi = \frac{9}{10}\Phi_i$, and $-2\Delta\Phi = \frac{1}{5}\Phi_i$. In reality the last scattering surface is just after the equality, so the contribution from the integral is somewhere between zero and $\frac{1}{5}\Phi_i$. Assuming η_* at pure matter-dominated epoch, the result (3.30) reads $\Theta_0(\eta_*) + \Psi(\eta_*) = (-\frac{1}{2} + \frac{1}{5})\Phi_i = -\frac{3}{10}\Phi_i$, in the limit $k \to 0$. This is exactly the same we would obtain from (2.36) and (2.40). Hence, our subhorizon solution is consistent with the superhorizon solution.

From our approximate adiabatic solution (3.28), the dipole is calculated as on the line after equation (2.101)

$$\Theta_1(\eta) = -\tfrac{3}{k}(\dot{\Theta}_0 + \dot{\Phi}) = \frac{3}{2}\frac{1}{\sqrt{3}}\frac{3}{\sqrt{1+R}}\Phi_i \sin(kr_s) - 3\int_{\eta_i}^{\eta} k\tilde{c}_s^2 \left[\Phi(\eta') - (1+R)\Psi(\eta')\right] \cos\left[kr_s(\eta) - kr_s(\eta')\right] d\eta'. \quad (3.31)$$

Neglecting the integral in (3.30) and a similar integral for Θ_1, the first two terms of the line of sight integration result (2.128) read now

$$\frac{\Theta_\ell(\eta_0, k)}{2\ell+1} = \left[\Theta_0 + \Psi + i\mu\Theta_1\right](\eta_*, k) \times j_\ell[k(\eta_0 - \eta_*)] = \left\{R\Phi(\eta_*) - \frac{1}{2}(1+2R)\Phi_i \left[\cos[kr_s(\eta_*)] - i\mu\tfrac{\sqrt{3}}{\sqrt{1+R}} \sin[kr_s(\eta_*)]\right]\right\} j_\ell[k(\eta_0 - \eta_*)]\,.$$

Naturally, if there were no baryons ($R = 0$), there would be no acoustic oscillations. This

is also seen from the above equation by realizing that $\langle|\mu|^2\rangle = 1/3$. Hence we would get

$$\left\langle \left| \frac{\Theta_\ell(\eta_0,k)}{2\ell+1} \right|^2 \right\rangle = \left\langle \left| -\frac{1}{2}\Phi_i \Big\{ \cos[kr_s(\eta_*)] - i\mu\sqrt{3}\sin[kr_s(\eta_*)] \Big\} \right|^2 \right\rangle j_\ell^2 = \frac{1}{4}\left\langle |\Phi_i|^2 \right\rangle j_\ell^2 .$$

This disappearance of the oscillatory behaviour is a result of monopole and dipole being in completely opposite phases both in time (sine vs. cosine) and in space (i in front of the dipole term). But when $R > 0$, the monopole and dipole terms do not cancel each other, since the amplitude of the dipole is only $1/\sqrt{1+R}$ times the amplitude of the monopole. In addition, the zero level of the monopole oscillation is shifted to $R\Phi$.

In (2.83) we found that typically $R_* = 0.55$—1. Hence, in the variance, the dipole amplitude is less than $(1/\sqrt{1+0.55})^2 = 65\%$ of the monopole. Moreover, the monopole and dipole are still in opposite phases in time (cosine vs. sine), which reduces the importance of the dipole, when determining the peaks of $\left\langle |\Theta_\ell(\eta_0,k)/(2\ell+1)|^2 \right\rangle$. Thus, in practice, in the C_ℓ spectrum there arise peaks at multipoles ℓ which correspond to such values of k that $\cos^2[kr_s(\eta_*)]$ takes its maximum value. In between the peaks there are valleys, but due to the dipole contribution, the amplitude is not zero anywhere. (Note also that $j_\ell^2(kD_*^A)$ picks some contribution to the C_ℓ from many other values of k than from exactly $k = \ell/D_*^A$, which in part smoothens the peaks and valleys.)

The first acoustic peak arises on a scale that obeys $kr_s(\eta_*) = \pi$. For the second peak we have $kr_s(\eta_*) = 2\pi$, and for the nth peak $k = n\pi/r_s(\eta_*)$. Consequently, in the angular power, our prediction for the position of the nth peak is $\ell_n = n\pi D_*^A/r_s(\eta_*)$. Plotting the monopole and dipole we realize that the $R\Phi$ shift in the zero level of the monopole results in an interesting effect for the heights of the peaks. The odd peaks become more pronounced than the even peaks. Since $R \propto \omega_b$, we realize that the physical baryon density can be determined by measuring the ratio of the heights of odd and even peaks. Around the concordance parameter values (see Sec. 4.3) Hu et al. find in [184] for the ratio H_2 of the second peak to the first peak the following scaling formula

$$\frac{\Delta H_2}{H_2} \approx 0.88\frac{\Delta n_{\rm ad}}{1} - 0.64\frac{\Delta\omega_b}{\omega_b} + 0.14\frac{\Delta\omega_m}{\omega_m}\,, \tag{3.32}$$

where the dependence on the spectral index n is easy to understand: positive tilt causes larger second peak compared to the first peak. The ω_m dependence comes from the early integrated SW effect, which we explain in Sec. 3.5.1.

Recall that the acoustic oscillations are a consequence of the competition between gravitational infall and the photon pressure. The first peak is caused by a k mode that has had time to oscillate one half of a period before the last scattering. The second peak comes from the mode that has oscillated through a full period, and so on. Hence, the odd peaks represent the compression maxima, and even peaks maximal rarefaction. Compared to the baryonless situation, the baryons increase the effective mass of the photon-baryon fluid causing the fluid to fall deeper into the gravitational potential wells. Finally, the photon pressure wins and rarefaction starts. This is the physical explanation of the $R\Phi$ offset and the enhancement of odd peaks over even peaks.

3.4.3 Gravitational driving

On scales that enter the horizon after equality but before decoupling the integral in (3.30) gives a negligible contribution, since Φ is practically a constant in matter-dominated era on all scales. On small scales, $k > k_{\rm eq}$, there occurs *gravitational driving*, since Φ (is oscillating and) its amplitude decreases very fast when it enters the horizon during radiation domination (say at $\eta = \eta_k^{\rm hor} = 1/k$) as described at the beginning of Sec. 2.7.3. Approximating Φ by a step function $\Phi = [1-\theta(\eta-\eta_k^{\rm hor})]\Phi_i$, we get an order of magnitude estimate for the integral in (3.30): $2\Phi_i \cos\left[kr_s(\eta_*) - kr_s(\eta_k^{\rm hor})\right] = 2\Phi_i \cos\left[kr_s(\eta_*) - 1/\sqrt{3}\right]$.

Neglecting R, for scales $k_*^{\rm hor} < k < k_{\rm eq}$, the anisotropy amplitude from (3.30) is $|\Theta_0(\eta_*) + \Psi(\eta_*)| \approx \frac{1}{2}|\Phi_i|$ while for scales that enter the horizon a little before equality, $k > k_{\rm eq}$, we have $|\Theta_0(\eta_*) + \Psi(\eta_*)| \approx |-\frac{1}{2}\Phi_i + 2\Phi_i| = \frac{3}{2}|\Phi_i|$. Hence, we have shown that the decay of potential on subhorizon scales in the radiation-dominated era boosts the anisotropy by a factor 3. (The angular power C_ℓ becomes boosted by a factor 9.) Compared to the SW results $\frac{3}{10}|\Phi_i|$ the boost factor is 5 [172]. However, the boost is not as profound as it might seem, since the diffusion damping starts to be effective also on scales $k > k_{\rm eq}$.

From (1.21) we have $k_{\rm eq} = \omega_m \times 0.0729\,{\rm Mpc}^{-1}$. For typical values $h = 0.7$ and $\omega_m = 0.147$ this leads to $k_{\rm eq} = 0.011\,{\rm Mpc}^{-1}$, and $\ell_{\rm eq} = 0.011 \times 14\,000 = 150$. Thus, all the acoustic peaks (including the first one) are boosted. If $\omega_m \gtrsim 0.2$, then $\ell_{\rm eq} > 210$, and the first acoustic peak does not become boosted. With even larger $\omega_m \sim 0.5$ the boosting starts after the second peak and so on. Small ω_m leads to more power around the first acoustics than large ω_m. This is easy to understand: with small ω_m, the equality comes later, so that larger scales become subhorizon during radiation domination and get boosted.

The gravitational driving introduces also a phase shift to acoustic oscillations [211]. Moreover, we used the relation $\ell_k \simeq kD_*^A$, but the spherical Bessel function $j_\ell(kD_*^A)$ actually peaks at about 10% smaller ℓ [94]. Taking into account these effects Hu et al. [184] find that the acoustic peak positions will be approximately $\ell_n = (n-\phi)\pi D_*^A/r_s(\eta_*)$ with the phase shift $\phi = 0.267(r_*/0.3)^{0.1}$, where $r_* = \rho_r(\eta_*)/\rho_m(\eta_*) = 0.042\omega_m^{-1}(z_*/10^3)$.

3.4.4 Damping on small scales

So far, we have implicitly assumed that the universe is completely opaque before decoupling. However, the ionization fraction decreases continuously, so that the "last scattering surface" is not infinitesimally thin, but has some thickness $\delta\eta_*$. This means that when looking into a particular direction in the sky, instead of seeing a point at a spherical shell at distance D_* from us, we will see the radial interval from D_* to $D_* + \delta\eta_*$. Oscillations on scales smaller than $\delta\eta_*$ do not show up as observable anisotropies in the sky, since any particular line of sight will encounter both overdense and underdense regions within D_* and $D_* + \delta\eta_*$. This effect is called the *cancellation* damping or the effect of *radial averaging.*

Let us estimate the scale of the radial averaging. Recombination begins around a

redshift $z_{\rm rec} = 1300$ and ends around $z_* = 1100$. Assuming a matter-dominated universe, the distance between these two reads

$$\delta\eta_* = \eta_* - \eta_{\rm rec} = \left(\frac{1}{\sqrt{z_*+1}} - \frac{1}{\sqrt{z_{\rm rec}+1}}\right)\eta_0 = 0.0024\eta_0 \approx 0.0024 D_*^A,$$

which corresponds to the multipole $\ell = \frac{2\pi D_*^A}{\delta\eta_*} = 2\pi \times 0.0024^{-1} = 2\,600$.

In Sec. 2.7.3 we discussed another small-scale damping effect, the diffusion damping. A numerical result corresponding to equation (2.117) is

$$k_D^{-1} \approx a^{5/4}\omega_m^{-1/4}\omega_b^{-1/2}(1 - Y_{\rm He})^{-1/2}\,, \tag{3.33}$$

where $Y_{\rm He}$ is the mass fraction of helium. Hu et al. [184] find a fitting formula

$$k_D^{-1}(\eta_*) \approx \frac{\left(\sqrt{1+r_*} - \sqrt{r_*}\right)^{1/2}}{1120}\left(\frac{z_*}{1000}\right)^{-5/4}\omega_b^{-0.24}\omega_m^{-0.39} \times 3000\ {\rm Mpc}\,. \tag{3.34}$$

With $\omega_b = 0.022$, $\omega_m = 0.15$, and $h = 0.7$ this gives $\ell_D = k_D D_*^A \simeq 0.10\,{\rm Mpc}^{-1} \times 14\,000\,{\rm Mpc} = 1400$.

After adding these two damping effects on top of the gravitational boosting, we end up with decreasing series of acoustic peaks, if the spectral index $n_{\rm ad}$ is moderate.

3.4.5 Adiabatic versus isocurvature initial conditions

In the isocurvature case we need to replace the cosines in Sec. 3.4.2 by sines and vice versa. Thus, the acoustic peak positions would be $\ell_n = [(n-1/2) - \phi]\pi D_*^A / r_s(\eta_*)$, where the phase shift due to the gravitational driving has not necessarily exactly the value as in the adiabatic case. However, we notice an important fact that the distance between two successive acoustic peaks is

$$\Delta\ell \stackrel{\rm def}{=} \ell_{n+1} - \ell_n = \frac{\pi D_*^A}{r_s(\eta_*)} \tag{3.35}$$

for both the adiabatic and the isocurvature case.

Substituting $k_{\rm eq}$ into the formula (2.97) for the sound horizon, using the Friedmann equation, and putting in numbers, we find

$$r_s(\eta_*) = \frac{2}{\sqrt{3}}\frac{1}{\sqrt{\omega_m}}\frac{1}{\sqrt{1+z_*}}\frac{1}{\sqrt{R_*}} \times \ln\frac{\sqrt{1+R_*} + \sqrt{R_*+r_*R_*}}{1+\sqrt{r_*R_*}} \times 3000\,{\rm Mpc}, \tag{3.36}$$

where, as before, $R_* = 3\rho_b(z_*)/4\rho_\gamma(z_*) = 30\omega_b(10^3/z_*)$ is the baryon to photon ratio, and $r_* = \rho_r(z_*)/\rho_m(z_*) = 0.042\omega_m^{-1}(z_*/10^3)$ is the radiation to matter ratio. The redshift of the last scattering surface z_* depends very weakly on ω_m and ω_b, see [184].

In Fig. 3.3 we plot $\Delta\ell$ using the above result for the sound horizon and (3.18) for the angular diameter distance to the last scattering surface. We use a parametrization where H_0 is a derived parameter. Consequently, H_0^{-1} in (3.18) gives a factor $\sqrt{(\Omega_m/\omega_m)} \times 3\,000\,{\rm Mpc}$ in D_*^A. The $1/\sqrt{\omega_m}$ part here cancels the similar factor in r_s. Hence, the end result $\Delta\ell$ depends only very weakly on ω_m via r_* and z_*. The ω_b dependence is also weak and comes only via R_* and z_*. Moreover, ω_m and ω_b become fixed very tightly by the

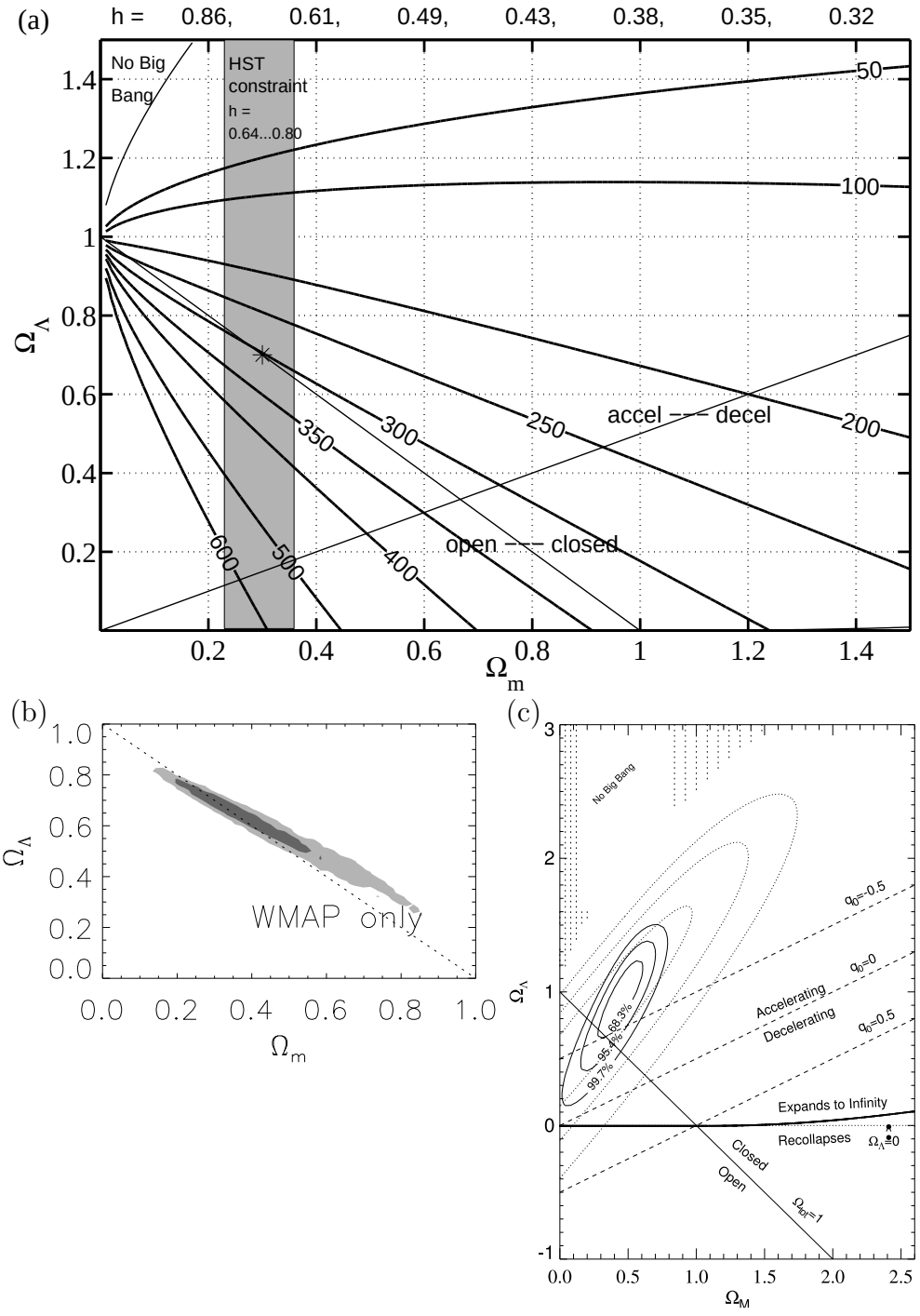

Figure 3.3: **Distance between successive acoustic peaks $\Delta\ell$, and observational constraints in $(\Omega_m, \Omega_\Lambda)$ plane. (a)** $\Delta\ell$ with $\omega_m = 0.147$, $\omega_b = 0.022$. The Hubble parameter is a derived parameter, $h = \sqrt{\omega_m/\Omega_m}$. Its values are indicated above the plot. We also show by the gray band the Huble Space Telescope constraint $h = 0.72 \pm 0.08$. **(b)** The 68% and 95% confidence level regions from WMAP observations. The allowed region follows closely the line $\Delta\ell \simeq 300$ of plot (a). **(c)** The 68%, 95%, and 99.7% confidence level regions from supernovae type Ia observations. The solid lines are for the year 2004 data and the dashed lines for the year 1999 data. The allowed region is nearly perpendicular to the WMAP region. The parts (b) and (c) have been reprinted with permission from [212] and [100], respectively.

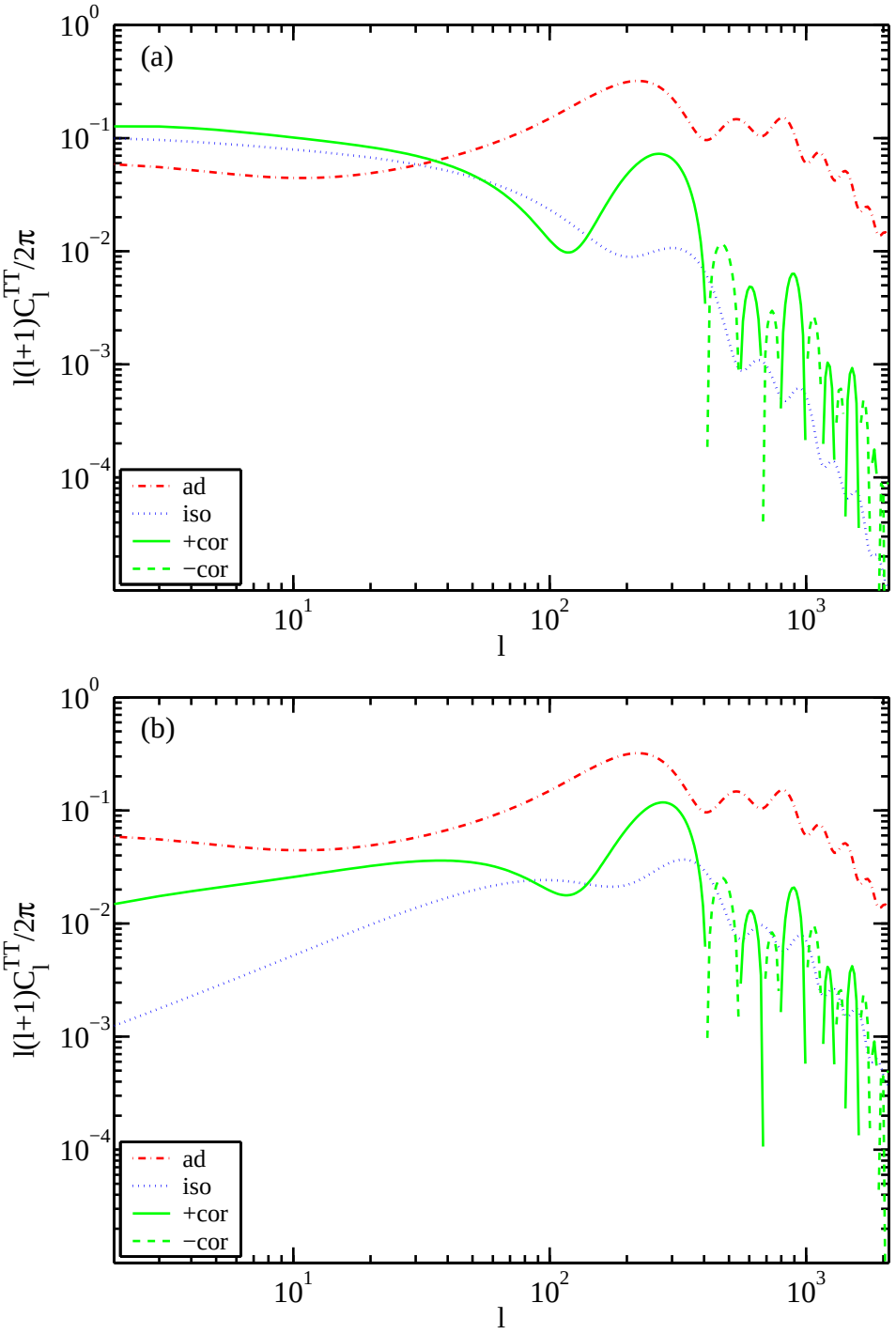

Figure 3.4: **Comparison of CMB temperature angular power** arising from unit amplitude adiabatic and isocurvature primordial perturbations, $\mathcal{P}_{\mathcal{R}_i} = 1 \times (k/k_0)^{n_{\rm ad}-1}$ and $\mathcal{P}_{\mathcal{S}_i} = 1 \times (k/k_0)^{n_{\rm iso}-1}$, respectively. We show also the correlation spectrum resulting from a "100% primordial correlation" $\mathcal{C}_{\mathcal{R}_i\mathcal{S}_i} = 1 \times (k/k_0)^{n_{\rm ad}/2+n_{\rm iso}/2-1}$. **(a)** The end result of scale-invariant primordial spectra $n_{\rm ad} = n_{\rm iso} = 1$. **(b)** The end result of $n_{\rm ad} = 1$ and $n_{\rm iso} = 2.252$. The plotted spectra have been calculated by CAMB [193] for a model with $\omega_b = 0.023$, $\omega_c = 0.12$, $\Omega_\Lambda = 0.71$, $\Omega_m = 0.29$, $\tau = 0.11$, and $h = 0.71$.

heights of the acoustic peaks, which are sensitive to these parameters. This motivates fixing the physical matter and baryon densities to some typical well-fitting values, and showing $\Delta\ell$ as a function of the remaining parameters Ω_Λ and $\Omega_m = \Omega_{\rm tot} - \Omega_\Lambda$.

The distance between acoustic peaks $\Delta\ell$ depends most strongly on the geometry of the universe (i.e. on $\Omega_{\rm tot}$). From Fig. 3.3 we find also some Ω_Λ dependence. Since $\Delta\ell$ is independent of the initial conditions of perturbations, it can be used the determine the geometry. In the data $\Delta\ell \simeq 300$, which implies nearly flat universe.

After fixing the total density parameter $\Omega_{\rm tot}$, we can now decide whether the primordial perturbations have been of adiabatic or isocurvature type. Taking into account the phase shift ϕ, the acoustic peaks arise at $\ell \simeq 200, 500, 800, \ldots$, in the adiabatic case. As seen in the beginning of this section, the isocurvature mode is approximately in the opposite phase, if the other cosmological parameters are the same as for the adiabatic model. So, isocurvature would produce peaks at $\ell \simeq 50, 350, 650, \ldots$. This conclusion is confirmed by exact numerical calculations. In Fig. 3.4a we show typical adiabatic and isocurvature angular power spectra for scale-invariant primordial perturbations. The first isocurvature "peak" at $\ell = 50$ is invisible, since the gravitational boosting has not raised its amplitude. We see also the diffusion damping effect which kills the power at large ℓ.

In addition to being in the opposite phase, the isocurvature perturbation mode differs from the adiabatic one in another respect, too. In Sec. 2.7.4 we found that the isocurvature monopole temperature perturbation amplitude is proportional to $(k_{\rm eq}/k)\mathcal{S}_i$. When converted to C_ℓ spectrum, this causes $(k_{\rm eq}/k)^2 \propto (\ell_{\rm eq}/\ell)^2$ behaviour, which is apparent from Fig. 3.4a. To maintain the ratio of the adiabatic and isocurvature power at approximately the same level on all scales, we would need to have $n_{\rm iso} \simeq n_{\rm ad} + 2$ to cancel the k^{-2} damping. This is demonstrated in Fig. 3.4b.

3.5 Secondary anisotropy sources

In this section we introduce effects arising after the last scattering, which can alter the anisotropy spectrum from that produced by the primary effects. Here we just mention some of these secondary effects. The most important ones are the early and late integrated Sachs-Wolfe effects which sometimes are even regarded as primary effects, since they are an essential part of the observed anisotropy spectrum.

3.5.1 Integrated Sachs-Wolfe effect

If the photons coming from the last scattering surface travel through time varying potential wells, then the integrated Sachs-Wolfe effect occurs. A constant potential well on the path of the photons does not alter the anisotropy spectrum, since the photons suffer gravitational redshift when climbing out of the well, which exactly cancels the blueshift caused by infall into the well. However, for example a decaying well gives rise to a net change in the energy of photons, since the redshift upon climbing out of the well is smaller than the blueshift upon falling in.

From classical mechanics the ISW effect on the temperature perturbation would be $\delta T^{ISW}/T = \int \dot{\Psi}(\eta, \vec{x}) d\eta$, where the integral is taken along the path of photons and Ψ is the Newtonian gravitational potential. However, this is not the whole truth. There is also a simultaneous general relativistic effect from stretching of space due to potential Φ. This approximately doubles the ISW effect, i.e., we obtain

$$\Theta^{ISW} = \int \left[\dot{\Psi}(\eta, \vec{x}) - \dot{\Phi}(\eta, \vec{x})\right] d\eta \,, \tag{3.37}$$

where $\Phi = -\Psi$, if there is no anisotropic stress. The exact formula in Fourier space for each multipole is given by the last term of (2.128)

$$\frac{\Theta_\ell^{ISW}(\eta, k)}{2\ell + 1} = \int_{\eta_*}^{\eta} [\dot{\Psi} - \dot{\Phi}](\eta', k) X_\nu^\ell(\tilde{\chi} - \tilde{\chi}') \, d\eta'. \tag{3.38}$$

The potentials remain constant in time on all scales, if the universe is strictly matter dominated ($\Omega_m(t) \gg \max\{\Omega_r(t), |\Omega_{de}(t)|, |\Omega_k(t)|\}$), and linear perturbation theory is valid ($\delta\rho/\rho \ll 1$). In the following we describe how these condition are violated in realistic cosmological models and determine the importance of the ISW effect in each case.

Early ISW effect

Consider the large scales first. In all viable models the last scattering occurs after matter to radiation equality, but it is only a slightly after ($a_*/a_{\rm eq} \simeq$ 3–100), which means that the universe is not yet fully matter dominated at the time of last scattering. Thus the gravitational potential Ψ is decaying (growing)[5] from the radiation-dominated value Ψ_i ($-\frac{1}{8} y \mathcal{S}_i$) to the matter-dominated value $\frac{9}{10}\Psi_i$ ($-\frac{1}{5}\mathcal{S}_i$) in pure adiabatic (isocurvature) models, see again the result (2.36). Since this kind of potential decay or growth happens at early times, the effect is called the early ISW (eISW) effect.

We can replace the upper limit in the integral (3.38) with some $\eta_1 \ll \eta_0$, where η_1 is in the fully matter-dominated epoch. Now $\tilde{\chi}_0 - \tilde{\chi}' \approx \tilde{\chi}_0$ and the integral becomes

$$\begin{aligned} \frac{\Theta_\ell^{eISW}(\eta_0, k)}{2\ell + 1} &\approx X_\nu^\ell(\tilde{\chi}_0) \int_{\eta_*}^{\eta_1} [\dot{\Psi} - \dot{\Phi}](\eta', k) d\eta' \\ &= X_\nu^\ell(\tilde{\chi}_0)[\Delta\Psi - \Delta\Phi] \\ &\approx 2\, X_\nu^\ell(\tilde{\chi}_0)\Delta\Psi, \end{aligned} \tag{3.39}$$

where $\Delta\Psi = \Psi(\mathrm{MD}) - \Psi(\eta_*)$ is the difference of the fully matter-dominated value of the potential and the value at the time of last scattering.

From the result (3.39) one realizes that the ordinary SW and ISW effect add to each

[5]Note that in this and in the following section we think of gravitational potential well $\Psi < 0$ caused by an overdensity. For underdensity ($\Psi > 0$) the terminology would be opposite, i.e., decaying $\leftrightarrow$ growing and redshift $\leftrightarrow$ blueshift.

other coherently (they both have $X_\nu^\ell(\tilde{\chi}_0)$). Thus the combined effect reads

$$\frac{\Theta_\ell^{SW+eISW}(\eta_0,k)}{2\ell+1} \approx \Big\{[\Theta_0+\Psi](\eta_*) + 2\Psi(\mathrm{MD}) - 2\Psi(\eta_*)\Big\} X_\nu^\ell(\tilde{\chi}_0). \tag{3.40}$$

The SW part can be written as $[\Theta_0+\Psi](\eta_*) = 2\Psi(\eta_*) + C$, where $C = -\frac{3}{2}\Psi_i$ in the adiabatic and zero in the isocurvature case, cf. Sec. 3.4.1 and the result (2.36). The term $2\Psi(\eta_*)$ from the SW effect cancels $-2\Psi(\eta_*)$ from the ISW effect, and the result (3.40) becomes independent of the value of the potential at the last scattering surface. Reading $\Psi(\mathrm{MD})$ from (2.36), we arrive at

$$\frac{\Theta_\ell^{SW+eISW}(\eta_0,k)}{2\ell+1} \approx X_\nu^\ell(\tilde{\chi}_0) \times \begin{cases} \frac{3}{10}\Psi_i & \text{(pure adiabatic)} \\ -\frac{2}{5}\mathcal{S}_i\,. & \text{(pure isocurvature)} \end{cases} \tag{3.41}$$

This is the same result which we would obtain for the ordinary SW effect by assuming that the last scattering occurs in the fully matter-dominated epoch, cf. equation (3.23).

Above, we have shown the following: In adiabatic models the eISW effect causes a blueshift, which approximately cancels the additional redshift the photons suffer due to the deeper potential well at the last scattering surface than in the fully matter-dominated epoch. In isocurvature models the eISW effect causes a redshift due to the growing potential, and again this cancels that part of the ordinary SW effect, which is caused by the fact that the potential well is lower at the time of last scattering than in the fully matter-dominated epoch. This is why ignoring the eISW effect and assuming that the last scattering occurs in the fully matter-dominated epoch, leads to very exact results on large scales. Hadn't the cancellation of $2\Psi(\eta_*)$ been so exact, the earliest studies, where only the ordinary SW effect was considered, would have led to misleading results.

Nevertheless, the eISW effect is important on intermediate scales which are approaching the sound horizon at last scattering. The reason for this is very similar to the reason for the gravitational driving effect of Sec. 3.4.3. On scales that enter the horizon between the equality and last scattering, the gravitational potential starts to decay as $(k\eta)^{-2}$ at horizon entry, see Sec. 2.7.3. This causes a strong eISW effect on these scales.

Discuss pure adiabatic models first. The sound horizon $r_s(\eta_*)$ is approximately $\tilde{c}_s\eta_*$ with $\tilde{c}_s \simeq 1/\sqrt{3}$. Thus the sound horizon is about $1/\sqrt{3}$ times the horizon size at last scattering. As the first acoustic peak arises at the sound horizon scale, the eISW effect affects the multipoles around and before the first acoustic peak, say $\ell < 300$. In the integral in (3.39) the lower bound is now η_{eq} and $-2\Psi(\eta_*)$ in (3.40) becomes replaced by $-2\Psi_i$. The SW term in (3.40) is just $-\frac{3}{2}\Psi_i$ and the term $2\Psi(\mathrm{MD})$ is close to zero, since the potential has decayed away. Taken together, the eISW effect adds a blueshift $-2\Psi(\eta_*)$ to the ordinary ISW effect. Thus the angular power around the first acoustic peak becomes larger than without the eISW effect, and the growth of the power starts well before the actual peak.

In isocurvature models the large-scale potential grows until the full matter domination ($\Psi/\mathcal{S}_i = -\frac{1}{8}y$) but when a given k-mode enters the horizon, the growth ends and the potential starts to decay causing a blueshift as in the adiabatic case. However, on super-

horizon scales the potential continues growing toward the value $-\frac{1}{5}\mathcal{S}_i$ as described above. Hence, on superhorizon scales, the eISW effect works in the opposite direction than on intermediate scales. We conclude that eISW reduces the angular power at $\ell_{\rm MD} \lesssim \ell \lesssim \ell_{\rm eq}$, where $\ell_{\rm MD}$ is a multipole corresponding to the scale that enters the horizon in strictly matter-dominated era, i.e., when the potential has settled down to its MD value. The eISW effect together with the factor $(k_{\rm eq}/k)^2$ causes a steep negative slope of $\ell(\ell+1)C_\ell$ on all scales in the isocurvature case even for $n_{\rm iso} = 1$ as shown in Fig. 3.4a.

The time of matter to radiation equality is the closer to the time of last scattering the smaller the matter density ω_m is. Thus the eISW effect becomes most pronounced in the universe with low matter density. The importance of the ISW effect also depends on the scale of the perturbation, which is going through the time varying potential. If the scale of the perturbation is much smaller than the time scale in which the potential decays (grows), then the perturbation suffers both negative and positive ISW contributions, which cancel each other. Time scale for the potential decay or growth is of the order of the size of the horizon at time of the decay. Thus the eISW effect is the most significant on large scales $\ell < 200$.

Late ISW effect

Both in adiabatic and isocurvature models the potential decays (grows) after the matter-dominated epoch, if the universe is not flat or if there exists the cosmological constant (or other dark energy). This comes about because $\tilde{a}$ in (2.36) starts to differ from y in the CD/ΛD case. This gives rise to the late ISW (lISW) effect. As the eISW effect, also the lISW effect is the most significant on modes with comparable scale to the time scale of the decay, which again is of the order of the horizon size during the decay. For example, the vacuum energy to matter energy equality occurs when $\Omega_m(a_0/a)^3 = \Omega_\Lambda$. This gives $a = 0.75a_0$ for $\Omega_m = 0.3$ and $\Omega_\Lambda = 0.7$. Thus the vacuum energy domination starts very recently, and affects the scales comparable to today's horizon, i.e., the lowest multipoles in the angular power.

The exact formula for the lISW contribution is

$$\frac{\Theta_\ell^{lISW}(\eta,k)}{2\ell+1} = 2C\int_{\eta_*}^{\eta}\frac{\tilde{a}}{a}\left(\frac{\dot{\tilde{a}}}{\tilde{a}}-\frac{\dot{a}}{a}\right)X_\nu^\ell(\tilde{\chi}-\tilde{\chi}')\,d\eta', \tag{3.42}$$

where $C = \frac{9}{10}\Psi_i$ in the adiabatic case and $C = -\frac{1}{5}\mathcal{S}_i$ in the isocurvature case. The integration lower bound can be replaced by the time when the vacuum or curvature domination begins.

The lISW effect of positive Ω_Λ causes the angular power to rise towards the lowest multipoles erasing the SW plateau. As discussed in paper **IV** the correlated isocurvature contribution is able to mimic (or cancel) this effect. Hence, the determination Ω_Λ is highly degenerate with the isocurvature. However, drawing "independent" constraints on the dark energy have become possible recently by cross-correlating the WMAP maps with large-scale structure surveys [213].

Rees-Sciama effect

The potential Ψ is constant in time in the matter-dominated epoch only in linear perturbation theory, which fails at very late times, when non-linear structure (such as galaxy clusters) forms causing the potential to grow [214]. This causes a special integrated SW effect called the Rees-Sciama effect. In hierarchical models, the smallest scales go non-linear first and thus the effect peaks toward small scales.

Some other ISW or gravitational effects

If there is a background of primordial gravitational waves, they introduce tensor perturbations in the metric, which leave a quadrupole signature on the distribution of the photons passing them. The gravitational waves redshift once they enter the horizon. Thus the possible effect of the gravitational waves occurs at low multipoles $\ell \lesssim 70$, cf. Sec. 3.3.

Also topological defects [215] can cause (time varying) spacetime curvature and hence an ISW effect.

Possible tensor perturbations are important in the CDM isocurvature models because they are very degenerate with the isocurvature amplitude and spectral index. The CMB data limits the isocurvature contribution tightly at higher multipoles, but at low multipoles significant isocurvature contribution is allowed. Note again also Fig. 3.4 and the fact that when $n_{\rm iso} \lesssim 3$ the isocurvature modifies the most the SW part — the same part of the spectrum where tensor modes would produce additional power. The polarization data can break this degeneracy. Recently, the CMB-galaxy cross-correlation has also been used to constrain the tensor contribution and gravity waves [216] In papers **I**–**V** we just assume that there are no tensor perturbations.

3.5.2 Gravitational lensing

From the previous discussion it should be clear that the ISW effect can be thought of as a momentum kick to a photon in the direction of its motion. This is caused by a time varying gradient of the gravitational field ($\nabla\Psi$) parallel to the path of flight of the photon. Gravity also kicks the photons in the transverse directions changing their direction of motion but not their energies (to first order). The result is weak gravitational lensing [217, 218], i.e., our image of the last scattering surface is distorted as if we looked at it through an irregular refracting medium. The consequence of this is a slight smearing of the angular power spectrum: Some power from the peaks will be moved into the valleys. Therefore the gravitational lensing smoothens the sharp features of the primary power spectrum.

3.5.3 Reionization

So far we have assumed that the photons do not scatter after the last scattering surface. However, the matter may become *locally reionized*, for instance, in hot clusters of galaxies.

Thus there exist free electrons from which the photons can (Thomson) scatter. In the direction of a cluster moving towards (away from) us, this will cause a Doppler blueshift (redshift), known as kinematic Sunyaev-Zel'dovich effect [219–222]. On the other hand, the high temperature of the free electrons distorts the blackbody spectrum: photons are transferred from the low-frequency region of the spectrum (Rayleigh-Jeans) into its high-frequency region (Wien), resulting in an intensification of power at the higher-frequency region and drop of power at frequencies lower than 217 GHz. The effect of local reionization (i.e. cluster Comptonization) on the CMB power spectrum is not negligible at multipoles of $\ell \gtrsim 1000$–3000 (the exact value depending on the cosmological model and cluster properties), where the primary spectrum is heavily suppressed due to Silk-damping.

The universe may also become *globally reionized*. From the Gunn-Petterson test it is known that the intergalactic medium is reionized out to redshifts of a few [223–225]. Usually it is assumed that the reionization occurs together with the formation of the earliest non-linear structure. Since this happens at moderate redshifts, the effect of reionization should be small. If the reionization somehow occurred much earlier, say at $z > 100$, it would alter the CMB anisotropy spectrum quite dramatically. First of all, the photons that come towards us from a particular direction need not to have originated from that direction, since the Thomson scattering could have changed their direction of propagation. This means that each direction in the observable sky contains photons that originate from a variety of locations at the last scattering surface. Thus the observed temperature is an average over some region at last scattering surface, and this removes especially the small-scale anisotropies. In fact, in severely reionized models the power suppression may begin at quite low ℓ-values, even so low as $\ell \sim 10$, and the acoustic peaks are completely washed out. On the other hand, the bulk flow and inhomogeneities of the reionized matter will cause new anisotropies.

As the optical depth τ appears in the visibility function $\dot{\tau}e^{-\tau}$, the CMB angular power probes more straightforwardly the optical depth due to reionization than the reionization redshift. (Note however, that the determination of the optical depth due to reionization is very degenerate with the spectral index and primordial amplitude of perturbations, since the main effect of the optical depth is just to lower the power at high multipoles. Polarization measurements are needed to break the degeneracy [54].) On the other hand, from the astrophysical observations one can try to determine z_{re} [226]. So it is worth deriving the relation between these two.

We start by writing the optical depth in the form

$$\tau = \int \dot{\tau} d\eta = \int \frac{d\tau}{dt}\frac{dt}{d\eta}\frac{d\eta}{da}da = \sigma_T \int n_{\rm free}\frac{a}{a_0}\frac{da}{\dot{a}}\,, \tag{3.43}$$

and assuming an instantaneous full reionization of the hydrogen at redshift z_{re}. This means that the number density of free electrons is practically zero between the last scattering surface and z_{re}. Instead, for $z < z_{re}$ we would have $n_{\rm free} = (1 - Y_{\rm He})\frac{\rho_b(t)}{m_p} = (1 - Y_{\rm He})\frac{\Omega_b}{m_p}\frac{3H_0^2}{8\pi G}\left(a/a_0\right)^{-3}$, where m_p is mass of the proton and $Y_{\rm He} \simeq 0.24$ is the mass

fraction of helium. Now the optical depth due to reionization becomes

$$\tau(z_{re}) = \int_{\eta_{re}}^{\eta_0} \dot{\tau}(\eta')d\eta' = (1 - Y_{\rm He})\frac{\Omega_b H_0^2}{m_p}\frac{3}{8\pi G}\sigma_T H_0^{-1}\mathcal{I}_{re}(z_{re}, 0)$$
$$= 0.069 \times (1 - Y_{\rm He})\,\omega_b\, h^{-1}\,\mathcal{I}_{re}(z_{re}, 0)\,, \qquad (3.44)$$

with

$$\mathcal{I}_{re}(z_{re}, 0) = \int_{\frac{1}{1+z_{re}}}^{1} \frac{dx}{x^2\sqrt{\Omega_\Lambda x^4 + \Omega_k x^2 + \Omega_m x + \Omega_r}}\,, \qquad (3.45)$$

which is very similar to (1.13), appeared again after employing the Friedmann equation (1.11). If τ has been determined by CMB observations, then we find the corresponding z_{re} by integrating numerically $\mathcal{I}(z, 0)$ until the above expression for $\tau(z)$ reaches the wanted value. For a model with $(\Omega_m \simeq 0.3, \Omega_\Lambda \simeq 0.7)$, $\Omega_b \simeq 0.05$, $h \simeq 0.7$ we find that $\tau_{re} = 0.12$ corresponds to $z_{re} = 14$.

3.6 Other anisotropy sources

This category contains sources for such anisotropies that are not truly the properties of the microwave background radiation, but merely some kind of contamination in the measured CMB data. The knowledge of these sources is needed in order to extract the actual CMB anisotropies from dirty data given by satellite, balloon, or ground based observations.

3.6.1 Extragalactic point sources

The sky is full of radio and infrared point sources, which must be removed from the CMB data. In order to do this one can try to use point source catalogs but unfortunately the information is poor in the microwave region of spectrum. Another possibility is to ignore all pixels containing a bright enough point source. In either case the result would be that only sources with a flux exceeding some cut-flux are eliminated. This is a consequence of the fact that for all practical purposes there are infinitely many point sources and thus one cannot eliminate all of them.

3.6.2 Galactic sources

The dust, free-free emission of photons, and synchrotron radiation from galaxies give their own contribution to the anisotropy spectrum. Furthermore, the whole band of the Milky Way in the sky is so contaminated that it must be ignored. This is why there is usually smooth structureless area in the CMB maps at equator — no data, no anisotropies to plot. However, the situation is not as bad as one might think, since a non-thermal shape of spectrum of the galactic sources (and an emission by inter-galactic dust) helps in distinguishing them from the primary anisotropies.

3.6.3 Local sources

Of course, also the sun, the moon, the earth and other planets affect the measurements. In addition, ground and balloon experiments suffer from the atmospheric emission.

Chapter 4

Short history of precision CMB cosmology

As mentioned in the Introduction, the exponential expansion of the interest in observational cosmology began from the definite detection of the first acoustic peak in 2000 by the Boomerang [21, 22] and Maxima [23, 24] teams. We start this chapter by introducing some CMB data sets. We do not try to be comprehensive but instead focus on the data chosen for papers **I**–**V**. Leaving certain data sets out of the discussion should not be regarded as our distrust in those sets. We merely have just used the sets that have been most easily available at the time of writing each paper. We have consciously limited the number of different data sets in our studies. The opposite approach would be to use as much data as possible. While both approaches have their place, using a smaller number of data sets at a time allows us to better discern what kind of constraints result from which kind of data. However, some external priors or data (like the amplitude of the rms mass perturbations in an $8h^{-1}\,\mathrm{Mpc}$ sphere, σ_8, in **I** & **II**, and matter power in **V**) are needed in order to break the degeneracies.

After describing the rapid improvement of the CMB data, we comment on developments of the likelihood analysis, which is straightly related to the parameter extraction and the complexity of the models that can be studied. After briefly discussing the current "concordance" model, we review the main results of papers **I**–**V**.

4.1 The CMB data sets

Although a breakthrough for the Big Bang theory, the detection of nearly isotropic 3 K background radiation in 1965 [8, 9] gave much less information of the history and particle contents of the universe than the anisotropies can offer.

The detection and determination of the amplitude of the anisotropy on large scales by COBE in 1992 [17] was an overwhelming victory for the theory of CMB perturbations that had been developed during 30 years. As we have seen, on large scales, the CMB perturbation amplitude is straightforwardly proportional to the primordial amplitude. Hence we can say that COBE measured the amplitude of the primordial perturbations.

However, in most models, this amplitude is a freely adjustable parameter. So the information offered by the COBE amplitude was very restricted. Take for example the inflation. We do not know what scalar field the inflaton is, and indeed it must result from some presently unknown extension of the standard model of particle physics.

Typically, in the simplest inflationary models, the amplitude of the power $\mathcal{P}_{\delta\phi}$ is related to the strength of the self-interaction of the inflaton field. But in the lack of particle physics knowledge of that field, we do not know the strength or even the type of self-coupling (e.g. whether it is $\propto m^2\phi^2,\ \lambda\phi^4$, a combination of these or maybe something more complicated). The COBE amplitude could be used to rule out only some types of inflaton potentials where one would have needed "unphysically strong" (or weak) couplings, see e.g. [156].

In addition to the amplitude, COBE measured the slope of $\ell(\ell+1)C_\ell/2\pi$ in the interval $\ell = 2$–21. The spectrum turned out to be nearly flat. Thus, in principle, COBE supported the scale invariant ($n = 1$) primordial spectrum. (The COBE data is described by the leftmost gray box in the Fig. 4.1a and by black diamonds in figures b&c. As we see, there is actually some freedom around the scale invariance.) Recalling that the cosmological constant causes an integrated SW effect in the part of the spectrum which COBE measured, one realizes that the determination of the spectral index is degenerate with the determination of Ω_Λ: the negative slope caused by positive Ω_Λ could be balanced by a positive tilt of the primordial spectrum. In lack of independent measurements of Ω_Λ the determination of the spectral index from the COBE data was usually accompanied by an ad hoc assumption $\Omega_\Lambda = 0$. The knowledge of the spectral index was then used to constrain the inflaton potential, which had to be such that the slow roll parameters were small enough to yield $n \approx 1$.

Constraining the geometry of the universe was also impossible with the COBE data alone. Moreover, isocurvature perturbations could have been fitted to the data as well as adiabatic perturbations. However, a strong belief in the scale-invariant adiabatic perturbations led to "ruling out" some models that, in principle, fit even the present-day CMB data. As a warning example, we note that the original implementation of the pre-Big Bang scenario [227] was ruled out in part because the spectral index $n = 4$ of the adiabatic perturbations coming from the dilaton was too large to fit the COBE data, and the second version [68] was ruled out because the axion with a spectral index $n = 1$ carried only isocurvature perturbations. Implementing the pre-Big Bang curvaton model for the axion [72, 73], but keeping the dilaton perturbations would lead to the type of the spectrum studied in paper **IV** with the spectral indices $n_1 = 4$ and $n_2 = 1$, which incidentally agree with the best-fit model we found in **IV**.

In Fig. 4.1a we show the status of the CMB observations at the end of the year 1999. There was already a hint of the first acoustic peak, though even a nearly straight line could have been fitted to the data. In any case, a curve with one small bump (e.g. parabola) would have yielded a perfect fit. Moreover, it is dangerous to combine so many different experiments. At the very least, the combined data analysis becomes very difficult, since one should know the possible correlation and relative normalizations of

different data sets. So, the most severe problem was the lack of a single experiment that would have covered the entire interval from large scales $\ell \sim 10$ to the scales smaller than the scale of the expected acoustic peak around $\ell \sim 200$ (in spatially flat adiabatic models). A bit exaggerating, the "peak" that one was willing to interpret as the acoustic peak could have resulted entirely from systematic calibration errors of the mid-scale experiments relative to the large- and small-scale experiments. However, the TOCO [228, 229] and Boomerang test flight [230] results covered the multipoles $\ell \simeq 60$–400 with high signal to noise ratio, and detected a peak at $\ell \sim 200$.

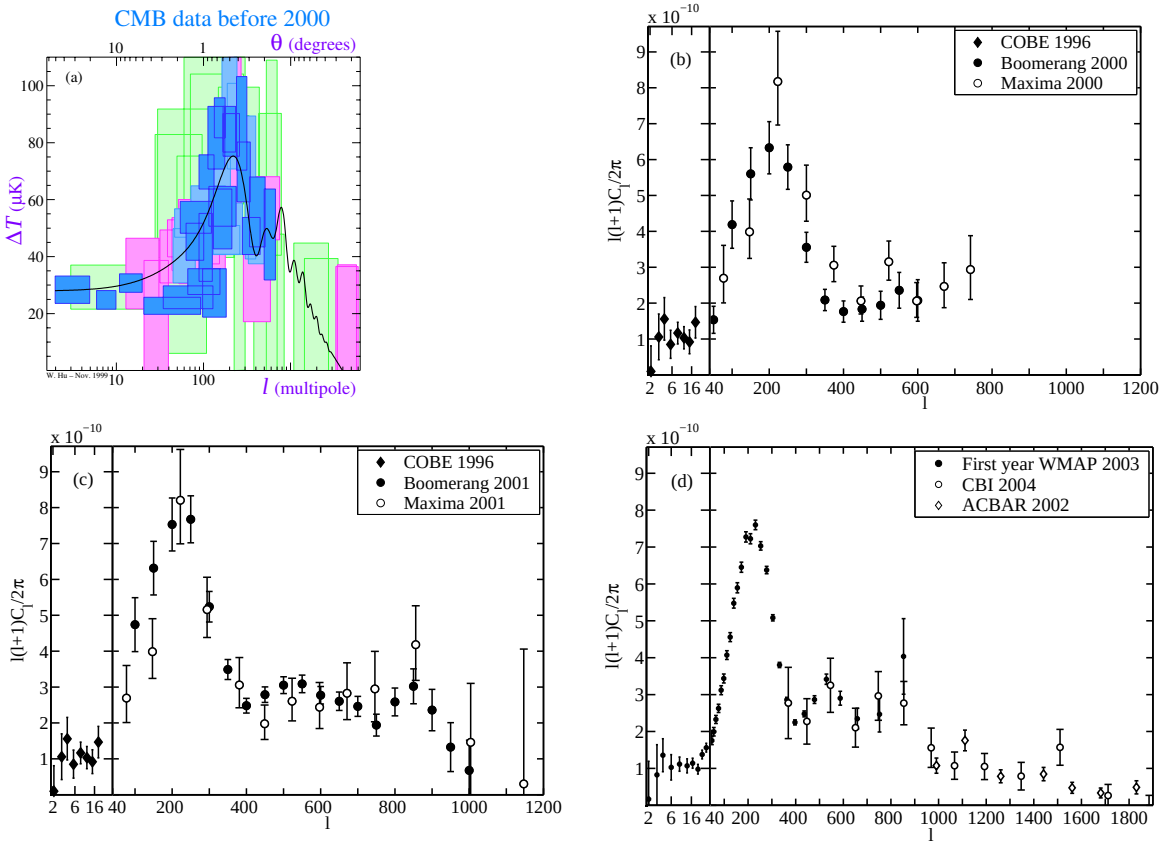

Figure 4.1: **The improvement of the CMB data. (a)** By the year 2000 the Sachs-Wolfe region (leftmost part of the spectrum) was probed accurately by COBE. However, the data in the acoustic peak region was messy, though several ground based experiments had scanned also these small angular scales. This compilation of data has been adopted from Wayne Hu's homepage at the end of year 1999 [231] (see also [90]). Note that the vertical axis is δT instead of $\ell(\ell+1)C_\ell/2\pi$ "$\propto$" $(\delta T)^2$ used in the other three plots in this figure. **(b)** The Boomerang [21] and Maxima [23] data from the year 2000 based on balloon flights above Antarctica and Texas, respectively. The COBE data in this plot is from [232], see also [233]. **(c)** Re-analyzed and enhanced data of the same Boomerang and Maxima flights as (b), but using more of the information collected during the flights. The error bars are smaller and the C_ℓ spectrum extends to smaller angular scales (larger ℓ), since larger patches of the sky were used than in the first data releases. **(d)** The WMAP first year data as published in [26]. We show also results from two ground based experiments CBI [37] and ACBAR [43] to demonstrate how they cover smaller angular scales, but the data is less accurate due to the smallness of the covered patches of sky. In (b) – (d) the horizontal axis is logarithmic up to $\ell = 40$, and linear for $\ell > 40$.

Finally, in May 2000 the experimental status of the CMB physics improved dramatically. In Fig. 4.1b we show the first complete Boomerang [21] and Maxima [23] data that span the multipoles $\ell = 50$–750. Both experiments were balloon borne ones. The Boomerang flight took 11 days at Antarctica and it scanned 750 square degrees of the sky (equivalent to less than 2% of the complete sky) while the Maxima flight lasted 4 days in Texas US and scanned 124 square degrees. Although the Maxima flight was shorter the error bars in the C_ℓ spectrum were about the same size as for Boomerang, since Maxima had more bolometers and they were more accurate than those of Boomerang. (During the shorter flight the bolometers could be kept cooler resulting in less noise.) However, the smallness of the analyzed patch of the sky increases the error bars. In any case, both experiments led to a definite determination of the position of the first acoustic peak. As can be seen from Fig. 4.1b the peak is around the multipole $\ell = 200$.

Absolute calibration of the measured temperature differences $\delta T(\vec{n})$ is a cumbersome task [234–237]. This was reflected by the fact that there was less consensus of the height of the peak, see Fig. 4.1b. As the calibration uncertainty in δT was 10% for Boomerang and 4% for Maxima, it became a common practice to lift up the Boomerang C_ℓ spectrum by multiplying it by 1.1^2 and divide Maxima data by 1.04^2 [23] to obtain consistency in the analysis where the both data sets were used (see also [238]). In [239] we adopted this approach. In paper **I** we performed our original analysis with the data sets as given in [21] and [23], but then we repeated the analysis with "corrected" amplitudes to check that the relative calibration error did not affect our results considerably.[1]

The Boomerang and Maxima data also showed definitely an overall decrease of the angular power towards small scales (large ℓ). As we have discussed, this can be interpreted as diffusion damping. Moreover, a hint of the second acoustic peak was seen although its relative amplitude compared to the first acoustic peak was uncertain due to large error bars. Since the peak was quite flat its position was even more speculative. However, a lot of attention was paid to the lack of prominence of the second peak. Many speculations were proposed [241–245], though cosmologists agreed that because of large experimental uncertainties in the data the lack of power was not statistically significant [246]. One had to wait for more accurate data to see whether the marginal lack of power of the second peak remained. A possible problem was that one would have needed a high baryon density $\omega_b \sim 0.03$ [247, 248] contradicting with Big Bang nucleosynthesis (BBN) calculations $\omega_b \sim 0.02$ [249] (for more a recent BBN value see e.g. [250]). In paper **I** we noticed that if a small portion of the power around the first and second peaks came from the CDM isocurvature perturbation, the observed spectrum could be fitted with a smaller

[1] As the number and precision of the data sets have increased dramatically in four years, dealing with relative normalization errors between data sets has become more and more important. Nowadays, the favourite approach is to vary the relative normalizations of different data sets when comparing to theoretical angular power spectrum and adopt for χ^2 of each model the smallest χ^2 among the values got by different normalizations (for χ^2 see Sec. 4.2). In other words, the relative normalization is marginalized over by maximizing the resulting likelihood for each theoretical model. Along a brute force numerical marginalization analytic methods have been developed [240].

ω_b than in a pure adiabatic case. This comes about because the isocurvature perturbation leads to an angular power that is completely out of phase from the adiabatic situation: isocurvature perturbations lead valleys at multipoles where adiabatic perturbations lead to peaks and vice versa. Hence the relative heights of the successive peaks can be modified by adding a small amount of isocurvature. Note, however, that this was just a side result of our isocurvature analysis, the main result being an upper bound for the isocurvature contribution.

A year after the first data releases, the Boomerang and Maxima teams published the second data releases [27] and [29], respectively. Remarkably, the deficit of power of the second acoustic peak had disappeared, and the peak itself had become evident, see Fig. 4.1c. The improved data was obtained by reanalyzing the sensitivity of the instruments. In particular, modeling of the scale dependence of the sensitivity was reconsidered. Another improvement was the use of CMB maps which covered larger patches of the sky. In paper **II** we used these second data releases along with COBE.

More than ten years of waiting after the COBE satellite ended in February 2003 when the first year WMAP data was released [25, 26], see Fig. 4.1d. The advantage of space based measurements over ground and balloon borne ones is that the entire sky can be scanned by a single apparatus. In addition, satellite based measurements do not suffer from the atmospheric emission and changing weather conditions. The fact that the cosmic variance is the dominant source of uncertainty up to the scale of the first acoustic peak instead of experimental errors reflects the impressive quality of the WMAP temperature power data. However, even in the single field case of inflation many types of inflationary potentials (small-field, large-field, hybrid) remain allowed by the CMB data [251].

4.2 From grid method to MCMC

In its simplest form the comparison of the data and theory proceeds as follows:

1 Decide the theoretical framework. For example, the adiabatic model with a power-law primordial spectrum. In other words, at this stage one must specify the parameters describing the theoretical model and the evolution equations to be used. The standard ΛCDM model could be described by the equations given in Chapter 2, by five background parameters (ω_c, ω_b, Ω_Λ, h, τ), and by two parameters related to primordial perturbation spectrum (the amplitude A and the spectral index $n_{\rm ad}$). Let us denote the cosmological parameters by $a_1, \ldots, a_n$. They form an n dimensional parameter space.

2 Find a physically interesting range for each parameter. At this stage one needs the literature, analytical (approximative) calculations, and, to some extent, intuition.

3 Although the parameter space specified in the steps 1 and 2 is continuous, one can give only a finite discrete set of values to a computer. These form a grid. For example, we could give for each parameter 30 linearly spaced values within their range.

4 Take a set of parameters (i.e. choose a grid point), integrate numerically the evolution equations, and form the theoretical angular power spectrum $C_\ell^{\rm th}$. There are publicly available codes like CAMB [193] and CMBfast [189] for this task.

5 Find how well the theoretical spectrum obtained in the step 4 fits the data. If the measured C_ℓ:s $\{C_{\ell_i}^{\rm meas}\}_{i=1,N}$ are uncorrelated, then a convenient measure of the goodness of the fit is[2]

$$\chi^2 = \sum_{i=1}^{N} (C_{\ell_i}^{\rm th} - C_{\ell_i}^{\rm meas}) \frac{1}{\sigma_i^2} (C_{\ell_i}^{\rm th} - C_{\ell_i}^{\rm meas}) \,, \tag{4.2}$$

where N is the number of data points and σ_i^2 is variance of an estimated measurement error of the ith data point reported by the experimental teams. The smaller the χ^2 is the better the fit is. As an alternative, one can use the likelihood $\mathcal{L}$ defined as $\mathcal{L} = e^{-\chi^2/2}$. For a better fit $\mathcal{L}$ receives a larger value.

6 Save the likelihood and return to the step 4. Repeat until the likelihood has been stored for all combinations of parameters, i.e., for all grid points.

7 The best-fit parameter combination is that one with the largest likelihood (or the smallest χ^2).

8 If the parameter ranges are chosen so that the best-fit is not near to the edges of the grid and the likelihood function is well-behaving, i.e., the data constrains reasonably well the parameters of the model studied, then the saved likelihoods can be regarded as an unnormalized probability density function. To put more exactly: the quantity

$$p(a_1, \ldots, a_n) da_1 \ldots da_n = \frac{\mathcal{L}(a_1, \ldots, a_n) da_1 \ldots da_n}{\int \mathcal{L}(a_1, \ldots, a_n) da_1 \ldots da_n} \tag{4.3}$$

gives the probability of the theoretical parameters to be within a box of volume $da_1 \ldots da_n$ at $(a_1, \ldots, a_n)$, if the observational data is the one we used in our analysis. The integration is actually a summation over all grid points. However, the function of several variables is difficult to visualize or tabulate. Hence, a common practice is to give the one-dimensional marginalized likelihood function for each parameter. For example, for a_1 it would be $\mathcal{L}(a_1) = \int \mathcal{L}(a_1, \ldots, a_n) da_2 \ldots da_n$.

9 In the literature, usually the 68% (or 95%) confidence levels (C.L.) for cosmological parameters are given in the form $a_1 = x^{+z}_{-y}$. Here x is the median of a_1. It is found by demanding $\int_{a_{1l}}^{x} \mathcal{L}(a_1) da_1 = 0.5 \times \int \mathcal{L}(a_1) da_1$, where the integration lower bound

[2]Estimated uncertainties in an experiment are described by the covariance matrix C (see e.g. [252] for WMAP). In the simplest case the measurements of different data points are independent processes and $C_{ij} = \delta_{ij} \times \sigma_i^2$, but in general C contains also off-diagonal terms, and then the goodness-of-fit can be described, e.g., by

$$\chi^2 = \sum_{ij} (C_{\ell_i}^{\rm th} - C_{\ell_i}^{\rm meas}) C_{ij}^{-1} (C_{\ell_j}^{\rm th} - C_{\ell_j}^{\rm meas}) \,, \tag{4.1}$$

where C^{-1} (which can depend on $\{C_{\ell_i}^{\rm th}\}$) is called the curvature matrix.

a_{1l} is the smallest value of a_1 in the grid. Then, in the case of the 68% region, y is found by demanding $\int_{a_{1l}}^{x-y} \mathcal{L}(a_1)da_1 = 0.16 \times \int \mathcal{L}(a_1)da_1$. Finally, z is is found from $\int_{x+z}^{a_{1u}} \mathcal{L}(a_1)da_1 = 0.16 \times \int \mathcal{L}(a_1)da_1$, where a_{1u} is the largest value of a_1 in the grid. Hence, the probability to get the observed angular power spectrum is $1.00 - 0.16 - 0.16 = 0.68$ if the parameter a_1 lies in the range $[x - y, x + z]$ and the other parameters can take any value (randomly picked from a uniform distribution) within their range. in the grid.

The step 8 needs an explanation, since the likelihood, for which we used a shorthand notation $\mathcal{L}(\{a_i\})$, is actually the unnormalized probability density for ending up with the measured data D, when the underlying model M is assumed to be true and the parameters have values $\{a_i\}$. In other words, our likelihood defined in 5 is $\mathcal{L}(D|\{a_i\}, M)$. With help of Bayes' theorem the argument can be turned around: the probability density for A when B is true can be written as $p(A|B) = p(B|A)p(A)/p(B)$. Applying this to our problem, we get (see e.g. [253])

$$\begin{aligned} p(\{a_i\}|D, M) &= \frac{\mathcal{L}(D|\{a_i\}, M) \ \times \ \pi(\{a_i\}, M)}{\int \mathcal{L}(D|\{a_i\}, M) \times \pi(\{a_i\}, M) da_1 \dots da_n} \\ &= \frac{\mathcal{L}(D|\{a_i\}, M) \ \times \ \pi(\{a_i\}, M)}{p(D|M)}. \end{aligned} \tag{4.4}$$

This states that when the theoretical model M, which is described by n parameters a_i, is assumed to be true and the data at hand is D, the probability density for the parameters to have values $\{a_i\}$ is given by the normalized likelihood of the data $\mathcal{L}$ multiplied by the prior probability distribution function (pdf) of the parameters of the model. If we do not have any prior knowledge of the values of the parameters, then π can be set, e.g., to be a flat pdf in the range of each parameter. Notably, our end result, the *posterior* pdf $p(\{a_i\}|D, M)$ change, if we assume a flat prior pdf for, e.g., $\{\sqrt{a_i}\}$ instead of the original set $\{a_i\}$.

As far as we do not want to compare different theoretical set-ups M, the denominator in (4.4) is just a normalization constant. However, to really discern between adiabatic and isocurvature models, one should calculate the denominator in the first line of (4.4). This leads one to a concept of Bayesian model selection (see e.g. [253–255]), which we comment on in Chapter 5.

In addition to the 1d marginalized likelihood mentioned in the step 8, the 2d marginalized likelihood is easy to visualize. For example, for a_1 and a_2 the 2d marginalized likelihood would be $\mathcal{L}(a_1, a_2) = \int \mathcal{L}(a_1, \dots, a_n) da_3 \dots da_n$. Now, e.g., the boundary of the 68% C.L. region can be represented by a contour on the (a_1, a_2) plane. However, it should be noted that the smallest and largest values of a_1 on that contour (i.e. the projected values) are not same as $x - y$ and $x + z$ of the step 9. Generally, the projected interval is wider than the 68% region found from the 1d marginalized likelihood. We could continue to define 3d likelihood etc. up to the original nd likelihood. In cosmology, the quoted values for parameters are nearly always (68% or 95%) confidence level regions of 1d likelihoods. This should be kept in mind when interpreting the "strict constraints"

given in the literature. Much wider intervals would have resulted, if the community had chosen to quote the projected intervals of the 68% (or 95%) volumes of the original nd likelihood.

The 68% and 95% C.L. regions can be defined even if $\mathcal{L}(a_1, \ldots a_n)$ is not an n-dimensional Gaussian function. For a Gaussian function the 1d likelihoods are symmetric and the median is the same as the mean. Moreover, the median and the mean are at the same position as the peak of the likelihood. Thus the 68% C.L. interval is symmetric and its limits correspond to subtracting 1σ from the mean and adding 1σ to the mean. The 95% interval correspons to [mean-2σ, mean$+2\sigma$]. Here σ is the standard deviation of the parameter considered. If all the 1d likelihoods are Gaussian, then the best-fit set of parameters $(a_{1b}, \ldots, a_{nb})$ is the same the set of parameters that gives the peak for each 1d likelihood. Since this is true only for strictly Gaussian distributions, the set of xs of the step 9 $(x_1, \ldots, x_n)$ differs from the best-fit set $(a_{1b}, \ldots, a_{nb})$ in general case. If some of 1d likelihoods are very far from a Gaussian shape, it may happen that, e.g., a_{1b} lies even outside of the 95% C.L. region of a_1. Still the 1d likelihood of a_1 can be nearly Gaussian. This kind of situations arise usually, when at least one of the parameters is not well constrained by the data. If all the parameters are well constrained, it is relatively safe to rely on Gaussianity of the likelihood function.

Often the quantities $x - y$ and $x + z$ of the step 9 are called the 1σ limits even if $\mathcal{L}$ was not nearly Gaussian. Similarly, the limits of 1d 95% C.L. region are called 2σ limits. This misleading habit may cause confusion. Fortunately, it is easy to check whether the quoted values result from a nearly Gaussian likelihood or not. If $y = z$ for all parameters and the 95% intervals are just the double of 68% intervals, then using the terms 1σ, 2σ, and regarding results as exclusion limits becomes justified.

For a Gaussian likelihood the σ limits are easy to convert to values of $\Delta\chi^2 = \chi^2 - \chi^2_{\rm best}$. In the case of 1d likelihood, the models whose χ^2 differs less than by one from the best-fit value ($\Delta\chi^2 \leq 1$) are within 1σ and models with $\Delta\chi^2 \leq 4$ are within 2σ. For 2d likelihood the limits are $\Delta\chi^2 \leq 2.3$ and $\Delta\chi^2 \leq 6.2$, respectively. More values can be found from the literature, see e.g. [256].

In addition to the marginalization by integration, there exists another method called the marginalization by maximization. Then 1d likelihood, e.g. for a_1, is formed by giving for $\mathcal{L}(a_1)$ at each grid point $a_1 = b$ the value $\max\{\mathcal{L}(a_1, \ldots, a_n)\}_{a_1=b}$. Obviously, the two methods are equivalent for a Gaussian $\mathcal{L}$. In papers **I** and **II** we used maximization while in papers **III**–**V** we applied integration.

The grid method is very straightforward and easy to implement. Problems arise because it is a brute force method — the theoretical angular power need to be calculated at every grid point. The calculation takes from a few seconds to a minute for each combination of parameters. Let us assume here 25 seconds for the average calculation time of one C_ℓ spectrum. By the grid method, the analysis performed in paper **V** where we have 11 parameters, would take gigayears. Actually, giving 30 values for each parameter (which would not even be enough) the CPU time needed would be $30^{11} \times 25$ s $= 14$ Gyrs. This is about the present age of the universe! However, constraining the study of the

standard ΛCDM model to the flat ($\Omega_{\rm tot} = 1$) case and fixing the optical depth due to reionization would leave one with 5 parameters. Then, with 18 values for each parameter, the job would be doable. Nevertheless, a powerful parallel computer is needed, since the CPU time consumption would be $18^5 \times 25$ s = 1.5 yrs.

In practice, to reduce the number of grid points to about less than a million, one is always forced to use a very coarse grid or strictly limited ranges of parameters. Five or six dimensional parameter space is the most complex case that can be analyzed by the grid method. This is why, in the literature, many parameters are usually kept fixed in the analysis. For example, nearly always a flat universe is assumed. Of course, the fixed parameters are chosen to be those that are less interesting for the author's specific model or whose values are considered to be already known with high precision.

The grid method demands also a lot of human work. One method to artificially increase the number of grid points is to find analytically, how one could estimate the power spectrum from the spectrum got in the nearby grid points, and then program sort of interpolation routines [257]. Closely related is a method where the results are "extrapolated". For example, the closed and open models can be approximated by calculating the C_ls for a "corresponding" flat model, and then scaling the peak positions. Since the sound horizon remains practically unchanged the scaling of ℓ is just $\ell_{\rm non-flat} = (D^A_{*\rm non-flat}/D^A_{*\rm flat})\ell_{\rm flat}$, where the ratio of the angular diameter distances can be calculated from Fig. 3.2 or from equation (3.18).

Other possibility to speed up the calculation is to try to pick the interesting parts of the parameter space and analyze only them. This method is based on some analytic and/or pragmatic knowledge of the behaviour of the angular power as a function of the cosmological parameters. By these arguments one can leave unanalyzed the regions where $\mathcal{L}$ is expected to be vanishingly small. The method demands lots of work since one needs to plot, analyze, and explain (analytically or semi-analytically) hundreds of C_ℓ curves to make decisions on a solid ground. We used this method in papers **I** and **II**. In **III** we restricted the range of the background cosmological parameters to a very narrow region around the best-fit adiabatic model and gave them only a few values. The parameters of our interest, related to the primordial curvature and isocurvature perturbations, were varied relatively freely. They had a wide ranges and we gave them tens of values within their ranges.

For a long time, the grid method was the only widely known and applied method in the cosmology community. However, at least with the WMAP data one had to consider faster methods. The data was so precise that even in the simplest 5 parameter flat adiabatic case the coarseness and limited range of the grid would have introduced larger errors than the actual measurement errors were. Between the years 2000 and 2003 cosmologists adopted the Markov Chain Monte Carlo method (MCMC) (see e.g. [258]) as their main likelihood analysis tool.

A brief cosmologist's introduction to MCMC can be found in the Appendix of [126]. Here we refer the main points. The first step in our analysis recipe remains unchanged. In the second step, quite wide ranges can be specified, since the speed of calculation

does not depend strongly on the ranges of parameters, if the data well constrains the parameters of the model. The actual calculation starts by picking randomly the starting point in the parameter space. The theoretical angular power for this set of parameters is calculated as in the step 4, and the likelihood is calculated by the step 5. Then a new set of parameters is picked randomly (from an n-dimensional Gaussian distribution centered at the original values of parameters). The steps 4 and 5 are repeated. If the likelihood of the new model is larger than the likelihood of the first model, the new model is "accepted" and its parameters are saved into a row in a file. If the original model was better, the new model is accepted only with the probability $\mathcal{L}_{\rm new}/\mathcal{L}_{\rm original}$. In the case that the new model is accepted it becomes as a "current" model. In other case, the original model remains as the current model, but its "multiplicity" is increased by one. Now the random picking of parameters is repeated (from a Gaussian distribution centered at the parameters of the current model). The above steps are repeated about 10^5–10^7 times. Every time, when the current model survives (i.e. the step trial is not accepted), the multiplicity of the current model is increased by one. After a run, one has a file containing rows of parameter values and the multiplicity of each row that describes how many trials had to be made before a step to another model (parameter set) was accepted.

The method is based on the fact that one wanders "randomly" in the parameter space, but spends more time in the regions of large $\mathcal{L}$ and less time in the regions of small $\mathcal{L}$. (It is more probable that a step towards a better model becomes accepted. If the current model is a very good fit to the data, then it is hard to find any better model. One stays many trials in the current model.) In other words, the multiplicity of models of large likelihood becomes larger than the multiplicity of models of small likelihood. Finally, the nd likelihood is proportional to the multiplicity (actually, the density of the accepted models) [259]. The run needs to be continued so long that the parameter space is well sampled.

Since the method is based on random processes, it is not enough to consider only one chain. One should produce several chains with distinct starting points, because all the chains do not necessarily wander to the region of a global likelihood maximum, but instead meet on their way some local likelihood maximum. If this kind of maximum is far from the global maximum and the likelihood is significantly larger than in the nearby surroundings, the chain gets stuck and does not find a way to the global maximum even if the global maximum had much larger $\mathcal{L}$ than the local one. This problem does not occur if the likelihood function is nearly Gaussian. Also, if all the 1d likelihoods have a clear single peak, the risk to get stuck is negligible. Unfortunately, even in the standard ΛCDM model the 1d likelihood of the optical depth τ is bimodal for the CMB data alone. Hence, some ad hoc (or an astrophysically motivated) prior for τ is needed.

For a successful run one needs a clever choice of the so-called jump function (proposal function, proposal matrix). It is a matrix that specifies the widths σ_i of an nd Gaussian distribution from which the step trial for each parameter is picked. With too narrow widths, sampling the parameter space takes forever, since one needs a huge number of

steps to wander from point A to point B. With large widths a risk to get stuck in some relatively good model becomes large. Thus, the CPU time needed to create a converged chain approaches infinity in both the limits $\sigma_i \to 0$ and $\sigma_i \to \infty$. The optimal width σ_i^2 is a few times the variance of the posterior likelihood of the corresponding parameter a_i. But this likelihood and variance we know only after a successful run. This is why, in practice, one needs all kinds of preliminary runs before the main run.

The marginalized 1d likelihood, e.g. for a_1, is formed by binning the range of a_1 to equally wide n_b bins centered at $a_1 = b_1, b_2, \ldots, b_{n_b}$. Then the multiplicities of all the rows with the parameter a_1 falling into the first bin are summed. This is an unnormalized $\mathcal{L}(a_1 = b_1)$. Similarly the value of $\mathcal{L}$ for some other bin is the sum of multiplicities of rows with a_1 having the value in the range of the considered bin.

With a good step function, the CPU time needed in the MCMC method is proportional to the number of parameters whereas in the grid method it was proportional to the number of grid points. The MCMC runs for paper **V** took about 2 CPU years instead of the age of the universe, which the grid method would have taken.

4.3 Concordance model and its shortcomings

The major part of the present cosmological and astrophysics data (CMB, large-scale structure, type Ia supernovae) is fit reasonably well by a simple cosmological model. This model has a spatially flat background geometry ($\Omega_{\rm tot} = 1$). It has five energy density components, "baryons" (meaning roughly speaking the ordinary matter), photons, massless neutrinos, CDM, and a constant vacuum energy (cosmological constant). The primordial scalar perturbations are Gaussian, adiabatic, and scale-free (spectral index $n_{\rm ad} = \text{constant}$).

The parameters to be determined from the data are the Hubble parameter h, two physical density parameters, ω_b and ω_c, and the amplitude A and spectral index $n_{\rm ad}$ of the primordial adiabatic scalar perturbations. The concordance values of the parameters are $h \simeq 0.7$, $\omega_b \simeq 0.023$, $\omega_c \simeq 0.12$, $n_{\rm ad} \simeq 1.0$, and $A \simeq 5 \times 10^{-5}$. Besides the 5 fundamental cosmological parameters, there are 2 additional parameters needed when the models are compared to CMB and large-scale structure (LSS) data: the optical depth τ due to reionization, and the bias parameter b relating the observed galaxy power spectrum to the underlying matter power spectrum.

There is no evidence in the cosmological data for the presence of additional features or ingredients beyond the concordance model, like (correlated) isocurvature or tensor perturbations, or neutrino masses, suggesting that they are probably so small as not to show up in the present data. However, the presence of an undetected contribution (whatever it is) may affect the determination of the main cosmological parameters. On the other hand, more accurate data, e.g., new WMAP, SDSS, SNIa, Boomerang (polarization) data [178, 260, 261] that are at hands or come in the near future may reveal some deviations from the concordance model.

Let us see how the data leads to the concordance values of parameters. We choose

the free parameters to be ω_m, ω_b, $\Omega_{\rm tot}$, Ω_Λ, $n_{\rm ad}$ and A. Each of these parameters has a particularly distinct imprint on the data, see [94]. The other parameters are derived parameters. For example, $\Omega_m = \Omega_{\rm tot} - \Omega_\Lambda$, $\omega_c = \omega_m - \omega_b$, and $h = \sqrt{\omega_m/(\Omega_{\rm tot} - \Omega_\Lambda)}$.

The relative heights of even and odd peaks are sensitive to ω_b fixing it very tightly. The combined effect of gravitational boosting, early ISW, and diffusion damping is sensitive to ω_m. Hence, the heights of the peaks compared to the SW part of the spectrum fix quite tightly ω_m to 0.145. The distance between the acoustic peaks in the CMB data is about $\Delta\ell = 300$. As we have seen in Fig. 3.3a, this corresponds approximately the line $\Omega_{\rm tot} = \Omega_m + \Omega_\Lambda = 1$. (Actually, for large Ω_m, the $\Delta\ell = 300$ line lies a little bit above the line $\Omega_\Lambda = -\Omega_m + 1$.) Hence, we must have $\Omega_{\rm tot} \approx 1$. Clearly, the primordial amplitude A^2 is fixed by the absolute amplitude of the C_ℓ spectrum. The spectral index affects the relative heights of the peaks and the SW part, but its effect (ℓ dependence of the effect) is slightly different than the one caused by the diffusion damping and gravitational driving. So, CMB fixes all the other parameters of the concordance model except Ω_Λ, which can vary quite freely between 0 and 1. Consequently the derived parameter Ω_m can vary between 1 and 0, see Fig. 3.3b. This is often called the *geometric degeneracy*, since models with different combinations of matter and vacuum energy lead to the same geometry and hence the similar CMB angular power.

From Fig. 3.3a we see that, actually even a model without the vacuum energy, i.e. $\Omega_\Lambda = 0$, is expected to fit the CMB data if $\Omega_m \simeq 1.28$. Then the Hubble parameter would be $h = \sqrt{0.145/1.28} = 0.34$. Usually, such a low value is regarded as unphysical. Restricting h one can break the geometric degeneracy. The Hubble Space Telescope Key project reports $h = 0.72 \pm 0.08$. This practically restricts ourselves to models with $\Omega_\Lambda = 1 - \omega_m/h^2 = 0.65$–$0.77$.

Another method to break the degeneracy is to use SN data, which probes a nearly perpendicular direction in the (Ω_m,Ω_Λ) plane. (As seen in 1.1.2, for example, the deceleration parameter, which SN data can probe, is $q_0 = \Omega_m/2 - \Omega_\Lambda$.) The role of the SNIa data becomes clear from Fig. 3.3c. Notably, the SNIa data alone prefer closed models with $\Omega_\Lambda > 0.7$ and $\Omega_m > 0.3$. The 68% C.L. regions of the CMB and SNIa data intersect only marginally with the parameter values of the concordance model $\Omega_\Lambda = 0.7$, $\Omega_m = 0.3$.

A third method to break the degeneracy, but not as powerful as the previous ones, is the use of LSS data. One can calculate the theoretical matter power spectrum $P_m(k) \stackrel{\rm def}{=} \langle|\delta\rho_m(\eta_0, \vec{k})/\rho_m(\eta_0)|^2\rangle$ and compare it to the galaxy clustering observations such as SDSS [126, 262] and 2dFGRS [263–265]. The matter density perturbations evolve differently on subhorizon scales in the radiation-dominated universe than in the matter-dominated universe. Actually, the perturbations start to decay as do the potentials Φ and Ψ after the horizon entry in the radiation-dominated epoch. On large scales $k < k_{\rm eq}$ the matter power reflects the primordial matter power $P_m(k) \propto P_{mi}(k)$, which is, according to the Poisson equation, proportional to $k^4 P_{\Phi_i}$. Thus we have $P_m(k) \propto k^4 P_{\mathcal{R}_i} \propto k^4 k^{-3} \mathcal{P}_{\mathcal{R}_i} = k\mathcal{P}_{\mathcal{R}_i}(k)$. For scales $k > k_{\rm eq}$, $\Phi \propto k^{-2}\Phi_i$, and we have approximately $P_m(k) \propto k^{-3}\mathcal{P}_{\mathcal{R}_i}(k)$. (See e.g. [94, 172] and [266, 267] for more exact calculations, for numerical fitting, and for an additional $\ln k$ dependence in the adiabatic case.) The key point here is that the shape of

the matter power spectrum, i.e., the scale where the described turnover appears, "fixes" $k_{\rm eq}$. But in (1.21) we saw that $k_{\rm eq} = \omega_m \times 0.0729h$ Mpc^{-1} $= h\Omega_m \times 0.0729h$ Mpc^{-1}. Here we separated h^2 into two parts, since, in the galaxy clustering observations, the length scale is known in units of h^{-1} Mpc. The quantity $\Gamma \stackrel{\rm def}{=} h\Omega_m$ is called the *shape parameter*. As the LSS data restricts Γ (say $\Gamma = C_1$) and the CMB data restricts ω_m (say $h^2\Omega_m = C_2$), we get an indirect constraint for the Hubble parameter, $h = C_2/C_1$. Hence, accurate LSS data breaks the geometric degeneracy.

Since it seems that the SNIa data are not completely consistent with CMB, we do not plug in our analysis the redshift-magnitude relation from SNIa observations. On the other hand, the direct determination of the Hubble parameter by observing nearby galaxies can be affected by our local gravitational potential. We could live in an underdense or overdense super cluster. Hence, we use the third method (matter power) in papers **I**, **II** and **V**. This saves us from speculating about supernovae dimming and reliability of the HST value of h. Notably, we would have missed the models with low ω_c and large h in **V**, had we used the additional constraints. In paper **IV** we test how badly degenerate the situation becomes in isocurvature models even with the accurate WMAP data, if one does not apply any additional priors or constraints. In [268] we again break the degeneracy by the SDSS data.

Although the concordance model fits the data relatively well [269], there are some unsatisfactory, less understood, aspects related to the model itself, the way its parameters are extracted from the observational data, or the lack of fundamental explanation of the observations. Here we list some "shortcomings":

(a) *Initial conditions of perturbations (adiabatic versus isocurvature).* Assuming purely adiabatic primordial perturbations leads to tightly constrained parameter values around the concordance model. In particular, as we have seen, the positions of acoustic peaks constrain the distance to the last scattering surface, and require nearly flat universe. However, small primordial correlated isocurvature contribution can adjust the position of the first peak (where the data is the most accurate) so that the flatness requirement is somewhat relaxed. Allowing for isocurvature may also affect the determination of other parameters. It should again be emphasized that, although less studied, the isocurvature perturbations are equally motivated as curvature perturbations.

(b) *Flatness.* Inflation is a strong theoretical motivation for the flatness assumption. However, if one wants to test observationally the flatness of the universe, one should allow for non-flat models in the analysis. This has been done in very few studies, and for the adiabatic case only, mainly because the task is computationally extremely hard. Based on the results of paper **V** one can expect that 5–10% deviation from flatness is allowed at the 95% C.L. in correlated isocurvature models. In particular, a closed model with $\Omega_{\rm tot} \simeq 1.10$ might fit the data reasonably well, yielding also less conflict between CMB and SNIa observations. On the other hand, with $-1 < w_{de} \leq -2/3$ (instead of $w_{de} = w_v = -1$) the $\Delta\ell = 300$ contour in Fig. 3.3a (see also footnote on page 94) would be at lower level, indicating that then $\Omega_{\rm tot}$ slightly less than one could fit the CMB data.

(c) *What field is the inflaton?* In the slow roll one-field inflation, quantum fluctuations of the inflaton field generate nearly scale-invariant Gaussian primordial curvature pertur-

bations. As the concordance model has this type of perturbation spectrum, the recent observational data has been regarded to give a strong support to inflation. However, in the particle physics standard model there is no a suitable candidate field. The situation is unsatisfactory, since all the matter (and radiation) of our universe should be decay products of some unknown field. Moreover, in the curvaton scenario [72, 74, 75, 164] that has recently got lot of publicity, the matter can be produced by decay of another scalar field, the curvaton (whose energy density is subdominant during inflation), instead of the inflaton that drives the expansion.

(d) *Neutrino masses.* Particle physics neutrino experiments show that neutrinos are not massless [270]. Allowing for their mass in a cosmological analysis does not yield large deviations from the concordance model in the adiabatic case. Massive neutrinos provide a part of dark matter so that the allowed amount of CDM becomes smaller, since CMB constrains the total amount of matter quite tightly. However, CDM is needed for forming gravitational potential wells in order to guarantee the large-scale structure formation. So LSS data forces the CDM density near to the concordance value and neutrino masses have to be very small. In contrast, in the (baryon) isocurvature models LSS can form even without the presence of CDM. Hence, much larger neutrino masses could become allowed and larger deviations from the concordance model might arise. For an interplay of cosmology and particle physics in determining neutrino masses see e.g. [271].

(e) *Dark matter.* Of the matter density in the concordance model 83% comes from an unknown form of matter, dark matter ($\Omega_{\rm dm} \approx 0.25$), while only 17% comes from the baryonic matter ($\Omega_b \approx 0.05$). The dark matter has practically no (local) interactions with the other particle species, but instead is detected by its gravitational implications. As neutrinos have light masses they could be the hot dark matter. However, at any rate, the concordance model does not explain what is the dark matter that form 25% of the total energy density of the universe.

(f) *Dark energy.* About 70% of the energy density is in the form of "dark energy" which must have negative pressure in order to cause the observed accelerating expansion of the universe [106]. In the concordance model, this mysterious dark energy is the vacuum energy with $\Omega_\Lambda \approx 0.70$. However, from particle physics point of view the vacuum energy density should either vanish by some symmetry or be 10^{60}–10^{122} times higher. Instead of a constant equation of state parameter, dark energy could have a time varying equation of state, $p_{\rm de}(t) = w_{\rm de}(t)\rho_{\rm de}(t)$, motivated, e.g., by quintessence models [272–278].

(g) *Features in the observed angular power.* The binned WMAP temperature angular power contains three "blips" (off-set data points) at multipoles $\ell \approx 22$, $\ell \approx 40$, and $\ell \approx 200$, which cannot be fitted by the concordance model. Originally, the WMAP team reported the blips as a possible technical problem in the measurement. However, the latest independent results by Archeops [48] also show the last two of these features. Hence, they may be imprints of some unknown physical phenomena. Another puzzle in the WMAP (and COBE) data is a low quadrupole ($\ell = 2$) power. While the low power can be just a rare chance caused by cosmic variance, it has raised lot of interest and may imply a need for new physics [177].

(h) *Supernovae observations.* As discussed above, the CMB and SNIa data are not completely "concordant" with each other. The former prefers flat models whereas the latter prefers closed models with a larger Ω_Λ and a little larger Ω_m.

4.4 Constraining isocurvature

As the isocurvature perturbations arise naturally in multi-field inflation, the literature dealing with isocurvature perturbations in context of inflation is nearly as numerous as the inflation literature itself. Isocurvature as a result of multi-field inflation has been considered, e.g., in [59, 60, 62, 144, 162, 201, 279–294] after COBE, in [153, 157–160, 163, 295–306] after Boomerang and Maxima, and in [307–314] after WMAP. Closely related are multi-component fluid studies [63, 81, 315–319]. In addition, the isocurvature literature with the focus on curvaton model is rich [65, 72, 74–78, 81, 164, 165, 320–325] as well as the literature with the focus on the pre-Big Bang [69–71, 73, 326–328] and non-Gaussianities [141, 203, 329–335]. Isocurvature perturbations can arise also in quintessence models [272–278], in brane world (and other extradimension) scenarios [146, 336–340], or as a result of topological defects [341–343] (see also [344]). Consequences of isocurvature perturbations to star formation have been studied in [345], to the superheavy dark matter in [346], to the primordial magnetic fields in [347, 348], to the Big Bang nucleosynthesis in [348–351], and to the large-scale structure formation in [284, 292, 337, 352–356]. Recently, isocurvature has also been mentioned in passing in various contexts [357–360].

Observational constraints on isocurvature have been considered before Boomerang and Maxima in [361–369], before WMAP in [49, 85, 86, 159, 370], and after WMAP in [58, 84, 87, 88, 253, 322, 371–378] with phenomenological primordial spectra and in [61, 379] with specific inflationary model in mind.

We devote this section to commenting the main results of papers **I**–**V**, and start by mentioning some of the most related literature. Before the Boomerang and Maxima data became available, limits to the isocurvature contribution in uncorrelated models had been obtained for the case $n_{\rm ad} = n_{\rm iso} = 1$, e.g., in [365], and with $n_{\rm ad}$ and $n_{\rm iso}$ as independent parameters in [281]. Predictions for WMAP and Planck had been considered, e.g., in [64, 380, 381]. Using among others the Boomerang and/or Maxima data, (correlated) isocurvature models with one independent spectral index have been studied, e.g., in [159], in [85, 86], and in [164, 165]. After WMAP, limits to correlated models were first obtained for the case of two independent spectral indices [87, 378]. Parkinson et al. [61] considered a particular inflation model producing correlated perturbations. Moodley et al. [88] considered models with up to three isocurvature modes (CDM and two neutrino modes) simultaneously present, but all sharing the same spectral index. Recently, the isocurvature contribution has been constrained in [84, 253, 255].

Uncorrelated isocurvature. While the main contribution comes from the usual adiabatic mode there can be a small fraction of isocurvature generated perturbations in the observed temperature (and polarization) anisotropy spectrum. We were the first to use Boomerang and Maxima data to set tight observational constraints on the CDM isocurvature contribution. In paper **I** we found that it could not be more than 13% of the power of the first acoustic peak in a flat universe. Nevertheless, this means that the amplitude of the primordial entropy perturbations in the very early universe could have been of the same order as the adiabatic amplitude, since the subsequent evolution of universe damps the isocurvature mode compared to the adiabatic one [recall the $(k_{\rm eq}/k)^2$ factor

in the isocurvature amplitude].

According to **I**, the isocurvature spectral index can take much larger values ($n_{\rm iso} > 1$) than the adiabatic index, which is constrained close to one. The large allowed values of $n_{\rm iso}$ are a direct consequence of the damping factor. Small values $n_{\rm iso} < 1$ are also allowed, since then the isocurvature modifies only the SW part of the spectrum where cosmic variance gives some freedom. As we have seen, one would need $n_{\rm iso} \sim 3$ to maintain the relative isocurvature contribution at the same level on all scales. As we did not study so large values in **I**, we conclude that within our grid the isocurvature added always more power to the SW region than to the acoustic peak region (recall Fig. 3.4). This means that we added to the adiabatic perturbations a small effectively negative spectral-tilt component. To compensate for this, adiabatic spectral indices of a little larger value than one became acceptable, although in pure adiabatic models they would have been ruled out.

Strong support for the near flatness of the universe. Although the position of the first acoustic peak was definitely that one of a typical adiabatic model with a flat geometry of the universe, the possibility of a well-fitting pure isocurvature model in the case of non-flat universe with a bit exotic combination of cosmological parameters remained unanswered. This was because changing the curvature (total energy density parameter) shifts the acoustic peaks so that the observed peak could have been fitted by the first isocurvature peak in the open universe case or by the second isocurvature peak in the closed case. After a comprehensive scan of the parameter space we concluded in paper **II** that even in curved space the pure CDM isocurvature is ruled out.

To speed up computation, CMB analysis is very often restricted to flat models. Prior to our study this was misleadingly justified by saying "the acoustic peak at multipole 200 implies the flatness". Obviously this was true only when assuming a purely adiabatic primordial perturbation mode. Hence, our result put the analyse relying on the flatness a on more solid ground. Of course, the second data releases of Boomerang and Maxima with a detection of the second peak position confirmed the near flatness by the right spacings[3] ($\Delta\ell \sim 300$) of the successive acoustic peaks. This result came when we were finalizing paper **II**. Hence, we reanalyzed our model. Naturally, the new data ruled out the pure isocurvature perturbations even more tightly than the first data releases of Boomerang and Maxima.

Although, as is obvious from Appendix A, the generalization of the calculation of C_ℓ to the curved space is very straightforward, it is worth pointing out that there arises one theoretical complication related to the shape of the primordial spectrum. In the flat case,

---

[3]Recall that $\Delta\ell$ does not depend on the initial conditions. It is basically a function of $\Omega_{\rm tot}$ only, see Fig. 3.3a. A rough scaling is [184]

$$\Delta\ell(w_{de}+\Delta w_{de}, \omega_m+\Delta\omega_m, \omega_b+\Delta\omega_b, \Omega_\Lambda+\Delta\Omega_\Lambda, \Omega_{\rm tot}+\Delta\Omega_{\rm tot})$$
$$\approx \left[1 + 0.11\frac{\Delta w_{de}}{w_{de}} - 0.24\frac{\Delta\omega_m}{\omega_m} + 0.07\frac{\Delta\omega_b}{\omega_b} - 0.17\frac{\Delta\Omega_\Lambda}{\Omega_\Lambda} - 1.1\frac{\Delta\Omega_{\rm tot}}{\Omega_{\rm tot}}\right]\Delta\ell(w_{de}, \omega_m, \omega_b, \Omega_\Lambda, \Omega_{\rm tot})$$

around a model ($w_{de} = -1$, $\omega_m = 0.148$, $\omega_b = 0.02$, $\Omega_\Lambda = 0.65$, $\Omega_{\rm tot} = 1$) for which $\Delta\ell \approx 301$.

there is no preferred length scale, but in open and closed models the spatial curvature introduces a length scale $\lambda_K \sim 1/k_K \stackrel{\text{def}}{=} \sqrt{1/|K|}$, which one expects to be reflected in the form of the power spectrum. In our analysis, we took $\Omega_{\text{tot}} = -1.1$–$3.4$, which gives $k_K = H_0\sqrt{|1-\Omega_{\text{tot}}|} \lesssim 1.45H_0$–$1.55H_0$. In the angular power this corresponds to $\ell_K \lesssim 10$. For very small scales $k^2 \gg |K|$, the curvature makes no difference to the flat case, but for large scales $k^2 \lesssim |K|$, the effect can be significant. Hence, we conclude that the spatial curvature can affect the lowest multipoles $\ell \lesssim \ell_K$.

In paper **II** we assumed for the shape of the primordial power spectrum the simplest generalization of the flat space power law spectrum, and employed with

$$\mathcal{P}_{\mathcal{S}_i}(k) = \mathcal{P}_{\text{gen.}}(k) \stackrel{\text{def}}{=} B\left(\sqrt{k^2-K}\right)^{n_{\text{iso}}-1} . \tag{4.5}$$

The motivation is that, in the curved space, the Laplacian has eigenvalues k^2-K instead of the k^2, see A.1. For $k \gg k_K$ our spectrum coincides with the flat space case.

Generically, as a consequence of inflation, the universe is flat. In the literature, various modifications of the basic inflationary scenario have been proposed to produce non-flat spatial geometry [190, 382–402]. Usually, the most viable ones include some kind of bubble formation. Then the resulting primordial power spectrum depends on the details of the bubbles, and the curvature scale. Schematically, we can write $\mathcal{P}_i(k) = f_K(k)\mathcal{P}_{\text{gen.}}(k)$, where $f_K(k) \to 1$ as $k/k_K \to \infty$. For $k \lesssim k_K$ there is no clear consensus of the form of $f_K(k)$ in the literature [190, 382–402]. However, in the data fit, the relative weight of the low multipoles $\ell \lesssim 10$ is small due to the cosmic variance. Although we simply assumed $f_K = 1$ for all scales, we showed in paper **II** that our conclusions can be drawn also from the Boomerang and Maxima data alone, i.e., by ignoring COBE data and considering $\ell \geq 50$ which are not affected by curvature in any case.

Scale dependent correlation. After paper **I** where an uncorrelated mixture of adiabatic and isocurvature perturbations was analyzed, correlated models became popular [59, 60, 157, 159]. In multi-field inflationary models a correlation arises, because the entropy perturbation can drive curvature perturbation [143, 152], see Sec. 1.2.3. Even the WMAP team considered this possibility in one of their papers [378]. However, from a theorist's point of view, they made a somewhat unmotivated assumption by treating the correlation amplitude as scale independent. Preliminary results of the scale dependent case, based on a grid method, were published in **III**.

Curvaton decay and resulting correlated perturbations. One possible mechanism that yields correlated perturbations is a decaying curvaton. The scenario was first addressed by Enqvist & Sloth [72] in the context of pre-Big Bang, and by Lyth & Wands [75] and Moroi & Takahashi [164] in the context of inflation. Gupta, Malik & Wands performed a curvaton decay calculation in the dust approximation [81]. With Francesc Ferrer & Syksy Räsänen we checked in **IV** the validity of the dust approximation by using efficient parallel computing and treating the curvaton as a genuine field instead of pressureless dust. We also included massive neutrinos in the analysis. Surprisingly, we found that the dust approximation leads to very precise results in wide range of parameter space. The CMB spectra arising from the curvaton decay are very similar to the ones produced by

the double inflation [61].

We used the MCMC method and modified the CosmoMC program [403] (see also [258]) to compare the CMB data with the inflaton-curvaton spectra. We found that the low quadrupole and octopole of the data can be fitted much better by an inflaton-curvaton spectrum than by the standard ΛCDM model. However, including the matter power spectrum in the analysis, the lowering of the low multipole CMB amplitude seems to become less pronounced [268].

Parameter estimation in the case of scale dependent correlation. Paper **V** is a follow-up paper of **III**. We tested how much the cosmological parameters can differ from the values of the standard ΛCDM model (i.e. from the concordance values). The results showed that the WMAP and SDSS [126, 262] data together force most of the parameters very near to the concordance values as noticed also by some other groups recently [84, 88]. This nicely demonstrates the importance of complementary observations in cosmology. However, we found that the CDM density ω_c and the vacuum energy density parameter Ω_Λ can differ significantly from the concordance values. This observation has an important impact for the dark matter and dark energy budget.

The isocurvature contribution in the primordial power at $k = 0.01$ Mpc^{-1} must be less than 18% at the 95% C.L. In the spirit of equation (3.4), we defined a nonadiabatic contribution to the temperature perturbation variance by

$$\alpha_T \stackrel{\text{def}}{=} \frac{\langle (\delta T^{\text{non-ad}})^2 \rangle}{\langle (\delta T^{\text{total}})^2 \rangle} = \frac{\sum_\ell (2\ell+1) \left(C_\ell^{\text{iso}} + C_\ell^{\text{cor}} \right)}{\sum_\ell (2\ell+1) C_\ell} \,. \tag{4.6}$$

The 95% C.L. upper limit found in **V** is 0.075. In order to demonstrate the rapidly improved constraining power of the data, I calculated the allowed CDM isocurvature contribution (at 95% C.L.) to the first acoustic peak from the MCMC chains that we had created for paper **V** but restricting the analysis to uncorrelated models. The result was 2.3% for the same model that four years ago in **I** with Boomerang and Maxima data yielded 13%. In the correlated case, the nonadiabatic contribution can lower the power at quadrupole ($\ell = 2$) by as much as 46% because of negative correlation. The 95% C.L. limit to the nonadiabatic contribution to the first acoustic peak at $\ell \simeq 200$ is only 8%. The cosmic variance is 63% for $\ell = 2$, and 7% for $\ell = 200$. Even for a bin of $\Delta\ell = 25$ it is 1.4% at the first acoustic peak. Notably, the allowed isocurvature contribution is only about the same size as these uncertainties.

The MCMC method is sensitive to the chosen parametrization. In correlated isocurvature models (with n_{ad} independent of n_{iso}) the isocurvature spectral index is not well constrained. This has caused major problems in the likelihood analysis. In particular, we found a strong dependence of the results on the pivot scale k_0. Using amplitudes at two different scales as primary parameters (instead of the spectral index and amplitude at one reference scale) could improve the situation. It should lead to faster convergence of the MCMC chains and more reliable results for other cosmological parameters (see the "Discussion" in **V**). Although the change in parametrization may seem tiny, it could decrease the CPU time demand by a factor of about four.

Chapter 5

Discussion

Our work answers two main questions: "*How much isocurvature is allowed if one adopts for the initial conditions a correlated or an uncorrelated mixture of adiabatic and CDM isocurvature perturbations?*" and "*How is the determination of the main cosmological parameters affected by an isocurvature contribution?*"

We have shown that pure CDM isocurvature primordial perturbations can be ruled out by the current data in flat, open, and closed universe. The rest of our analysis has been restricted to the flat case. Not surprisingly, we also find that the observed CMB anisotropies are generated from predominantly adiabatic primordial perturbations. This holds even for the model in which we allow for different spectral indices of the adiabatic and isocurvature perturbation spectra, and a scale-dependent correlation amplitude. In particular, combining CMB with observations of the matter power spectrum tightly constrains the isocurvature contribution. This is because the geometric degeneracy becomes broken so that one cannot adjust the parameters to values that would "favour" the isocurvature. Both the CMB and matter power spectra have definitely the "adiabatic pattern", and only small deviations (in practice, of the order of measurement errors) are allowed. The main consequence of allowing for the CDM isocurvature mode is to decrease the accuracy of the determination of (the main) cosmological parameters. One should, in principle, always include the isocurvature mode(s) in the analysis or at least give the results with it in comparison with the pure adiabatic case. Performing the CMB analysis by relying on the assumption of adiabaticity, one can overestimate the power of CMB measurements. By including the isocurvature one gets a bit more conservative (i.e. larger) error estimate of the determination of the cosmological parameters.

If CMB alone is used, as in paper **IV**, degeneracies between the isocurvature and main cosmological parameters result in much larger uncertainties in the determination of all parameters than in the pure adiabatic case. For example, in the pure adiabatic case, we find the physical baryon density to be $\omega_b = 0.0238^{+0.0026}_{-0.0015}$ whereas the correlated isocurvature model of **IV** leads to $\omega_b = 0.0315^{+0.0107}_{-0.0044}$ at 68% C.L.

According to **V** where we supplement the CMB data with the matter power, allowing for a correlated isocurvature has the strongest effect on the determination of the physical cold dark matter density ω_c and the vacuum energy density parameter Ω_Λ. Compared to

the standard ΛCDM model, smaller ω_c and larger Ω_Λ become acceptable in our model. This effect is caused by a positive correlation which effectively can shift the first acoustic peak toward larger values. To compensate for this one needs a larger Ω_Λ in flat models. (Had we allowed for non-flat models, the compensation would have resulted most easily in closed models with Ω_Λ slightly larger than 0.7 and the matter density parameter Ω_m slightly larger than 0.3.) Then the distance between the successive acoustic peaks, $\Delta\ell$, becomes smaller. However, the data around the second and third peaks is not as accurate as around the first peak. So, a possible worsening of the fit at high multipoles does not overrule the improvement around the first peak. In the future, more accurate data at high ℓ can be used either to rule out the large values of Ω_Λ or to detect the "correlation effect". If the current interpretation (see Fig. 3.3c) of the high redshift supernovae type Ia data remained unchanged, it would exclude the large Ω_Λ in flat models. However, slightly closed ($\Omega_{\rm tot} \simeq 1.05$–$1.10$) models with a small positively correlated isocurvature contribution could lead to a very good fit to the CMB and to a better "concordance" between the current supernovae and CMB data.

At the wavenumber $k_0 = 0.01$ Mpc^{-1}, which, in typical models, corresponds to a slightly lower multipole than the first acoustic peak in CMB, the 95% C.L. upper limit on the relative isocurvature contribution in the primordial perturbation power is $\alpha(k_0) = \mathcal{P}_{\mathcal{S}_i}(k_0)/[\mathcal{P}_{\mathcal{R}_i}(k_0)+\mathcal{P}_{\mathcal{S}_i}(k_0)] = 0.18$, where $\mathcal{P}_{\mathcal{R}_i}(k)$ is the adiabatic (i.e. curvature) perturbation power and $\mathcal{P}_{\mathcal{S}_i}(k)$ is the isocurvature (i.e. entropy) perturbation power on scale $\lambda = 2\pi/k$.

Implications of allowing for (say 18% of) isocurvature are numerous for the underlying fundamental theory of physics. First of all, not insisting on the adiabatic primordial perturbations opens up a whole variety of new possibilities of theory building. For example, in the inflaton-curvaton model the energy scale of inflation can be lowered [77, 404–406]. However, certain fine tuning problems can arise. Since the isocurvature amplitude cannot be the dominant one, one must ask: "Could the adiabatic and isocurvature amplitudes be of the same order?" Wouldn't it be more natural for the one to dominate over the other? In the context of multi-field inflation this is usually the case. In this sense, the observation that the CMB perturbations are mostly adiabatic can be regarded to support *pure* adiabaticity.

The 95% C.L. upper limit to the nonadiabatic contribution to the CMB temperature anisotropy variance is $\langle(\delta T^{\rm non-ad})^2\rangle/\langle(\delta T)^2\rangle = 0.075$. In the observed CMB temperature angular power C_ℓ, the allowed nonadiabatic contribution in the range from the quadrupole ($\ell = 2$) to the acoustic peak scale ($\ell \simeq 200$) is only about the size of the cosmic variance. This suggests that the isocurvature mode with spectral index $n_{\rm iso} \lesssim 3$ can never be constrained much better by the CMB temperature anisotropy measurements. This comes about because one needs $n_{\rm iso} > 3$ to get a nondecaying isocurvature contribution at large multipoles $\ell \gtrsim 150$ where the uncertainty due to cosmic variance is smaller. Neither can matter power directly improve the constraints, since in any case [with $\alpha(k_0) < 0.18$] the isocurvature contribution there is at least an order of magnitude less than the adiabatic contribution (see Fig. 2 in paper **V**). On the other hand,

improved CMB data around the second and third acoustic peaks could tightly limit the isocurvature modes with $n_{\rm iso} > 3$. In addition, the very small-scale matter power would be sensitive to these modes. Improved polarization data could lead to tighter limits also in the case $n_{\rm iso} < 3$.

As the observed C_ℓ spectrum is purely adiabatic at the level of the accuracy of the measurements, one should ask "*Are the additional degrees of freedom introduced by the CDM isocurvature mode motivated?*" We have not answered this question, since the likelihood analysis, as presented in papers **I**–**V** and in most of the current literature, has a focus on the parameter estimation assuming that the studied theoretical model is true. The method does not punish much for the additional parameters, but comparing the best-fit χ^2 divided by the reduced number of degrees of freedom shows that the goodness-of-fit of the isocurvature model is not better than that of the pure adiabatic ΛCDM model. To really discern the models, one should apply, for example, the Bayesian model selection criteria. This is computationally extremely time-consuming and has been done only very recently [255]. Fortunately, rapidly developing analytical methods [253, 407] will make the computation easier.

In [255], a so-called evidence ratio (Bayes factor) in favour of the adiabatic models against (nearly our type of) correlated isocurvature models is found to be 3:1. In [253], an evidence ratio 1000:1 against 100% correlated isocurvature model with $n_{\rm ad} = n_{\rm iso}$ is predicted. The discrepancy demonstrates that the Bayesian selection criteria are sensitive to the details of the isocurvature model. Moreover, different parametrizations of the same model may lead to considerably different end results. This has been discussed briefly in [253] and at length in paper **V**. An underlying problem is that, for example, the isocurvature spectral index is not well constrained, when the overall isocurvature amplitude is small. In case of some unconstrained parameters, the likelihood analysis becomes sensitive to the chosen parametrization. Using $\sqrt{\alpha(k_0)}$ instead of $\alpha(k_0)$ to characterize the relative isocurvature contribution would change our flat prior distribution of α to nonflat resulting in a different weighting in the integration when marginalizing the likelihoods. In our considerations, the most dramatic parametrization effect comes from the choice of the pivot scale k_0 where we specify the isocurvature fraction α. To get rid of the ambiguity related to unconstrained $n_{\rm iso}$ and the choice of k_0 I propose in **V** that, in future studies of isocurvature models, one should parametrize the isocurvature spectrum by amplitudes at two different scales instead of the conventional parametrization by an amplitude at one pivot scale and by a spectral index.

As a final comment, let us stress that although the CDM isocurvature is very tightly constrained, the neutrino isocurvature modes, which lead to less deviation from the adiabatic peak structure, may form about a half of the observed temperature variance. In fact, there is an explicit example where CDM and neutrino isocurvature modes together give a major contribution to all of the observed acoustic peaks [89].

Appendix A

Normal mode decomposition in curved space

Usually, the cosmological perturbation theory is done in Fourier space. In the linear theory, each k-mode (or scale) behaves independently and the evolution equations take an easily (numerically) solvable form. In paper **II** along with the flat geometry also the open and closed geometries of the universe are allowed. In this chapter we briefly review the derivation of a generalization of the normal Fourier transformation to the curved space. The angular power is a multipole expansion of the temperature perturbation so that we also need a generalization of the usual multipole expansion.

A.1 Generalization of the Fourier transformation

As in the normal Fourier analysis, any square integrable scalar function $F(\vec{x})$ can be represented in terms of eigenfunctions Q of the Helmholtz equation

$$\nabla^2 Q \stackrel{\text{def}}{=} \gamma^{ij} Q_{|ij} = -k^2 Q, \tag{A.1}$$

where $|$ represents a covariant derivative with respect to the unperturbed three-metric γ_{ij} (1.6) of constant curvature K

$$\gamma_{ij}\, dx^i\, dx^j = |K|^{-1}[\, d\tilde{\chi}^2 + \sin_K^2\tilde{\chi}\, (\, d\theta^2 + \sin^2\theta\; d\varphi^2)]. \tag{A.2}$$

In what follows, the combination $|K|^{1/2}\chi$ will appear so frequently that we defined here a shorthand notation $\tilde{\chi} = |K|^{1/2}\chi$ for the dimensionless radial coordinate. Note that in the case of flat space in rectangular coordinates we have $\gamma_{ij} = \delta_{ij}$ and then, for example, the usual plane wave $Q(\vec{x}, \vec{k}) = e^{i\vec{k}\cdot\vec{x}}$ is a solution to (A.1).

It can be shown that the eigenfunctions $Q(\vec{x}, \vec{k})$ are complete for $|\vec{k}| \geq \sqrt{-K}$ in the open universe [91, 408]. (For the spectrum in the closed universe see below.) Hence we have an expansion

$$F(\vec{x}) = \sum_{|\vec{k}|\geq\sqrt{|K|}} F(\vec{k})Q(\vec{x}, \vec{k}) \text{“} = \text{”} \frac{V}{(2\pi)^3} \int_{|\vec{k}|\geq\sqrt{|K|}}^{\infty} d^3\vec{k}\, F(\vec{k})Q(\vec{x}, \vec{k}), \tag{A.3}$$

which is a *generalization of the Fourier transformation into curved space.*

A.1.1 Solution of the Helmholtz equation — radial functions

Let us first solve the Helmholtz equation[1] in general case with $K \neq 0$. The Laplacian on the right hand side of (A.1) is given by

$$\begin{aligned}\nabla^2 Q &= \gamma^{ij}(Q_{,i})_{|j} = \gamma^{ij}(Q_{,ij} - \Gamma^b_{\ ij}Q_{,b}) \\ &= \gamma^{ij}[Q_{,ij} - \frac{1}{2}(\gamma_{bj,i} + \gamma_{ib,j} - \gamma_{ij,b})Q_{,}^{\ b}] \\ &= |K| \sin_K^{-2}\tilde{\chi}\left[\frac{\partial}{\partial\tilde{\chi}}\left(\sin_K^2\tilde{\chi}\frac{\partial Q}{\partial\tilde{\chi}}\right) + \sin^{-1}\theta\frac{\partial}{\partial\theta}\left(\sin\theta\frac{\partial Q}{\partial\theta}\right) + \sin^{-2}\theta\frac{\partial^2 Q}{\partial\varphi^2}\right]. \quad \text{(A.4)}\end{aligned}$$

In the flat space limit ($K \to 0$) this would be the normal Laplacian in spherical coordinates.

Now the Helmholtz equation (A.1) can be solved by separation of variables. Putting $Q(\vec{x}) = f(\tilde{\chi})g(\theta,\varphi)$ leads to

$$\frac{1}{f}\frac{\partial}{\partial\tilde{\chi}}\left(\sin_K^2\tilde{\chi}\frac{\partial f}{\partial\tilde{\chi}}\right) + \frac{k^2}{|K|}\sin_K^2\tilde{\chi} = -\frac{1}{g}\left[\sin^{-1}\theta\frac{\partial}{\partial\theta}\left(\sin\theta\frac{\partial g}{\partial\theta}\right) + \sin^{-2}\theta\frac{\partial^2 g}{\partial\varphi^2}\right], \quad \text{(A.5)}$$

where the left hand side depends on $\tilde{\chi}$ only and the right hand side on θ and φ only. Hence both sides must be equal to same constant; say $\ell(\ell+1)$. Now we immediately see that

$$g(\theta,\varphi) = Y_{\ell m}(\theta,\varphi), \quad \ell = 0,1,2,\ldots, \quad m = -\ell, -\ell+1, \ldots, \ell, \quad \text{(A.6)}$$

where functions $Y_{\ell m}$ are the spherical harmonics [182, 206]. For $f(\tilde{\chi})$ we get a little bit more complicated equation, which under substitution $f(\tilde{\chi}) = \Pi(\tilde{\chi})\sin_K^{-1/2}\tilde{\chi}$ reduces to

$$\frac{1}{\sin_K\tilde{\chi}}\frac{d}{d\tilde{\chi}}\left[\sin_K\tilde{\chi}\frac{d}{d\tilde{\chi}}\Pi(\tilde{\chi})\right] + \left[\mu(\mu+1) - \frac{(\ell+\frac{1}{2})^2}{\sin_K^2\tilde{\chi}}\right]\Pi(\tilde{\chi}) = 0, \quad \text{(A.7)}$$

where we put $\mu(\mu+1) \stackrel{\text{def}}{=} \frac{k^2}{|K|} \pm \frac{3}{4}$ with upper sign for closed ($K > 0$) and lower sign for open ($K < 0$) universe. In addition, we will write from now on $\nu^2 \stackrel{\text{def}}{=} \frac{k^2}{|K|} \pm 1$ just for convenience.

Let us, for a while, analyze closed, open and flat cases separately:

K > 0

Using the definitions of μ and ν, we get a second degree equation for μ: $\mu(\mu+1) = \nu^2 - \frac{1}{4}$, which gives $\mu_{1,2} = -\frac{1}{2} \pm \nu$. Remembering that $\sin_K\tilde{\chi} = \sin\tilde{\chi}$ we find equation (A.7) to be the (associated) Legendre differential equation [206] with the solutions $P^{-1/2-\ell}_{-1/2+\nu}(\cos\tilde{\chi})$ and $P^{+1/2+\ell}_{-1/2+\nu}(\cos\tilde{\chi})$. These Legendre functions with non-integer indices are defined in terms of hypergeometric functions, see e.g. [210, 409]. Note that we can take these as independent solutions instead of P^β_α and the Legendre function of second kind, Q^β_α, since

[1] Note that as there is k^2 in the Helmholtz equation, it does not specify the dependence on the direction of $\vec{k}$. Thus it gives only the quantity $Q(\vec{x}) \stackrel{\text{def}}{=} Q(\vec{x}, |\vec{k}|)$, not the whole $Q(\vec{x}, \vec{k})$, which appears in the expansion (A.3). The dependence on the direction of $\vec{k}$ will be fixed later by demanding the analogy to the flat space plane wave to be as close as possible.

$\ell + 1/2$ is a half-integer. Furthermore, μ_2 gives nothing more because $P^{\beta}_{\alpha} = P^{\beta}_{-1-\alpha}$, i.e. $P^{\beta}_{-1/2+\nu} = P^{\beta}_{-1/2-\nu}$. So it is enough to consider non-negative values of ν. Now, from the definition of ν it follows that $\nu \geq 1$. Demanding $f(\tilde{\chi})$ to be regular at the origin eliminates the solution $P^{+1/2+\ell}_{-1/2+\nu}(\cos\tilde{\chi})$ and leaves us with $P^{-1/2-\ell}_{-1/2+\nu}(\cos\tilde{\chi})$. Thus we get for the radial function

$$f(\tilde{\chi}) = X^{\ell}_{\nu}(\tilde{\chi}) = N_K(\ell,\nu)\,\sin^{-1/2}\tilde{\chi}\; P^{-1/2-\ell}_{-1/2+\nu}(\cos\tilde{\chi}), \tag{A.8}$$

where N_K is a normalization constant.

In the closed universe the radial coordinate $\tilde{\chi}$ can take values from 0 to π. Assuming that X^{ℓ}_{ν} is the radial part of the "wave function of the whole universe" [16, 410], one can demand $|X^{\ell}_{\nu}|^2$ to be single valued (that is periodic). This implies that $P^{-1/2-\ell}_{-1/2+\nu}(\cos(\tilde{\chi}+\pi)) = \pm P^{-1/2-\ell}_{-1/2+\nu}(\cos\tilde{\chi})$. But here $\cos(\tilde{\chi}+\pi) = -\cos\tilde{\chi}$, and we obtain $P^{-1/2-\ell}_{-1/2+\nu}(-\cos\tilde{\chi}) = \pm P^{-1/2-\ell}_{-1/2+\nu}(\cos\tilde{\chi})$. On the other hand, we find from tables the following identity

$$P^{\mu}_{\nu}(-x) = \cos[\pi(\nu+\mu)]P^{\mu}_{\nu}(x) - (2/\pi)\sin[\pi(\nu+\mu)]Q^{\mu}_{\nu}(x).$$

Thus we must have $\cos[\pi(\nu-\ell-1)] = \pm 1$ and $\sin[\pi(\nu-\ell-1)] = 0$, i.e., ν must be a positive integer. Now $P^{-1/2-\ell}_{-1/2+\nu}(x)$ is non-zero only if $\nu \geq \ell$, since both ℓ and ν are non-negative integers. In addition, $\nu = 1$ and $\nu = 2$ give modes, which are unnecessary gauge terms [14]. So the final spectrum of eigenvalues in the closed universe will be

$$k^2 = K(\nu^2 - 1), \quad \text{with } \nu = 3,\, 4,\, 5,\, \ldots \quad \text{and} \quad \nu \geq \ell.$$

K < 0

First we replace $\tilde{\chi}$ by $i\tilde{\chi}$ everywhere in equation (A.7) and use the formula $\sinh(i\tilde{\chi}) = i\sin\tilde{\chi}$ to get

$$\frac{1}{\sin\tilde{\chi}}\frac{d}{d\tilde{\chi}}\left[\sin\tilde{\chi}\frac{d}{d\tilde{\chi}}\Pi(i\tilde{\chi})\right] + \left[-\mu(\mu+1) - \frac{(\ell+\frac{1}{2})^2}{\sin^2\tilde{\chi}}\right]\Pi(i\tilde{\chi}) = 0.$$

This gives $\Pi(i\tilde{\chi}) = P^{-1/2-\ell}_{-1/2+i\nu}(\cos\tilde{\chi})$, which leads to $\Pi(\tilde{\chi}) = P^{-1/2-\ell}_{-1/2+i\nu}(\cosh\tilde{\chi})$, where ν can now take any non-negative real value. So we have

$$f(\tilde{\chi}) = X^{\ell}_{\nu}(\tilde{\chi}) = N_K(\ell,\nu)\,\sinh^{-1/2}\tilde{\chi}\; P^{-1/2-\ell}_{-1/2+i\nu}(\cosh\tilde{\chi}), \tag{A.9}$$

where $\tilde{\chi}$ can take values from zero to infinity.

K = 0

In this case, the equation for f reduces at once to the spherical Bessel equation with solution

$$f(\tilde{\chi}) = X^{\ell}_{\nu}(\tilde{\chi}) = j_{\ell}(\nu\tilde{\chi}), \tag{A.10}$$

where $\tilde{\chi} \in [0,\infty]$ and $\nu\tilde{\chi} = (k^2/|K| \pm 1)^{1/2}\,|K|^{1/2}\chi = (k^2 \pm |K|)^{1/2}\chi = k\chi$ as $|K| \to 0$. The closure relation for spherical Bessel functions [206] gives

$$\int_0^{\infty} X^{\ell}_{\nu}(\tilde{\chi})X^{\ell\,*}_{\nu'}(\tilde{\chi})\,\tilde{\chi}^2 d\tilde{\chi} = \frac{\pi}{2\nu^2}\delta(\nu-\nu'). \tag{A.11}$$

We can generate $X^\ell_\nu(\tilde\chi)$ with $\ell > 0$ from $X^0_\nu(\tilde\chi) = \frac{\sin(k\chi)}{k\chi}$ via the familiar recursion formula for j_ℓ [411]

$$\frac{d}{d\chi}X^\ell_\nu(\tilde\chi) = \frac{\ell}{2\ell+1}kX^{\ell-1}_\nu(\tilde\chi) - \frac{\ell+1}{2\ell+1}kX^{\ell+1}_\nu(\tilde\chi). \tag{A.12}$$

Note that for radially moving photons we have here $d\chi = d\eta$.

Now we return to analyze the properties of the radial function

$$X^\ell_\nu(\tilde\chi) = N_K(\ell,\nu)\sin_K^{-1/2}\tilde\chi\, P^{-1/2-\ell}_{-1/2+(i)\nu}(\cos_K\tilde\chi) \tag{A.13}$$

with $K > 0$ (or $K < 0$). From tables (e.g [210]) or from "the famous Bateman's shoe-boxes[2]" [409] one finds many expressions for the associated Legendre functions, which could be used to find a more explicit form for the radial solution as is done in [16]. However, we will need only the following orthogonality and recursion relations:

$$\int P^{-m}_n(z)P^{-m}_{n'}(z)^*\,dz = \frac{2}{2n+1}\frac{(n-m)!}{(n+m)!}\;\delta_{n,n'}, \tag{A.14}$$

$$\frac{dP^\mu_\nu(z)}{dz} = (\nu+\mu)(\nu-\mu+1)(z^2-1)^{-1/2}P^{\mu-1}_\nu(z) \pm \frac{\mu z}{z^2-1}P^\mu_\nu(z), \tag{A.15}$$

$$P^{\mu+1}_\nu(z) + 2\mu z(z^2-1)^{-1/2}P^\mu_\nu(z) = \mp(\nu-\mu+1)(\nu+\mu)P^{\mu-1}_\nu(z). \tag{A.16}$$

In (A.14) we integrate from -1 (1) to 1 (∞) in closed (open) case. Upper signs are for closed case and lower signs for open case. In equations (A.15) and (A.16) $z = \cosh\tilde\chi$ for open case. In closed case we must replace z with x and $1-z^2$ with x^2-1, where $x = \cos\tilde\chi$.

Generalizing (A.14) to our case of Legendre functions with non-integer indices, we get

$$\int X^\ell_\nu(\tilde\chi)X^{\ell\,*}_{\nu'}(\tilde\chi)\,\sin^2_K\tilde\chi\,d\tilde\chi = |N_K(\ell,\nu)|^2\int_{-1\,(1)}^{1\,(\infty)} P^{-1/2-\ell}_{-1/2+(i)\nu}(z)[P^{-1/2-\ell}_{-1/2+(i)\nu'}(z)]^*\,dz$$

$$= |N_K(\ell,\nu)|^2\left|[(i)\nu]^{-1}\frac{1}{[(i)\nu+\ell][(i)\nu+\ell-1]\cdots[(i)\nu-\ell]}\right|\delta(\nu-\nu').$$

We demand the normalization to be similar to the flat space case (A.11), i.e.,

$$\int X^\ell_\nu(\tilde\chi)X^{\ell\,*}_{\nu'}(\tilde\chi)\,\sin^2_K\tilde\chi\,d\tilde\chi = \frac{\pi}{2\nu^2}\delta(\nu-\nu'). \tag{A.17}$$

Hence we choose

$$N_K(\ell,\nu) = \left[\frac{\pi}{2\nu^2}\right]^{1/2}\left[\prod_{\ell'=0}^{\ell}(\nu^2 \mp \ell'^2)\right]^{1/2}. \tag{A.18}$$

From this we obtain

$$\frac{N_K(\ell,\nu)}{N_K(\ell+1,\nu)} = \left[\nu^2 \mp (\ell+1)^2\right]^{-1/2} \quad\text{and}\quad \frac{N_K(\ell,\nu)}{N_K(\ell-1,\nu)} = \left[\nu^2 \mp \ell^2\right]^{1/2}. \tag{A.19}$$

[2]For explanation read Preface and Foreword of [409].

For photons we have $d\eta = |K|^{-1/2} d\tilde{\chi}$. Thus, derivating (A.13), we obtain

$$\frac{dX_\nu^\ell(\tilde{\chi})}{d\eta} = |K|^{1/2} N_K(\ell,\nu) \left[-\tfrac{1}{2} \sin_K^{-3/2}\tilde{\chi} \cos_K\tilde{\chi} \mp \sin_K^{1/2}\tilde{\chi} \tfrac{d}{d(\cos_K\tilde{\chi})} \right] P^{-1/2-\ell}_{-1/2+(i)\nu}(\cos_K\tilde{\chi}).$$

Evaluating the second term with help of (A.15) and then applying the recurrence relation (A.16) leads to

$$\begin{aligned}\frac{dX_\nu^\ell(\tilde{\chi})}{d\eta} &= |K|^{1/2} N_K(\ell,\nu) \sin_K^{-1/2}\tilde{\chi} \\ &\quad \times \left\{ \frac{\ell}{2\ell+1} P^{-1/2-(\ell-1)}_{-1/2+(i)\nu}(\cos_K\tilde{\chi}) \mp [\pm\nu^2 - (\ell+1)^2] \frac{\ell+1}{2\ell+1} P^{-1/2-(\ell+1)}_{-1/2+(i)\nu}(\cos_K\tilde{\chi}) \right\}.\end{aligned}$$

With help of (A.19) this reduces to

$$\frac{d}{d\eta} X_\nu^\ell(\tilde{\chi}) = \frac{\ell}{2\ell+1} k K_\ell^{1/2} X_\nu^{\ell-1}(\tilde{\chi}) - \frac{\ell+1}{2\ell+1} k K_{\ell+1}^{1/2} X_\nu^{\ell+1}(\tilde{\chi}), \tag{A.20}$$

where

$$K_\ell \stackrel{\text{def}}{=} 1 - (\ell^2-1)K/k^2, \quad \ell \geq 1.$$

Note that in the limit $K \to 0$ this recursion formula gives just the flat space relation (A.12).

We immediately see (cf. equations (A.7) and (A.17)) that

$$X_\nu^0(\tilde{\chi}) = \frac{\sin(\nu\tilde{\chi})}{\nu \sin_K\tilde{\chi}} \tag{A.21}$$

is a properly normalized solution for $\ell = 0$. From this we can derive all other solutions with $\ell \geq 1$ by using (A.20). Hence this recursion relation is all we need to know about the radial solutions.

A.1.2 Direction dependence of the expansion functions

To complete our discussion of the generalization of the Fourier transformation, we must specify the whole $Q(\vec{x},\vec{k})$, which depends on the direction of $\vec{k}$. Let us start with flat space. In this case we immediately find a solution to the Helmholtz equation (A.1) to be

$$Q_{\vec{u}} = e^{i\vec{u}\cdot\vec{x}},$$

where direction of the vector $\vec{u}$ can be arbitrary but its length must be $|\vec{u}| = |\vec{k}|$. The general solution is a sum of these solutions

$$Q = \int C(\theta_u,\varphi_u) Q_{\vec{u}} d\Omega_u, \tag{A.22}$$

where, as indicated, the multipliers C depend only on the direction of $\vec{u}$. From this general solution one finds particular solutions needed in different physical situations by fixing the multipliers. For example, in scattering theory one would probably set $C(\theta_u,\varphi_u) = 1$ leading to the formula $Q(\vec{x},\vec{k}) = 4\pi\frac{\sin(kx)}{kx}$. Now we want to do the normal Fourier analysis and thus we choose $C(\theta_u,\varphi_u) = \delta(\cos\theta_u - \cos\theta_k)\delta(\varphi_u - \varphi_k)$ to get the plane wave solution $Q(\vec{x},\vec{k}) = e^{i\vec{k}\cdot\vec{x}}$. Expanding $e^{i\vec{k}\cdot\vec{x}}$ in terms of $Y^*_{\ell m}(\theta_k,\varphi_k)$ as on page 52 in (2.126), and

remembering that in flat space $j_\ell(k\chi)$ is just the radial function $X^\ell_\nu(\tilde\chi)$, we get

$$Q_{\rm flat}(\vec{x},\vec{k}) = 4\pi \sum_{\ell=0}^{\infty}\sum_{m=-\ell}^{\ell} i^\ell X^\ell_\nu(\tilde\chi) Y_{\ell m}(\theta,\varphi) Y^*_{\ell m}(\theta_k,\varphi_k). \tag{A.23}$$

Note that if we had chosen other than the plane wave solution in (A.22), the coefficients in the expansion (A.23) would differ from $4\pi i^\ell$.

In curved space the whole $Q(\vec{x},\vec{k})$ (or general solution to the Helmholtz equation) can be written as

$$Q_{\rm curv}(\vec{x},\vec{k}) = \sum_{\ell=0}^{\infty}\sum_{m=-\ell}^{\ell} X^\ell_\nu(\tilde\chi) Y_{\ell m}(\theta,\varphi) b_{\ell m}(\theta_k,\varphi_k), \tag{A.24}$$

where quantities $b_{\ell m}$ are arbitrary functions of the direction of $\vec{k}$. Since we are looking for a generalization for the normal Fourier transformation, we choose these functions in such a way that our $Q_{\rm curv}$ has an as close as possible relation to the flat space Q. Putting more accurately, we demand

$$\lim_{|K|\to 0} Q_{\rm curv} = Q_{\rm flat}. \tag{A.25}$$

But the only quantity in (A.23) or (A.24) which the curvature affects is $X^\ell_\nu(\tilde\chi)$. Thus (A.25) fixes the functions $b_{\ell m}$ to be $b_{\ell m}(\theta_k,\varphi_k) = 4\pi i^\ell Y^*_{\ell m}(\theta_k,\varphi_k)$, and we get

$$Q(\vec{x},\vec{k}) = 4\pi \sum_{\ell=0}^{\infty}\sum_{m=-\ell}^{\ell} i^\ell X^\ell_\nu(\tilde\chi) Y_{\ell m}(\theta,\varphi) Y^*_{\ell m}(\theta_k,\varphi_k). \tag{A.26}$$

This is valid in curved space as well as in flat space, if we just pick the right X^ℓ_ν for each case from the previous subsection.

In what follows, we need the result

$$\begin{aligned}
&\int Q^*(\vec{x},\vec{k}) Q(\vec{x},\vec{k}') d^3\vec{x} \\
&= |K|^{-3/2}(4\pi)^2 \sum_{\ell m}\sum_{\ell' m'} \Bigg[(-i)^\ell i^{\ell'} Y_{\ell m}(\theta_k,\varphi_k) Y^*_{\ell' m'}(\theta_{k'},\varphi_{k'}) \\
&\quad \times \int X^{\ell *}_\nu(\tilde\chi) X^{\ell'}_{\nu'}(\tilde\chi)\, \sin^2_K\tilde\chi\, d\tilde\chi \int Y^*_{\ell m}(\theta,\varphi) Y_{\ell' m'}(\theta,\varphi) d\Omega \Bigg] \\
&= |K|^{-3/2}(4\pi)^2 \sum_{\ell m}\sum_{\ell' m'} \left[(-i)^\ell i^{\ell'} Y_{\ell m}(\theta_k,\varphi_k) Y^*_{\ell' m'}(\theta_{k'},\varphi_{k'}) \frac{\pi}{2\nu^2}\delta(\nu-\nu')\delta_{\ell\ell'}\delta_{mm'} \right] \\
&= |K|^{-3/2}(4\pi)^2 \frac{\pi}{2\nu^2}\delta(\nu-\nu') \sum_{\ell m} Y_{\ell m}(\theta_k,\varphi_k) Y^*_{\ell m}(\theta_{k'},\varphi_{k'}) \\
&= |K|^{-3/2}(4\pi)^2 \frac{\pi}{2\nu^2}\delta(\nu-\nu')\delta(\cos\theta_k - \cos\theta_{k'})\delta(\varphi_k-\varphi_{k'}),
\end{aligned} \tag{A.27}$$

where the first step follows from (A.26) and from the fact

$$d^3\vec{x} = |K|^{-3/2} \sin^2_K\tilde\chi\, d\tilde\chi\, d\Omega, \tag{A.28}$$

see the metric (A.2). Then we used the normalization condition (A.17) and just the familiar properties of the spherical harmonics, see e.g. [206, 411]. Recall that the Dirac

delta function satisfies

$$\delta\left(f(x)\right) = \frac{1}{\left|\frac{df}{dx}(x_0)\right|}\delta(x - x_0), \tag{A.29}$$

where x_0 is a zero point of f; $f(x_0) = 0$. Now

$$\frac{d\nu}{dk} = \frac{k/|K|}{\sqrt{k^2/|K| \pm 1}} \tag{A.30}$$

and (A.27) becomes

$$\int Q^*(\vec{x},\vec{k})Q(\vec{x},\vec{k}')d^3\vec{x}$$

$$= |K|^{-3/2}(4\pi)^2\frac{\pi}{2\nu^2}\frac{\sqrt{k'^2/|K| \pm 1}}{k'/|K|}\delta(k-k')\delta(\cos\theta_k - \cos\theta_{k'})\delta(\varphi_k - \varphi_{k'}), \tag{A.31}$$

where, as before, upper sign stands for $K > 0$ and lower sign for $K < 0$.

With help of this result we find what we actually mean by $d^3\vec{k}$ in (A.3). In flat space we can write $d^3\vec{k} = k^2 dk\, d\Omega_k$, where $k = |\vec{k}|$ and $d\Omega_k = d(\cos\theta_k)\, d\varphi_k$. In curved space we must be more careful. So, let us write $d^3\vec{k} = \mu(k) dk\, d\Omega_k$ and specify the "measure" $\mu(k)$ by performing subsequent inverse transformation and transformation to the identity function.

The identity function in k-space can be written as an inverse transformation of the identity function in x-space

$$\hat{1}(\vec{k}) = \frac{1}{V}\int 1(\vec{x})Q^*(\vec{x},\vec{k})d^3\vec{x}.$$

On the other hand, here $1(\vec{x})$ is given by a transformation of $\hat{1}(\vec{k}')$

$$1(\vec{x}) = \frac{V}{(2\pi)^3}\int \hat{1}(\vec{k}')Q(\vec{x},\vec{k}')d^3\vec{k}'.$$

Thus we have after changing the order of integrations

$$\hat{1}(\vec{k}) = \frac{1}{(2\pi)^3}\int \hat{1}(\vec{k}')\left[\int Q^*(\vec{x},\vec{k})Q(\vec{x},\vec{k}')d^3\vec{x}\right] d^3\vec{k}'.$$

The quantity in square brackets is given in (A.31) and we arrive at

$$\hat{1}(\vec{k}) = \frac{1}{(2\pi)^3}\int \hat{1}(\vec{k}')\left[|K|^{-3/2}(4\pi)^2\frac{\pi}{2\nu^2}\frac{\sqrt{k'^2/|K| \pm 1}}{k'/|K|}\right.$$

$$\left.\times\,\delta(\nu-\nu')\delta(\cos\theta_k - \cos\theta_{k'})\delta(\varphi_k - \varphi_{k'})\right]\mu(k')dk'\, d\Omega_{k'}.$$

Noting that actually the identity function is direction independent i.e. $\hat{1}(\vec{k}) = \hat{1}(k)$, we can perform the integration to get

$$\hat{1}(k) = \mu(k)\,|K|^{-3/2}\frac{\sqrt{k^2/|K| \pm 1}}{k/|K|}\frac{1}{\nu^2}\hat{1}(k).$$

This leads to

$$\mu(k) = |K|^{3/2}\frac{k/|K|}{\sqrt{k^2/|K| \pm 1}}\,\nu^2, \tag{A.32}$$

where recall that $\nu^2 = k^2/|K| \pm 1$. Note that in the limit $|K| \to 0$ the term ± 1 becomes negligible and we get $\mu(k) \to |K|^{3/2} \frac{k/|K|}{\sqrt{k^2/|K|}} k^2/|K| = k^2$ as pointed out earlier. Thus we may write

$$d^3\vec{k} = |K|^{3/2} \frac{k/|K|}{\sqrt{k^2/|K| \pm 1}} \nu^2 dk\, d\Omega_k \tag{A.33}$$

in all three cases of geometry.

A.2 Full multipole expansion

In addition to the position $\vec{x}$ the temperature perturbation function Θ depends on the direction $\vec{\gamma}$. Thus we need a generalization of the expansion (A.3). That is

$$F(\vec{x}, \vec{\gamma}) = \sum_{|\vec{k}| \geq \sqrt{|K|}} \sum_{\ell=0}^{\infty} \tilde{F}_\ell(\vec{k})\, G_\ell(\vec{x}, \vec{\gamma}, \vec{k}), \tag{A.34}$$

where

$$G_\ell(\vec{x}, \vec{\gamma}, \vec{k}) = \gamma^{i_1}\gamma^{i_2} \ldots \gamma^{i_\ell}\, Q^{(\ell)}_{i_1 i_2 \ldots i_\ell}(\vec{x}, \vec{k}). \tag{A.35}$$

Here $Q^{(\ell)}$ is an ℓth order tensor constructed from Q, its covariant derivatives and the metric tensor γ_{ij}. For practical calculations the first three are enough. Those can be chosen as [15]

$$\begin{aligned} Q^{(0)} &= Q, \\ Q^{(1)}_i &= (-k)^{-1} Q_{|i} \stackrel{\text{def}}{=} Q_i, \\ \frac{2}{3} Q^{(2)}_{ij} &= (-k)^{-2} Q_{|ij} + \frac{1}{3}\gamma_{ij} Q \stackrel{\text{def}}{=} Q_{ij}. \end{aligned} \tag{A.36}$$

Construction of higher $Q^{(\ell)}$s becomes extremely difficult.

In fact, when expressions for general G_ℓ are needed, they are usually written in terms of Legendre tensors [408, 412][3]

$$G_\ell(\vec{x}, \vec{\gamma}, \vec{k}) = (-k)^{-\ell} Q_{|\, i_1 i_2 \ldots i_\ell}(\vec{x}, \vec{k})\, P^{i_1 i_2 \ldots i_\ell}_{(\ell)}(\vec{x}, \vec{\gamma}). \tag{A.37}$$

Tensors $P_{(\ell)}$ are defined recursively

$$\begin{aligned} P_0 = 1, \qquad P^i_1 = \gamma^i, \qquad P^{ij}_2 &= \frac{1}{2}(3\gamma^i\gamma^j - \gamma^{ij}), \\ P^{i_1 \ldots i_{\ell+1}}_{\ell+1} &= \frac{2\ell+1}{\ell+1}\gamma^{(i_1} P^{i_2 \ldots i_{\ell+1})}_\ell - \frac{\ell}{\ell+1}\gamma^{(i_1 i_2} P^{i_3 .. i_{\ell+1})}_{\ell-1}, \end{aligned}$$

where parentheses around indices denote symmetrization. Using this relation one can derive the following recursion formula for G_ℓ

$$\gamma^i G_{\ell\,|i} = k\left(\frac{\ell}{2\ell+1} K_\ell G_{\ell-1} - \frac{\ell+1}{2\ell+1} G_{\ell+1}\right). \tag{A.38}$$

[3] Wilson and Gouda et al. put in [408, 412] an extra $i^{-\ell}$ into expansions such as our (A.34). Thus they have $i^{-\ell}$ also in the definition of G_ℓ. We have dropped $i^{-\ell}$ from multipole expansion (A.34) and thus we get $(-1)^{-\ell}$ instead of $i^{-\ell}$ in the definition of G_ℓ.

White and Scott [413] derive these results in detail by using induction. See also the papers by Hu et al. [414, 415] for their modern and powerful "total angular momentum method", which unifies the treatment of temperature and polarization anisotropies. Though we will omit the polarization completely here, it should not be too difficult to generalize our formulas to include polarization by using their method. Note that the same expansion (A.34) with G_ℓ defined in (A.37) can be used, in addition to the polarization, also when investigating other tensor anisotropies such as gravitational waves [416].

If one thinks the perturbations along the radial path of photons, then $\gamma^2 = \gamma^3 = 0$ and $\gamma_{11}(\gamma^1)^2 = 1$ i.e. $\gamma^1 = \sqrt{|K|}$. In this case, the left hand side of (A.38) is simply

$$\gamma^i G_{\ell\,|i} = \sqrt{|K|}\frac{d}{d\tilde{\chi}}G_\ell = \frac{d}{d\eta}G_\ell[\vec{x}(\eta), \vec{\gamma}(\eta)], \tag{A.39}$$

and we observe by comparing (A.38) to equation (A.20) that

$$G_\ell[\vec{x}(\eta), \vec{\gamma}(\eta)] = M_\ell^{1/2} X_\nu^\ell(\eta), \tag{A.40}$$

where $M_\ell = \prod_{\ell'=0}^{\ell} K_{\ell'}$ with $K_0 = 1$.

Hence in order to maintain the same normalization as in the previous section we must redefine $\tilde{F}_\ell$ in (A.34) to be $\tilde{F}_\ell = M_\ell^{-1/2} F_\ell$. So our final form of the multipole decomposition will be

$$F(\vec{x}, \vec{\gamma}) = \sum_{|\vec{k}| \geq \sqrt{|K|}} \sum_{\ell=0}^{\infty} F_\ell(\vec{k})\, M_\ell^{-1/2} G_\ell(\vec{x}, \vec{\gamma}, \vec{k}). \tag{A.41}$$

We need also the following properties (see [413]) of the properly normalized expansion functions $M_\ell^{-1/2} G_\ell(\vec{x}, \vec{\gamma}, \vec{k})$. Since the tensors $P_{(\ell)}$ are symmetric, we have

$$\int G_\ell d\Omega_k \propto \int Q(\vec{x}, \vec{k}) P_\ell(\hat{k} \cdot \vec{\gamma}) d\Omega_k, \tag{A.42}$$

where $\hat{k}$ is a unit vector in the direction of $\vec{k}$ and P_ℓ is the Legendre polynomial. The second useful property is

$$\int ||M_\ell^{-1/2} G_\ell||^2 d\Omega_k = \int ||M_{\ell-1}^{-1/2} G_{\ell-1}||^2 d\Omega_k = \ldots = \int ||G_0||^2 d\Omega_k = \int ||Q||^2 d\Omega_k, \tag{A.43}$$

where the norm is defined by

$$||G_\ell||^2 \stackrel{\text{def}}{=} \int G_\ell^*(\vec{x}, \vec{\gamma}, \vec{k}) G_\ell(\vec{x}, \vec{\gamma}, \vec{k}) d^3\vec{x}. \tag{A.44}$$

A.3 Decomposed brightness equation

Now we proceed to find the decomposition of the collisional brightness equation (2.50)

$$\frac{d}{d\eta}(\Theta + \Psi) = \dot{\Psi} - \dot{\Phi} + \dot{\tau}[(\Theta_0 - \Theta) + \gamma_i v_b^i + \frac{1}{16}\gamma_i\gamma_j \Pi_\gamma^{ij}], \tag{A.45}$$

where we wrote $\dot{\Psi} = \frac{\partial \Psi}{\partial \eta}$, $\dot{\Phi} = \frac{\partial \Phi}{\partial \eta}$ and $\dot{\tau} = \frac{d\tau}{d\eta}$. Since the perturbations in the metric (Ψ and Φ) are scalar quantities, we have from (A.41)

$$\Psi(\eta, \vec{x}) = \sum_{|\vec{k}| \geq \sqrt{|K|}} \Psi_0(\eta, \vec{k})\, M_0^{-1/2} G_0(\vec{x}, \vec{\gamma}, \vec{k}) = \sum_{\vec{k}} \Psi(\eta, \vec{k}) Q(\vec{x}, \vec{k}) \tag{A.46}$$

and similar expression for Φ (and Θ_0). For brevity we will omit the indexes 0 and the arguments of $\Psi_0(\eta, \vec{k})$ and $\Phi_0(\eta, \vec{k})$ from now on. For the temperature perturbation the full multipole expansion stands as

$$\Theta(\eta, \vec{x}, \vec{\gamma}) = \sum_{|\vec{k}| \geq \sqrt{|K|}} \sum_{\ell=0}^{\infty} \Theta_\ell(\eta, \vec{k})\, M_\ell^{-1/2} G_\ell(\vec{x}, \vec{\gamma}, \vec{k}). \tag{A.47}$$

In addition we have defined $V_b(\eta, \vec{k})$ and $\Pi_\gamma(\eta, \vec{k})$ in such a way that

$$\gamma_i v_b^i(\eta, \vec{x}, \vec{\gamma}) = \sum_{|\vec{k}| \geq \sqrt{|K|}} V_b(\eta, \vec{k}) M_1^{-1/2} G_1(\vec{x}, \vec{\gamma}, \vec{k}) \tag{A.48}$$

and

$$\gamma_i \gamma_j \Pi_\gamma^{ij}(\eta, \vec{x}, \vec{\gamma}) = \sum_{|\vec{k}| \geq \sqrt{|K|}} \Pi_\gamma(\eta, \vec{k}) M_2^{-1/2} G_2(\vec{x}, \vec{\gamma}, \vec{k}). \tag{A.49}$$

When we substitute equations (A.46) – (A.49) into the Boltzmann equation (A.45), we obtain for each k

$$\begin{aligned}\left[\sum_{\ell=0}^{\infty} M_\ell^{-1/2} \tfrac{d}{d\eta} (\Theta_\ell G_\ell)\right] + M_0^{-1/2} \tfrac{d}{d\eta}(\Psi G_0) = M_0^{-1/2} \tfrac{\partial}{\partial \eta}(\Psi G_0) - M_0^{-1/2} \tfrac{\partial}{\partial \eta}(\Phi G_0) \\ + \dot{\tau} \left[- \left(\sum_{\ell=1}^{\infty} M_\ell^{-1/2} \Theta_\ell G_\ell \right) + M_1^{-1/2} V_b G_1 + \tfrac{1}{16} M_2^{-1/2} \Pi_\gamma G_2 \right].\end{aligned}$$

With help of the recursion relation (A.38) this gives

$$\begin{aligned}&\sum_{\ell=0}^{\infty} M_\ell^{-1/2} \left[\dot{\Theta}_\ell G_\ell + \Theta_\ell k \left(\frac{\ell}{2\ell+1} K_\ell G_{\ell-1} - \frac{\ell+1}{2\ell+1} G_{\ell+1} \right) \right] + M_0^{-1/2} \dot{\Psi} G_0 - M_0^{-1/2} \Psi k G_1 \\ &= M_0^{-1/2} \dot{\Psi} G_0 - M_0^{-1/2} \dot{\Phi} G_0 + \dot{\tau} \left[- \left(\sum_{\ell=1}^{\infty} M_\ell^{-1/2} \Theta_\ell G_\ell \right) + M_1^{-1/2} V_b G_1 + \tfrac{1}{16} M_2^{-1/2} \Pi_\gamma G_2 \right].\end{aligned}$$

Now we equalize the multipliers of each G_ℓ to obtain our final result:

$$\begin{aligned}\dot{\Theta}_0 &= -\frac{k}{3}\Theta_1 - \dot{\Phi}, \\ \dot{\Theta}_1 &= k \left[\Theta_0 + \Psi - \frac{2}{5} K_2^{1/2} \Theta_2 \right] - \dot{\tau}(\Theta_1 - V_b), \\ \dot{\Theta}_2 &= k \left[\frac{2}{3} K_2^{1/2} \Theta_1 - \frac{3}{7} K_3^{1/2} \Theta_3 \right] - \frac{9}{10} \dot{\tau} \Theta_2, \\ \dot{\Theta}_\ell &= k \left[\frac{\ell}{2\ell-1} K_\ell^{1/2} \Theta_{\ell-1} - \frac{\ell+1}{2\ell+3} K_{\ell+1}^{1/2} \Theta_{\ell+1} \right] - \dot{\tau} \Theta_\ell \quad (\ell > 2).\end{aligned} \tag{A.50}$$

In the third line we made use of the fact that the anisotropic stress is $\Pi_\gamma = \frac{8}{5}\Theta_2$, see equation (2.61). This is the standard Boltzmann hierarchy which we discuss in Sec. 2.5.

References

[1] J. C. Mather *et. al.*, *Calibrator design for the COBE Far-Infrared Absolute Spectrophotometer (FIRAS)*, Astrophys. J. **512** (1999) 511, [astro-ph/9810373].

[2] R. C. Tolman, *Relativity, thermodynamics, and cosmology*, Clarendon Press (1934).

[3] G. Gamow, *Evolution of the universe*, Nature **162** (1948) 680–682.

[4] G. Gamow, *The origin of elements and the separation of galaxies*, Phys. Rev. **74** (1948) 505–506.

[5] R. A. Alpher and R. C. Herman, *Evolution of the universe*, Nature **162** (1948) 774–775.

[6] R. A. Alpher, *A neutron-capture theory of the formation and relative abundance of the elements*, Phys. Rev. **74** (1948) 1577–1589.

[7] R. A. Alpher and R. C. Herman, *Remarks on the evolution of an expanding universe*, Phys. Rev. **75** (1949), no. 7 1089–1095.

[8] A. A. Penzias and R. W. Wilson, *A measurement of excess antenna temperature at 4080-Mc/s*, Astrophys. J. **142** (1965) 419–421.

[9] R. H. Dicke, P. J. E. Peebles, P. G. Roll, and D. T. Wilkinson, *Cosmic black-body radiation*, Astrophys. J. **142** (1965) 414–419.

[10] D. T. Wilkinson, *Measurement of the cosmic microwave background at 8.56-mm wavelength*, Phys. Rev. Lett. **19** (1967), no. 20 1195–1198.

[11] R. A. Stokes, R. B. Partridge, and D. T. Wilkinson, *New measurements of the cosmic microwave background at lambda = 3.2 cm and lambda = 1.58 cm - evidence in support of a blackbody spectrum*, Phys. Rev. Lett. **19** (1967), no. 20 1199–1202.

[12] P. Grenier, J. Roucher, and B. Talureau, *Measurement of the millimetric background radiation*, Astronomy and Astrophysics **53** (1976), no. 2 249–251.

[13] R. K. Sachs and A. M. Wolfe, *Perturbations of a cosmological model and angular variations of the microwave background*, Astrophys. J. **147** (1967) 73–90.

[14] J. M. Bardeen, *Gauge invariant cosmological perturbations*, Phys. Rev. **D22** (1980) 1882–1905.

[15] H. Kodama and M. Sasaki, *Cosmological perturbation theory*, Prog. Theor. Phys. Suppl. **78** (1984) 1–166.

[16] L. F. Abbott and R. K. Schaefer, *A general, gauge invariant analysis of the cosmic microwave anisotropy*, Astrophys. J. **308** (1986) 546.

[17] G. F. Smoot *et. al.*, *Structure in the COBE DMR first year maps*, Astrophys. J. **396** (1992) L1–L5.

[18] C. L. Bennett *et. al.*, *Cosmic temperature fluctuations from two years of COBE differential microwave radiometers observations*, Astrophys. J. **436** (1994) 423–442.

[19] J. Silk, *Cosmic black body radiation and galaxy formation*, Astrophys. J. **151** (1968) 459–471.

[20] M. White and W. Hu, *The Sachs–Wolfe effect*, Astronomy and Astrophysics **321** (1997), no. 2 8 – 9.

[21] **Boomerang** Collaboration, P. de Bernardis *et. al.*, *A flat universe from high-resolution maps of the cosmic microwave background radiation*, Nature **404** (2000) 955–959, [astro-ph/0004404].

[22] **Boomerang** Collaboration, A. E. Lange *et. al.*, *Cosmological parameters from the first results of Boomerang*, Phys. Rev. **D63** (2001) 042001, [astro-ph/0005004].

[23] S. Hanany *et. al.*, *Maxima-1: A measurement of the cosmic microwave background anisotropy on angular scales of 10 arcminutes to 5 degrees*, Astrophys. J. **545** (2000) L5, [astro-ph/0005123].

[24] A. Balbi *et. al.*, *Constraints on cosmological parameters from Maxima-1*, Astrophys. J. **545** (2000) L1–L4, [astro-ph/0005124].

[25] C. L. Bennett *et. al.*, *First Year Wilkinson Microwave Anisotropy Probe (WMAP) observations: Preliminary maps and basic results*, Astrophys. J. Suppl. **148** (2003) 1, [astro-ph/0302207].

[26] G. Hinshaw *et. al.*, *First Year Wilkinson Microwave Anisotropy Probe (WMAP) observations: Angular power spectrum*, Astrophys. J. Suppl. **148** (2003) 135, [astro-ph/0302217].

[27] **Boomerang** Collaboration, C. B. Netterfield *et. al.*, *A measurement by Boomerang of multiple peaks in the angular power spectrum of the cosmic microwave background*, Astrophys. J. **571** (2002) 604–614, [astro-ph/0104460].

[28] P. de Bernardis *et. al.*, *Multiple peaks in the angular power spectrum of the cosmic microwave background: Significance and consequences for cosmology*, Astrophys. J. **564** (2002) 559–566, [astro-ph/0105296].

[29] A. T. Lee *et. al.*, *A high spatial resolution analysis of the Maxima-1 cosmic microwave background anisotropy data*, Astrophys. J. **561** (2001) L1–L6, [astro-ph/0104459].

[30] R. Stompor *et. al.*, *Cosmological implications of the Maxima-I high resolution cosmic microwave background anisotropy measurement*, Astrophys. J. **561** (2001) L7–L10, [astro-ph/0105062].

[31] E. M. Leitch *et. al.*, *Experiment design and first season observations with the Degree Angular Scale Interferometer*, Astrophys. J. **568** (2002) 28–37, [astro-ph/0104488].

[32] N. W. Halverson *et. al.*, *DASI first results: A measurement of the cosmic microwave background angular power spectrum*, Astrophys. J. **568** (2002) 38–45, [astro-ph/0104489].

[33] C. Pryke *et. al.*, *Cosmological parameter extraction from the first season of observations with DASI*, Astrophys. J. **568** (2002) 46–51, [astro-ph/0104490].

[34] S. Padin *et. al.*, *First intrinsic anisotropy observations with the Cosmic Background Imager*, Astrophys. J. **549** (2001) L1–L5, [astro-ph/0012211].

[35] B. S. Mason *et. al.*, *The anisotropy of the microwave background to l = 3500: Deep field observations with the Cosmic Background Imager*, Astrophys. J. **591** (2003) 540–555, [astro-ph/0205384].

[36] T. J. Pearson *et. al.*, *The anisotropy of the microwave background to l = 3500: Mosaic observations with the Cosmic Background Imager*, Astrophys. J. **591** (2003) 556–574, [astro-ph/0205388].

[37] A. C. S. Readhead *et. al.*, *Extended mosaic observations with the Cosmic Background Imager*, Astrophys. J. **609** (2004) 498–512, [astro-ph/0402359].

[38] P. F. Scott *et. al.*, *First results from the Very Small Array – III. The CMB power spectrum*, Mon. Not. Roy. Astron. Soc. **341** (2003) 1076, [astro-ph/0205380].

[39] K. Grainge *et. al.*, *The CMB power spectrum out to l=1400 measured by the VSA*, Mon. Not. Roy. Astron. Soc. **341** (2003) L23, [astro-ph/0212495].

[40] A. Slosar *et. al.*, *Cosmological parameter estimation and bayesian model comparison using VSA data*, Mon. Not. Roy. Astron. Soc. **341** (2003) L29, [astro-ph/0212497].

[41] R. Rebolo *et. al.*, *Cosmological parameter estimation using Very Small Array data out to l=1500*, astro-ph/0402466.

[42] C. Dickinson *et. al.*, *High sensitivity measurements of the CMB power spectrum with the extended Very Small Array*, astro-ph/0402498.

[43] **ACBAR** Collaboration, C.-l. Kuo *et. al.*, *High resolution observations of the CMB power spectrum with ACBAR*, Astrophys. J. **600** (2004) 32–51, [astro-ph/0212289].

[44] J. H. Goldstein *et. al.*, *Estimates of cosmological parameters using the CMB angular power spectrum of ACBAR*, Astrophys. J. **599** (2003) 773–785, [astro-ph/0212517].

[45] M. C. Runyan *et. al.*, *The Arcminute Cosmology Bolometer Array Receiver*, Astrophys. J. Suppl. **149** (2003) 265, [astro-ph/0303515].

[46] A. Benoit *et. al.*, *Archeops: A high resolution, large sky coverage balloon experiment for mapping CMB anisotropies*, astro-ph/0106152.

[47] **Archeops** Collaboration, A. Benoit *et. al.*, *The cosmic microwave background anisotropy power spectrum measured by Archeops*, Astron. Astrophys. **399** (2003) L19–L23, [astro-ph/0210305].

[48] M. Tristram *et. al.*, *The CMB temperature power spectrum from an improved analysis of the Archeops data*, astro-ph/0411633.

[49] M. Bucher, K. Moodley, and N. Turok, *Constraining isocurvature perturbations with CMB polarization*, Phys. Rev. Lett. **87** (2001) 191301, [astro-ph/0012141].

[50] E. M. Leitch *et. al.*, *Measuring polarization with DASI*, Nature **420** (2002) 763–771, [astro-ph/0209476].

[51] J. Kovac *et. al.*, *Detection of polarization in the cosmic microwave background using DASI*, Nature **420** (2002) 772–787, [astro-ph/0209478].

[52] E. M. Leitch *et. al.*, *DASI three-year cosmic microwave background polarization results*, astro-ph/0409357.

[53] A. C. S. Readhead *et. al.*, *Polarization observations with the Cosmic Background Imager*, astro-ph/0409569.

[54] A. Kogut *et. al.*, *Wilkinson Microwave Anisotropy Probe (WMAP) first year observations: TE polarization*, Astrophys. J. Suppl. **148** (2003) 161, [astro-ph/0302213].

[55] http://www.rssd.esa.int/Planck.

[56] A. Melchiorri, *Cosmological constraints from microwave background anisotropy and polarization*, hep-ph/0311319.

[57] A. Melchiorri, *Multiple peaks in the CMB*, astro-ph/0201237.

[58] J. Valiviita, *Correlated adiabatic and isocurvature CMB fluctuations in the light of the WMAP data*, astro-ph/0310206. To appear in the proceedings of 15th Rencontres de Blois: Physical Cosmology: New Results in Cosmology and the Coherence of the Standard Model (Blois 2003), Blois, France, 15-20 Jun 2003.

[59] D. Langlois, *Correlated adiabatic and isocurvature perturbations from double inflation*, Phys. Rev. **D59** (1999) 123512, [astro-ph/9906080].

[60] D. Langlois and A. Riazuelo, *Correlated mixtures of adiabatic and isocurvature cosmological perturbations*, Phys. Rev. **D62** (2000) 043504, [astro-ph/9912497].

[61] D. Parkinson, S. Tsujikawa, B. A. Bassett, and L. Amendola, *Testing for double inflation with WMAP*, Phys. Rev. **D71** (2005) 063524, [astro-ph/0409071].

[62] K. Enqvist and J. McDonald, *Observable isocurvature fluctuations from the Affleck-Dine condensate*, Phys. Rev. Lett. **83** (1999) 2510–2513, [hep-ph/9811412].

[63] M. Bucher, K. Moodley, and N. Turok, *The general primordial cosmic perturbation*, Phys. Rev. **D62** (2000) 083508, [astro-ph/9904231].

[64] M. Bucher, K. Moodley, and N. Turok, *Characterising the primordial cosmic perturbations using MAP and PLANCK*, Phys. Rev. **D66** (2002) 023528, [astro-ph/0007360].

[65] C. Gordon and A. Lewis, *Observational constraints on the curvaton model of inflation*, Phys. Rev. **D67** (2003) 123513, [astro-ph/0212248].

[66] S. Weinberg, *Can non-adiabatic perturbations arise after single-field inflation?*, Phys. Rev. **D70** (2004) 043541, [astro-ph/0401313].

[67] E. J. Copeland, R. Easther, and D. Wands, *Vacuum fluctuations in axion-dilaton cosmologies*, Phys. Rev. **D56** (1997) 874–888, [hep-th/9701082].

[68] R. Durrer, M. Gasperini, M. Sakellariadou, and G. Veneziano, *Seeds of large-scale anisotropy in string cosmology*, Phys. Rev. **D59** (1999) 043511, [gr-qc/9804076].

[69] J. E. Lidsey, D. Wands, and E. J. Copeland, *Superstring cosmology*, Phys. Rept. **337** (2000) 343–492, [hep-th/9909061].

[70] F. Vernizzi, A. Melchiorri, and R. Durrer, *CMB anisotropies from pre-big bang cosmology*, Phys. Rev. **D63** (2001) 063501, [astro-ph/0008232].

[71] M. Gasperini and G. Veneziano, *The pre-big bang scenario in string cosmology*, Phys. Rept. **373** (2003) 1–212, [hep-th/0207130].

[72] K. Enqvist and M. S. Sloth, *Adiabatic CMB perturbations in pre big bang string cosmology*, Nucl. Phys. **B626** (2002) 395–409, [hep-ph/0109214].

[73] M. S. Sloth, *Superhorizon curvaton amplitude in inflation and pre-big bang cosmology*, Nucl. Phys. **B656** (2003) 239–251, [hep-ph/0208241].

[74] S. Mollerach, *Isocurvature baryon perturbations and inflation*, Phys. Rev. **D42** (1990) 313–325.

[75] D. H. Lyth and D. Wands, *Generating the curvature perturbation without an inflaton*, Phys. Lett. **B524** (2002) 5–14, [hep-ph/0110002].

[76] D. H. Lyth, C. Ungarelli, and D. Wands, *The primordial density perturbation in the curvaton scenario*, Phys. Rev. **D67** (2003) 023503, [astro-ph/0208055].

[77] K. Dimopoulos and D. H. Lyth, *Models of inflation liberated by the curvaton hypothesis*, Phys. Rev. **D69** (2004) 123509, [hep-ph/0209180].

[78] N. Bartolo and A. R. Liddle, *The simplest curvaton model*, Phys. Rev. **D65** (2002) 121301, [astro-ph/0203076].

[79] K. Enqvist, *Curvatons in the minimally supersymmetric standard model*, Mod. Phys. Lett. **A19** (2004) 1421–1434, [hep-ph/0403273].

[80] D. Langlois and F. Vernizzi, *Mixed inflaton and curvaton perturbations*, Phys. Rev. **D70** (2004) 063522, [astro-ph/0403258].

[81] S. Gupta, K. A. Malik, and D. Wands, *Curvature and isocurvature perturbations in a three-fluid model of curvaton decay*, Phys. Rev. **D69** (2004) 063513, [astro-ph/0311562].

[82] F. Ferrer, S. Rasanen, and J. Valiviita, *Correlated isocurvature perturbations from mixed inflaton- curvaton decay*, JCAP **0410** (2004) 010, [astro-ph/0407300].

[83] S. Weinberg, *Must cosmological perturbations remain non-adiabatic after multi-field inflation?*, Phys. Rev. **D70** (2004) 083522, [astro-ph/0405397].

[84] M. Beltran, J. Garcia-Bellido, J. Lesgourgues, and A. Riazuelo, *Bounds on CDM and neutrino isocurvature perturbations from CMB and LSS data*, Phys. Rev. **D70** (2004) 103530, [astro-ph/0409326].

[85] R. Trotta, A. Riazuelo, and R. Durrer, *Reproducing cosmic microwave background anisotropies with mixed isocurvature perturbations*, Phys. Rev. Lett. **87** (2001) 231301, [astro-ph/0104017].

[86] R. Trotta, A. Riazuelo, and R. Durrer, *The cosmological constant and general isocurvature initial conditions*, Phys. Rev. **D67** (2003) 063520, [astro-ph/0211600].

[87] P. Crotty, J. Garcia-Bellido, J. Lesgourgues, and A. Riazuelo, *Bounds on isocurvature perturbations from CMB and LSS data*, Phys. Rev. Lett. **91** (2003) 171301, [astro-ph/0306286].

[88] K. Moodley, M. Bucher, J. Dunkley, P. G. Ferreira, and C. Skordis, *Constraints on isocurvature models from the WMAP first-year data*, Phys. Rev. **D70** (2004) 103520, [astro-ph/0407304].

[89] M. Bucher, J. Dunkley, P. G. Ferreira, K. Moodley, and C. Skordis, *The initial conditions of the universe: how much isocurvature is allowed?*, Phys. Rev. Lett. **93** (2004) 081301, [astro-ph/0401417].

[90] J. Väliviita, *An analytic approach to cosmic microwave background radiation anisotropies*, Master's thesis, University of Helsinki, 1999. http://www.helsinki.fi/∼jvalivii.

[91] W. T. Hu, *Wandering in the background: a cosmic microwave background explorer.* PhD thesis, University of California at Berkeley, 1995. astro-ph/9508126.

[92] A. R. Liddle and D. H. Lyth, *Cosmological inflation and large-scale structure.* Cambridge University Press, 2000.

[93] J. A. Peacock, *Cosmological Physics.* Cambridge University Press, 1999.

[94] S. Dodelson, *Modern cosmology.* Academic Press, 2003.

[95] E. W. Kolb and M. S. Turner, *The Early Universe.* Addison-Wesley, 1993.

[96] E. P. Hubble, *A relation between distance and radial velocity among extragalactic nebulae*, Proceedings of the National Academy of Sciences of the United States of America **15** (1929) 169–173.

[97] W. L. Freedman *et. al.*, *Final results from the Hubble Space Telescope Key Project to measure the Hubble constant*, Astrophys. J. **553** (2001) 47–72, [astro-ph/0012376].

[98] R. M. Wald, *General Relativity.* The University of Chicago Press, 1984.

[99] C. W. Misner, K. S. Thorne, and J. A. Wheeler, *Gravitation.* W. H. Freeman and Company, 1973.

[100] **Supernova Search Team** Collaboration, A. G. Riess *et. al.*, *Type Ia supernova discoveries at $z > 1$ from the Hubble Space Telescope: Evidence for past deceleration and constraints on dark energy evolution*, Astrophys. J. **607** (2004) 665–687, [astro-ph/0402512].

[101] R. A. Daly and S. G. Djorgovski, *Direct determination of the kinematics of the universe and properties of the dark energy as functions of redshift*, astro-ph/0403664.

[102] I. Ferreras, A. Melchiorri, and D. Tocchini-Valentini, *Using bright ellipticals as dark energy cosmic clocks*, Mon. Not. Roy. Astron. Soc. **344** (2003) 257, [astro-ph/0302180].

[103] A. Melchiorri, *New constraints on dark energy*, astro-ph/0406652.

[104] A. Melchiorri, L. Mersini-Houghton, C. J. Odman, and M. Trodden, *The state of the dark energy equation of state*, Phys. Rev. **D68** (2003) 043509, [astro-ph/0211522].

[105] S. M. Carroll, *Spacetime and geometry: An introduction to general relativity.* Addison Wesley, 2004.

[106] **Supernova Search Team** Collaboration, A. G. Riess *et. al.*, *Observational evidence from supernovae for an accelerating universe and a cosmological constant*, Astron. J. **116** (1998) 1009–1038, [astro-ph/9805201].

[107] **Supernova Cosmology Project** Collaboration, S. Perlmutter *et. al.*, *Measurements of Omega and Lambda from 42 high-redshift supernovae*, Astrophys. J. **517** (1999) 565–586, [astro-ph/9812133].

[108] **Supernova Search Team** Collaboration, J. L. Tonry *et. al.*, *Cosmological results from high-z supernovae*, Astrophys. J. **594** (2003) 1–24, [astro-ph/0305008].

[109] R. A. Knop *et. al.*, *New constraints on Ω_M, Ω_Λ, and w from an independent set of eleven high-redshift supernovae observed with HST*, Astrophys. J. **598** (2003) 102, [astro-ph/0309368].

[110] B. J. Barris *et. al.*, *23 high redshift supernovae from the IfA Deep Survey: Doubling the SN sample at $z > 0.7$*, Astrophys. J. **602** (2004) 571–594, [astro-ph/0310843].

[111] **Supernova Cosmology Project** Collaboration, S. Nobili *et. al.*, *Restframe I-band Hubble diagram for type Ia supernovae up to redshift $z \sim 0.5$*, astro-ph/0504139.

[112] C. Csaki, N. Kaloper, and J. Terning, *Dimming supernovae without cosmic acceleration*, Phys. Rev. Lett. **88** (2002) 161302, [hep-ph/0111311].

[113] C. Csaki, N. Kaloper, and J. Terning, *Effects of the intergalactic plasma on supernova dimming via photon axion oscillations*, Phys. Lett. **B535** (2002) 33–36, [hep-ph/0112212].

[114] E. Mortsell, L. Bergstrom, and A. Goobar, *Photon axion oscillations and type Ia supernovae*, Phys. Rev. **D66** (2002) 047702, [astro-ph/0202153].

[115] E. Mortsell and A. Goobar, *Constraining photon axion oscillations using quasar spectra*, JCAP **0304** (2003) 003, [astro-ph/0303081].

[116] L. Ostman and E. Mortsell, *Limiting the dimming of distant type Ia supernovae*, JCAP **0502** (2005) 005, [astro-ph/0410501].

[117] D. L. Wiltshire, *Viable exact model universe without dark energy from primordial inflation*, gr-qc/0503099.

[118] B. M. N. Carter, B. M. Leith, S. C. C. Ng, A. B. Nielsen, and D. L. Wiltshire, *Exact model universe fits type IA supernovae data with no cosmic acceleration*, astro-ph/0504192.

[119] E. J. Guerra, R. A. Daly, and L. Wan, *Global cosmological parameters determined using classical double radio galaxies*, Astrophys. J. **544** (2003) 659–670.

[120] S. Podariu, R. A. Daly, M. P. Mory, and B. Ratra, *Radio galaxy redshift-angular size data constraints on dark energy*, Astrophys. J. **584** (2003) 577–579, [astro-ph/0207096].

[121] R. A. Daly and E. J. Guerra, *Quintessence, cosmology, and FRIIb radio galaxies*, Astron. J. **124** (2002) 1831, [astro-ph/0209503].

[122] R. A. Daly and S. G. Djorgovski, *A model-independent determination of the expansion and acceleration rates of the universe as a function of redshift and constraints on dark energy*, Astrophys. J. **597** (2003) 9–20, [astro-ph/0305197].

[123] U. Alam, V. Sahni, T. D. Saini, and A. A. Starobinsky, *Is there supernova evidence for dark energy metamorphosis?*, astro-ph/0311364.

[124] S. Weinberg, *Curvature dependence of peaks in the cosmic microwave background distribution*, Phys. Rev. **D62** (2000) 127302, [astro-ph/0006276].

[125] A. Riotto, *Inflation and the theory of cosmological perturbations*, hep-ph/0210162.

[126] **SDSS** Collaboration, M. Tegmark *et. al.*, *Cosmological parameters from SDSS and WMAP*, Phys. Rev. **D69** (2004) 103501, [astro-ph/0310723].

[127] S. Masi *et. al.*, *The BOOMERanG experiment and the curvature of the universe*, Prog. Part. Nucl. Phys. **48** (2002) 243–261, [astro-ph/0201137].

[128] A. H. Guth, *The inflationary universe: A possible solution to the horizon and flatness problems*, Phys. Rev. **D23** (1981) 347–356.

[129] A. A. Starobinsky, *Spectrum of relict gravitational radiation and the early state of the universe*, JETP Lett. **30** (1979) 682–685.

[130] A. A. Starobinsky, *A new type of isotropic cosmological models without singularity*, Phys. Lett. **B91** (1980) 99–102.

[131] J. M. Bardeen, P. J. Steinhardt, and M. S. Turner, *Spontaneous creation of almost scale-free density perturbations in an inflationary universe*, Phys. Rev. **D28** (1983) 679.

[132] E. D. Stewart and D. H. Lyth, *A more accurate analytic calculation of the spectrum of cosmological perturbations produced during inflation*, Phys. Lett. **B302** (1993) 171–175, [gr-qc/9302019].

[133] A. Vilenkin, *The birth of inflationary universes*, Phys. Rev. **D27** (1983) 2848.

[134] A. D. Linde, *Chaotic inflation*, Phys. Lett. **B129** (1983) 177–181.

[135] D. H. Lyth, *Large scale energy density perturbations and inflation*, Phys. Rev. **D31** (1985) 1792–1798.

[136] L. A. Kofman, *What initial perturbations may be generated in inflationary cosmological models*, Phys. Lett. **B173** (1986) 400.

[137] A. D. Linde, *Generation of isothermal density perturbations in the inflationary universe*, Phys. Lett. **B158** (1985) 375–380.

[138] A. D. Linde, *Eternally existing selfreproducing chaotic inflationary universe*, Phys. Lett. **B175** (1986) 395–400.

[139] L. A. Kofman and A. D. Linde, *Generation of density perturbations in the inflationary cosmology*, Nucl. Phys. **B282** (1987) 555.

[140] M. Sasaki and E. D. Stewart, *A general analytic formula for the spectral index of the density perturbations produced during inflation*, Prog. Theor. Phys. **95** (1996) 71–78, [astro-ph/9507001].

[141] A. D. Linde and V. Mukhanov, *Nongaussian isocurvature perturbations from inflation*, Phys. Rev. **D56** (1997) 535–539, [astro-ph/9610219].

[142] T. Vachaspati and M. Trodden, *Causality and cosmic inflation*, Phys. Rev. **D61** (2000) 023502, [gr-qc/9811037].

[143] D. Wands, K. A. Malik, D. H. Lyth, and A. R. Liddle, *A new approach to the evolution of cosmological perturbations on large scales*, Phys. Rev. **D62** (2000) 043527, [astro-ph/0003278].

[144] F. Finelli and R. H. Brandenberger, *Parametric amplification of metric fluctuations during reheating in two field models*, Phys. Rev. **D62** (2000) 083502, [hep-ph/0003172].

[145] G. German, G. G. Ross, and S. Sarkar, *Low-scale inflation*, Nucl. Phys. **B608** (2001) 423–450, [hep-ph/0103243].

[146] M. Bastero-Gil, V. Di Clemente, and S. F. King, *A supersymmetric standard model of inflation with extra dimensions*, Phys. Rev. **D67** (2003) 083504, [hep-ph/0211012].

[147] V. F. Mukhanov, H. A. Feldman, and R. H. Brandenberger, *Theory of cosmological perturbations. Part 1. Classical perturbations. Part 2. Quantum theory of perturbations. part 3. extensions*, Phys. Rept. **215** (1992) 203–333.

[148] R. H. Brandenberger, *Inflationary cosmology: Progress and problems*, hep-ph/9910410.

[149] J. R. Bond *et. al.*, *The cosmic microwave background and inflation, then and now*, AIP Conf. Proc. **646** (2003) 15–33, [astro-ph/0210007].

[150] E. R. Harrison, *Fluctuations at the threshold of classical cosmology*, Phys. Rev. **D1** (1970) 2726–2730.

[151] Y. B. Zeldovich, *A hypothesis, unifying the structure and the entropy of the Universe*, Mon. Not. Roy. Astron. Soc. **160** (1972) 1P–3P.

[152] J. Garcia-Bellido and D. Wands, *Metric perturbations in two-field inflation*, Phys. Rev. **D53** (1996) 5437–5445, [astro-ph/9511029].

[153] C. Gordon, *Adiabatic and entropy perturbations in cosmology*, astro-ph/0112523.

[154] L. Covi, D. H. Lyth, A. Melchiorri, and C. J. Odman, *The running-mass inflation model and WMAP*, Phys. Rev. **D70** (2004) 123521, [astro-ph/0408129].

[155] L. Covi, D. H. Lyth, and A. Melchiorri, *New constraints on the running-mass inflation model*, Phys. Rev. **D67** (2003) 043507, [hep-ph/0210395].

[156] D. H. Lyth and A. Riotto, *Particle physics models of inflation and the cosmological density perturbation*, Phys. Rept. **314** (1999) 1–146, [hep-ph/9807278].

[157] C. Gordon, D. Wands, B. A. Bassett, and R. Maartens, *Adiabatic and entropy perturbations from inflation*, Phys. Rev. **D63** (2001) 023506, [astro-ph/0009131].

[158] G. Rigopoulos, *On second order gauge invariant perturbations in multi-field inflationary models*, Class. Quant. Grav. **21** (2004) 1737–1754, [astro-ph/0212141].

[159] L. Amendola, C. Gordon, D. Wands, and M. Sasaki, *Correlated perturbations from inflation and the cosmic microwave background*, Phys. Rev. Lett. **88** (2002) 211302, [astro-ph/0107089].

[160] D. Wands, N. Bartolo, S. Matarrese, and A. Riotto, *An observational test of two-field inflation*, Phys. Rev. **D66** (2002) 043520, [astro-ph/0205253].

[161] L. A. Kofman and D. Y. Pogosian, *Nonflat perturbations in inflationary cosmology*, Phys. Lett. **B214** (1988) 508–514.

[162] D. Polarski and A. A. Starobinsky, *Isocurvature perturbations in multiple inflationary models*, Phys. Rev. **D50** (1994) 6123–6129, [astro-ph/9404061].

[163] S. Tsujikawa, D. Parkinson, and B. A. Bassett, *Correlation-consistency cartography of the double inflation landscape*, Phys. Rev. **D67** (2003) 083516, [astro-ph/0210322].

[164] T. Moroi and T. Takahashi, *Effects of cosmological moduli fields on cosmic microwave background*, Phys. Lett. **B522** (2001) 215–221, [hep-ph/0110096].

[165] T. Moroi and T. Takahashi, *Cosmic density perturbations from late-decaying scalar condensations*, Phys. Rev. **D66** (2002) 063501, [hep-ph/0206026].

[166] R. Jeannerot, J. Rocher, and M. Sakellariadou, *How generic is cosmic string formation in SUSY GUTs*, Phys. Rev. **D68** (2003) 103514, [hep-ph/0308134].

[167] P. J. E. Peebles, *Principles of Physical Cosmology*. Princeton University Press, 1993.

[168] S. Weinberg, *Gravitation and Cosmology*. Wiley, 1972.

[169] R. Durrer, *The theory of CMB anisotropies*, J. Phys. Stud. **5** (2001) 177–215, [astro-ph/0109522].

[170] R. Durrer, *Cosmological perturbation theory*, astro-ph/0402129.

[171] H. Kodama and M. Sasaki, *Evolution of isocurvature perturbations. I: Photon - baryon universe*, Int. J. Mod. Phys. **A1** (1986) 265.

[172] W. Hu and N. Sugiyama, *Small scale cosmological perturbations: An analytic approach*, Astrophys. J. **471** (1996) 542–570, [astro-ph/9510117].

[173] W. Hu and N. Sugiyama, *Anisotropies in the cosmic microwave background: An analytic approach*, Astrophys. J. **444** (1995) 489–506, [astro-ph/9407093].

[174] W. Hu and N. Sugiyama, *Toward understanding CMB anisotropies and their implications*, Phys. Rev. **D51** (1995) 2599–2630, [astro-ph/9411008].

[175] V. N. Lukash, *Production of phonons in an isotropic universe*, Sov. Phys. JETP **52** (1980) 807–814.

[176] J. Foster and J. D. Nightingale, *A Short Course in General Relativity*. Springer, 1994.

[177] G. Rocha *et. al.*, *Measuring α in the early universe: CMB polarization, reionization and the Fisher matrix analysis*, Mon. Not. Roy. Astron. Soc. **352** (2004) 20, [astro-ph/0309211].

[178] T. Montroy *et. al.*, *Measuring CMB polarization with Boomerang*, astro-ph/0305593.

[179] C. J. A. P. Martins *et. al.*, *WMAP constraints on varying α and the promise of reionization*, Phys. Lett. **B585** (2004) 29–34, [astro-ph/0302295].

[180] C. J. A. P. Martins *et. al.*, *Measuring α in the early universe I: CMB temperature, large-scale structure and Fisher matrix analysis*, Phys. Rev. **D66** (2002) 023505, [astro-ph/0203149].

[181] J. R. Bond and G. Efstathiou, *Cosmic background radiation anisotropies in universes dominated by nonbaryonic dark matter*, Astrophys. J. **285** (1984) L45–L48.

[182] E. Merzbacher, *Quantum Mechanics*. Wiley, third ed., 1998.

[183] P. J. E. Peebles and J. T. Yu, *Primeval adiabatic perturbation in an expanding universe*, Astrophys. J. **162** (1970) 815–836.

[184] W. Hu, M. Fukugita, M. Zaldarriaga, and M. Tegmark, *CMB observables and their cosmological implications*, Astrophys. J. **549** (2001) 669, [astro-ph/0006436].

[185] M. R. Spiegel, *Mathematical Handbook of Formulas and Tables*. Schaum's outline series. McGraw-Hill, 1968.

[186] S. I. Grossman, *Multivariable Calculus, Linear Algebra, and Differential Equations*. Harcourt Brace Jovanovich, second ed., 1984.

[187] E. Kreyszig, *Advanced Engineering Mathematics*. Wiley, seventh ed., 1993.

[188] U. Seljak and M. Zaldarriaga, *A line of sight approach to cosmic microwave background anisotropies*, Astrophys. J. **469** (1996) 437–444, [astro-ph/9603033].

[189] U. Seljak and M. Zaldarriaga. http://www.cmbfast.org/.

[190] M. Zaldarriaga, U. Seljak, and E. Bertschinger, *Integral solution for the microwave background anisotropies in non-flat universes*, Astrophys. J. **494** (1998) 491, [astro-ph/9704265].

[191] M. Zaldarriaga and U. Seljak, *CMBFAST for spatially closed universes*, Astrophys. J. Suppl. **129** (2000) 431–434, [astro-ph/9911219].

[192] U. Seljak, N. Sugiyama, M. J. White, and M. Zaldarriaga, *A comparison of cosmological Boltzmann codes: are we ready for high precision cosmology?*, Phys. Rev. **D68** (2003) 083507, [astro-ph/0306052].

[193] A. Lewis and A. Challinor. http://camb.info/.

[194] A. Lewis, A. Challinor, and A. Lasenby, *Efficient computation of CMB anisotropies in closed FRW models*, Astrophys. J. **538** (2000) 473–476, [astro-ph/9911177].

[195] A. Lewis and A. Challinor, *Evolution of cosmological dark matter perturbations*, Phys. Rev. **D66** (2002) 023531, [astro-ph/0203507].

[196] H. K. Eriksen, F. K. Hansen, A. J. Banday, K. M. Gorski, and P. B. Lilje, *Asymmetries in the CMB anisotropy field*, Astrophys. J. **605** (2004) 14–20, [astro-ph/0307507].

[197] F. K. Hansen, P. Cabella, D. Marinucci, and N. Vittorio, *Asymmetries in the local curvature of the WMAP data*, Astrophys. J. **607** (2004) L67–L70, [astro-ph/0402396].

[198] D. J. Schwarz, G. D. Starkman, D. Huterer, and C. J. Copi, *Is the low-l microwave background cosmic?*, Phys. Rev. Lett. **93** (2004) 221301, [astro-ph/0403353].

[199] F. K. Hansen, A. J. Banday, and K. M. Gorski, *Testing the cosmological principle of isotropy: local power spectrum estimates of the WMAP data*, astro-ph/0404206.

[200] A. Slosar and U. Seljak, *Assessing the effects of foregrounds and sky removal in WMAP*, Phys. Rev. **D70** (2004) 083002, [astro-ph/0404567].

[201] A. R. Liddle and A. Mazumdar, *Perturbation amplitude in isocurvature inflation scenarios*, Phys. Rev. **D61** (2000) 123507, [astro-ph/9912349].

[202] G. Polenta *et. al.*, *Search for non-gaussian signals in the BOOMERanG maps: pixel-space analysis*, Astrophys. J. **572** (2002) L27–L32, [astro-ph/0201133].

[203] N. Bartolo, E. Komatsu, S. Matarrese, and A. Riotto, *Non-Gaussianity from inflation: Theory and observations*, Phys. Rept. **402** (2004) 103–266, [astro-ph/0406398].

[204] http://lambda.gsfc.nasa.gov/product/map/map_tt_powspec.cfm.

[205] E. F. Bunn, *Calculations of cosmic background radiation anisotropies and implications*, astro-ph/9607088.

[206] G. Arfken, *Mathematical Methods for Physicists*. Academic Press, third ed., 1985.

[207] M. Tegmark, *Doppler peaks and all that: CMB anisotropies and what they can tell us*, astro-ph/9511148.

[208] C. H. Lineweaver, *Gold in the Doppler hills: Cosmological parameters in the microwave background*, astro-ph/9702042.

[209] J. Hwang, T. Padmanabhan, O. Lahav, and H. Noh, *On the 1/3 factor in the CMB Sachs-Wolfe effect*, Phys. Rev. **D65** (2002) 043005, [astro-ph/0107307].

[210] M. Abramowitz and I. A. Stegun, eds., *Handbook of Mathematical Functions*. Dover Publications, 1965.

[211] S. Weinberg, *Fluctuations in the cosmic microwave background I: Form factors and their calculation in synchronous gauge*, Phys. Rev. **D64** (2001) 123511, [astro-ph/0103279].

[212] **WMAP** Collaboration, D. N. Spergel *et. al.*, *First year Wilkinson Microwave Anisotropy Probe (WMAP) observations: Determination of cosmological parameters*, Astrophys. J. Suppl. **148** (2003) 175, [astro-ph/0302209].

[213] P.-S. Corasaniti, T. Giannantonio, and A. Melchiorri, *Constraining dark energy with cross-correlated CMB and large scale structure data*, astro-ph/0504115.

[214] W. Hu, N. Sugiyama, and J. Silk, *The physics of microwave background anisotropies*, Nature **386** (1997) 37–43, [astro-ph/9604166].

[215] R. Durrer, M. Kunz, and A. Melchiorri, *Cosmic structure formation with topological defects*, Phys. Rept. **364** (2002) 1–81, [astro-ph/0110348].

[216] A. Cooray, P.-S. Corasaniti, T. Giannantonio, and A. Melchiorri, *An indirect limit on the amplitude of primordial gravitational wave background from CMB – galaxy cross correlation*, astro-ph/0504290.

[217] M. Bartelmann and P. Schneider, *Weak gravitational lensing*, Phys. Rept. **340** (2001) 291–472, [astro-ph/9912508].

[218] U. Seljak, *Gravitational lensing effect on cosmic microwave background anisotropies: A power spectrum approach*, Astrophys. J. **463** (1996) 1, [astro-ph/9505109].

[219] R. A. Sunyaev and Y. B. Zeldovich, *The velocity of clusters of galaxies relative to the microwave background. The possibility of its measurement*, Mon. Not. Roy. Astron. Soc. **190** (1980) 413–420.

[220] M. Birkinshaw, *The Sunyaev-Zel'dovich effect*, Phys. Rept. **310** (1999) 97–195, [astro-ph/9808050].

[221] J. E. Carlstrom, G. P. Holder, and E. D. Reese, *Cosmology with the Sunyaev-Zel'dovich effect*, Ann. Rev. Astron. Astrophys. **40** (2002) 643, [astro-ph/0208192].

[222] Y. Rephaeli, *Comptonization of the cosmic microwave background: The Sunyaev-Zeldovich effect*, Ann. Rev. Astron. Astrophysics **33** (1995) 541–580.

[223] E. Giallongo *et. al.*, *The Gunn-Peterson effect in the spectrum of the z=4.7 QSO 1202-0725: The intergalactic medium at very high redshift*, astro-ph/9402035.

[224] **SDSS** Collaboration, R. H. Becker *et. al.*, *Evidence for reionization at $z \sim 6$: Detection of a Gunn- Peterson trough in a z=6.28 quasar*, Astron. J. **122** (2001) 2850, [astro-ph/0108097].

[225] S. P. Oh and S. R. Furlanetto, *How universal is the Gunn-Peterson trough at $z \sim 6$?: A closer look at the quasar SDSS J1148+5251*, Astrophys. J. **620** (2005) L9–L12, [astro-ph/0411152].

[226] L. Hui and Z. Haiman, *The thermal memory of reionization history*, Astrophys. J. **596** (2003) 9–18, [astro-ph/0302439].

[227] R. Brustein, M. Gasperini, M. Giovannini, V. F. Mukhanov, and G. Veneziano, *Metric perturbations in dilaton driven inflation*, Phys. Rev. **D51** (1995) 6744–6756, [hep-th/9501066].

[228] A. D. Miller *et. al.*, *A measurement of the angular power spectrum of the CMB from l = 100 to 400*, Astrophys. J. **524** (1999) L1–L4, [astro-ph/9906421].

[229] E. Torbet *et. al.*, *A measurement of the angular power spectrum of the microwave background made from the high Chilean Andes*, Astrophys. J. **521** (1999) L79–L82, [astro-ph/9905100].

[230] **Boomerang** Collaboration, P. D. Mauskopf *et. al.*, *Measurement of a peak in the cosmic microwave background power spectrum from the North American test flight of Boomerang*, Astrophys. J. **536** (2000) L59–L62, [astro-ph/9911444].

[231] W. Hu, "An introduction to the cosmic microwave background."
In the year 1999 at http://www.sns.ias.edu/∼whu/beginners/introduction.html
Currently at http://background.uchicago.edu/∼whu/beginners/introduction.html.

[232] C. L. Bennett *et. al.*, *4-Year COBE DMR cosmic microwave background observations: Maps and basic results*, Astrophys. J. **464** (1996) L1–L4, [astro-ph/9601067].

[233] M. Tegmark and M. Zaldarriaga, *Current cosmological constraints from a 10 parameter CMB analysis*, Astrophys. J. **544** (2000) 30–42, [astro-ph/0002091].

[234] S. Masi *et. al.*, *Boomerang: a scanning telescope for 10 arcminutes resolution CMB maps*, astro-ph/9911520.

[235] F. Piacentini *et. al.*, *The Boomerang North America instrument: a balloon-borne bolometric radiometer optimized for measurements of cosmic background radiation anisotropies from 0.3 to 4 degrees*, astro-ph/0105148.

[236] K. Coble *et. al.*, *Observations of galactic and extra-galactic sources from the Boomerang and SEST telescopes*, astro-ph/0301599.

[237] B. Rabii *et. al.*, *Maxima: A balloon-borne cosmic microwave background anisotropy experiment*, astro-ph/0309414.

[238] X. Wang, M. Tegmark, and M. Zaldarriaga, *Is cosmology consistent?*, Phys. Rev. **D65** (2002) 123001, [astro-ph/0105091].

[239] J. Valiviita, K. Enqvist, and H. Kurki-Suonio, *Limits on isocurvature fluctuations from Boomerang and Maxima*, in *Cosmology And Particle Physics CAPP2000* (R. Durrer, J. Garcia-Bellido, and M. Shaposhnikov, eds.), vol. 555 of *AIP conference proceedings*, pp. 320 – 323, American Institute of Physics, 2001.
Available at: http://www.helsinki.fi/%7Ejvalivii/subpage/capp2000_talk.html.

[240] S. L. Bridle *et. al.*, *Analytic marginalization over CMB calibration and beam uncertainty*, Mon. Not. Roy. Astron. Soc. **335** (2002) 1193, [astro-ph/0112114].

[241] H. Kurki-Suonio and E. Sihvola, *Inhomogeneous Big Bang nucleosynthesis and the high baryon density suggested by Boomerang and Maxima*, Phys. Rev. **D63** (2001) 083508, [astro-ph/0011544].

[242] J. Barriga, E. Gaztanaga, M. G. Santos, and S. Sarkar, *Evidence for an inflationary phase transition from the LSS and CMB anisotropy data*, Nucl. Phys. Proc. Suppl. **95** (2001) 66–69, [astro-ph/0012284].

[243] J. Barriga, E. Gaztanaga, M. G. Santos, and S. Sarkar, *On the APM power spectrum and the CMB anisotropy: Evidence for a phase transition during inflation?*, Mon. Not. Roy. Astron. Soc. **324** (2001) 977, [astro-ph/0011398].

[244] S. Hannestad, S. H. Hansen, and F. L. Villante, *Probing the power spectrum bend with recent CMB data*, Astropart. Phys. **16** (2001) 137–144, [astro-ph/0012009].

[245] J. P. Kneller, R. J. Scherrer, G. Steigman, and T. P. Walker, *When does CMB + BBN = new physics?*, Phys. Rev. **D64** (2001) 123506, [astro-ph/0101386].

[246] E. Gawiser, *Interpreting CMB anisotropy observations: Trying to tell the truth with statistics*, astro-ph/0105010.

[247] T. Padmanabhan and S. K. Sethi, *Constraints on Omega_B, Omega_m and h from Maxima and Boomerang*, Astrophys. J. **555** (2001) 125, [astro-ph/0010309].

[248] M. Tegmark and M. Zaldarriaga, *New CMB constraints on the cosmic matter budget: trouble for nucleosynthesis?*, Phys. Rev. Lett. **85** (2000) 2240, [astro-ph/0004393].

[249] S. Burles, K. M. Nollett, and M. S. Turner, *Big-bang nucleosynthesis predictions for precision cosmology*, Astrophys. J. **552** (2001) L1–L6, [astro-ph/0010171].

[250] **Particle Data Group** Collaboration, K. Hagiwara *et. al.*, *Review of particle physics*, Phys. Rev. **D66** (2002) 010001.

[251] W. H. Kinney, E. W. Kolb, A. Melchiorri, and A. Riotto, *Inflationary physics from the Wilkinson Microwave Anisotropy Probe*, Phys. Rev. **D69** (2004) 103516, [hep-ph/0305130].

[252] L. Verde *et. al.*, *First Year Wilkinson Microwave Anisotropy Probe (WMAP) observations: Parameter estimation methodology*, Astrophys. J. Suppl. **148** (2003) 195, [astro-ph/0302218].

[253] R. Trotta, *Applications of Bayesian model selection to cosmological parameters*, astro-ph/0504022.

[254] A. R. Liddle, *How many cosmological parameters?*, Mon. Not. Roy. Astron. Soc. **351** (2004) L49–L53, [astro-ph/0401198].

[255] M. Beltran, J. Garcia-Bellido, J. Lesgourgues, A. R. Liddle, and A. Slosar, *Bayesian model selection and isocurvature perturbations*, Phys. Rev. **D71** (2005) 063532, [astro-ph/0501477].

[256] W. H. Press, S. A. Teukolsky, W. T. Vetterling, and B. P. Flannery, *Numerical recipes in FORTRAN. The art of scientific computing.* Cambridge University Press, 1992.

[257] J. Dunkley, M. Bucher, P. G. Ferreira, K. Moodley, and C. Skordis, *Fast and reliable MCMC for cosmological parameter estimation*, astro-ph/0405462.

[258] A. Lewis and S. Bridle, *Cosmological parameters from CMB and other data: a Monte-Carlo approach*, Phys. Rev. **D66** (2002) 103511, [astro-ph/0205436].

[259] D. Gamerman, *Markov Chain Monte Carlo: Stochastic simulation from Bayesian inference*. Chapman & Hall, 1997.

[260] P. de Bernardis *et. al.*, *Maps of the millimetre sky from the BOOMERanG experiment*, astro-ph/0311396.

[261] J. e. Ruhl *et. al.*, *Improved measurement of the angular power spectrum of temperature anisotropy in the CMB from two new analyses of Boomerang observations*, Astrophys. J. **599** (2003) 786–805, [astro-ph/0212229].

[262] **SDSS** Collaboration, M. Tegmark *et. al.*, *The 3D power spectrum of galaxies from the SDSS*, Astrophys. J. **606** (2004) 702–740, [astro-ph/0310725].

[263] **The 2dFGRS** Collaboration, W. J. Percival *et. al.*, *The 2dF galaxy redshift survey: The power spectrum and the matter content of the universe*, Mon. Not. Roy. Astron. Soc. **327** (2001) 1297, [astro-ph/0105252].

[264] **The 2dFGRS** Collaboration, M. Colless *et. al.*, *The 2dF galaxy redshift survey: Spectra and redshifts*, Mon. Not. Roy. Astron. Soc. **328** (2001) 1039, [astro-ph/0106498].

[265] M. Colless *et. al.*, *The 2dF galaxy redshift survey: Final data release*, astro-ph/0306581.

[266] J. M. Bardeen, J. R. Bond, N. Kaiser, and A. S. Szalay, *The statistics of peaks of Gaussian random fields*, Astrophys. J. **304** (1986) 15–61.

[267] J. A. Peacock and S. J. Dodds, *Reconstructing the linear power spectrum of cosmological mass fluctuations*, Mon. Not. Roy. Astron. Soc. **267** (1994) 1020–1034, [astro-ph/9311057].

[268] F. Ferrer, S. Rasanen, and J. Valiviita, 2005. In prep.

[269] C. J. Odman, A. Melchiorri, M. P. Hobson, and A. N. Lasenby, *Constraining the shape of the CMB: A peak-by-peak analysis*, Phys. Rev. **D67** (2003) 083511, [astro-ph/0207286].

[270] K. Zuber, *Experimental neutrino physics*, hep-ex/0502039.

[271] A. Melchiorri *et. al.*, *Constraints on the sum of neutrino masses from cosmology and their impact on world neutrino data*, astro-ph/0501531.

[272] M. Doran, C. M. Muller, G. Schafer, and C. Wetterich, *Gauge-invariant initial conditions and early time perturbations in quintessence universes*, Phys. Rev. **D68** (2003) 063505, [astro-ph/0304212].

[273] M.-z. Li, X.-l. Wang, B. Feng, and X.-m. Zhang, *Quintessence and spontaneous leptogenesis*, Phys. Rev. **D65** (2002) 103511, [hep-ph/0112069].

[274] T. Takahashi, *Cosmic microwave background anisotropy in models with quintessence*, astro-ph/0111159.

[275] J.-c. Hwang and H. Noh, *Quintessential perturbations during scaling regime*, Phys. Rev. **D64** (2001) 103509, [astro-ph/0108197].

[276] M. Kawasaki, T. Moroi, and T. Takahashi, *Isocurvature fluctuations in tracker quintessence models*, Phys. Lett. **B533** (2002) 294–301, [astro-ph/0108081].

[277] M. Kawasaki, T. Moroi, and T. Takahashi, *Cosmic microwave background anisotropy with cosine-type quintessence*, Phys. Rev. **D64** (2001) 083009, [astro-ph/0105161].

[278] L. R. W. Abramo and F. Finelli, *Attractors and isocurvature perturbations in quintessence models*, Phys. Rev. **D64** (2001) 083513, [astro-ph/0101014].

[279] K. Enqvist and J. McDonald, *Inflationary Affleck-Dine scalar dynamics and isocurvature perturbations*, Phys. Rev. **D62** (2000) 043502, [hep-ph/9912478].

[280] B. A. Bassett, C. Gordon, R. Maartens, and D. I. Kaiser, *Restoring the sting to metric preheating*, Phys. Rev. **D61** (2000) 061302, [hep-ph/9909482].

[281] E. Pierpaoli, J. Garcia-Bellido, and S. Borgani, *Microwave background anisotropies and large scale structure constraints on isocurvature modes in a two-field model of inflation*, JHEP **10** (1999) 015, [hep-ph/9909420].

[282] G. N. Felder, L. Kofman, and A. D. Linde, *Inflation and preheating in NO models*, Phys. Rev. **D60** (1999) 103505, [hep-ph/9903350].

[283] K. A. Malik and D. Wands, *Dynamics of assisted inflation*, Phys. Rev. **D59** (1999) 123501, [astro-ph/9812204].

[284] R. A. Battye and J. Weller, *Cosmic structure formation in hybrid inflation models*, Phys. Rev. **D61** (2000) 043501, [astro-ph/9810203].

[285] K. Koyama and J. Soda, *Baryon isocurvature perturbation in the Affleck-Dine baryogenesis*, Phys. Rev. Lett. **82** (1999) 2632–2635, [astro-ph/9810006].

[286] T. Kanazawa, M. Kawasaki, N. Sugiyama, and T. Yanagida, *Isocurvature fluctuations of the M-theory axion in a hybrid inflation model*, Prog. Theor. Phys. **100** (1998) 1055–1062, [hep-ph/9803293].

[287] S. Kasuya, M. Kawasaki, and T. Yanagida, *Domain wall problem of axion and isocurvature fluctuations in chaotic inflation models*, Phys. Lett. **B415** (1997) 117–121, [hep-ph/9709202].

[288] T. Chiba, N. Sugiyama, and J. Yokoyama, *Imprints of the metrically coupled dilaton on density perturbations in inflationary cosmology*, Nucl. Phys. **B530** (1998) 304–324, [gr-qc/9708030].

[289] W.-l. Lee and L.-Z. Fang, *Density perturbations of thermal origin during inflation*, Int. J. Mod. Phys. **D6** (1997) 305–322, [astro-ph/9706101].

[290] D. H. Lyth, *Models of inflation and the spectral index of the density perturbation*, hep-ph/9609431.

[291] D. Langlois, *Cosmic microwave background dipole induced by double inflation*, Phys. Rev. **D54** (1996) 2447–2450, [gr-qc/9606066].

[292] M. Kawasaki, N. Sugiyama, and T. Yanagida, *Isocurvature and adiabatic fluctuations of axion in chaotic inflation models and large scale structure*, Phys. Rev. **D54** (1996) 2442–2446, [hep-ph/9512368].

[293] A. A. Starobinsky and J. Yokoyama, *Density fluctuations in Brans-Dicke inflation*, gr-qc/9502002.

[294] L. M. Krauss, *COBE, inflation, and light scalars*, hep-ph/9207243.

[295] F. Di Marco, F. Finelli, and R. Brandenberger, *Adiabatic and isocurvature perturbations for multifield generalized Einstein models*, Phys. Rev. **D67** (2003) 063512, [astro-ph/0211276].

[296] P. R. Ashcroft, C. van de Bruck, and A. C. Davis, *Inflationary dynamics with two scalar fields and generalized potentials*, Phys. Rev. **D69** (2004) 083516, [astro-ph/0210597].

[297] S. Tsujikawa and B. A. Bassett, *When can preheating affect the CMB?*, Phys. Lett. **B536** (2002) 9–17, [astro-ph/0204031].

[298] D. Wands, *Primordial perturbations from inflation*, astro-ph/0201541.

[299] A. A. Starobinsky, S. Tsujikawa, and J. Yokoyama, *Cosmological perturbations from multi-field inflation in generalized Einstein theories*, Nucl. Phys. **B610** (2001) 383–410, [astro-ph/0107555].

[300] N. Bartolo, S. Matarrese, and A. Riotto, *Adiabatic and isocurvature perturbations from inflation: Power spectra and consistency relations*, Phys. Rev. **D64** (2001) 123504, [astro-ph/0107502].

[301] S. Groot Nibbelink and B. J. W. van Tent, *Scalar perturbations during multiple field slow-roll inflation*, Class. Quant. Grav. **19** (2002) 613–640, [hep-ph/0107272].

[302] N. Bartolo, S. Matarrese, and A. Riotto, *Oscillations during inflation and cosmological density perturbations*, Phys. Rev. **D64** (2001) 083514, [astro-ph/0106022].

[303] J.-c. Hwang and H. Noh, *Cosmological perturbations with multiple scalar fields*, Phys. Lett. **B495** (2000) 277–283, [astro-ph/0009268].

[304] W. Lee and L.-Z. Fang, *A relativistic calculation of super-Hubble suppression of inflation with thermal dissipation*, Class. Quant. Grav. **17** (2000) 4467–4480, [astro-ph/0009060].

[305] A. N. Taylor and A. Berera, *Perturbation spectra in the warm inflationary scenario*, Phys. Rev. **D62** (2000) 083517, [astro-ph/0006077].

[306] K. Enqvist and A. Mazumdar, *Cosmological consequences of MSSM flat directions*, Phys. Rept. **380** (2003) 99–234, [hep-ph/0209244].

[307] F. Di Marco and F. Finelli, *Slow-roll inflation for generalized two-field Lagrangians*, astro-ph/0505198.

[308] K. R. S. Balaji, R. H. Brandenberger, and A. Notari, *Single field baryogenesis and the scale of inflation*, hep-ph/0412197.

[309] P. Fox, A. Pierce, and S. Thomas, *Probing a QCD string axion with precision cosmological measurements*, hep-th/0409059.

[310] F. Vernizzi, *Cosmological perturbations from varying masses and couplings*, Phys. Rev. **D69** (2004) 083526, [astro-ph/0311167].

[311] W. Lee and L.-Z. Fang, *Correlated hybrid fluctuations from inflation with thermal dissipation*, Phys. Rev. **D69** (2004) 023514, [astro-ph/0310856].

[312] B. van Tent, *Multiple-field inflation and the CMB*, Class. Quant. Grav. **21** (2004) 349–370, [astro-ph/0307048].

[313] A. Mazumdar and M. Postma, *Evolution of primordial perturbations and a fluctuating decay rate*, Phys. Lett. **B573** (2003) 5–12, [astro-ph/0306509].

[314] A. Mazumdar, *A model for fluctuating inflaton coupling: (s)neutrino induced adiabatic perturbations and non-thermal leptogenesis*, Phys. Rev. Lett. **92** (2004) 241301, [hep-ph/0306026].

[315] N. Bartolo, P. S. Corasaniti, A. R. Liddle, and M. Malquarti, *Perturbations in cosmologies with a scalar field and a perfect fluid*, Phys. Rev. **D70** (2004) 043532, [astro-ph/0311503].

[316] I. M. Khalatnikov, A. Y. Kamenshchik, M. Martellini, and A. A. Starobinsky, *Quasi-isotropic solution of the Einstein equations near a cosmological singularity for a two-fluid cosmological model*, JCAP **0303** (2003) 001, [gr-qc/0301119].

[317] K. A. Malik, D. Wands, and C. Ungarelli, *Large-scale curvature and entropy perturbations for multiple interacting fluids*, Phys. Rev. **D67** (2003) 063516, [astro-ph/0211602].

[318] J.-c. Hwang and H. Noh, *Cosmological perturbations with multiple fluids and fields*, Class. Quant. Grav. **19** (2002) 527–550, [astro-ph/0103244].

[319] F. Perrotta and C. Baccigalupi, *Early time perturbations behaviour in scalar field cosmologies*, Phys. Rev. **D59** (1999) 123508, [astro-ph/9811156].

[320] E. J. Chun, K. Dimopoulos, and D. Lyth, *Curvaton and QCD axion in supersymmetric theories*, Phys. Rev. **D70** (2004) 103510, [hep-ph/0402059].

[321] A. Gruzinov, *Post-inflationary curvature perturbations*, astro-ph/0401407.

[322] C. Gordon and K. A. Malik, *WMAP, neutrino degeneracy and non-Gaussianity constraints on isocurvature perturbations in the curvaton model of inflation*, Phys. Rev. **D69** (2004) 063508, [astro-ph/0311102].

[323] K. Hamaguchi, M. Kawasaki, T. Moroi, and F. Takahashi, *Curvatons in supersymmetric models*, Phys. Rev. **D69** (2004) 063504, [hep-ph/0308174].

[324] D. H. Lyth and D. Wands, *The CDM isocurvature perturbation in the curvaton scenario*, Phys. Rev. **D68** (2003) 103516, [astro-ph/0306500].

[325] K. Dimopoulos, G. Lazarides, D. Lyth, and R. Ruiz de Austri, *The Peccei-Quinn field as curvaton*, JHEP **05** (2003) 057, [hep-ph/0303154].

[326] V. Bozza, M. Gasperini, M. Giovannini, and G. Veneziano, *Constraints on pre-big bang parameter space from CMBR anisotropies*, Phys. Rev. **D67** (2003) 063514, [hep-ph/0212112].

[327] V. Bozza, M. Gasperini, M. Giovannini, and G. Veneziano, *Assisting pre-big bang phenomenology through short-lived axions*, Phys. Lett. **B543** (2002) 14–22, [hep-ph/0206131].

[328] F. Vernizzi, A. Melchiorri, and R. Durrer, *CMB anisotropies in pre-big bang cosmology*, astro-ph/0011197.

[329] L. Boubekeur and D. H. Lyth, *Detecting a small perturbation through its non-Gaussianity*, astro-ph/0504046.

[330] A. P. Andrade, C. A. Wuensche, and A. L. B. Ribeiro, *Predictions of mixed non-Gaussian cosmological density fields for the cosmic microwave background radiation*, Astrophys. J. **602** (2004) 555–564, [astro-ph/0312028].

[331] F. Bernardeau and J.-P. Uzan, *Non-Gaussianity in multi-field inflation*, Phys. Rev. **D66** (2002) 103506, [hep-ph/0207295].

[332] N. Bartolo, S. Matarrese, and A. Riotto, *Non-Gaussianity from inflation*, Phys. Rev. **D65** (2002) 103505, [hep-ph/0112261].

[333] M. J. White, *Higher order moments of the density field in a parameterized sequence of non-gaussian theories*, astro-ph/9811227.

[334] M. Bucher and Y. Zhu, *Non-Gaussian isocurvature perturbations from Goldstone modes generated during inflation*, Phys. Rev. **D55** (1997) 7415–7422, [astro-ph/9610223].

[335] K. Yamamoto and M. Sasaki, *Skewness of CMB anisotropies in an inflationary isocurvature baryon model*, Astrophys. J. **435** (1994) L83–L85, [astro-ph/9407046].

[336] K. Koyama, *CMB anisotropies in brane worlds*, Phys. Rev. Lett. **91** (2003) 221301, [astro-ph/0303108].

[337] M. Bastero-Gil, V. Di Clemente, and S. F. King, *Large scale structure from the Higgs fields of the supersymmetric standard model*, Phys. Rev. **D67** (2003) 103516, [hep-ph/0211011].

[338] A. Notari and A. Riotto, *Isocurvature perturbations in the ekpyrotic universe*, Nucl. Phys. **B644** (2002) 371–382, [hep-th/0205019].

[339] K. Koyama and J. Soda, *Bulk gravitational field and cosmological perturbations on the brane*, Phys. Rev. **D65** (2002) 023514, [hep-th/0108003].

[340] C. van de Bruck and M. Dorca, *On cosmological perturbations on a brane in an anti-de Sitter bulk*, hep-th/0012073.

[341] N. Deruelle, D. Langlois, and J.-P. Uzan, *Cosmological perturbations seeded by topological defects: Setting the initial conditions*, Phys. Rev. **D56** (1997) 7608–7620, [gr-qc/9707035].

[342] R. Durrer and M. Sakellariadou, *Microwave background anisotropies from scaling seed perturbations*, Phys. Rev. **D56** (1997) 4480–4493, [astro-ph/9702028].

[343] W. Hu, D. N. Spergel, and M. J. White, *Distinguishing causal seeds from inflation*, Phys. Rev. **D55** (1997) 3288–3302, [astro-ph/9605193].

[344] L. Conversi, A. Melchiorri, L. Mersini-Houghton, and J. Silk, *Are domain walls ruled out?*, Astropart. Phys. **21** (2004) 443–449, [astro-ph/0402529].

[345] N. Sugiyama, S. Zaroubi, and J. Silk, *Isocurvature fluctuations induce early star formation*, Mon. Not. Roy. Astron. Soc. **354** (2004) 543, [astro-ph/0310593].

[346] D. J. H. Chung, E. W. Kolb, A. Riotto, and L. Senatore, *Isocurvature constraints on gravitationally produced superheavy dark matter*, astro-ph/0411468.

[347] M. Giovannini, *Primordial magnetic fields*, hep-ph/0208152.

[348] M. Giovannini and M. E. Shaposhnikov, *Primordial magnetic fields, anomalous isocurvature fluctuations and big bang nucleosynthesis*, Phys. Rev. Lett. **80** (1998) 22–25, [hep-ph/9708303].

[349] T. Moroi and H. Murayama, *CMB anisotropy from baryogenesis by a scalar field*, Phys. Lett. **B553** (2003) 126–134, [hep-ph/0211019].

[350] H. Kurki-Suonio, K. Jedamzik, and G. J. Mathews, *Stochastic isocurvature baryon fluctuations, baryon diffusion, and primordial nucleosynthesis*, Astrophys. J. **479** (1997) 31–39, [astro-ph/9606011].

[351] C. J. Copi, K. A. Olive, and D. N. Schramm, *Large scale baryon isocurvature inhomogeneities*, Astrophys. J. **451** (1995) 51, [astro-ph/9410007].

[352] W. Hu, *An isocurvature mechanism for structure formation*, Phys. Rev. **D59** (1999) 021301, [astro-ph/9809142].

[353] P. J. E. Peebles, *An isocurvature CDM cosmogony. I. A worked example of evolution through inflation*, astro-ph/9805194.

[354] P. J. E. Peebles, *An isocurvature CDM cosmogony. II. Observational tests*, astro-ph/9805212.

[355] P. J. E. Peebles, *Issues for the next generation of galaxy surveys*, astro-ph/9805167.

[356] A. A. de Laix and R. J. Scherrer, *Another look at gaussian isocurvature hot dark matter models for large-scale structure*, Astrophys. J. **464** (1996) 539, [astro-ph/9509075].

[357] C. M. Hirata and U. Seljak, *Can superhorizon cosmological perturbations explain the acceleration of the universe?*, astro-ph/0503582.

[358] A. Mazumdar and A. Perez-Lorenzana, *Sneutrino condensate as a candidate for the hot big bang cosmology*, Phys. Rev. **D70** (2004) 083526, [hep-ph/0406154].

[359] A. Mazumdar and A. Perez-Lorenzana, *Sneutrino bangs*, Phys. Rev. Lett. **92** (2004) 251301, [hep-ph/0311106].

[360] E. W. Kolb, S. Matarrese, A. Notari, and A. Riotto, *Cosmological influence of super-Hubble perturbations*, astro-ph/0410541.

[361] T. Kanazawa, M. Kawasaki, N. Sugiyama, and T. Yanagida, *Observational implications of axionic isocurvature fluctuations*, Prog. Theor. Phys. **102** (1999) 71–87, [astro-ph/9805102].

[362] D. Langlois, *Cosmological CMBR dipole in open universes?*, gr-qc/9706024.

[363] M. Kawasaki and T. Yanagida, *Are isocurvature fluctuations of the M-theory axion observable?*, Prog. Theor. Phys. **97** (1997) 809–812, [hep-ph/9703261].

[364] M. J. White and W. Hu, *Testing inflation with small scale CMB anisotropies*, astro-ph/9606138.

[365] R. Stompor, A. J. Banday, and M. Gorski, Krzysztof, *Flat dark matter dominated models with hybrid adiabatic plus isocurvature initial conditions*, Astrophys. J. **463** (1996) 8, [astro-ph/9511087].

[366] W. Hu, E. F. Bunn, and N. Sugiyama, *COBE constraints on baryon isocurvature models*, Astrophys. J. **447** (1995) L59–L64, [astro-ph/9501034].

[367] N. Sugiyama and J. Silk, *The imprint of omega on the cosmic microwave background*, Phys. Rev. Lett. **73** (1994) 509–513, [astro-ph/9406026].

[368] W. Hu and N. Sugiyama, *Thermal history constraints on the isocurvature baryon model*, Astrophys. J. **436** (1994) 456–466, [astro-ph/9403031].

[369] T. Chiba, N. Sugiyama, and Y. Suto, *Microwave background anisotropies in primeval isocurvature baryon models: Constraints on the cosmological parameters*, Astrophys. J. **429** (1994) 427–433, [astro-ph/9311012].

[370] M. Bucher, K. Moodley, and N. Turok, *Primordial isocurvature perturbations: Testing the adiabaticity of the CMB anisotropy*, astro-ph/0011025.

[371] R. Trotta, *Cosmic microwave background anisotropies: Beyond standard parameters*, astro-ph/0410115.

[372] G. Lazarides, R. R. de Austri, and R. Trotta, *Constraints on a mixed inflaton and curvaton scenario for the generation of the curvature perturbation*, Phys. Rev. **D70** (2004) 123527, [hep-ph/0409335].

[373] C. Gordon and W. Hu, *A low CMB quadrupole from dark energy isocurvature perturbations*, Phys. Rev. **D70** (2004) 083003, [astro-ph/0406496].

[374] J. Garcia-Bellido, *Bounds on isocurvature perturbations from CMB and LSS*, astro-ph/0406488.

[375] R. Trotta and R. Durrer, *Testing the paradigm of adiabaticity*, astro-ph/0402032.

[376] T. Moroi and T. Takahashi, *Correlated isocurvature fluctuation in quintessence and suppressed CMB anisotropies at low multipoles*, Phys. Rev. Lett. **92** (2004) 091301, [astro-ph/0308208].

[377] R. Trotta, *The cosmological constant and the paradigm of adiabaticity*, New Astron. Rev. **47** (2003) 769–774, [astro-ph/0304525].

[378] H. V. Peiris *et. al.*, *First year Wilkinson Microwave Anisotropy Probe (WMAP) observations: Implications for inflation*, Astrophys. J. Suppl. **148** (2003) 213, [astro-ph/0302225].

[379] F. J. Cao, H. J. de Vega, and N. G. Sanchez, *The quantum inflaton, primordial perturbations and CMB fluctuations*, Phys. Rev. **D70** (2004) 083528, [astro-ph/0406168].

[380] K. Enqvist and H. Kurki-Suonio, *Constraining isocurvature fluctuations with the Planck Surveyor*, Phys. Rev. **D61** (2000) 043002, [astro-ph/9907221].

[381] L. A. Popa, C. Burigana, and N. Mandolesi, *Testing the principle of equivalence with Planck surveyor*, astro-ph/0209497.

[382] K. M. Gorski, B. Ratra, R. Stompor, N. Sugiyama, and A. J. Banday, *COBE-DMR-normalized open CDM cosmogonies*, Astrophys. J. Suppl. **114** (1998) 1–30, [astro-ph/9608054].

[383] B. Ratra and P. J. E. Peebles, *Inflation in an open universe*, Phys. Rev. **D52** (1995) 1837–1894.

[384] B. Ratra and P. J. E. Peebles, *CDM cosmogony in an open universe*, Astrophys. J. **432** (1994) L5–L9.

[385] D. H. Lyth and A. Woszczyna, *Large scale perturbations in the open universe*, Phys. Rev. **D52** (1995) 3338–3357, [astro-ph/9501044].

[386] A. D. Linde and A. Mezhlumian, *Inflation with Omega not = 1*, Phys. Rev. **D52** (1995) 6789–6804, [astro-ph/9506017].

[387] A. D. Linde, *Inflation with variable Omega*, Phys. Lett. **B351** (1995) 99–104, [hep-th/9503097].

[388] K. Yamamoto, M. Sasaki, and T. Tanaka, *Quantum fluctuations and CMB anisotropies in one-bubble open inflation models*, Phys. Rev. **D54** (1996) 5031–5048, [astro-ph/9605103].

[389] M. Bucher, A. S. Goldhaber, and N. Turok, *An open universe from inflation*, Phys. Rev. **D52** (1995) 3314–3337, [hep-ph/9411206].

[390] K. Yamamoto, M. Sasaki, and T. Tanaka, *Large angle CMB anisotropy in an open universe in the one bubble inflationary scenario*, Astrophys. J. **455** (1995) 412–418, [astro-ph/9501109].

[391] M. Kamionkowski and D. N. Spergel, *Large angle cosmic microwave background anisotropies in an open universe*, Astrophys. J. **432** (1994) 7, [astro-ph/9312017].

[392] B. Ratra *et. al.*, *CMB anisotropy constraints on open and flat-lambda CDM cosmogonies from UCSB South Pole, ARGO, MAX, White Dish, and SuZIE Data*, Astrophys. J. **517** (1999) 549, [astro-ph/9901014].

[393] J. Garcia-Bellido, A. R. Liddle, D. H. Lyth, and D. Wands, *The open universe Grishchuk-Zeldovich effect*, Phys. Rev. **D52** (1995) 6750–6759, [astro-ph/9508003].

[394] J. Garcia-Bellido, *Density perturbations from quantum tunneling in open inflation*, Phys. Rev. **D54** (1996) 2473–2482, [astro-ph/9510029].

[395] J. Garcia-Bellido, *Open inflation*, Nucl. Phys. Proc. Suppl. **48** (1996) 128–130, [astro-ph/9511078].

[396] J. Garcia-Bellido, A. R. Liddle, D. H. Lyth, and D. Wands, *Normalization of modes in an open universe*, Phys. Rev. **D55** (1997) 4596–4602, [astro-ph/9608106].

[397] J. Garcia-Bellido and A. R. Liddle, *Complete power spectrum for an induced gravity open inflation model*, Phys. Rev. **D55** (1997) 4603–4613, [astro-ph/9610183].

[398] J. Garcia-Bellido and A. D. Linde, *Open hybrid inflation*, Phys. Rev. **D55** (1997) 7480–7488, [astro-ph/9701173].

[399] J. Garcia-Bellido, *Open inflation models and gravitational wave anisotropies in the CMB*, Phys. Rev. **D56** (1997) 3225–3237, [astro-ph/9702211].

[400] J. Garcia-Bellido, J. Garriga, and X. Montes, *Quasi-open inflation*, Phys. Rev. **D57** (1998) 4669–4685, [hep-ph/9711214].

[401] J. Garcia-Bellido, *Single-bubble open inflation: An overview*, hep-ph/9803270.

[402] J. Garcia-Bellido, J. Garriga, and X. Montes, *Microwave background anisotropies in quasiopen inflation*, Phys. Rev. **D60** (1999) 083501, [hep-ph/9812533].

[403] A. Lewis. http://cosmologist.info/cosmomc/.

[404] D. H. Lyth, *Can the curvaton paradigm accommodate a low inflation scale*, Phys. Lett. **B579** (2004) 239–244, [hep-th/0308110].

[405] K. Dimopoulos, D. H. Lyth, and Y. Rodriguez, *Low scale inflation and the curvaton mechanism*, JHEP **02** (2005) 055, [hep-ph/0411119].

[406] Y. Rodriguez, *Low scale inflation and the immediate heavy curvaton decay*, hep-ph/0411120.

[407] J. Skilling, *Nested sampling for general Bayesian computation*, http://www.inference.phy.cam.ac.uk/bayesys/.

[408] M. L. Wilson, *On the anisotropy of the cosmological background matter and radiation distribution. 2. the radiation anisotrophy in models with negative spatial curvature*, Astrophys. J. **273** (1983) 2–15.

[409] A. Erdélyi, ed., *Higher Transcendental Functions*, vol. I of *Bateman manuscript project*. McGraw-Hill, 1953.

[410] E. R. Harrison, *Normal modes of vibrations of the universe*, Rev. Mod. Phys. **39** (1967) 862 – 882.

[411] J. D. Jackson, *Classical Electrodynamics*. Wiley, second ed., 1974.

[412] N. Gouda, N. Sugiyama, and M. Sasaki, *Large angle anisotropy of the cosmic microwave background in an open universe*, Prog. Theor. Phys. **85** (1991) 1023–1040.

[413] M. J. White and D. Scott, *Why not consider closed universes?*, Astrophys. J. **459** (1996) 415, [astro-ph/9508157].

[414] W. Hu and M. J. White, *CMB anisotropies: Total angular momentum method*, Phys. Rev. **D56** (1997) 596–615, [astro-ph/9702170].

[415] W. Hu, U. Seljak, M. J. White, and M. Zaldarriaga, *A complete treatment of CMB anisotropies in a FRW universe*, Phys. Rev. **D57** (1998) 3290–3301, [astro-ph/9709066].

[416] W. Hu and M. J. White, *Tensor anisotropies in an open universe*, Astrophys. J. **486** (1997) L1, [astro-ph/9701210].